

Palaeoclimate history of the Arabian Peninsula: humid phases recorded in lake deposits

Inauguraldissertation
der Philosophisch-naturwissenschaftlichen Fakultät
der Universität Bern

vorgelegt von
Thomas M. Rosenberg
von Beinwil AG

Leiter der Arbeit:

Prof. Dr. F. Preusser

Department of Physical Geography and Quaternary Geology, Stockholm University

Prof. Dr. D. Fleitmann

Institut für Geologie und Oeschger-Zentrum für Klimaforschung, Universität Bern

Palaeoclimate history of the Arabian Peninsula: humid phases recorded in lake deposits

Inauguraldissertation
der Philosophisch-naturwissenschaftlichen Fakultät
der Universität Bern

vorgelegt von
Thomas M. Rosenberg
von Beinwil AG

Leiter der Arbeit:
Prof. Dr. F. Preusser
Department of Physical Geography and Quaternary Geology, Stockholm University
Prof. Dr. D. Fleitmann
Institut für Geologie und Oeschger-Zentrum für Klimaforschung, Universität Bern

Von der Philosophisch-naturwissenschaftlichen Fakultät angenommen.

Bern, 25.11.2011

Der Dekan:
Prof. Dr. S. Decurtins

CONTENTS

| | |
|--|------------|
| Abstract | III |
| Acknowledgments | V |
| 1 Introduction and outline | 1 |
| 1.1 Introduction | 1 |
| 1.2 Luminescence dating | 2 |
| 1.3 Outline | 3 |
| 1.4 References | 5 |
| 2 A comparison of single and multiple aliquot TT-OSL data sets for sand-sized quartz from the Arabian Peninsula | 7 |
| 2.1 Introduction | 8 |
| 2.2 Material and methods | 9 |
| 2.3 Performance of OSL and TT-OSL SAR protocols | 12 |
| 2.4 Discussion | 18 |
| 2.5 Conclusions | 20 |
| 2.6 References | 21 |
| 3 Faunal evidence of a Holocene pluvial phase in Southern Arabia with remarks on the morphological variability of <i>Helenina anderseni</i> | 23 |
| 3.1 Introduction | 24 |
| 3.2 Geological setting | 24 |
| 3.3 Material and methods | 25 |
| 3.4 Micropaleontology | 26 |
| 3.5 Discussion | 30 |
| 3.6 Conclusions | 37 |
| 3.7 References | 39 |
| 4 Humid periods in southern Arabia - windows of opportunity for modern human dispersal | 45 |
| 4.1 Introduction | 46 |
| 4.2 Material and methods | 47 |

| | | |
|-------------------|---|------------|
| 4.3 | Chronology and environmental reconstructions | 47 |
| 4.4 | Discussion | 49 |
| 4.5 | Conclusions | 52 |
| 4.6 | References | 53 |
| 5 | Late Pleistocene palaeolake in the interior of Oman: A potential key area for the dispersal of anatomically modern humans out of Africa? | 57 |
| 5.1 | Introduction | 58 |
| 5.2 | Palaeolake Saiwan | 60 |
| 5.3 | Results and Discussion | 61 |
| 5.4 | References | 63 |
| 6 | Nafud palaeolakes fill the gap between southern and northern Arabian climate archives | 65 |
| 6.1 | Introduction | 66 |
| 6.2 | Regional palaeoclimate history | 68 |
| 6.3 | Materials and methods | 70 |
| 6.4 | Results from the Nafud palaeolake deposits | 75 |
| 6.5 | Discussion | 83 |
| 6.6 | Conclusions | 87 |
| 6.7 | References | 89 |
| 7 | Conclusions and outlook | 97 |
| Appendices | | |
| | Appendix A – Conference contributions | 99 |
| | Appendix B – Supplementals to Chapter 2 | 101 |
| | Appendix C – Supplementals to Chapter 3 | 103 |
| | Appendix D – Supplementals to Chapter 4 | 105 |
| | Appendix E – Supplementals to Chapter 5 | 143 |
| | Erklärung gemäss Art. 28 Abs. 2 RSL 05 | 147 |
| | Curriculum vitae | 149 |

Abstract

The dispersal of anatomically modern humans (AMH, *Homo sapiens*) out of Africa is a pivotal event in the global expansion of our species. As the major dispersal routes cut through the vast Arabian Desert, favourable climatic and environmental conditions with sufficient supply of surface water must have been critical factors for AMH expansion into Arabia and beyond. The modern climate of Arabia is governed by subtropical high pressure with very scarce moisture, generally delivered by northwesterly winds. A limited area in the far south experiences tropical summer precipitation under the influence of the Indian Summer Monsoon. From regional climate archives it is known, that the northern limit of monsoon rainfall was highly variable in the past, reaching latitudinal positions far north of its present summer position. How far north, however, remains unknown because of large gaps between clusters of existing climate archives. Relict lake deposits scattered among the dunes are the primary repository of past climate conditions in Arabia due to their potential to record environmental conditions during humid periods. Yet, until a few years ago, dating of Pleistocene relict lake deposits was limited to contaminated radiocarbon ages of the 70s, systematically underestimating the real ages. Hence, this PhD study focused on re-dating the relict lake deposits using optically stimulated luminescence (OSL). Owing to early signal saturation, the OSL dating limit was reached at ages of ~100 ka and required the testing of a novel measuring protocol to expand the dating range. Application of the approved protocol on samples from south-western Saudi Arabia revealed humid phases with a savannah like environment at ~80 ka (MIS 5a), ~100 ka (MIS 5c) and ~125 ka (MIS 5e). A second study on fluvial and lacustrine deposits in the interior of Oman, suggested a short humid period sometime between 132 and 104 ka. A final study on relict lake deposits from northern Saudi Arabia indicated humid periods centered at ~410 and ~320, 125 and 100 ka. A comparison with speleothem records of the southern Negev desert shows a very similar timing for humid periods. The agreement with the southern Negev, and disagreement with the central and northern Negev, makes a Mediterranean moisture source unlikely and suggests a tropical source, possibly from an enhanced African Monsoon. Favourable environmental conditions during all these periods allowed AMH to migrate across Arabia. Between ~75 and 10.5 ka arid conditions prevailed and turned Arabia into a natural barrier for human dispersal. Thus, expansion of AMH into Arabia and beyond must have taken place before 75 ka, possibly in multiple dispersals.

Thank you!

This thesis was initiated by Albert Matter together with Frank Preusser and Dominik Fleitmann. Albert Matter enabled the project owing to his valuable networking with local authorities, established through a lifelong engagement in Arabia. Albert Matter furthermore had a leading role in organising fieldwork and kindly supported me whenever I needed it. Back in Bern, and also in Oman, Frank Preusser spent a lot of his precious time to advise me in a very respectful and encouraging way. I felt understood and that we share a common work approach. Frank was, as far as I can judge, the best supervisor I could have had. When we both were sometimes a bit too efficient in finishing a manuscript we could count on Dominik Fleitmann, who looked at the texts with great care and came up with a number of critical improvements. Besides the team of my supervisors many more were involved in the success of this project. First of all I would like to thank my officemate Sally Lowick, who I shared a lot with and who helped me extensively with comments and English corrections. It was also through Sally that I got in touch with Ann Wintle, who's help on my first manuscript made it possible to publish it in *Radiation Measurements*. For the study in Oman, Ingo Blechschmidt joined us. I very much enjoyed fieldwork with him and his continuous support back in Switzerland was of great value. Further I would like to thank Karl Ramseier and Dirk Rike-Zapp for their advice and help. In the polishing workshop Stephan Brechbühl and Thomas Aebi were always very kind and helpful, even when I asked the nearly impossible, such as making oriented thin sections out of chalky diatomite or cutting rocks in the dark. At the beginning of my PhD Damian Steffen and Luca Abbühl introduced me to the secrets of the institute and motivated me to run and participate in running competitions. Thank you as well to my friends Thomas Scheiber, Raphael Worni, Mareike Trauerstein, Dănu Rufer, Anamaria Häuselmann and Dorian Gaar who were of great support many times. Anamaria's never ending supply of sweets was often crucial for my working spirit.

When I was fourteen, extra chemistry lessons with my teacher Felix Bauer for the first time familiarised me with the adventure of natural sciences. Later, at the age of eighteen Nikolaus Greeff, Professor at the Institute of Physiology of the University of Zürich, supervised me for a school thesis on electrical signals in plants. He gave me the opportunity to follow my curiosity by making experiments under his guidance and support. We looked at electric signals in *Mimosa* plants, used to trigger the closing of leaves after stimulation.

Finally I would like to close these acknowledgments with a big THANK YOU to my parents Agnes and Stephan and to Mélanie Jost for their endless support and understanding.

This work was financed by the Swiss National Science Foundation (grant 200021-117985/1).

1 Introduction and outline

1.1 Introduction

Today, an arid to hyper arid climate prevails in most of Arabia with a landscape dominated by sand and stone deserts. In contrast, the widespread occurrence of relict lake deposits is striking evidence of a more humid climate in the past. The modern climate is governed by subtropical high pressure with very scarce moisture, generally delivered by the northwesterlies. A limited area in the far south, namely the Yemeni highlands and the Dhofar region, experiences tropical summer precipitation under the influence of the Indian Summer Monsoon. From speleothems and marine cores of the Arabian Sea (Clemens and Prell, 2003; Fleitmann et al., 2011) it is known that monsoon strength was highly variable over the past 350 ka. The growth and isotopic records of speleothems from Hoti cave in Oman (Burns et al., 2001) and Mukalla cave in Yemen (Fleitmann et al., 2011) indicate, that during peak interglacial periods, the limit of monsoon rainfall was shifted north of its present location (Fig. 1.1). How far north, however, remains unknown.

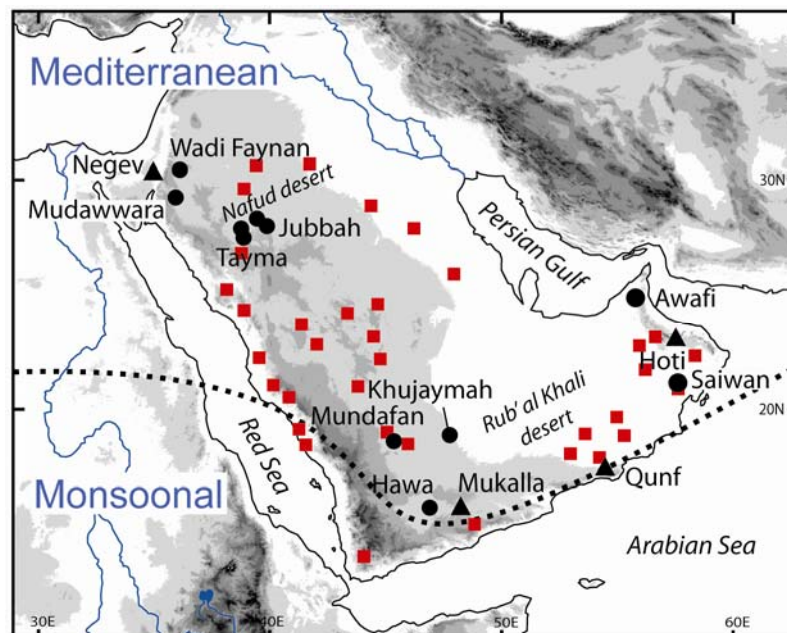


Fig. 1.1. The Arabian Peninsula. Black circles indicate relict lake deposits and black triangles cave sites. Red squares show a simplified distribution of Lower and Middle Palaeolithic archaeological sites (Petraglia and Alsharekh, 2003). The dashed line separates modern precipitation regimes (adapted from Gasse (2000)). “Mediterranean” = winter rainfall, “Monsoonal” = summer monsoon rainfall.

Despite being a key-area for understanding climate dynamics, the Pre-Holocene climate history of the Arabian Peninsula has major spatial and temporal gaps. Palaeoclimate archives (Fig. 1.1) do not cover the central part of the peninsula leaving a large gap between clusters of archives in the north and south. Besides its key location for understanding past climate dynamics, Arabia is of crucial importance for reconstruction of when and where anatomically modern humans (AMH) moved out of Africa and spread over the planet. From genetic mutation rates, it is assumed that the genetic diversion from the African gene-pool occurred some time between 85,000 and 65,000 years ago (Forster and Matsumura, 2005; Macaulay et al., 2005). This time slot, together with the nearly simultaneous first appearance of modern humans in Indonesia (Mellars, 2006; Oppenheimer, 2009), led a number of authors to suggest a single rapid southern dispersal across the Bab al Mandab strait and along the southern coast of Arabia. Regardless of whether AMH took the southern route or a northern route across the Sinai Peninsula, favourable environmental conditions with enough fresh water and food must have been a key factor. Thus, climate change on the Arabian Peninsula played a critical role in the timing of the out of Africa dispersal of AMH and therewith the global expansion of our species.

The potential to record not only humidity, but also environmental conditions during humid periods, makes relict lake deposits the primary repository of past climate conditions in Arabia. Yet, until a few years ago, dating of the relict lake deposits was limited to radiocarbon on carbonate-rich bulk sediments and shells. New evidence of recent studies using U/Th and optically stimulated luminescence (OSL) (Petit-Maire et al., 2010; Rosenberg et al., in press) strongly suggests that most of the relict lake deposits are considerably older than the previously suggested 40-20 ka (McClure, 1976; McClure, 1984; Sanlaville, 1992; Whitney, 1983a; Whitney et al., 1983b).

The aim of this study was to investigate relict lake deposits of the Arabian deserts as archives of past environmental conditions using OSL for dating, and ostracods, foraminifera, charophytes, diatoms, shells and molluscs as environmental proxies. Situated between existing clusters of palaeoclimate archives the results might offer an important contribution towards filling the spatial and temporal gaps in the Arabian climate record.

1.2 Luminescence dating

Optically stimulated luminescence (OSL) dating is used to identify when sedimentary grains were last exposed to daylight. During burial, the sedimentary grains absorb energy from the naturally occurring radioactivity of the surrounding sediment. OSL dating allows the estimation of the amount of radiation absorbed since burial using an optically and thermally

sensitive light signal in minerals such as quartz and feldspar. During exposure to light the luminescence signal within the grains is erased. By first measuring the natural luminescence and then the response to a series of known rising doses it is possible to identify the amount of radiation equivalent to the absorbed dose during burial (D_e), measured in Gray (1 Gy = 1 J kg⁻¹). The time elapsed since the last exposure to daylight is calculated as the ratio of D_e to the annual radiation flux, or dose rate (D_r), at the sampling location.

$$\text{Luminescence age [a]} = \frac{D_e \text{ [Gy]}}{D_r \text{ [Gy a}^{-1}\text{]}}$$

The single aliquot regenerative dose (SAR) protocol (Murray and Wintle, 2000) is now widely used to measure the equivalent dose (D_e). A minimum set of tests is required for every sample to assess the performance of the protocol (Wintle and Murray, 2006).

1.3 Outline

The major limiting factor with regard to the dating range of OSL dating of quartz is the saturation of the fast OSL component in the range of a few hundred Gray. For the samples from Saudi Arabia and Oman, the quartz OSL signals start to saturate at doses of about 100-150 Gy. In order to date dune sands with greater expected doses, a previously published, single-aliquot regenerative-dose protocol (SAR) for thermally-transferred optically stimulated luminescence (TT-OSL) (Porat et al., 2009) was tested and the results are presented in **Chapter 2**.

Although foraminifera have been found living in inland saline lakes isolated from the sea, this phenomenon has rarely been recognized in the fossil record. **Chapter 3** documents the occurrence of benthic foraminifera in Holocene lake sediments located nearly 500 km inland from the Red Sea, in the south-western Rub' al Khali in Saudi Arabia.

As southern Arabia is a key-area for the dispersal of AMH out of Africa, dating results and environmental proxies of the south-western Rub' al Khali are combined to provide a regional climate reconstruction, and set into the archaeological context. Given its modern hostile environment, the question of timing of the dispersal is also a question of climatic conditions. **Chapter 4** presents the first climatic and environmental framework that supports the hypothesis of a successful out of Africa dispersal of AMH before ca. 75 ka.

Uncertain access to Saudi Arabia in 2009 led us to choose a second site in central Oman, near Saiwan where palaeolake sediments were known from an earlier

reconnaissance study. The area is noted for its rich archaeological evidence, although no study had been carried out on the relict lake deposits before. Climatic and archaeological results of this study are summarized in **Chapter 5**.

After further access was granted in 2010 a third study was carried out in the Great Nafud desert of northern Saudi Arabia. The area is a key area for palaeolake archive research because of its position between clusters of existing archives, but also because of the quality and thickness of the palaeolake sequences. Rich vertebrate fossil finds (Thomas et al., 1998) indicated an Early Pleistocene age for some of the relict lake deposits but no absolute dating existed apart from questionable radiocarbon ages. The intermediate results of this study are presented in **Chapter 6**.

Overall final conclusions are drawn in **Chapter 7** and a list of publications resulting from this PhD thesis is shown in Tab. 1.1.

Table 1.1. List of publications included as chapters in this PhD-thesis

| | |
|-----------|--|
| Chapter 2 | Rosenberg, T. M., Preusser, F., and Wintle, A. G. (2011). A comparison of single and multiple aliquot TT-OSL data sets for sand-sized quartz from the Arabian Peninsula. <i>Radiation Measurements</i> 46, 573-579. |
| Chapter 3 | Gennari, G., Rosenberg, T., Spezzaferri, S., Berger, J.-P., Fleitmann, D., Preusser, F., Al-Shanti, M., and Matter, A. (2011). Faunal evidence of a Holocene pluvial phase in southern Arabia with remarks on the morphological variability of <i>Helena Anderseni</i> . <i>Journal of Foraminiferal Research</i> 41, 248-259. |
| Chapter 4 | Rosenberg, T. M., Preusser, F., Fleitmann, D., Schwalb, A., Penkman, K., Schmid, T. W., Kadi, K., Al-Shanti, M. A., and Matter, A. (2011). Humid periods in southern Arabia - windows of opportunity for modern human dispersal. <i>Geology</i> , 39, 1115-1118. |
| Chapter 5 | Rosenberg, T. M., Preusser, F., Blechschmidt, I., Fleitmann, D., Jagher, R., and Matter, A. (accepted). Late Pleistocene palaeolake in the interior of Oman: A potential key-area for the dispersal of anatomically modern humans out-of-Africa? <i>Journal of Quaternary Science</i> . |
| Chapter 6 | Rosenberg, T. M., Preusser, F., Fleitmann, D., Risberg, J., Pliik, A., Kadi, K., and Matter, A. (in prep.). Nafud palaeolakes fill the gap between southern and northern Arabian climate archives. |

1.4 References

- Burns, S. J., Fleitmann, D., Matter, A., Neff, U., and Mangini, A. (2001). Speleothem evidence from Oman for continental pluvial events during interglacial periods. *Geology* 29, 623-626.
- Clemens, S. C., and Prell, W. L. (2003). A 350,000 year summer-monsoon multi-proxy stack from the Owen Ridge, Northern Arabian Sea. *Marine Geology* 201, 35-51.
- Fleitmann, D., Burns, S. J., Pekala, M., Mangini, A., Al-Subbary, A., Al-Aowah, M., Kramers, J., and Matter, A. (2011). Holocene and Pleistocene pluvial periods in Yemen, southern Arabia. *Quaternary Science Reviews* 30, 783-787.
- Forster, P., and Matsumura, S. (2005). EVOLUTION: Enhanced: Did Early Humans Go North or South? *Science* 308, 965-966.
- Gasse, F. (2000). Hydrological changes in the African tropics since the Last Glacial Maximum. *Quaternary Science Reviews* 19, 189-211.
- Macaulay, V., Hill, C., Achilli, A., Rengo, C., Clarke, D., Meehan, W., Blackburn, J., Semino, O., Scozzari, R., Cruciani, F., Taha, A., Shaari, N. K., Raja, J. M., Ismail, P., Zainuddin, Z., Goodwin, W., Bulbeck, D., Bandelt, H.-J., Oppenheimer, S., Torroni, A., and Richards, M. (2005). Single, Rapid Coastal Settlement of Asia Revealed by Analysis of Complete Mitochondrial Genomes. *Science* 308, 1034-1036.
- McClure, H. A. (1976). Radiocarbon chronology of late Quaternary lakes in the Arabian Desert. *Nature* 263, 755-756.
- McClure, H. A. (1984). "Late Quaternary palaeoenvironments of the Rub' Al-Khali. Unpublished PhD Thesis, University College, London, 245p."
- Mellars, P. (2006). Going East: New Genetic and Archaeological Perspectives on the Modern Human Colonization of Eurasia. *Science* 313, 796-800.
- Murray, A. S., and Wintle, A. G. (2000). Luminescence dating of quartz using an improved single-aliquot regenerative-dose protocol. *Radiation Measurements* 32, 57-73.
- Oppenheimer, S. (2009). The great arc of dispersal of modern humans: Africa to Australia. *Quaternary International* 202, 2-13.
- Petit-Maire, N., Carbonel, P., Reyss, J. L., Sanlaville, P., Abed, A., Bourrouilh, R., Fontugne, M., and Yasin, S. (2010). A vast Eemian palaeolake in Southern Jordan (29°N). *Global and Planetary Change* 72, 368-373.
- Petraglia, M. D., and Alsharekh, A. (2003). The Middle Palaeolithic of Arabia: Implications for modern human origins, behaviour and dispersals. *Antiquity* 77, 671-684.
- Porat, N., Duller, G.A.T., Roberts, H.M., Wintle, A.G., 2009. A simplified SAR protocol for TT-OSL. *Radiation Measurements* 44, 538-542.

-
- Rosenberg, T. M., Preusser, F., Fleitmann, D., Schwalb, A., Penkman, K., Schmid, T. W., Kadi, K., Al-Shanti, M. A., and Matter, A. (2011b). Humid periods in southern Arabia - windows of opportunity for modern human dispersal. *Geology* 39, 1115-1118.
- Sanlaville, P. (1992). Changements climatiques dans la péninsule arabique durant le Pléistocène supérieure et l'Holocène. *Paléorient* 18, 5–26.
- Thomas, H., Geraads, D., Vaslet, D., Memesh, A., Billiou, D., Bocherens, H., Dobigny, G., Eisenmann, V., Gayet, M., France de Lapparent de, B., Petter, G., and Halawani, M. (1998). First Pleistocene faunas from the Arabian Peninsula: An Nafud desert, Saudi Arabia. *Comptes Rendus de l'Académie des Sciences - Series IIA - Earth and Planetary Science* 326, 145-152.
- Whitney, J. W. (1983a). *Erosional history and surficial geology of western Saudi Arabia. United States Geological Survey Technical Record 04-1.*
- Whitney, J. W., Faulkender, D. J., and Rubin, M. (1983b). *The environmental history and present condition of Saudi Arabia's northern sand seas. USGS Open-File Report 83-749, 42.*
- Wintle, A. G., and Murray, A. S. (2006). A review of quartz optically stimulated luminescence characteristics and their relevance in single-aliquot regeneration dating protocols. *Radiation Measurements* 41, 369-391.

2 A comparison of single and multiple aliquot TT-OSL data sets for sand-sized quartz from the Arabian Peninsula

Thomas M. Rosenberg ^{a,b}, Frank Preusser ^{a,c}, Ann G. Wintle ^d

^a Institute of Geological Sciences, University of Bern, Switzerland

^b Oeschger Centre for Climate Change Research, University of Bern, Switzerland

^c Present address: Department of Physical Geography and Quaternary Geology, Stockholm University, Sweden

^d Institute of Geography and Earth Sciences, Aberystwyth University, UK

Published in Radiation Measurements (2011), 46, 573-579

Abstract: The quartz OSL signals from dune sands from Saudi Arabia and Oman start to saturate at doses of about 100 Gy. In order to try to date dune sands with greater expected doses, a previously published, single-aliquot, regenerative-dose protocol (SAR) for thermally-transferred optically stimulated luminescence (TT-OSL) was tested. Dose recovery tests, recycling and recuperation ratios showed robust functioning and dose response curves demonstrated the potential to extend the dose range to beyond 600 Gy. Multiple aliquot additive dose (MAAD) TT-OSL protocols were used to test for sensitivity changes in the SAR TT-OSL protocol up to doses of 1200 Gy. A strong dose dependent deviation of the SAR TT-OSL relative to the MAAD TT-OSL dose response is observed. Comparison of the TT-OSL and OSL sensitivity data obtained from the MAAD and SAR data sets shows a lack of proportionality between TT-OSL and OSL for the SAR data which will result in a problem when SAR dose response curves are constructed using many regeneration points with doses above 300Gy.

2.1 Introduction

In optically stimulated luminescence (OSL) dating of quartz, saturation of the fast OSL component in the range of a few hundred Gray is the major limiting factor with regard to the dating range. In some samples, including the ones of this study, saturation starts as early as about 100 Gy (Roberts and Duller, 2004). To overcome the problem of saturation, the use of thermally transferred optically stimulated luminescence (TT-OSL) signals has been suggested, as this signal shows a much higher saturation level (Wang et al., 2006). Thermal transfer of charge has long been known as the unwanted effect of recuperation (Aitken and Smith, 1988; Aitken, 1998) but recently TT-OSL signals were tested for their potential use in dating applications (e.g., Wang et al., 2006; Tsukamoto et al., 2008; Kim et al., 2009; Nian et al., 2009; Porat et al., 2009; Stevens et al., 2009; Sun et al., 2009; Athanassas and Zacharias, 2010; Adamiec et al., 2010). Compared with the fast OSL signal, two adverse properties of the TT-OSL signal have been found: first, the source of the thermally transferred charge is less optically sensitive (Adamiec et al., 2008) and second, its thermal stability is an order of magnitude lower, with a lifetime at 10°C of 4.5 Ma compared to 3800 Ma of the fast OSL trap (Adamiec et al., 2010).

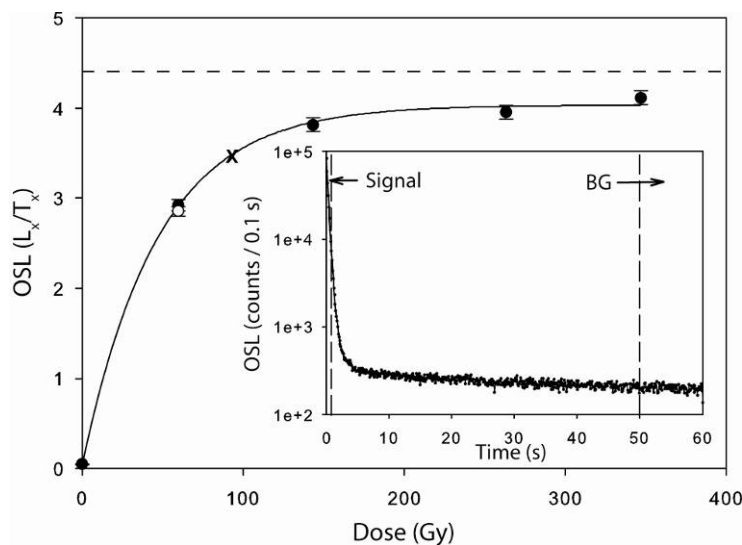


Fig. 2.1. OSL dose response curve of a coarse-grained sample (8327.1/1) obtained using a 6 mm aliquot. The $2D_0$ value of the single saturating exponential is marked with a cross at 95 Gy. The dashed line shows the value of the natural L_n/T_n ratio. The open circle is a repeated measurement. The inset shows a typical OSL decay curve on a semi-log scale with the regions indicated for signal and background estimations.

The procedure to obtain the TT-OSL signal includes an initial measurement of the OSL signal, a subsequent transfer preheat (e.g. 10 s at 260°C), followed by a second OSL measurement, giving the TT-OSL signal. While the first measurement empties the fast OSL

trap, the transfer preheat moves charge from the TT-OSL trap into the fast OSL trap. Understanding the process behind this thermal transfer is still a challenge (Pagonis et al., 2009) with competition for charge by different traps during thermal transfer being expected to have a major influence on the final amount of charge reaching the fast OSL trap. These processes may affect the shape of the dose response curve and therefore the performance of the measurement protocol applied.

The recuperated TT-OSL measurement protocol originally suggested by Wang et al. (2006) comprised 15 steps including the removal of the so-called Basic Transferred OSL (BT-OSL) signal (Aitken, 1998), that remains after repeated measurements of the TT-OSL signal. Porat et al. (2009) have shown that the BT-OSL signal is dose dependent in a way that is similar to TT-OSL and this led Porat et al. (2009) to suggest a shorter protocol of only nine steps. Although the BT-OSL is small, it interferes with the TT-OSL signal and has to be removed when not measured separately. Porat et al. (2009) suggested a heating step of 300°C for 100 seconds to remove the BT-OSL signal at the end of each measurement cycle.

The present study focuses on sand-sized quartz extracted from aeolian dune sands from the Arabian Peninsula, for which early saturation of the quartz fast OSL component had been observed. The properties of the TT-OSL signal of the samples under consideration are investigated and the recently suggested single aliquot regenerative dose (SAR) protocol (Porat et al., 2009) is tested. In this protocol, the OSL response to a test dose is used to monitor the sensitivity. However, when using the SAR protocol of Wang et al. (2007), Stevens et al. (2009) reported a non-linear relationship between the regenerative dose TT-OSL and test dose OSL; this led them to suggest a protocol that included a TT-OSL test dose correction, but they needed to use much larger test doses.

In the current study, particular attention is paid to the sensitivity correction for TT-OSL measurements when using the OSL response and this is examined by comparing the SAR data set and multiple aliquot additive dose (MAAD) data set obtained for a modern naturally bleached sample. Due to the limited experience with TT-OSL for sand-sized grains (e.g. Porat et al., 2009; Tsukamoto et al., 2008; Athanassas and Zacharias, 2010), the results obtained are expected to be important for related studies on similar deposits from other regions.

2.2 Material and methods

The samples originated from two sites in Saudi Arabia (18°34'N, 45°21'E and 18°32'N, 47°14'E) and one site in Oman (20°58'N, 57°22'E). Seventeen samples were investigated, including a modern surface sand (18°32'N, 47°14'E). The grain size 200-250

μm was isolated and treated with HCl and H_2O_2 to remove carbonates and organic matter. A two step heavy-liquid separation using LST Fastfloat (2.70 and 2.58 g cm^{-3}) was carried out and the quartz fraction was subsequently etched in HF (40%) for 60 min to remove feldspars and the outer part of the quartz grains influenced by alpha irradiation during burial. After washing with HCl to dissolve fluorides, the samples were re-sieved at $150 \mu\text{m}$ to remove any feldspar grains that might have been only partly etched, rather than removed. The coarse-grained quartz was then mounted on steel discs using silicone spray. For all measurements the aliquot size was 6 mm. Measurements were made in a Risø TL/OSL-DA-20 reader with blue diodes ($470 \pm 30 \text{ nm}$; $\sim 41 \text{ mW cm}^{-2}$) and with a calibrated $40 \text{ mCi } ^{90}\text{Sr}/^{90}\text{Y}$ beta source delivering $\sim 0.13 \text{ Gy s}^{-1}$ to the grains. Luminescence signals were measured with an EMI 9635Q photomultiplier tube through a 7.5 mm Hoya U340 filter. Typical OSL and TT-OSL decay curves are shown in the inset in Figure 2.1 and in Figure 2.2B, respectively.

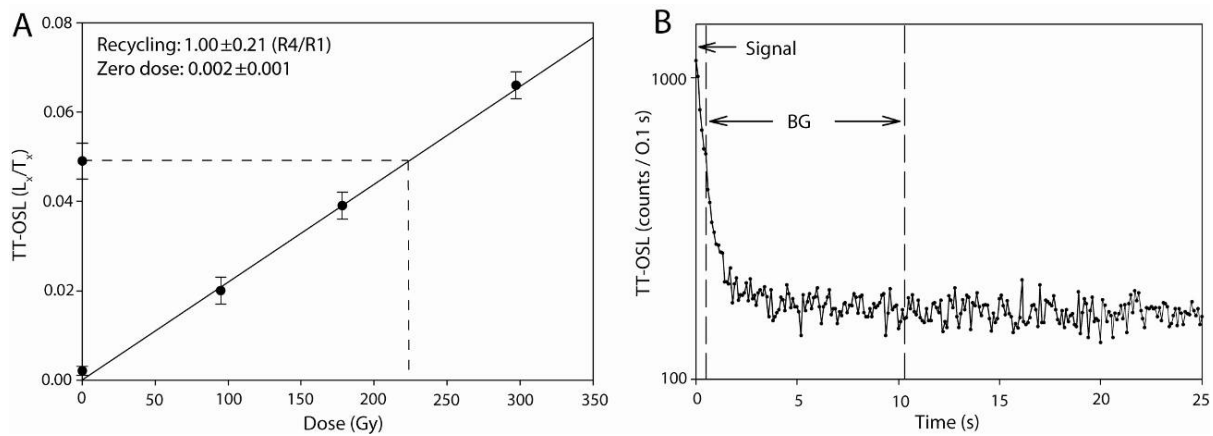


Fig. 2.2. (A) TT-OSL dose response curve of the same sample as in Figure 2.1 (8327.1/1), also using a 6 mm aliquot. Dose response points are linearly fitted and forced through the origin. The natural L_n/T_n ratio projected onto the curve results in a D_e of $233 \pm 8 \text{ Gy}$. The recycling ratio ($R4/R1$) is 1.00 ± 0.21 and the zero dose L_x/T_x ratio is 0.002 ± 0.001 . **(B)** Typical natural TT-OSL decay curve on a semi-log scale with the regions indicated used for signal and background estimations.

Two protocols were used to determine the equivalent dose (D_e) for each of the sixteen non-modern samples: a standard SAR protocol for OSL (Murray and Wintle, 2000) and a SAR protocol for TT-OSL (Porat et al., 2009). In addition, a multiple aliquot additive dose (MAAD) protocol for TT-OSL was used to construct a dose response curve using the modern sample.

For the SAR OSL protocol, samples were initially characterized using preheat plateau and dose recovery tests (Appendix B). A preheat of 260°C for 10 s together with a cut-heat of 240°C were selected for D_e determination. The test dose size was always 10 Gy. The dose response curve was constructed by plotting L_x/T_x versus dose (Fig. 2.1), where L_x is the OSL signal from the regenerative dose and T_x is the response to the test dose. The initial 0.4 s OSL signal minus a background estimated from the 50-60 s integral was used for OSL dose

determinations. These regions of the decay curve are shown in the inset to Figure 2.1. Aliquots were rejected if the recycling ratio was outside the range 1.0 ± 0.2 or the IR-OSL depletion ratio (Duller, 2003) was less than 0.8. All heating was ramped at 5°C s^{-1} .

As in the SAR protocol for TT-OSL originally proposed by Wang et al. (2007), the luminescence sensitivity was monitored using an OSL signal. For our study, the Porat et al. (2009) SAR protocol for TT-OSL (Table 2.1) was used. The test dose was 1 Gy for the modern sample and 10 Gy for all other samples (except 6.5 Gy in the case of the same repeated regenerative dose). The initial 0.4 s TT-OSL signal minus an early background estimated from the 0.4-10.4 s integral, as suggested by Ballarini et al. (2007), was used for TT-OSL dose determinations to better cope with the small TT-OSL signals. A TT-OSL dose response curve is shown in Figure 2.2A and signal and background integrals are shown in Figure 2.2B.

A multiple aliquot additive dose (MAAD) TT-OSL response curve was constructed using a modern naturally bleached sample (laboratory number 8326.2) which had a residual TT-OSL signal equivalent to 5.5 ± 2.6 Gy (residual OSL dose was 0.02 ± 0.04 Gy). In the MAAD procedure the same protocol as for SAR (Table 1) was used, but each aliquot was used only once, first to measure the TT-OSL signal from the natural plus one added laboratory dose ($N + \beta$ giving L_x), and then to measure the OSL response (T_x) to a test dose of 1 Gy.

A D_e value for each sample was obtained using the central age model (Galbraith et al., 1999), with at least eight aliquots for TT-OSL D_e values and with at least 15 aliquots for OSL D_e values.

Table 2.1

Simplified TT-OSL SAR protocol as suggested by Porat et al. (2009). For TT-OSL MAAD the same procedures were carried out, but only once per aliquot (no return to 1).

| Step | Treatment | Measurement |
|------|---|-------------|
| 1 | Dose, D_i | |
| 2 | Preheat at 200°C for 10 s | |
| 3 | Blue stimulation at 125°C for 300 s | |
| 4 | Transfer preheat at 260°C for 10 s | |
| 5 | Blue stimulation at 125°C for 100 s | L_x |
| 6 | Test dose, D_t | |
| 7 | Preheat at 220°C for 10 s | |
| 8 | Blue stimulation at 125°C for 100 s | T_x |
| 9 | Heat at 300°C for 100 s | |
| 10 | Return to 1 | |

2.3 Performance of OSL and TT-OSL SAR protocols

The features investigated in this study are (i) the saturation of the OSL signal as measured with the SAR protocol, (ii) TT-OSL SAR dose recovery tests, (iii) the performance of the sensitivity correction for the TT-OSL SAR protocol, (iv) the comparison of the equivalent doses determined from both TT-OSL and OSL SAR measurements, and (v) the offset between the SAR and MAAD TT-OSL dose response curves.

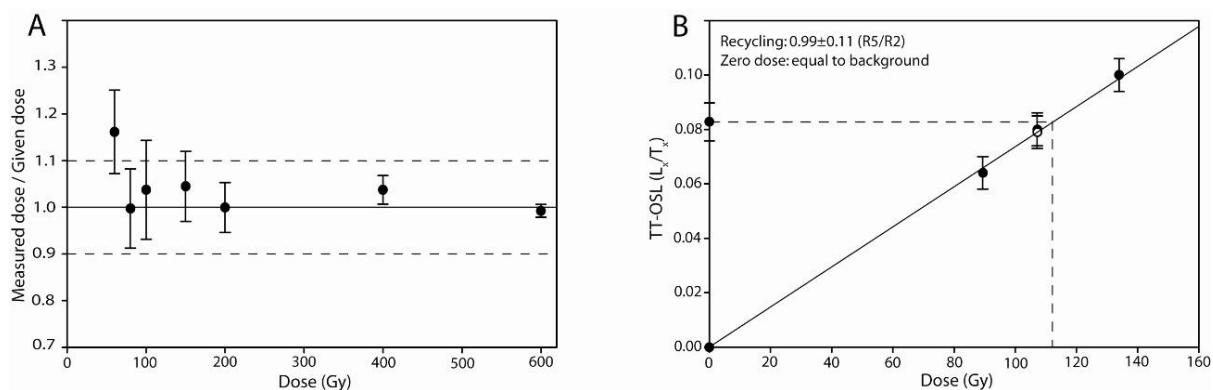


Fig. 2.3. (A) TT-OSL dose recovery test, average data for 6 discs obtained using TT-OSL SAR protocol for seven doses given to a modern naturally bleached sample (8326.2) with a residual dose of 5.5 ± 2.6 Gy; this value was subtracted from the measured doses. **(B)** TT-OSL dose response curve of an aliquot of the same sample given a laboratory dose of 100 Gy. The recycling ratio ($R5/R2$) is 0.99 ± 0.11 and the zero dose L_x/T_x ratio measured at the end of the SAR sequence is equal to the background signal. Error bars represent standard errors.

2.3.1 Saturation of the OSL signal

OSL dose response curves were obtained for all 16 samples using the SAR protocol and a typical curve is shown in Figure 2.1. The OSL data sets were fitted with a saturating exponential function $I = I_0(1 - \exp[-D/D_0])$, where I_0 is the asymptotic value of L_x/T_x when plotted as a function of the laboratory dose D and D_0 is the dose that characterizes the rate at which saturation occurs. For several aliquots, D_0 values were as low as 47.5 Gy (Fig. 2.1). Wintle and Murray (2006) recommended that the $2D_0$ value of a single exponential dose response curve should be the upper threshold for dating because it is 15% below the asymptotic value and therefore prevents large and asymmetric uncertainties in the calculation of D_e . The average $2D_0$ values for all our samples were approximately 150 Gy and are comparable with values of 110 Gy reported by Roberts and Duller (2004) for NE Tasmanian coarse-grained quartz which are among the smallest reported (Wintle and Murray, 2006). For a typical environmental dose rate in the Rub' al Khali desert of 1.2 Gy ka^{-1} , for example a $2D_0$ value of 95 Gy gives 79 ka as the upper limit for dating (shown in Fig. 2.1 for sample 8327.1/1). In addition, for the aliquot in Figure 2.1, it was not possible to obtain a value of D_e since L_x/T_x for the natural signal was above the asymptotic value for the

regenerated data set. Thus, to provide a chronology further back in time, it is necessary to investigate another luminescence signal, in this case TT-OSL.

2.3.2 TT-OSL SAR dose recovery test

Applying the TT-OSL SAR protocol of Porat et al. (2009) with regeneration doses of 95, 178 and 297 Gy to the same sample (8327.1/1), results in a linear TT-OSL dose response curve (Fig. 2.2A) with an excellent recycling ratio of 1.00 ± 0.21 and a De of 233 ± 8 Gy. The recycle point and the zero dose value were measured after the measurements for the dose response curve and the linear fit shown in Fig. 2.2A is forced through the origin.

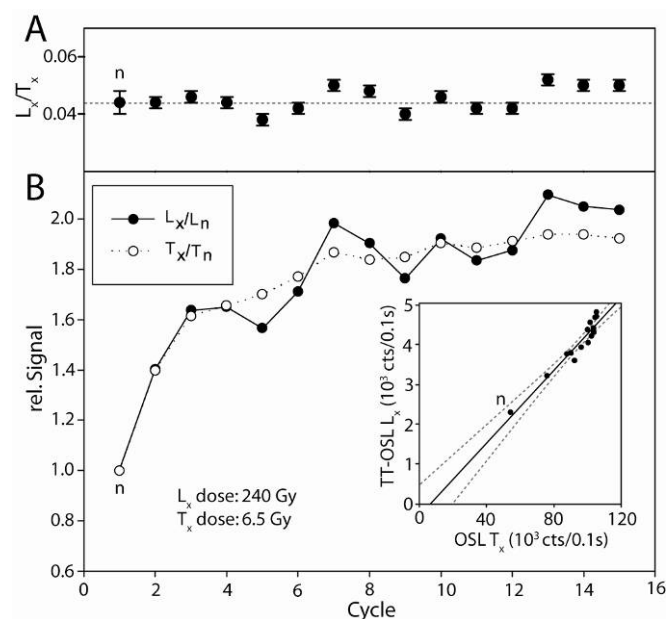


Fig. 2.4. Sensitivity change of the TT-OSL signal L_x and related OSL signal from the test dose (T_x) of 6.5 Gy through fourteen repeated cycles of the Porat et al. (2009) protocol for a dose of 240 Gy on one single disc of a sample (8327.1/1) with a natural De of 233 ± 8 Gy. **(A)** L_x/T_x ratio and **(B)** L_x and T_x separately normalized to their first cycle (lower figure) and L_x as a function of T_x (inset). n refers to the natural measurement. The dotted lines in the inset show the 95% confidence band.

To confirm the effectiveness of the protocol in recovering a laboratory dose, dose recovery tests were undertaken on the modern naturally bleached surface sample (8326.2). Doses of 60, 80, 100, 150, 200, 400 and 600 Gy were administered to six aliquots of untreated sample for each dose and the TT-OSL was subsequently measured in order to obtain the De . Figure 2.3A shows the results as the ratio of measured to given dose. The dose of 5.5 ± 2.6 Gy measured for the modern sample using the TT-OSL SAR protocol was subtracted from the measured doses. The agreement of measured and administered dose is within 10 %, except for the 60 Gy dose. Of particular note is the excellent recovery of a given dose of 600 Gy (Fig. 2.3A) which suggests that it should be possible to obtain De values of 600 Gy from natural samples. Figure 2.3B shows the dose response curve of one of the

aliquots that had received a previous laboratory dose of 100 Gy. For this aliquot the measured dose is greater than the given dose, even though recycling is excellent for a dose of 110 Gy; this result contributes to the range seen in Fig. 2.3A for the 100 Gy dose.

2.3.3 Performance of the sensitivity correction for the TT-OSL SAR protocol

For OSL measurements, Wintle and Murray (2006) recommended testing the performance of the sensitivity correction in the SAR procedure by repeating the SAR protocol using the same regeneration and test dose. In a similar test for the TT-OSL SAR protocol, Stevens et al. (2009) showed non linear sensitivity relationships between the TT-OSL signal and the OSL test dose signal. In the current study, identical cycles of the Porat et al. (2009) TT-OSL SAR protocol were repeated using a small test dose as recommended by Wang et al. (2007). Figure 2.4 shows the ratio of L_x/T_x (Fig. 2.4A) and normalized values of L_x and T_x (Fig. 2.4B) for repeated cycles with a dose of 240 Gy for the TT-OSL signal (L_x), and a test dose of 6.5 Gy for the OSL signal (T_x). Data are normalized to the first measurement (the natural), as indicated by the point labeled as n in Figure 2.4. The sample is the same as in the previous two sections (8327.1/1), having a D_e of 233 ± 8 Gy (as obtained by the TT-OSL SAR protocol), indistinguishable from the repeated laboratory dose of 240 Gy. The overall change in sensitivity with repeated cycle relative to the first cycle is very similar for the TT-OSL signal and the OSL test dose signal (Fig. 2.4B), thus resulting in the consistent response for the ratio L_x/T_x (Fig. 2.4A). In the inset of Figure 2.4B, L_x and T_x plot on a line, indicating a nearly proportional relationship between the TT-OSL signal from 240 Gy and the OSL signal from the 6.5 Gy test dose.

2.3.4 Comparison of D_e values obtained by TT-OSL and OSL

For 16 samples, D_e values were determined by TT-OSL using the SAR protocol of Porat et al. (2009) and compared to the D_e values obtained for the same samples by the standard OSL protocol. The doses obtained were in the range of 50-200 Gy (as measured by TT-OSL) and are shown in Figure 2.5. For TT-OSL, dose response curves with only 2 regeneration doses were used. OSL and TT-OSL D_e values agree reasonably for doses below the range where the OSL signal starts to saturate (i.e. at ~ 150 Gy). When the natural sensitivity corrected OSL is above the $2D_0$ value of the dose response curve (as shown in Fig. 2.1), the aliquots could not be included in the calculation of D_e values for each sample using the central age model (Galbraith et al., 1999). Their enforced rejection leads to the D_e value for the OSL measurements being a lower limit, and hence the dose obtained is shown in Figure 2.5 with an infinite upper error bar.

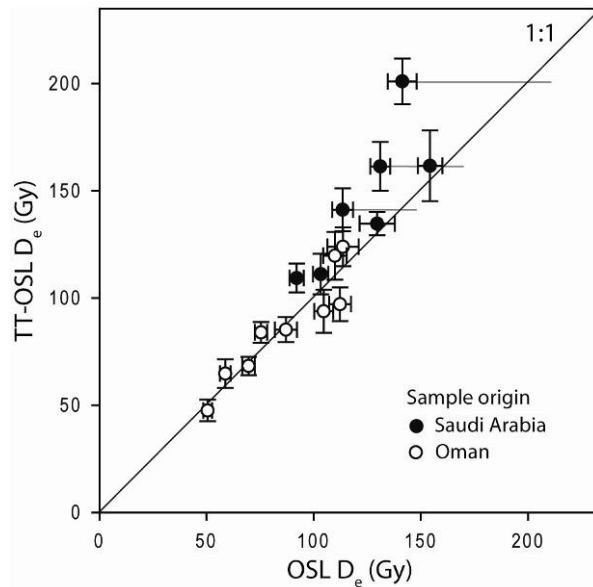


Fig. 2.5. Comparison of TT-OSL and OSL D_e values for 16 samples. The OSL signal starts to saturate at 100-150 Gy leading to an underestimation of OSL D_e values, which are thus drawn with an infinite upper error bar. The TT-OSL D_e values were obtained using only two regeneration points.

2.3.5 The comparison between SAR and MAAD dose response curves

In section 3.3, it has been shown that the OSL sensitivity changes measured in a TT-OSL SAR sequence in response to a small test dose appear to be appropriate (inset to Fig. 2.4B). In section 3.4, the paired D_e values obtained using the TT-OSL SAR protocol and the OSL SAR protocol are similar for doses below 120 Gy (Fig. 2.5). Both sets of results suggest that it is correct to use the OSL response to a test dose in the TT-OSL SAR protocol. However, the test in Fig. 2.4 is for a regeneration dose of 240 Gy and in Fig. 2.5 the largest D_e is ~ 200 Gy. To check the L/T response for larger doses, it is necessary to compare the dose response curves and sensitivity measurements made using a TT-OSL SAR sequence and a TT-OSL MAAD sequence.

For the modern, naturally bleached aliquot, Figure 2.6 shows the mean L_x/T_x ratios obtained for a TT-OSL SAR sequence using six aliquots given regeneration doses up to 1200 Gy. Above 300 Gy the sensitivity corrected TT-OSL changes slope with dose. A MAAD data set with six aliquots for each of a large number of doses up to 2600 Gy is also shown in Figure 2.6. Up to 1000 Gy the sensitivity corrected TT-OSL shows consistent growth. The same test dose (1 Gy) was used for both data sets, thus allowing the absolute values of L_x/T_x to be compared. It should be noted that the MAAD L_x/T_x data set for our sample is more scattered than those published by Nian et al. (2009) using 4-11 μm grains and by Sun et al. (2009) using 40-63 μm grains. This is most likely related to the smaller number of grains making up each of our aliquots with grains of 200-250 μm diameter. In addition, for the

MAAD data set, the non-linear response as a function of dose seen above 1000 Gy would limit application of the MAAD procedure. The deviation of the SAR and MAAD data is a cause for concern, given that the L_x values measured in the MAAD experiment should be representative of the natural signal of the same dose level.

To investigate whether the higher values for the sensitivity-corrected TT-OSL L_x/T_x data set for the SAR protocol were being caused by build up of the TT-OSL signal during the repeated cycles, two zero dose measurements were made in the fifth (R5) and tenth (R10) cycles. The results are shown in the inset to Figure 2.6. The size of L_x/T_x when no dose is given, even after ten cycles with increasing regenerative doses, is too small to be an explanation for the difference in L_x/T_x for the SAR and MAAD curves above 300 Gy (Figure 2.6).

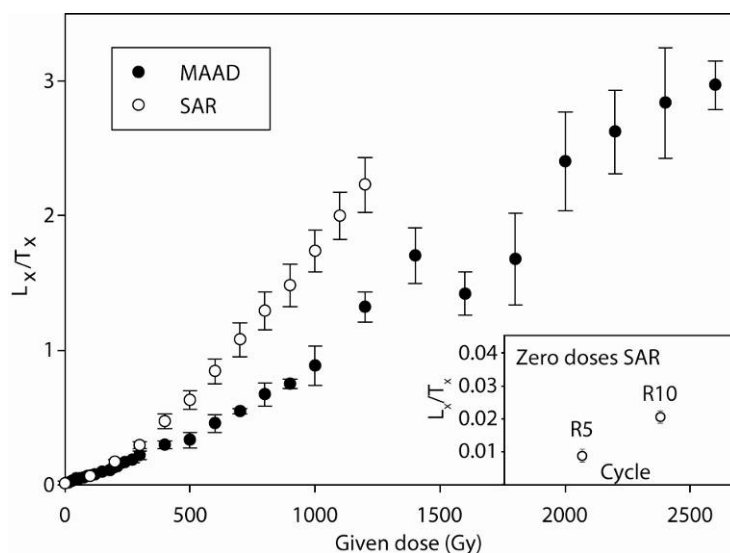


Fig. 2.6. TT-OSL MAAD and SAR dose response curves for a modern naturally bleached sample (8326.2) with a residual TT-OSL dose equal to 5.5 ± 2.6 Gy. Both data sets involve sensitivity correction using the OSL response to a test dose of 1 Gy. The inset shows two zero dose measurements of the SAR dose response curve at cycle R5 and R10. Data points are mean values of six discs. Error bars represent standard errors.

The deviation of the MAAD and SAR data above 300 Gy suggest that T_x is not correctly monitoring the sensitivity for one, or both, data sets. Figure 2.7 shows dose normalized L_x versus T_x for the MAAD and SAR measurements of Figure 2.6. The values are background subtracted and divided by the received dose. A straight line is fitted to the MAAD data set (Fig. 2.7A) and the same line is also shown together with the SAR data sets (Fig. 2.7B). The dose range for both data sets in Figure 2.7 is limited to 1200 Gy to facilitate the comparison. For the MAAD data set (Fig. 2.7A), the sensitivity (L_x/D) of the TT-OSL response to added dose (D) increases in proportion to the measured OSL sensitivity (T_x) (i.e. with the fitted line passing through the origin), though the data are scattered, since each data point is derived from a separate aliquot of coarse-grained quartz. For the SAR data set obtained

using up to 12 regenerative doses, the plots of L_x versus T_x for the six aliquots (Fig. 2.7B) show little scatter within the data set for each aliquot, but none of the data sets fall on a line that passes exactly through the origin. The intersection with the x axis is more pronounced than for the results obtained when identical regenerative doses were applied (inset in Fig. 2.4).

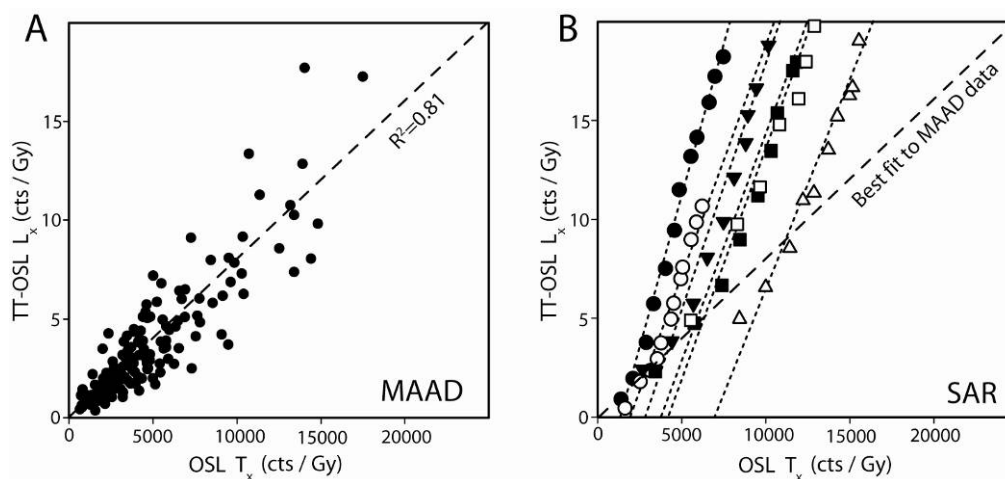


Fig. 2.7. L_x versus T_x for MAAD and SAR measurements obtained for a modern sample. Values are background subtracted and divided by the received dose, which was 1 Gy for the test dose. **(A)** A straight line (dashed) is fitted to the MAAD data set. The same dashed line is also shown in **(B)**. While each data point in **(A)** represents one aliquot, the data in figure **(B)** originates from 6 aliquots (different symbols). Best linear fits are shown by dotted lines. Only regeneration dose points up to 1200 Gy are plotted for both data sets to facilitate comparison.

In order to determine whether the OSL response (T_x) is dose dependent, the values on the x axes of Figures 2.7A and 2.7B can also be plotted as a function of dose D , given to obtain the TT-OSL signal. The average values of OSL sensitivity (T_x/T_D), obtained for a test dose T_D of 1 Gy, are shown plotted as a function of D in Figure 2.8. No error bars are given as the values for the MAAD data set are based on 132 discs (6 for each dose); they are scattered since there is no appropriate method of normalization between aliquots. Several MAAD runs were made to obtain the data set, and it is thought that the lower dose response between 240 and 600 Gy was the result of smaller amounts of quartz being mounted on the disc.

For the SAR data set (based on 6 discs) the range of values for a single dose is also large; this can be seen by looking at the highest values of L and T obtained for each of the discs in Figure 2.7B. For five of the discs (excluding the open circle data), similar values of TT-OSL sensitivity (L_x/D) was shown, but there was a factor of 2 spread in the OSL sensitivity (T_x/T_D). However, the trend in T_x/T_D was consistent for each disc, thus resulting in a smooth plot of T_x/T_D versus D .

The measurement of sensitivity change using a fixed regenerative dose of 240 Gy, as carried out in section 3.3, was repeated for the modern sample, but using a test dose of 1 Gy. The results for two aliquots (circles in Fig. 2.9) show that for a test dose of 1 Gy, the sensitivities of the TT-OSL and OSL are even less proportional (i.e. intersect with the x axis further from the origin) than for the older sample (downward triangles in Fig. 2.9) for which a test dose of 6.5 Gy was used (data previously shown in Figure 2.4). The reason for this different behaviour is not known.

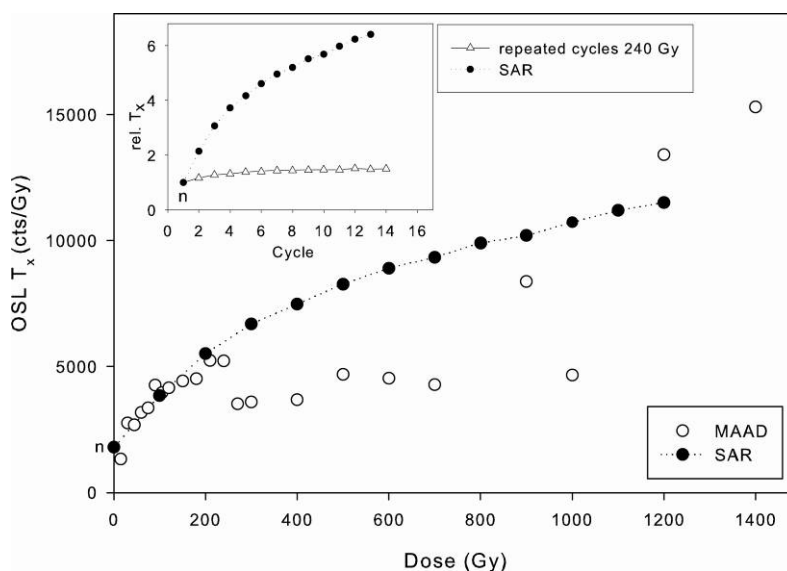


Fig. 2.8. Average value of six measurements (filled circles) of T_x (OSL response to 1 Gy) plotted as a function of dose given in the same cycle for the SAR data set in Fig. 2.6. Average of six measurements (open circles) of T_x for MAAD data set in Fig. 2.6 plotted as a function of dose given to each aliquot. Inset is the same SAR data set taken from Fig. 2.6 but normalized to the first measurement (designated n) and a data set for 14 repeated measurements of a regenerative dose of 240 Gy and a test dose of 1 Gy (triangles, data from Fig. 2.9).

2.4 Discussion

Dose recovery tests, recycling ratios and recuperation ratios showed robust functioning of the Porat et al. (2009) SAR TT-OSL protocol when applied to sands from sites in Saudi Arabia and Oman. Dose response curves obtained using a small number of laboratory doses were used in the dose recovery tests; excellent dose recovery was achieved, and the results showed the potential to extend the range of dose usable for dating to 600 Gy (Fig. 2.3A). The sensitivity correction procedure using the OSL signal from a test dose to normalize the TT-OSL signal was tested by giving a repeated 240 Gy dose. For one sample (with a natural D_e of ~233 Gy) the two signals show what is thought to be good proportionality (Fig. 2.4 and Fig. 2.9), but for the modern sample the proportionality is less good (Fig. 2.9). The reason for this difference in behavior is not known.

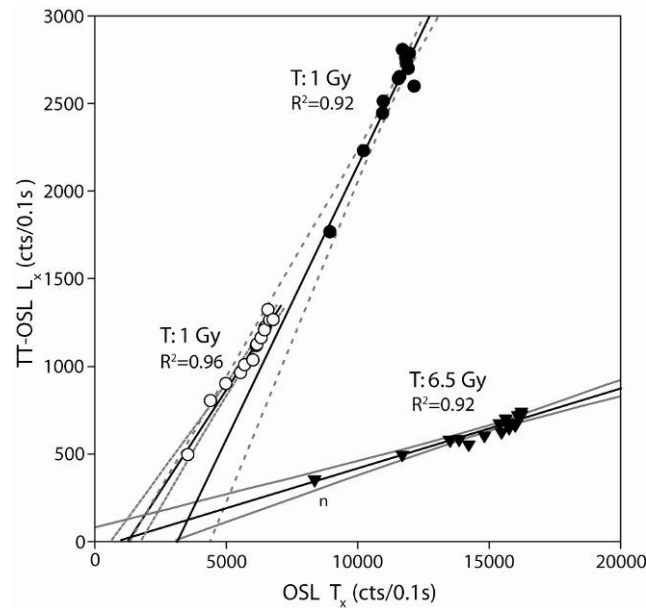


Fig. 2.9. L_x versus T_x using a fixed regenerative dose of 240 Gy. The test dose was 1 Gy for two discs of the modern sample (circles) and 6.5 Gy for the sample with a natural dose of 233 ± 8 Gy (data set from Fig. 2.4). The T_x values of the latter data set are divided by their test dose (6.5 Gy). The data sets are linearly fitted, with the gray lines showing the 95% confidence bands.

When comparing SAR TT-OSL dose response curves constructed with many regeneration points over a wide dose range to MAAD TT-OSL dose response curves, we found an increase of SAR L_x/T_x ratios with dose additional to the increase seen in the MAAD dose response (Fig. 2.6). This suggests that there is a dose dependent signal in the SAR dose response, which is not present in the MAAD dose response. In the region below 300 Gy, a SAR TT-OSL dose response curve constructed with only 2 regeneration doses was used to obtain to D_e , and the values were well correlated with the D_e values from OSL (Fig. 2.5). When the signals used to construct the SAR dose response curve up to 1200 Gy were examined, it was found (Fig. 2.7B) that the TT-OSL and OSL signals were not proportional. In addition, for any one disc the change of sensitivity with increasing dose as found to be both cycle and dose dependent. The apparent non-linearity of the MAAD TT-OSL measurements (Fig. 2.6) and the scatter observed when doses up to 2500 Gy were employed, suggests that this approach should be used with caution.

2.5 Conclusions

The SAR TT-OSL of Porat et al. (2009) can be used when the expected doses are below 300 Gy. However, the lack of proportionality observed between the TT-OSL and related OSL sensitivity measurements for doses between 300 and 1200 Gy will result in incorrect D_e determination. Before a SAR procedure can be accepted, it is crucial that the related TT-OSL and OSL responses are monitored using repetition of the same regenerative dose and using a range of doses.

Acknowledgments

We are indebted to Albert Matter for initiation and support of the project in the Rub' al Khali and we would like to thank two anonymous reviewers for constructive comments on the manuscript. This research is funded by the Swiss National Science Foundation (project 200021-117985/1) and fieldwork by the Saudi Geological Survey.

2.6 References

- Adamiec, G., Bailey, R.M., Wang, X.L., Wintle, A.G., 2008. The mechanism of thermally transferred optically stimulated luminescence in quartz. *Journal of Physics D: Applied Physics* 41, 135503.
- Adamiec, G., Duller, G.A.T., Roberts, H.M., Wintle, A.G., 2010. Improving the TT-OSL SAR protocol through source trap characterisation. *Radiation Measurements* 45, 768-777.
- Aitken, M.J., Smith, B.W., 1988. Optical dating: recuperation after bleaching. *Quaternary Science Reviews* 7, 387-394.
- Aitken, M.J., 1998. *An Introduction to Optical Dating*. Oxford University Press, Oxford.
- Athanassas, C., Zacharias, N., 2010. Recuperated-OSL dating of quartz from Aegean (South Greece) raised Pleistocene marine sediments: current results. *Quaternary Geochronology* 5, 65-75.
- Ballarini, M., Wallinga, J., Wintle, A.G., Bos, A.J.J., 2007. A modified SAR protocol for optical dating of individual grains from young quartz samples. *Radiation Measurements* 42, 360-369.
- Duller, G.A.T., 2003. Distinguishing quartz and feldspar in single grain luminescence measurements. *Radiation Measurements* 37, 161-165.
- Galbraith, R.F., Roberts, R.G., Laslett, G.M., Yoshida, H., Olley, J.M., 1999. Optical dating of single and multiple grains of quartz from Jinmium rock shelter, Northern Australia: Part I, Experimental design and statistical models. *Archaeometry* 41, 339-364.
- Kim, J.C., Duller, G.A.T., Roberts, H.M., Wintle, A.G., Lee, Y.I., Yi, S.B., 2009. Dose dependence of thermally transferred optically stimulated luminescence signals in quartz. *Radiation Measurements* 44, 132-143.
- Murray, A.S., Wintle, A.G., 2000. Luminescence dating of quartz using an improved single-aliquot regenerative-dose protocol. *Radiation Measurements* 32, 57-73.
- Nian, X.M., Zhou, L.P., Qin, J.T., 2009. Comparisons of equivalent dose values obtained with different protocols using a lacustrine sediment sample from Xuchang, China. *Radiation Measurements* 44, 512-516.
- Pagonis, V., Wintle, A.G., Chen, R., Wang, X.L., 2009. Simulations of thermally transferred OSL experiments and of the ReSAR dating protocol for quartz. *Radiation Measurements* 44, 634-638.
- Porat, N., Duller, G.A.T., Roberts, H.M., Wintle, A.G., 2009. A simplified SAR protocol for TT-OSL. *Radiation Measurements* 44, 538-542.
- Roberts, H.M., Duller, G.A.T., 2004. Standardised growth curves for optical dating of sediment using multiple-grain aliquots. *Radiation Measurements* 38, 241-252.

-
- Stevens, T., Buylaert, J.P., Murray, A.S., 2009. Towards development of a broadly-applicable SAR TT-OSL dating protocol for quartz. *Radiation Measurements* 44, 639-645.
- Sun, X., Mercier, N., Falgueres, C., Bahain, J.-J., Despriee, J., Bayle, G., and Lu, H., 2010. Recuperated optically stimulated luminescence dating of middle-size quartz grains from the Palaeolithic site of Bonneval (Eure-et-Loir, France). *Quaternary Geochronology*, 5, 342-347.
- Tsukamoto, S., Duller, G.A.T., Wintle, A.G., 2008. Characteristics of thermally transferred optically stimulated luminescence (TT-OSL) in quartz and its potential for dating sediments. *Radiation Measurements* 43, 1204-1218.
- Wang, X.L., Lu, Y.C., Wintle, A.G., 2006. Recuperated OSL dating of fine-grained quartz in Chinese loess. *Quaternary Geochronology* 1, 89-100.
- Wang, X.L., Wintle, A.G., Lu, Y.C., 2007. Testing a single-aliquot protocol for recuperated OSL dating. *Radiation Measurements* 42, 380-391.
- Wintle, A.G., Murray, A.S., 2006. A review of quartz optically stimulated luminescence characteristics and their relevance in single-aliquot regeneration dating protocols. *Radiation Measurements* 41, 369-391

3 Faunal evidence of a Holocene pluvial phase in Southern Arabia with remarks on the morphological variability of *Helenina anderseni*

Giordana Gennari ^a, Thomas M. Rosenberg ^{b,c}, Silvia Spezzaferri ^a,
Jean-Pierre Berger ^a, Dominik Fleitmann ^{b,c}, Frank Preusser ^{b,d}, Mahmoud Al-Shanti ^e
and Albert Matter ^b

^a Department of Geosciences, Earth Sciences, University of Fribourg, Switzerland

^b Institute of Geological Sciences, University of Bern, Switzerland

^c Oeschger Centre for Climate Change Research, University of Bern, Switzerland

^d Present address: Department of Physical Geography and Quaternary Geology, Stockholm University, Sweden

^e Saudi Geological Survey, Jeddah, Saudi Arabia

Published in the Journal of Foraminiferal Research (2011), 41, 248-259

Abstract: Although foraminifera have been found living in inland saline lakes isolated from the sea, this phenomenon has rarely been recognized in the fossil record. This study documents the occurrence of benthic foraminifera in Holocene lake sediments located nearly 500 km inland from the Red Sea, in the Al-Mundafan region of southern Saudi Arabia. The lake formed during a regional pluvial period, 10,500–6000 yr BP. The presence of foraminifera and brackish charophytes in the studied section represent an interval when the lake was slightly brackish due to high evaporation. The studied sediments yielded a bispecific benthic foraminiferal fauna comprised of *Helenina anderseni* and *Trichohyalus aguayoi*, as well as the brackish charophyte genus *Lamprothamnium*. The benthic foraminifera are species characteristic of mangrove swamps, salt marshes, and lagoons, which are environments currently widespread along the Red Sea coasts. Because the Al Mundafan area was never connected to the sea during the Quaternary, wading birds must have been the vector that transported the foraminifera to the paleolake.

3.1 Introduction

There have been numerous reports of benthic foraminifera occurring in both Recent and ancient sediments of inland lakes, ponds, springs, and rivers (see summaries in Patterson and others, 1990; Lévy and others, 1995; Patterson and others, 1997; and Wennrich and others, 2007). Nevertheless, these are enigmatic occurrences, each of which presents an enticing challenge to research. In the present study, we document the presence of foraminifera in inland paleolake deposits of southern Arabia, and seek an explanation for this local phenomenon.

The climate of southern Arabia is strongly affected by the African-Asian monsoon. Periods of intensified monsoonal circulation during the late Pleistocene and Holocene caused significantly higher precipitation over the southern Arabian Peninsula (e.g., Fleitmann and others, 2003a). Since lacustrine sediments can provide a detailed record of paleoclimate variability, a multiproxy study of Pleistocene–Holocene lake deposits in the Empty Quarter of Saudi Arabia (Rub' al Khali) was undertaken as part of a Swiss National Science Foundation project seeking to better understand this pluvial period in what is still a largely unexplored region.

During fieldwork in the Al Mundafan region in March 2008, ten outcrops were sampled (Fig. 3.1). A total of 68 samples were taken for micropaleontological analysis and radiocarbon and OSL dating. One of these outcrops yielded two samples with foraminifera and charophytes (Fig. 3.2). The primary aim of our study is to reinvestigate this benthic foraminiferal fauna, first reported in the Al Mundafan area by McClure and Swain (1980), and to place it into a paleoenvironmental context.

3.2 Geological setting

The study area is located 700 km southeast of Mecca at the southern end of the Tuwayq sedimentary escarpment, where Holocene lakebeds are exposed within a single depression of approximately 15 square kilometers. The depression is bordered by the escarpment to the north and by dunes to the south. A modern sabkha occupies the western part of the depression.

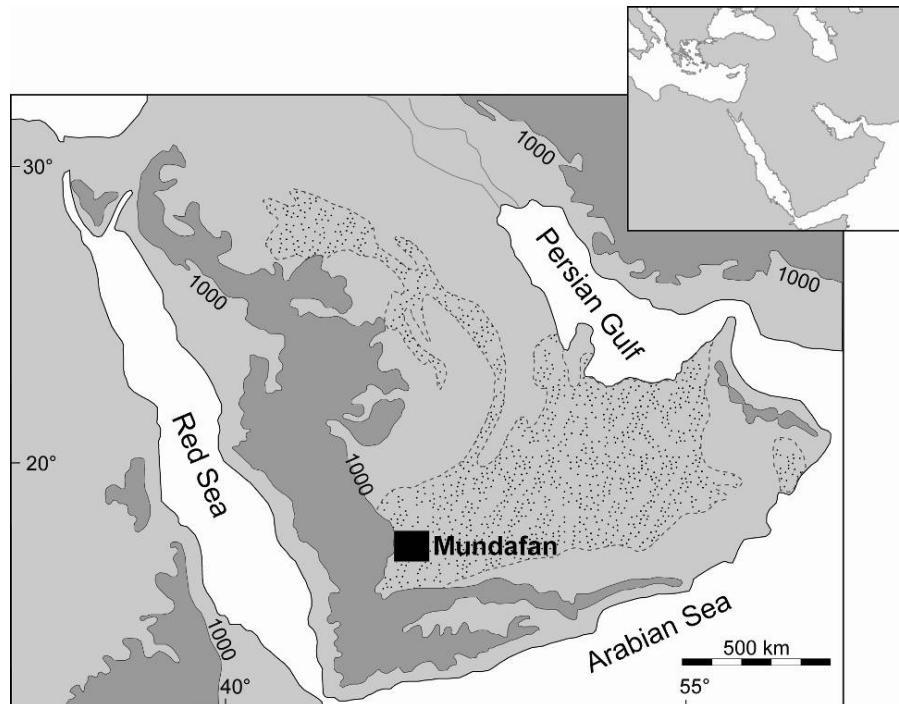


Fig. 3.1. Simplified relief map of the Arabian Peninsula and surroundings showing the location of Al Mundafan. Dark grey areas are >1000 m in elevation; dotted areas are large areas of sand dunes.

3.3 Material and methods

Sediment samples were prepared for micropaleontological quantitative analysis first by drying at room temperature. Aliquots of ~40 and 30 g for samples A4 and A5, respectively, were then washed through a 32- μm satilon net. The two residues were left at room temperature and once dry each was sieved into 250, 125, 63, and 32 μm -size fractions. Each fraction was split three times and the foraminiferal content of one of those splits was quantitatively studied. Approximately 200 adult specimens were picked from the 125–250 μm size-fraction and mounted on slides. Each specimen was analyzed for morphometric parameters using a KEYENCE VHX-600 digital microscope at a magnification of 200 \times . Measurements were taken of spiral diameters (D and B) and height (H), as well as intersutural length (ISL) of the first and penultimate chambers of the last whorl (Fig. 3.3) following Pearson and others, 2001. Multivariate (Principal Component Analysis) statistical treatment on morphometric data was performed with the software PRIMER 6 after data normalization (Clarke and Warwick, 2001; Clarke and Gorley, 2006). Scanning electron microscope (SEM) images were obtained at the Department of Geosciences, University of Fribourg.

The chronology of Section 8321.1 is based on radiocarbon dating, measured by accelerator mass spectrometry (AMS) at the ETH/PSI facility in Zurich (Table 1). In order to

avoid age offsets due to the so-called “hard water effect”, the carbonate fraction was dissolved using 5M HCl and only phytoclasts were used for dating. The Holocene radiocarbon age was calibrated to calendar years using OxCal 3.10 with atmospheric data from Bronk Ramsey (2005).

An additional age for the sand layers underlying Section 8321.1 is based on Optically Stimulated Luminescence (OSL) dating (Table 1). Details on preparation and measurement techniques are described in Wintle and Murray (2006) and Preusser and others (2008). The OSL measurements were performed at the University of Bern using an automated Risoe TL/OSL-DA-20 reader with an attachment for measuring single grains.

3.4 Micropaleontology

Although several samples from Section 8321.1 were investigated, only samples A4 and A5 (Fig. 3.2) contain well-preserved and relatively abundant benthic foraminifera (Table 3.2; Figs. 3.4 and 3.5). These two samples, as well as several others from the same and adjacent sections contain rare to abundant gyrogonites of charophytes ascribed to the genera *Chara* and *Lamprothamnium* (Fig. 3.6).

3.4.1 Foraminiferal Assemblages

Two foraminiferal species were identified in the lowermost lacustrine deposits (samples A4 and A5): *Helenina anderseni* (Warren), which was dominant, and *Trichohyalus aguayoi* (Bermudéz) (Table 2). Both adult and juvenile growth stages were present, with adult forms strongly dominating and representing at least 84% of the species populations. Those juvenile specimens picked from the 32- μ m size-fraction that could not be identified at generic level accounted for ~6% of the total assemblage in each sample (Table 2). In each of the adult populations of both *H. anderseni* and *T. aguayoi*, microspheric forms always outnumbered the megalospheric ones. Test abnormalities, mainly deformed chambers and aberrant chamber arrangements, were restricted to *H. anderseni* and accounted for 2–6% of its populations.

3.4.2 Morphological Variability and Morphometry of *Helenina anderseni*

In the studied material, *Helenina anderseni* showed a high degree of morphological variability (Fig. 3.4). The test outline and shape of the sutures were the most variable features, so we used them to distinguish two extreme morphotypes. Morphotype A has a subcircular profile and the sutures on its spiral side are tangential and deeply incised; sutures on the umbilical side are curved to tangential (Fig. 3.4.1). Morphotype A closely resembles

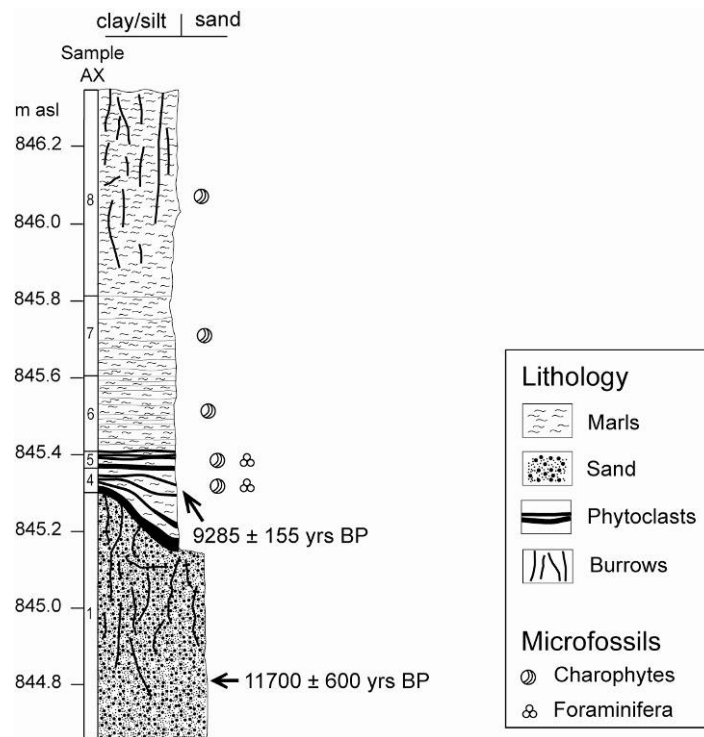


Fig. 3.2. Sedimentological profile of outcrop 8321.1 ($18^{\circ}32'43.0''N$, $45^{\circ}21'27.1''E$).

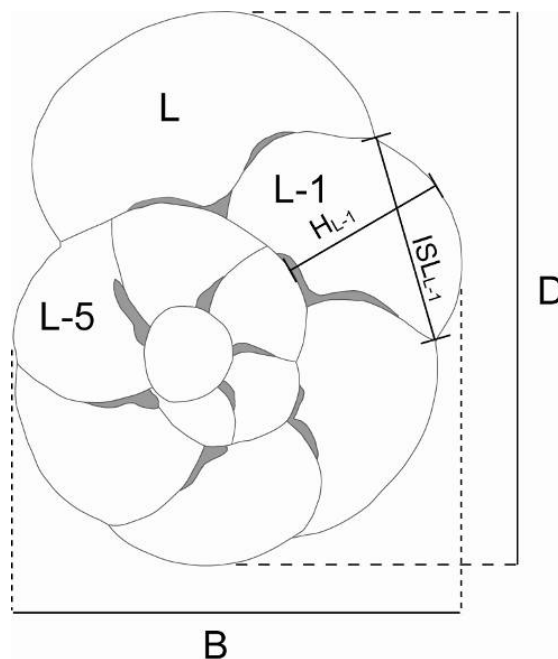


Fig. 3.3. Morphometric parameters measured on the dorsal side of *Helenina anderseni*. Last whorl's chambers were numbered from the last one (L) backward to the first one (L-5 in this case). D = greatest spiral diameter; B = spiral diameter perpendicular to D; H = chamber's height; ISL = intersutural length.

the holotype. In contrast, morphotype B has an ovate profile and the sutures on both its spiral and umbilical sides are straight to slightly curved and deeply incised; its supplementary sutural apertures are generally wider than those of morphotype A (Fig. 3.4.4-6).

A morphometric study was performed to verify the characters that distinguish morphotypes A and B. The morphometric parameters considered were 1) the spiral diameters ratio (D/B), which measures the degree of roundness of the test outline, 2) the Chamber Expansion Index (CEI), which indicates the increase in chamber size in the last whorl, and 3) the Dorsal Chamber View Index (DCVI), which is a measure of the degree of elongation of the penultimate chamber (see Pearson and others, 2001 for equations).

The results of the univariate and multivariate analysis (PCA) are shown in Figures 3.7 and 3.8, where they are plotted separately according to whether they have six or seven chambers in the outer whorl (Figs. 3.7A-C and 3.8A vs. Figs. 3.7D-F and 3.8B). For each group, an equal number of microspheric and megalospheric forms were measured (50 specimens each). Frequency histograms (univariate analysis) for both subsamples have a clear unimodal distribution, showing a continuous transition of the considered morphometric parameters. Results of the PCA are plotted in a PC1-PC2 graph, since the first two components account for >80% of the variation (Table 3). The PCA plot shows a great morphometric correspondence between specimens attributed to the two identified morphotypes.

Table 3.1. Results of AMS ¹⁴C and OSL dating.

| Lab code | Outcrop | Sample | Material | Method | n | OD | Age (yr BP) | Calibrated age (yr BP) |
|------------|---------|--------|-------------|-----------------|----|-------|-------------|------------------------|
| ETH-37792 | 8321.1 | A4 | Phytoclasts | ¹⁴ C | - | - | 8300 ± 45 | 9285 ± 155 |
| ROT-77/160 | 8321.1 | A1 | Qtz grains | OSL | 24 | 9.70% | 11700 ± 600 | |

3.4.3 Systematics and Ecology of Foraminiferal Species

Family Heleninidae Loeblich and Tappan, 1987

Genus *Helenina* Saunders, 1961

Helenina anderseni (Warren)

Figures 3.4.1-6, 3.5.1-4

1957 *Pseudoeponides anderseni* Warren, pl. 4, figs. 12-15.

1957 *Helenia anderseni* (Warren), Saunders, p. 374.

1961 *Helenina anderseni* (Warren), Saunders, p. 136, pl. 3, fig. 3.

1996 *Helenina anderseni* (Warren), Culver and others, p. 480, figs. 9.10, 9.11.

1999 *Helenina* sp., Lipps and Langer, pl. 2, figs. 2, 5.

2003 *Helenina anderseni* (Warren), Javaux and Scott, p. 24, figs. 6.3, 6.4.

2005a *Helenina* cf. *H. anderseni* (Warren), Kawagata and others, pl. 2, figs. 8-12.

2005b *Helenina* cf. *H. anderseni* (Warren), Kawagata and others, p. 224, pl. 1, figs. 5-13.

Ecology. This species has been described from estuarine environments, marshes, lagoons, low salinity mangrove swamps including those in North America (Culver and Horton, 2005), South America (Steinker and Butcher, 1981; Culver, 1990), the western Pacific (Lipps and Langer, 1999; Kawagata and others, 2005a, 2005b), New Zealand (Gregory, 1973; Hayward and Hollis, 1994; Hayward and others, 1999), New Caledonia and Australia (Debenay and Guillou, 2002), the Red Sea (Halicz and others, 1984), and the Venice lagoon (Serandrei Barbero and others, 2004). Very rarely has it been found in hypersaline lagoons (Debenay and others, 2001). It is purportedly an infaunal species (Culver and Horton, 2005).

Family Trichohyalidae Saidova, 1981

Genus *Trichohyalus* Loeblich and Tappan, 1953

Trichohyalus aguayoi (Bermudéz)

Figures 3.5.5-7

1935 *Discorbis aguayoi* Bermudéz, pl. 15, figs. 10-14.

1950 *Discorbina lacunae* Silvestri, pl. 3, figs. 9, 10.

1991 *Trichohyalus lacunae* (Silvestri), Albani and others, pl. 1, figs. 9, 10.

2004 *Discorinopsis aguayoi* (Bermudéz), Foresi and others, pl. 2, figs. 1-11, pl. 3, figs. 1-12, pl. 4, figs. 1-13.

Remarks. We retain the assignment of this genus to *Trichohyalus* because of its truly calcareous wall texture as opposed to *Discorinopsis*, which is agglutinated with calcareous particles. Foresi and others (2004) placed *T. lacunae* in synonymy with *T. aguayoi* because they concluded that chamber shape is highly variable in this species. Features that they considered as invariant characteristics determined by genetic characters include the numerous chambers in the last whorl, primary and secondary apertures, coarse pores, limbation of the sutures, depressed sutures in the last whorl, and test contortion. Although taxonomy is beyond the scope of this paper, we note that *T. aguayoi* was present in our material as two quite distinct forms that differ in chamber shape in umbilical view. One is *T. aguayoi* sensu stricto (Fig. 3.5.5) with slightly curved sutures, while the other has the *T. lacunae* morphology (Figs. 3.5.6, 3.5.7) with sigmoid sutures resulting from the overlapping of chambers in the last whorl.

Table 3.2. Relative abundance (%) of *Helenina anderseni* and *Trichohyalus aguayoi* in total assemblage. For each species, the relative abundance of adults (microspheric and megalospheric forms), juveniles, and abnormal specimens are also indicated. *Juveniles (in 32- μ m fraction) not identified at generic level.

| Sample | A4 | A5 |
|--|------------------------|-------------|
| Weight dry sediment (g) | 40 | 30 |
| Total number of counted specimens | 3227 | 2354 |
| Species | Relative abundance (%) | |
| <i>Helenina anderseni</i> in total assemblage | 93.5 | 87.9 |
| adults | 95 | 94 |
| <i>microspheric forms</i> | 62 | 59.2 |
| <i>megalospheric forms</i> | 38 | 40.8 |
| juveniles | 5 | 6 |
| abnormal specimens | 1.9 | 6.1 |
| <i>Trichohyalus aguayoi</i> in total assemblage | 0.7 | 5.9 |
| adults | 95.5 | 84.2 |
| <i>microspheric forms</i> | 52.4 | 60.7 |
| <i>megalospheric forms</i> | 47.6 | 39.3 |
| juveniles | 4.5 | 15.8 |
| abnormal specimens | - | - |
| Indet. juveniles* in total assemblage | 5.8 | 6.2 |

Ecology. This species can tolerate a wide range of salinities. Most often, it has been reported in fresh to brackish waters (Wantland, 1975; Javaux and Scott, 2003) and mangrove swamps (Steinker and Butcher, 1981; Javaux and Scott, 2003). It has also been recorded in the Montecatini thermal pool and Orbetello lagoon (Zampi and others, 1996; Foresi and others, 2004). Occurrences in hypersaline lagoons are rare (Debenay and others, 2001).

3.5 Discussion

3.5.1 Paleoenvironmental Interpretation

Regional climate records (McClure, 1976; Lezine and others, 1998; Burns and others, 2001; Preusser and others, 2002; Radies and others, 2005; Fleitmann and others, 2007) indicate an early Holocene wet phase in southern Arabia. In particular, speleothems from Oman provide a record of pluvial intervals between 10,500–6,000 yr BP (Fleitmann and others, 2003a, 2003b, 2007). The radiocarbon age of 9285 \pm 155 cal. yr BP we obtained from sample A4 phytoclasts falls within this interval (Table 1). As a result of increased monsoon precipitation at that time, the Al Mundafan depression, presently occupied by a sabkha, was

a large paleolake of ~15 km². Enhanced wadi flow into the depression and possibly groundwater infiltration, produced a lake with temporarily brackish conditions in which foraminifera could thrive.

This investigation found adults and juveniles in association for both *H. anderseni* and *T. aguayoi*. The presence of both growth stages indicates that a population is reproducing and is a good indication that the environment is favorable to the species (Wennrich and others, 2007). In our study, the adults were always strongly dominant (Table 2), which suggests that the lake conditions were sufficiently stable to allow juveniles to reach maturity (Almogi-Labin and others, 1992).

The adult populations of *H. anderseni* and *T. aguayoi* were characterized by a preponderance of microspheric tests (i.e., the main form of reproduction was sexual). This is peculiar because most natural populations of benthic foraminifera are predominantly asexually produced megalospheric tests (see Alve and Goldstein, 2003 and references therein). Alve and Goldstein (2003) proposed that an unusual abundance of microspheric forms may be due to the different dispersal potentials of microspheric versus megalospheric proloculi. Such a dimorphic ratio has also been linked to unfavorable or highly variable environmental conditions (Boltovskoy and Wright, 1976; Hallock, 1985) and to seasonality (Alve and Goldstein, 2003). In particular, the presence of abundant microspheric individuals in unstable environments may result in higher genetic variability and different ecological preferences (Alve and Goldstein, 2003). Morphology, which for some benthic foraminifera is also related to environmental preference, may also be affected. The presence of morphotypes in *H. anderseni* and possibly in *T. aguayoi* (see Figs. 3.5.5-7) suggests that the hypothesis of unstable environmental conditions or seasonality cannot be ruled out. Further studies on the ecology and biology of *H. anderseni* are needed, including its poorly understood reproductive cycle.

Alve (1991) noted that some degree of environmental stress is suggested by populations with >1% abnormal tests. In our study, deformed *H. anderseni* ranged 2-6%, below the 10-20% values reported from highly stressed paralic environments (see review in Geslin and others, 2002).

Charophytes present throughout the studied section provide additional paleoenvironmental information. The family Characeae is represented by six living genera (*Chara*, *Lamprothamnium*, *Lychnothamnus*, *Nitellopsis*, *Nitella*, and *Tolypella*), determined at the specific level on the basis of the morphology of both vegetative parts and reproductive organs (gyrogonites).



Fig. 3.4. 1 *Helenina anderseni*, specimen strongly resembling the holotype, morphotype A: a, spiral view; b, side view; c, umbilical view. 2, 3 *H. anderseni*, intermediate morphotype: a, spiral view; b, side view; c, umbilical view. 4–6 *H. anderseni*, morphotype B: a, spiral view; b, side view; c, umbilical view. Scale bars = 100 μm .

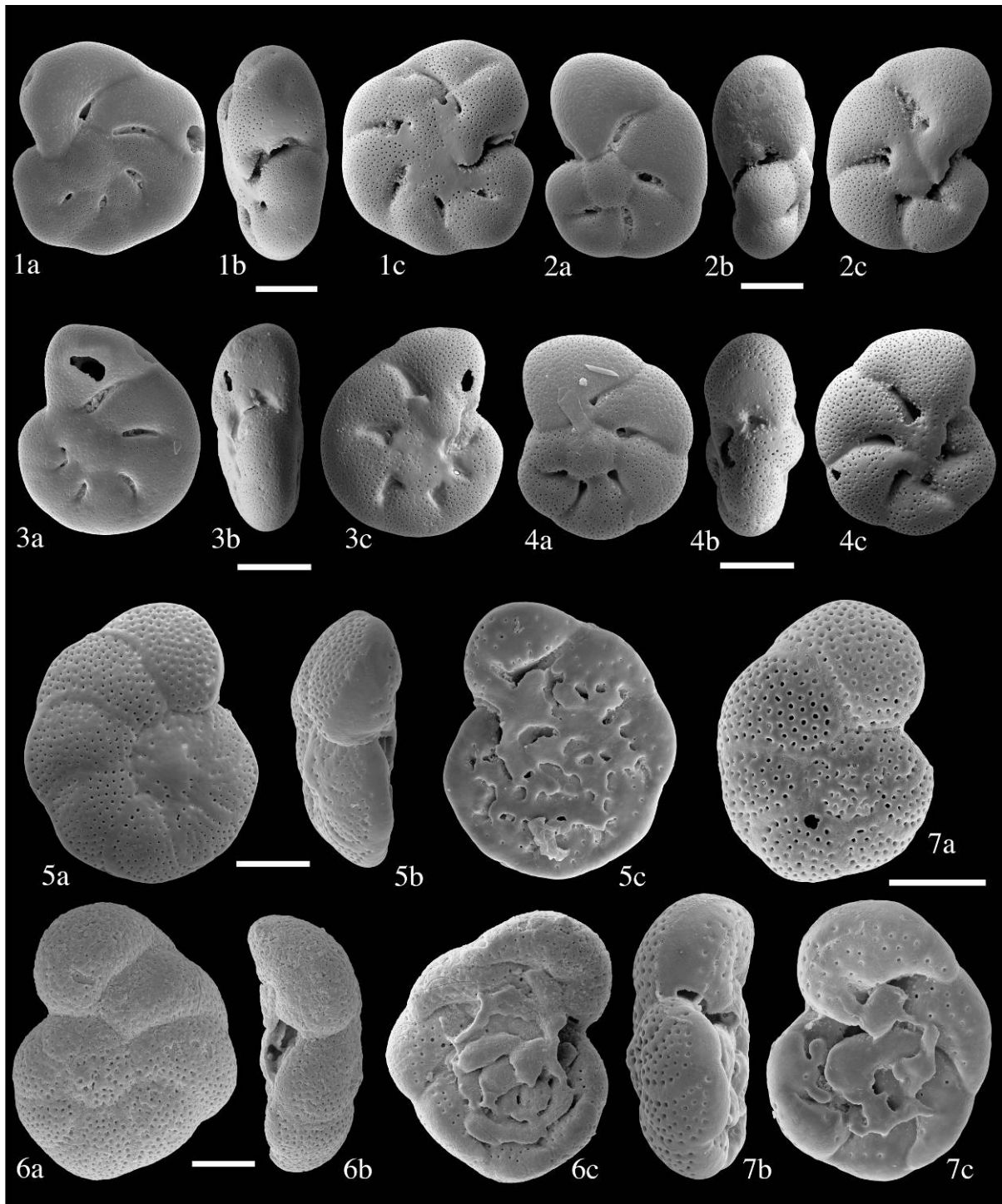


Fig. 3.5. 1–4 *Helenina anderseni*, juvenile specimens: a, spiral view; b, side view; c, umbilical view. 5 *Trichohyalus aguayoi* (sensu stricto): a, spiral view; b, side view; c, umbilical view. 6, 7 *T. aguayoi* (*T. lacunae*-type): a, spiral view; b, side view; c, umbilical view. Scale bars 1–4 = 50 μm , 5–7 = 100 μm .

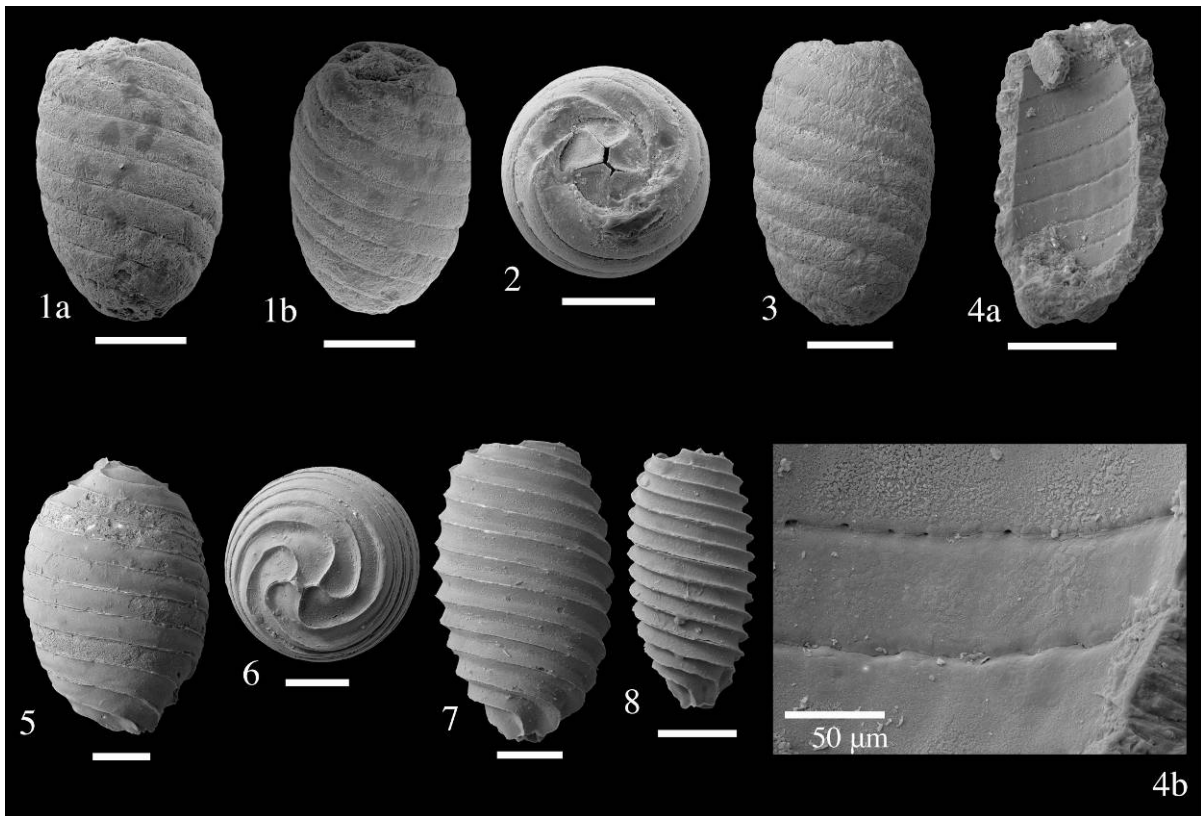


Fig. 3.6. 1 *Lamprothamnium* sp.: a, lateral view; b, oblique lateral view. 2 apical view; 3 *Lamprothamnium* sp., lateral view. 4 *Lamprothamnium* sp.: a, internal view; b, internal view: undulated intercellular sutures. 5-8 *Chara* sp. (?*Ch. globularis* var. *aspera*): 5, regular morphotype, lateral view; 6, regular morphotype, apical view; 7, large elongate morphotype, lateral view; 8, small elongate morphotype, lateral view. Scale bars = 200 µm, unless otherwise specified.

Thus, fossil charophytes are typically assumed to be freshwater indicators. The charophyte assemblage of Al Mundafan is represented mostly by forms very similar to *Chara globularis* var. *aspera* (Figs. 3.6.6-8) with very elongated morphotypes characteristic of slightly brackish environments (salinity ~2‰; Soulie-Märsche, 1989). Levels A7, A8, and possibly A6 yielded rare specimens ascribed to *Lamprothamnium* (Figs. 3.6.1-5), which is one of the most typical brackish genera (Corillion, 1972). Large amounts of fragile gyrogonites are strong indication that these fossil floras are in situ. This implies that deposition occurred in water depths shallower than six meters, which is the limit for charophytes to fructify (Becker and others, 2002; Picot, 2003).

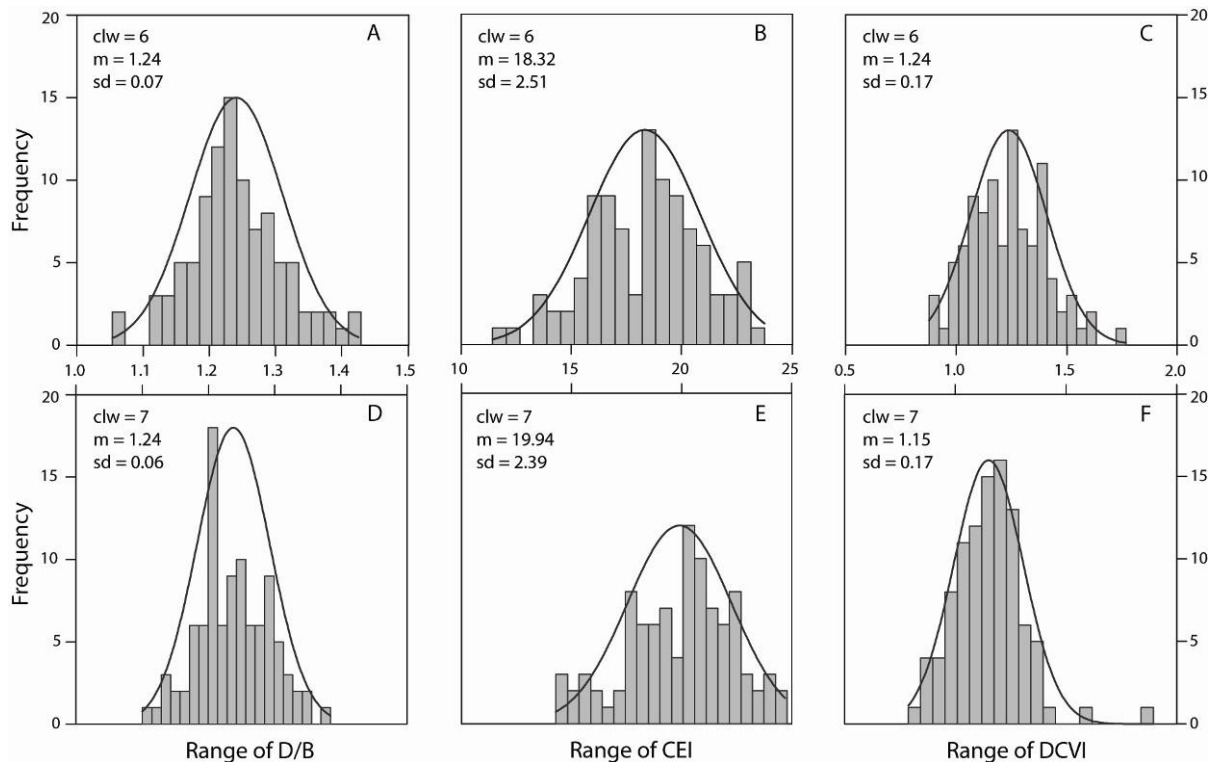


Fig. 3.7. Morphometric data measured on *Helenina anderseni* plotted as standard histograms (frequency). Normal Curve Shape is shown as a solid line. D/B = spiral diameters ratio; CEI = Chamber Expansion Index; DCVI = Dorsal Chamber View Index; clw = number of chambers in last whorl; m = mean; sd = standard deviation (Pearson and others, 2001).

3.5.2 Transportation Mechanism and Provenance of Benthic Foraminifera

The presence of benthic foraminifera in inland saline or brackish waters is rare, but cannot be considered unusual (Resig, 1974). Most of their fossil record has probably been erased primarily because they have thin shells that are susceptible to dissolution (e.g., Jonasson and Patterson, 1992; Culver and Horton, 2005).

As reported by Resig (1974), three hypotheses have been proposed to explain the occurrence of these forms in inland waters that were never connected to the sea: endemism (Daday, 1884), marine reliction (Brodsky, 1928; Gauthier-Lièvre, 1935), and transport via avian or human means (Arnal, 1954; Almogi-Labin and others, 1992; Patterson and others, 1997).

Species diversity in comparable environments varies considerably. In the Hawaiian Salt Lake, Resig (1974) recorded 41 species, including calcareous and agglutinated forms. In stark contrast, Almogi-Labin and others (1992) reported monospecific assemblages of *Ammonia tepida* in the Dead Sea, and Wennrich and others (2007) found only two species in two inland brackish lakes (Salziger See and Suesser See) in central Germany. Moderate

numbers of species were documented by Abu-Zied and others (2007), with 15 calcareous species from Lake Qarun (Egypt). In the meromictic Mecherchar Jellyfish Lake in Palau, Lipps and Langer (1999) identified 15 species (agglutinated and calcareous) in surface sediments, while Kawagata and others (2005b) observed 10 calcareous species in a sediment core retrieved from the same lake, with only two species (*Helenina* cf. *H. anderseni* and *Bolivina striatula*) common to the two studies. All of these studies discussed the provenance of their benthic foraminiferal assemblages from nearby or relatively far marine coastal environments when there were temporary connections with the sea or dry intervals characterized by increasing salinity.

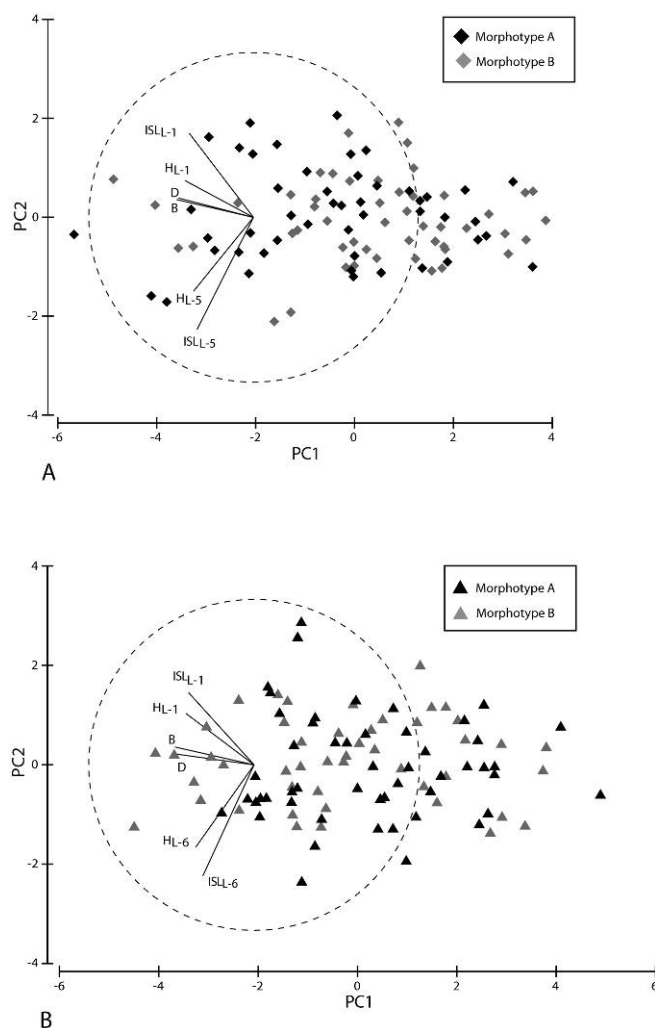


Fig. 3.8. Principal component analysis applied to morphometric measurements of *Helenina anderseni*. A = specimens with six chambers in the last whorl; B = specimens with seven chambers in the last whorl. D = greatest spiral diameter; B = spiral diameter perpendicular to D; H = chamber's height; ISL = inter-sutural length.

In our materials, benthic foraminifera are represented by two genera (*Helenina* and *Trichohyalus*) characteristic of mangrove swamps, salt marshes, and lagoons (e.g., Tufesco, 1969; Javaux and Scott, 2003; Culver and Horton 2005). To explain the presence of benthic

foraminifera in the Mundafan region, we can exclude endemism and marine reliction as it was never connected to the sea during the Quaternary. The most likely explanation for their occurrence in the Mundafan paleolake is avian-mediation, which Patterson and others (1997) suggested to be a much more important foraminiferal dispersal mechanism than usually realized. Although there is extensive literature on the mangrove swamps, salt marshes, and lagoons flanking the Red Sea (e.g., Mohamed, 1984; Saleh, 2007), little is known about their foraminifera. Because these transitional environments are suitable habitats for *H. anderseni* and *T. aguayoi*, it is reasonable to assume that those along the Egyptian-Sudanese and Saudi Arabian coasts of the Red Sea most likely are the provenance of the *H. anderseni* and *T. aguayoi* specimens that pioneered the Mundafan paleolake. The absence of other taxa in the paleolake may relate to the low diversity of the foraminiferal faunas in mangrove swamps (e.g., Culver, 1990). Therefore, we postulate that avian-mediated transport from the margins of the Red Sea introduced the two foraminiferal species that colonized the Mundafan brackish paleolake.

Table 3.3. Principal components analysis: eigenvalues and eigenvectors (coefficients in the linear combinations of variables making up the principal components) for the six analyzed variables. *Normalized before PCA analysis.

| No. ch. | PC | Eigenvalues | | | Variable | Eigenvectors | | | | | |
|---------|----|--------------|-------------|------------------|--------------------|--------------|--------|--------|--------|--------|--------|
| | | Eigen-values | % Variation | Cum. % Variation | | PC1 | PC2 | PC3 | PC4 | PC5 | PC6 |
| 6 | 1 | 4.17 | 69.4 | 69.4 | D | -0.455 | 0.118 | 0.016 | -0.048 | 0.715 | 0.515 |
| | 2 | 0.756 | 12.6 | 82 | B | -0.467 | 0.108 | -0.039 | -0.105 | 0.274 | -0.826 |
| | 3 | 0.504 | 8.4 | 90.4 | H _{L-1} | -0.416 | 0.223 | -0.473 | -0.541 | -0.47 | 0.199 |
| | 4 | 0.284 | 4.7 | 95.2 | ISL _{L-1} | -0.39 | 0.511 | 0.25 | 0.627 | -0.353 | 0.079 |
| | 5 | 0.198 | 3.3 | 98.4 | H _{L-5} | -0.364 | -0.448 | 0.718 | -0.294 | -0.244 | 0.07 |
| | 6 | 9.34E-02 | 1.6 | 100 | ISL _{L-5} | -0.342 | -0.68 | -0.443 | 0.462 | -0.091 | 0.036 |
| 7 | 1 | 3.93 | 65.5 | 65.5 | D | -0.473 | 0.065 | -0.028 | 0.013 | -0.576 | -0.663 |
| | 2 | 0.922 | 15.4 | 80.8 | B | -0.478 | 0.108 | -0.046 | 0.022 | -0.45 | 0.745 |
| | 3 | 0.478 | 8 | 88.8 | H _{L-1} | -0.412 | 0.311 | 0.255 | 0.69 | 0.436 | -0.051 |
| | 4 | 0.335 | 5.6 | 94.4 | ISL _{L-1} | -0.396 | 0.437 | -0.022 | -0.691 | 0.415 | -0.047 |
| | 5 | 0.275 | 4.6 | 99 | H _{L-6} | -0.353 | -0.498 | -0.728 | 0.092 | 0.297 | -0.023 |
| | 6 | 6.07E-02 | 1 | 100 | ISL _{L-6} | -0.31 | -0.67 | 0.634 | -0.194 | 0.123 | 0.017 |

3.6 Conclusions

The presence of two benthic foraminiferal species, *Helenina anderseni* and *Trichohyalus aguayoi* and charophytes in lacustrine sediments of the Al Mundafan section are linked to the continental pluvial periods that occurred in the area 10,500–6,000 yr BP (Fleitmann and others, 2003a, 2003b, 2007). Enhanced precipitation created a freshwater lake with temporarily brackish conditions. This is corroborated by the presence of

reproducing populations of foraminifera and in situ brackish charophytes. Because the Al Mundafan paleo-lake was never connected to the sea, the foraminifera were most likely introduced by avian-mediated transport from mangrove swamps along the coasts of the Red Sea.

Acknowledgments

We warmly thank Irka Hajdas, ETH Zurich, for AMS radiocarbon dating. We also thank John Murray and an anonymous reviewer for their useful revision of the manuscript. Kenneth Finger is kindly acknowledged for editing the manuscript. This research was funded by the Swiss National Foundation Projects 200021-117985, 206021-117374 and 200021-111694 and by the Saudi Geological Survey.

Author contributions: GG and SS carried out the foraminiferal study and wrote the paper; TR did the fieldwork, described and sampled the section, performed the OSL dating and contributed to writing; J-PB. studied the charophytes, AM initiated the project, organized and supervised the fieldwork; DF and FP supervised the project and contributed to the discussion, and MA-S was responsible for the field logistics.

For taxonomic notes on *Helenina anderseni* (Warren) see Appendix C.

3.7 References

- Abu-Zied, R. H., Keatings, K. W., and Flower, R. J., 2007, *Environmental controls on foraminifera in Lake Qarun, Egypt: Journal of Foraminiferal Research*, v. 37, p. 136–149.
- Albani, A., Favero, V. M., and Serandrei Barbero, R., 1991, *The distribution and ecological significance of Recent foraminifera in the lagoon south of Venice (Italy): Revista Española de Micropaleontología*, v. 23, p. 29–45.
- Almogi-Labin, A., Perelis-Grossovicz, L., and Raab, M., 1992, *Living Ammonia from a hypersaline inland pool, Dead Sea area, Israel: Journal of Foraminiferal Research*, v. 22, p. 257–266.
- Alve, E., 1991, *Benthic foraminifera in sediment cores reflecting heavy metal pollution in Sør fjord, western Norway: Journal of Foraminiferal Research*, v. 21, p. 1–19.
- Alve, E., and Goldstein, S. T., 2003, *Propagule transport as a key method of dispersal in benthic foraminifera (Protista): Limnology and Oceanography*, v. 48, p. 2163–2170.
- Arnal, R. E., 1954, *Preliminary report on the sediments and foraminifera of the Salton Sea, southern California: Geological Society of America Bulletin*, v. 65, p. 1227–1228.
- Becker, D., Picot, L., and Berger, J.-P., 2002, *Stable isotopes ($\delta^{13}\text{C}$ and $\delta^{18}\text{O}$) of charophytes gyrogonites: example from the Brochnene Fluh section (late Oligocene–early Miocene, Switzerland): Geobios*, v. 35, p. 89–97.
- Bermudéz, P. J., 1935, *Foraminiferos de la costa norte de Cuba: Memorias de la Sociedad Cubana de Historia Natural*, v. 9, p. 129–224.
- Boltovskoy, E., and Wright, R., 1976, *Recent Foraminifera: W. Junk, The Hague*, 515 p.
- Brodsky, A. A., 1928, *Foraminifera (Polythalamia) in the wells of the Kara-Kum desert: Trudy Sredne-Aziatskogo Gosudarstvennogo Universiteta; Serija 8a, Zoologija*, v. 8, p. 6–36. (In Russian).
- Bronk Ramsey, C., 2005, *Improving the resolution of radiocarbon dating by statistical analysis*, in Levy, E. E., and Higham, T. F. G. (eds.), *The Bible and radiocarbon dating: Archeology, Text and Science: Equinox*, London, p. 57–64.
- Burns, S. J., Fleitmann, D., Matter, A., Neff, U., and Mangini, A., 2001, *Speleothem evidence from Oman for continental pluvial events during interglacial periods: Geology*, v. 29, p. 623–626.
- Clarke, K. R., and Gorley, R. N., 2006, *PRIMER v6: user Manual/Tutorial: PRIMER-E, Plymouth*, 190 p.
- Clarke, K. R., and Warwick, R. M., 2001, *Change in marine communities: an approach to statistical analysis and interpretation, 2nd Edition: PRIMER-E, Plymouth*, 172 p.

-
- Corillion, R., 1972, *Les Charophycées de France et de l'Europe Occidentale*: Otto Koeltz Verlag, Koenigstein, 499 p.
- Culver, S. J., 1990, *Benthic foraminifera of Puerto Rican mangrove-lagoon systems: potential for paleoenvironmental interpretations*: *Palaios*, v. 5, p. 34–51.
- Culver, S. J. and Horton, B. P., 2005, *Infaunal marsh foraminifera from the Outer Banks, North Carolina, U.S.A.*: *Journal of Foraminiferal Research*, v. 35, p. 148–170.
- Culver, S. J., Jun Woo, H., Oertel, G. F., and Buzas, M. A., 1996, *Foraminifera of coastal depositional environments, Virginia, U.S.A.: distribution and taphonomy*: *Palaios*, v. 11, p. 459–486.
- Daday, E. V., 1884, *Über eine Polythalamie der Kochsalztümpel bei Deva in Siebenbürgen*: *Zeitschrift für Wissenschaftliche Zoologie*, v. 40, p. 465–480.
- Debenay, J.-P., and Guillou, J.-J., 2002, *Ecological transitions indicated by foraminiferal assemblages in paralic environments*: *Estuaries*, v. 25, p. 1107–1120.
- Debenay, J.-P., Geslin, E., Beck Eichler, B., Duleba, W., Sylvestre, F., and Eichler, P., 2001, *Foraminiferal assemblages in an hypersaline lagoon, Araruma (R.J.), Brazil*: *Journal of Foraminiferal Research*, v. 31, p. 133–151.
- Fleitmann, D., Burns, S. J., Neff, U., Mangini, A., and Matter, A., 2003a, *Changing moisture sources over the last 330,000 years in northern Oman from fluid inclusion evidence in speleothems*: *Quaternary Research*, v. 60, p. 223–232.
- Fleitmann, D., Burns, S. J., Mudelsee, M., Neff, U., Kramers, J., Mangini, A., and Matter, A., 2003b, *Holocene forcing of the Indian monsoon recorded in a stalagmite from southern Oman*: *Science*, v. 300, p. 1737–1739.
- Fleitmann, D., Burns, S. J., Mangini, A., Mudelsee, M., Kramers, J., Villa, I., Neff, U., Al-Subbary, A. A., Buettner, A., Hippler, D., and Matter, A., 2007, *Holocene ITCZ and Indian monsoon dynamics recorded in stalagmites from Oman and Yemen (Socotra)*: *Quaternary Science Reviews*, v. 26, p. 170–188.
- Foresi, L. M., Zampi, M., and Focardi, S., 2004, *Test morphology and organic layer of *Discorinopsis aguayoi* (Bermudéz): relationships with environmental conditions*: *Revista Española de Micropaleontología*, v. 36, p. 323–347.
- Gauthier-Lièvre, L., 1935, *Sur une des singularités de l'Oued Rhir: Des foraminifères thalassoïdes vivant dans des eaux sahariennes*: *Bulletin de la Société d'Histoire Naturelle de l'Afrique du Nord*, v. 26, p. 142–147.
- Geslin, E., Debenay, J.-P., Duleba, W., and Bonetti, C., 2002, *Morphological abnormalities of foraminiferal tests in Brazilian environments: comparison between polluted and non-polluted areas*: *Marine Micropaleontology*, v. 45, p. 151–168.
- Gregory, M. R., 1973, *Benthonic foraminifera from a mangrove swamp, Whhangaparapara, Great Barrier Island*: *Tane*, v. 19, p. 193–204.

- Halicz, E., Noy, N., and Reiss, Z., 1984, *Foraminifera from Shura Arwashie mangrove (Sinai)*, in Por, F. D., and Dor, I. (eds.), *Hydrobiology of the Mangal: Dr. W. Junk b.v., The Hague*, p. 145–149.
- Hallock, P., 1985, *Why are larger foraminifera large?: Paleobiology*, v. 11, p. 195–208.
- Hayward, B. W., and Hollis, C. J., 1994, *Brackish foraminifera in New Zealand: a taxonomic and ecologic review: Micropaleontology*, v. 40, p. 185–222.
- Hayward, B. W., Grenfell, H. R., and Scott, D. B., 1999, *Tidal range of marsh foraminifera for determining former sea-level heights in New Zealand: New Zealand Journal of Geology & Geophysics*, v. 42, p. 395–413.
- Javaux, E. J., and Scott, D. B., 2003, *Illustration of modern benthic foraminifera from Bermuda and remarks on distribution in other tropical/subtropical areas: Palaeontologia Electronica*, v. 6, p. 29, 2.1MB, http://palaeo-electronica.org/paleo/20031/benthic/issue1_03.htm.
- Jonasson, K. E., and Patterson, R. T., 1992, *Preservation potential of salt marsh foraminifera from the Fraser River delta, British Columbia: Micropaleontology*, v. 38, p. 289–301.
- Kawagata, S., Yamasaki, M., and Jordan, R. W., 2005a, *Acarotrochus lobulatus, a new genus and species of shallow-water benthic foraminifera from Mecherchar Jellyfish Lake, Palau, NW Equatorial Pacific Ocean: Journal of Foraminiferal Research*, v. 35, p. 44–49.
- Kawagata, S., Yamasaki, M., Genka, R., and Jordan, R. W., 2005b, *Shallow-water benthic foraminifera from Mecherchar Jellyfish Lake (Ongerul Tketau Uet), Palau: Micronesica*, v. 37, p. 215–233.
- Lévy, A., Mathieu, R., Poignant, A., and Fernandez-Gonzalez, M., 1995, *Sur la signification des foraminifères dans les dépôts continentaux: Oceanologica Acta*, v. 18, p. 597–605.
- Lézine, A. M., Saliège, J. F., Robert, C., Wertz, F., and Inizan, M. L., 1998, *Holocene lakes from Ramlat as-Sab'atayn (Yemen) illustrate the impact of monsoon activity in southern Arabia: Quaternary Research*, v. 50, p. 290–299.
- Lipps, J. H., and Langer, M. R., 1999, *Benthic foraminifera from the meromictic Mecherchar Jellyfish Lake, Palau (western Pacific): Micropaleontology*, v. 45, p. 278–284.
- Loeblich, A. R., Jr., and Tappan, H., 1953, *Studies of Arctic foraminifera: Smithsonian Miscellaneous Collections*, v. 121 (7), p. 1–150.
- Loeblich, A. R., Jr., and Tappan, H., 1987, *Foraminiferal Genera and Their Classification: Van Nostrand Reinhold Company, New York*, 2 vol., 1182 p.
- McClure, H. A., 1976, *Radiocarbon chronology of late Quaternary lakes in Arabian deserts: Nature*, v. 263, p. 755–756.
- McClure, H. A. and Swain, F. M., 1980, *Fresh-water and brackish-water fossil Quaternary Ostracoda from the Rub' al Khali ("Empty Quater"), Saudi Arabia: Actes du VIe*

- Mohamed, B. F., 1984, *Ecological observations on the mangroves of the Red Sea shores of Sudan: Hydrobiologia, v. 110, p. 109-111.*
- Pearson, P. N., Norris, R. D., and Empson, A. J., 2001, *Mutabella mirabilis gen. et sp. nov., a Miocene microperforate planktonic foraminifera with an extreme level of intraspecific variability: Journal of Foraminiferal Research, v. 31, p. 120–132.*
- Patterson, R. T., Scott, D. B., and McKillop, W. B., 1990, *Recent marsh-type agglutinated foraminifera in Lake Winnipegosis, Manitoba, in Hemleben, C., Kaminski, M. A., Kuhnt, W., and Scott, D. B. (eds.), Paleoecology, Biostratigraphy, Paleoceanography and Taxonomy of Agglutinated Foraminifera. Nato Science Series C, 327: Kluwer Academic Publisher, Dordrecht, p. 765–781.*
- Patterson, R. T., McKillop, W. B., Kroker, S., Nielsen, E., and Reinhardt, E. G., 1997, *Evidence of rapid avian-mediated foraminiferal colonization of Lake Winnipegosis, Manitoba, during the Holocene Hypsithermal: Journal of Paleolimnology, v. 18, p. 131–143.*
- Picot, L., 2003, *Le Paléogène des synclinaux du Jura et de la bordure sud-rhénane: paléontologie (ostracodes), paléoécologie, biostratigraphie et paléogéographie, Geofocus, v. 5, 240 p.*
- Preusser, F., Radies, D., and Matter, A., 2002, *A 160,000-year record of dune development and atmospheric circulation in southern Arabia: Science, v. 296, p. 2018–2020.*
- Preusser, F., Degering, D., Fuchs, M., Hilgers, A., Kadereit, A., Klasen, N., Krbetschek, M., Richter, D., and Spencer, J., 2008, *Luminescence dating: basics, methods and applications: Eiszeitalter & Gegenwart (Quaternary Science Journal), v. 57, p. 95–149.*
- Radies, D., Hasiotis, S. T., Preusser, F., Neubert, E., and Matter, A., 2005, *Paleoclimatic significance of early Holocene faunal assemblages in wet interdune deposits of the Wahiba Sand Sea, Sultanate of Oman: Journal of Arid Environments, v. 62, p. 109–125.*
- Resig, J. M., 1974, *Recent foraminifera from a landlocked Hawaiian lake: Journal of Foraminiferal Research, v. 4, p. 69–76.*
- Saidova, K. M., 1981, *On an up-to-date system of supraspecific taxonomy of Cenozoic benthonic foraminifera: Institut Okeanologi P. P. Shirshova, Akademiya Nauk SSSR, Moscow, 73 p. (In Russian).*
- Saleh, M. A., 2007, *Assessment of mangrove vegetation on Abu Minqar Island of the Red Sea: Journal of Arid Environments, v. 68, p. 331–336.*
- Saunders, J. B., 1957, *Emendation of the foraminiferal genus Palmerinella Bermudez, 1934, and erection of the foraminiferal genus Helenia: Washington Acad. Sci., Jour., Baltimore, Maryland, v. 47, p. 374.*

- Saunders, J. B., 1961, *Helenina Saunders, new name for the foraminiferal genus Helenia Saunders, 1957, non Helenia Walcott, 1880: Contribution from the Cushman Foundation for Foraminiferal Research*, v. 12, p. 128
- Serandrei Barbero, R., Albani, A. D., and Bonardi, M., 2004, *Ancient and modern salt marshes in the lagoon of Venice: Palaeogeography, Palaeoclimatology, Palaeoecology*, v. 202, p. 229–244.
- Silvestri, A., 1950, *Foraminiferi della Laguna Veneta: Bollettino Pesca, Piscicoltura e Idrobiologia*, v. 5, p. 22–98.
- Soulie-Marsche I., 1989, *Etude Comparée de Gyrogonites de Charophytes Actuelles et Fossiles et Phylogénie des Genres Actuels: Imprimerie des Tilleuls, Millau, France*. 237 p.
- Steinker, D. C., and Butcher, W. A., 1981, *Foraminifera from mangrove shores, Bermuda: Micron*, v. 12, p. 223–224.
- Tufesco, M., 1969, *Sur la présence de Trichohyalus aguayoi (Bermudez) dans la Mer Noire: Revue de Micropaléontologie*, v. 12, p. 46–52.
- Wantland, K. F., 1975, *Distribution of Holocene benthonic foraminifera on the Belize Shelf*, in Wantland, K. F., and Pursey, W. C., III (eds.), *Belize Shelf – Carbonate Sediments, Clastic Sediments and Ecology: American Association of Petroleum Geologists Studies in Geology*, v. 2, p. 332–399.
- Warren, A. D., 1957, *Foraminifera of the Buras-Scofield Bayou region, southeast Louisiana: Contributions of the Cushman Foundation for Foraminiferal Research*, v. 8, p. 29–40.
- Wennrich, V., Meng, S., and Schmiedl, G., 2007, *Foraminifers from Holocene sediments of two inland brackish lakes in central Germany: Journal of Foraminiferal Research*, v. 37, p. 318–326.
- Wintle, A. G., and Murray, A. S., 2006, *A review of quartz optically stimulated luminescence characteristics and their relevance in single-aliquot regeneration dating protocols: Radiation Measurements*, v. 41, p. 369–391.
- Zampi, M., Foresi, L. M., and Benocci, S., 1996, *Nuove osservazioni su morfologia ed ecologia di Miliammina fusca (Brady) e Discorinopsis aguayoi (Bermudez) rinvenuti in una vasca termale in Montecatini Terme (Pistoia): Atti della Società Toscana di Scienze Naturali, Serie A*, v. 103, p. 17–25.

4 Humid periods in southern Arabia: windows of opportunity for modern human dispersal

Thomas M. Rosenberg ^{a,b}, Frank Preusser ^{a,c}, Dominik Fleitmann ^{a,b}, Antje Schwalb ^d,
Kirsty Penkman ^e, Thomas W. Schmid ^f, Mahmoud Al-Shanti ^g, Khalid Kadi ^g,
Albert Matter ^a

^a Institute of Geological Sciences, University of Bern, Switzerland

^b Oeschger Centre for Climate Change Research, University of Bern, Switzerland

^c Present address: Department of Physical Geography and Quaternary Geology, Stockholm University, Sweden

^d Institut für Umweltgeologie, Technische Universität Braunschweig, Germany

^e BioArCh, Department of Chemistry, University of York, UK

^f Geological Institute, ETH Zurich, Switzerland

^g Saudi Geological Survey, Jeddah, Saudi Arabia

Published in Geology (2011), 39, 1115-1118

(American English)

Abstract: Arabia is a key-area for the dispersal of anatomically modern humans (AMH, *Homo sapiens*) out of Africa. Given its modern hostile environment, the question of the timing of dispersal is also a question of climatic conditions. Fresh water and food were crucial factors facilitating AMH expansions into Arabia. By dating relict lake deposits, four periods of lake formation were identified: one during the Early Holocene and three during the Late Pleistocene centered at ca. 80, ca. 100 and ca. 125 ka. Favorable environmental conditions during these periods allowed AMH to migrate across southern Arabia. Between ca. 75 and 10.5 ka arid conditions prevailed and turned southern Arabia into a natural barrier for human dispersal. Thus, expansion of AMH through the southern corridor into Asia must have taken place before 75 ka, possibly in multiple dispersals.

4.1 Introduction

The dispersal of anatomically modern humans (AMH, *Homo sapiens*) out of Africa is a pivotal event in the global expansion of our species (Macaulay et al., 2005; Mellars, 2006; Petraglia et al., 2007). The routes of movement, however, from Africa into Asia and Europe are the subject of an ongoing discussion due to the paucity of fossil finds and environmental data from key areas, and uncertainties associated with the interpretation of the genetic evidence (Beyin, 2006; Petraglia et al., 2010; Petraglia, 2011). Currently, two main routes are considered to be most likely. One route follows the western Red Sea coast and Nile River into the Levant (northern dispersal route) and has been regarded traditionally as the primary corridor for human dispersal (Van Peer, 1998; Vermeersch, 2001; Drake et al., 2011). A second route, from the Horn of Africa across the Red Sea (Bab al Mandab Strait) and southern Arabia (southern dispersal route) into Asia, has also been proposed (Lahr and Foley, 1994; Macaulay et al., 2005; Armitage et al., 2011). Support for a rapid dispersal along the southern dispersal route at some time between ca. 85 and ca. 60 ka arises from genetic evidence and archaeological data (Forster and Matsumura, 2005; Macaulay et al., 2005; Mellars, 2006). As the southern dispersal route cuts through the vast Arabian Desert belt, favorable climatic and environmental conditions with sufficient supply of surface water must have been critical factors for human expansion into southern Arabia and beyond (Petraglia et al., 2010). During arid climate intervals the region was a natural barrier for human expansion. Therefore, key questions are when did the Arabian deserts turn into a green and penetrable corridor for AMH, and whether the timing of pluvial periods in southern Arabia is consistent with genetic and archaeological evidence for the proposed successful expansion of AMH along the southern dispersal route.

Today, an arid to hyperarid climate prevails in most of southern Arabia and the landscape is dominated by sand and stone deserts, with little to no vegetation. Only a few areas, such as the Yemeni highlands, the Dhofar region, and the Oman Mountains, receive enough precipitation to support preindustrial human settlements. Relict lake deposits in the deserts of southern Arabia are evidence for periods of pronounced humidity in the past (Figs. 4.1 and 4.2). Radiocarbon dates (^{14}C) indicate that these lakes formed between 40–20 ka and 10.5–6 ka (McClure, 1976; Whitney, 1983) (Fig. 4.3F), much later than the proposed main period of human dispersal, between ca. 130 and ca. 60 ka (Walter et al., 2000; Macaulay et al., 2005; Armitage et al., 2011). Until now there was no solid evidence whether the environmental conditions would have allowed AMH to disperse along the southern dispersal route into Asia. Here we present new geochronological and environmental data of

relict lake deposits in the southwestern Rub' al Khali desert to support the hypothesis for pre-Holocene human dispersal along the southern dispersal route.

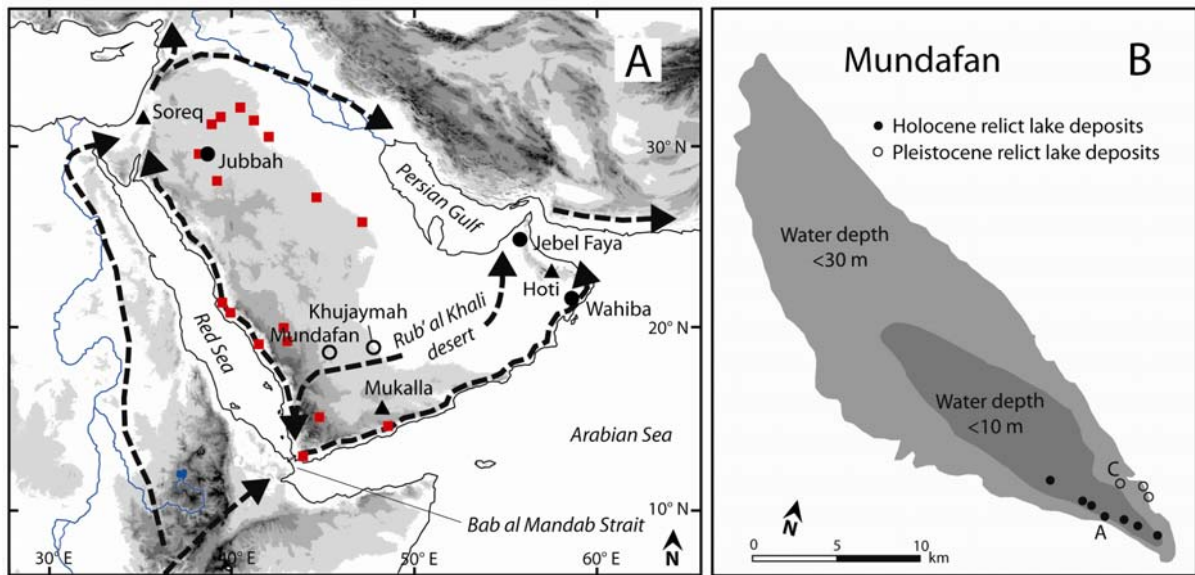


Fig. 4.1. A: Location of sites and possible anatomically modern humans (AMH) dispersal routes. The open circles are the sites of this study, triangles represent cave sites, closed circles indicate other sites mentioned in the text. Red squares show a simplified distribution of Middle Palaeolithic archaeological sites (Petraglia and Alsharekh, 2003). **B:** Outcrops of Holocene and Pleistocene relict lake deposits at Mundafan with inferred lake levels.

4.2 Material and methods

Relict lake deposits (dm to 2 m thick) in the south western Rub' al Khali at Mundafan ($18^{\circ}33'N$, $45^{\circ}21'E$) and Khujaymah ($18^{\circ}33'N$, $47^{\circ}14'E$) consist mainly of grey marls deposited on dune sands. We dated these deposits using radiocarbon, optically stimulated luminescence (OSL) and amino acid racemization (AAR). All radiocarbon ages reported in this study were calibrated with OxCal 4.10 using the IntCal09 curve (Bronk Ramsey, 2009). Faunal (in particular ostracodes) and floral remains, as well as geomorphologic evidence, were used to reconstruct environmental conditions. Full Methods and any associated references are available in Appendix D.

4.3 Chronology and environmental reconstructions

Based on the spatial extent of lacustrine deposits of Holocene age at Mundafan, the lake had a surface area of $\sim 50\text{ km}^2$ and a maximum depth of $\sim 10\text{ m}$. Layers of black phytoclasts are intercalated in the Holocene lacustrine sequences (Fig. 4.2A and Appendix D Fig. DR2), possibly representing redeposited ash from bush fires. Radiocarbon ages of phytoclasts ranging between 9.6 ± 0.09 and $7.9 \pm 0.1\text{ ka}$ match the well-documented early

Holocene wet phase in this area (Fleitmann et al., 2007). In Figure 4.2A, the OSL age of 10.1 ± 0.5 ka of the underlying eolian sand overlaps with the radiocarbon age of 9.6 ± 0.09 ka at the base of the lacustrine sequence, indicating the onset of lake formation. The ostracode species assemblage from the lower part of the section reflects shallowwater environments (*Paracandona* sp.), but with freshwater conditions (*Cypretta* sp.). The latter observation is confirmed by the diatom assemblage and freshwater sponges (McClure, 1978). The presence of the ostracode *Darwinula stevensoni* indicates that the lake was perennial (Griffiths et al., 2001). The ubiquitous presence of characeae, phragmites, and typha plants in the sediments reveals a vegetated lake fringed by reeds, whereas the $\delta^{13}\text{C}_{\text{org}}$ values (-23 to -26‰) of phytoclasts (microscopic plant fragments; Appendix D Table DR7) and the pollen content indicate a predominance of C3 plants in a cooler and wetter climate than today (Lézine et al., 2010; Parker, 2009). Vertebrate remains in the deposits of Figure 4.2A are of gazelle.

The youngest set of the Pleistocene deposits is dated by OSL just beneath these units, to ca. 80 ka (Marine Isotope Stage, MIS 5a) in three sections (Fig. 4.2B and Appendix D, Fig. DR4 and DR7). The OSL ages are supported by AAR ratios (for details, see Appendix D), which rule out substantially younger ages for the lake deposits due to ratios in the range of the robustly dated Pleistocene deposits. The dominance of ostracode *D. stevensoni* suggests freshwater conditions, as during the Holocene with perennial lakes.

On a second set of Pleistocene deposits, radiocarbon ages of *Melanoides tuberculata* (39.5 ± 0.9 ka and 45.4 ± 1.2 ka) are chronologically inverted (Fig. 4.2C). OSL ages of ca. 100 ka (MIS 5c) determined for eolian deposits from above and below the same lacustrine sequence are considered to reflect the real depositional age. The inferred area of the lake is ~ 300 km², with an average depth of ~ 12 m and a maximum depth of 25-30 m. The lake at Mundafan was substantially larger ca. 100 ka than during the early Holocene (Fig. 4.1B), and therefore implies pronounced humid conditions. Ostracodes indicate permanent (*Darwinula stevensoni*) but partly shallow freshwater conditions (*Candonocypris* sp.). Such water conditions are also indicated by the presence of the shell *Unio* sp. Vertebrate remains found in the sediments are of grazing animals (McClure, 1978).

The third set of Pleistocene deposits (Fig. 4.2D) is dated by OSL to MIS 5e (ca. 125 ka). The presence of ostracode *D. stevensoni* together with the *Unio* sp. shells indicates conditions with fresh open running water. A radiocarbon age of 19.3 ± 0.3 ka for shells contradicts two overlapping OSL ages (Fig. 4.2D).

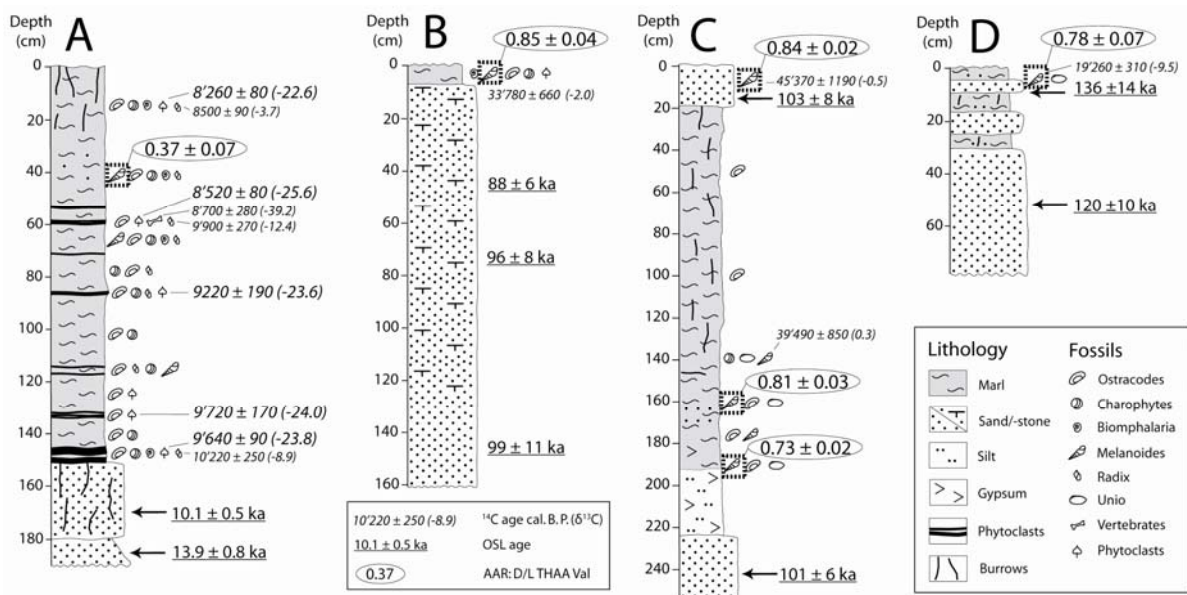


Fig. 4.2. Lake deposits from Mundafan (**A, C**) and Khujaymah (**B, D**). Underlined ages are optically stimulated luminescence (OSL) ages. $\delta^{13}\text{C}$ values of the radiocarbon ages are given in brackets. Given in ellipses are amino acid racemization (AAR) values as D/L ratios of total hydrolysable amino acid fraction (THAA) for Valine (Val) from *Melanoides tuberculata*.

4.4 Discussion

The first important result of this study is that re-dating of lacustrine sediments from Mundafan and Khujaymah does not support a humid period between 40 and 20 ka (McClure, 1976; Whitney, 1983) (Fig. 4.3F). The obvious discrepancy between OSL and radiocarbon ages is most likely the result of contamination with younger ^{14}C from meteoric water during the Holocene wet period, leading to consistently younger radiocarbon ages. This effect has been reported previously from similar environments (Fontes and Gasse, 1989). Instead, OSL dating supported by AAR ratios reveals that the lakes formed ca. 125 ka (MIS 5e), ca. 100 ka (MIS 5c), and ca. 80 ka (MIS 5a) (Fig. 4.2), a timing that is in good agreement with periods of enhanced speleothem growth in Oman (Hoti Cave) and Yemen (Mukalla Cave) (Fleitmann et al., 2011). During these periods within MIS 5, high summer insolation pulled the Intertropical Convergence Zone and the associated monsoonal rainfall belt into southern Arabia (Fig. 4.3H) (Fleitmann et al., 2011). Summer monsoon precipitation was sufficient to sustain perennial lakes during MIS 5a, 5c, and 5e. The lakes were surrounded by savannah and populated by herbivores, turning southern Arabia into a viable habitat for AMH. Hydroclimatic conditions during all of these three periods were at least as humid as during the early Holocene wet period when AMH were prevalent in southern Arabia (McCorriston and Martin, 2009).

However, climate during MIS 5 was not continuously humid. A return to arid conditions, with desiccation of the lakes and transformation from a savannah-type into a desert-like landscape, occurred between ca. 115 and 105 ka, and 95 and 85 ka. This agrees with growth discontinuities in speleothem records (indicative of low effective moisture) from Oman and Yemen (Fleitmann et al., 2003, 2011) and dune movements in the Wahiba Sands in Oman (Radies et al., 2004) (Fig. 4.3C). Thus, during MIS 5d and 5b the southern corridor turned again into a hostile habitat and AMH were either forced to retreat to refugia or became extinct there.

Having shown that there were only three windows of opportunity for a successful eastward expansion of AMH along the southern dispersal route, the question of when the dispersal took place arises. Studies of the DNA of living populations suggest that the genetic diversion from the African gene pool occurred between ca. 85 and ca. 60 ka (Forster, 2004; Macaulay et al., 2005). Thus, until very recently this would have suggested that the dispersal took place during MIS 5a (80-75 ka). Petraglia et al. (2011) proved the presence of Middle Paleolithic hominines at Jubbah in the Nafud desert in northern Saudi Arabia ca. 75 ka. However, artifacts attributed to AMH dated to ca. 125 ka at Jebel Faya might change this view (Fig. 4.1A) (Armitage et al., 2011). The timing of humid periods, the presence of AMH at the Red Sea (Walter et al., 2000) and in the Levant during MIS 5e, and the narrow width of the Bab al Mandab Strait of ~10 km at the transition of MIS 6 to MIS 5 (Fig. 4.3G) would all be in favor of a MIS 5e dispersal, while additional later dispersal pulses during MIS 5c and 5a could explain the late genetic diversion found in modern populations.

The timing of pluvial periods in southern Arabia, when combined with paleoclimate data from the Levant (Bar-Matthews et al., 2003; Vaks et al., 2007), has important implications for the dispersal of AMH along the northern and southern dispersal routes. Lacustrine as well as speleothem data from southern Arabia show that the change from humid to arid conditions ca. 75 ka barred the southern corridor for human expansion until the early Holocene. At the same time, a marked shift toward arid conditions occurred in the Levant (northern dispersal route) (Vaks et al., 2007) and led to the extinction of AMH there (Shea, 2008). The concurrent climatic and environmental deterioration in the areas of the northern and southern dispersal routes at the transition from MIS 5 to MIS 4 would have limited, or even prevented human dispersal into Asia for several tens of thousands of years until at least ca. 45 ka, when AMH were again present in the Levant (Shea, 2008).

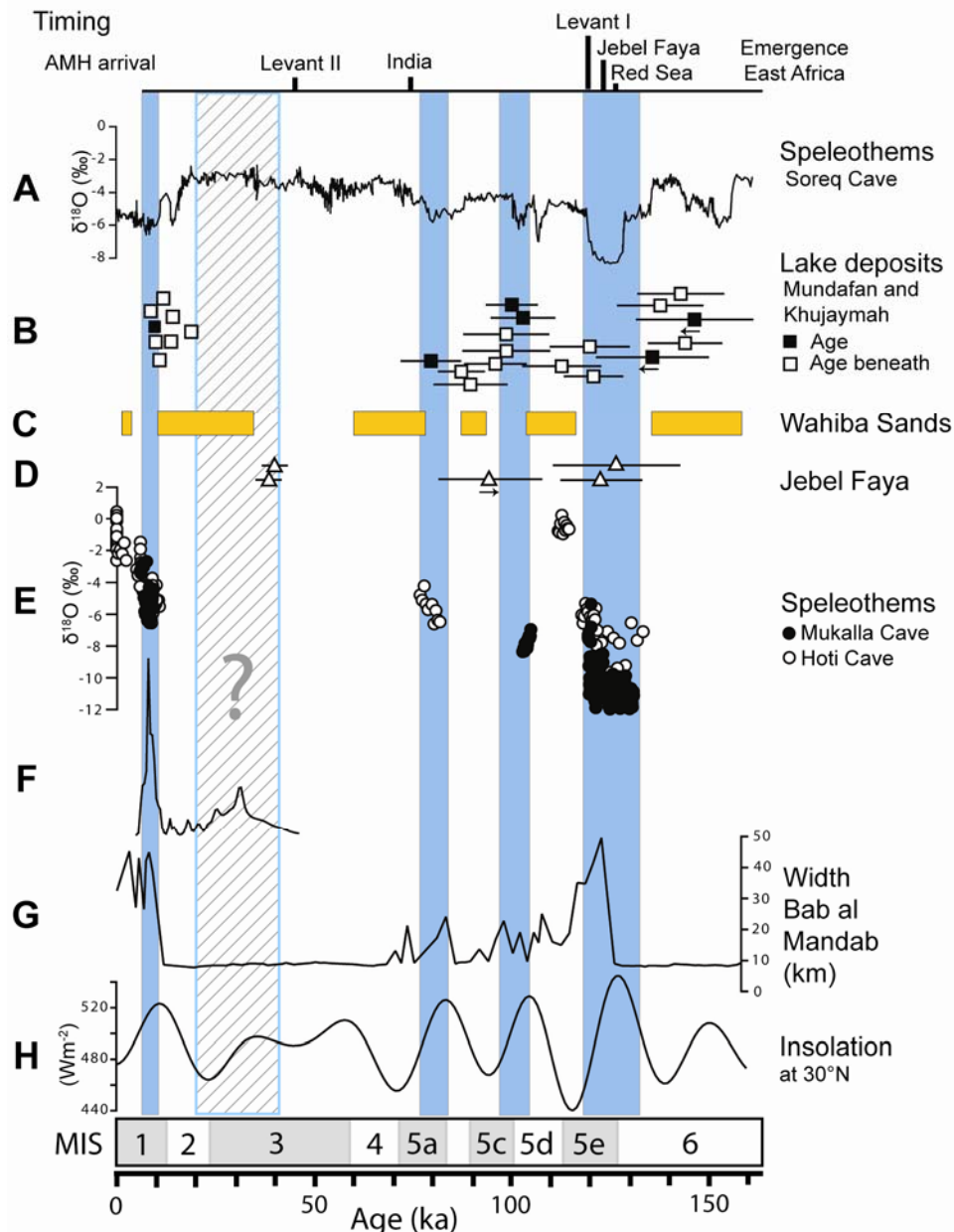


Fig. 4.3. Compilation of southern dispersal route proxy records. Blue bars represent humid periods. **A:** Oxygen isotope ($\delta^{18}\text{O}$) record from Soreq Cave (Bar-Matthews et al., 2003). **B:** OSL ages from lake deposits at Mundafan and Khujaymah. OSL ages obtained for sand beneath lake deposits are interpreted to just predate the onset of lake formation. Small arrows indicate OSL ages overestimating due to problems with dose rate determination **C:** Phases of eolian dune accumulation in the Wahiba Sands, Oman (Radies et al., 2004). **D:** OSL ages from occupation phases at Jebel Faya (Armitage et al., 2011). **E:** Oxygen isotope ($\delta^{18}\text{O}$) data set from Mukalla and Hoti Cave (Fleitmann et al., 2011). **F:** Probability density plot of existing ^{14}C ages on the lake deposits at Mundafan and Khujaymah (McClure, 1976; Whitney, 1983). **G:** Width of the Bab al Mandab Strait calculated from Red Sea sea level (Siddall et al., 2003) and bathymetry at the position marked in Fig. 4.1. **H:** Summer insolation for 30°N (Berger and Loutre, 1991). Timing of anatomically modern human (AMH) dispersal is according to Shea (2008), Petraglia et al. (2010) and Armitage et al. (2011). MIS - marine isotope stage.

4.5 Conclusions

Overall, our reconstructions from southern Arabia provide a chronological and environmental framework that supports the hypothesis of a successful dispersal of AMH before ca. 75 ka along the southern dispersal route into Asia (Macaulay et al., 2005). Lakes existed in southern Arabia ca. 80 ka (MIS 5a), ca. 100 ka (MIS 5c), and ca. 125 ka (MIS 5e), making this region suitable for occupation by AMH. As arid conditions prevailed in southern Arabia between ca. 75 and ca. 10.5 ka, MIS 5a was the last climatic window of opportunity for AMH to disperse eastward along the southern dispersal route into Asia.

Acknowledgments

We thank S.E. Lowick, R.G. Roberts, and two anonymous referees for their constructive comments on previous versions of the manuscript, as well as R. Allen for technical assistance. We acknowledge support from the Swiss National Science Foundation (grant 200021- 117985/1) and the Saudi Geological Survey.

4.6 References

- Armitage, S.J., Jasim, S.A., Marks, A.E., Parker, A.G., Usik, V.I., and Uerpmann, H.-P., 2011, The southern route “out of Africa”: Evidence for an early expansion of modern humans into Arabia: *Science*, v. 331, no. 6016, p. 453–456.
- Bar-Matthews, M., Ayalon, A., Gilmour, M., Matthews, A., and Hawkesworth, C.J., 2003, Sea-land oxygen isotopic relationships from planktonic foraminifera and speleothems in the Eastern Mediterranean region and their implication for paleorainfall during interglacial intervals: *Geochimica et Cosmochimica Acta*, v. 67, no. 17, p. 3181–3199.
- Berger, A., and Loutre, M.F., 1991, Insolation values for the climate of the last 10 million years: *Quaternary Science Reviews*, v. 10, no. 4, p. 297–317.
- Beyin, A., 2006, The Bab al Mandab vs the Nile-Levant: An appraisal of the two dispersal routes for early modern humans out of Africa: *African Archaeological Review*, v. 23.
- Bronk Ramsey, C., 2009, Bayesian analysis of radiocarbon dates: *Radiocarbon*, v. 51, p. 337–360.
- Drake, N.A., Blench, R.M., Armitage, S.J., Bristow, C.S., and White, K.H., 2011, Ancient watercourses and biogeography of the Sahara explain the peopling of the desert: *Proceedings of the National Academy of Sciences of the United States of America*, v. 108, no. 2, p. 458–462.
- Fleitmann, D., Burns, S.J., Neff, U., Mangini, A., and Matter, A., 2003, Changing moisture sources over the last 330,000 years in Northern Oman from fluid-inclusion evidence in speleothems: *Quaternary Research*, v. 60, no. 2, p. 223–232.
- Fleitmann, D., Burns, S.J., Mangini, A., Mudelsee, M., Kramers, J., Villa, I., Neff, U., Al-Subbary, A.A., Buettner, A., Hippler, D., and Matter, A., 2007, Holocene ITCZ and Indian monsoon dynamics recorded in stalagmites from Oman and Yemen (Socotra): *Quaternary Science Reviews*, v. 26, no. 1–2, p. 170–188.
- Fleitmann, D., Burns, S.J., Pekala, M., Mangini, A., Al-Subbary, A., Al-Aowah, M., Kramers, J., and Matter, A., 2011, Holocene and Pleistocene pluvial periods in Yemen, southern Arabia: *Quaternary Science Reviews*, v. 30, no. 7–8, p. 783–787.
- Fontes, J.C., and Gasse, F., 1989, On the ages of humid Holocene and Late Pleistocene phases in North Africa—Remarks on “Late Quaternary climatic reconstruction for the Maghreb (North Africa)” by P. Rognon: *Palaeogeography, Palaeoclimatology, Palaeoecology*, v. 70, no. 4, p. 393–398.
- Forster, P., 2004, Ice Ages and the mitochondrial DNA chronology of human dispersals: a review: *Philosophical Transactions of the Royal Society of London. Series B, Biological Sciences*, v. 359, no. 1442, p. 255–264.
- Forster, P., and Matsumura, S., 2005, *EVOLUTION: Enhanced: Did early humans go North or South?: Science*, v. 308, no. 5724, p. 965–966.

-
- Griffiths, H.I., Schwalb, A., and Stevens, L.R., 2001, *Environmental change in southwestern Iran: The Holocene ostracod fauna of Lake Mirabad: The Holocene*, v. 11, no. 6, p. 757–764.
- Lahr, M. M., and Foley, R., 1994, *Multiple dispersals and modern human origins: Evolutionary Anthropology: Issues, News, and Reviews*, v. 3, no. 2, p. 48-60.
- Lézine, A.-M., Robert, C., Cleuziou, S., Inizan, M.-L., Braemer, F., Saliège, J.-F., Sylvestre, F., Tiercelin, J.-J., Crassard, R., Méry, S., Charpentier, V., and Steimer-Herbet, T., 2010, *Climate change and human occupation in the Southern Arabian lowlands during the last deglaciation and the Holocene: Global and Planetary Change*, v.72, p. 412-428.
- Macaulay, V., Hill, C., Achilli, A., Rengo, C., Clarke, D., Meehan, W., Blackburn, J., Semino, O., Scozzari, R., Cruciani, F., Taha, A., Shaari, N.K., Raja, J.M., Ismail, P., Zainuddin, Z., Goodwin, W., Bulbeck, D., Bandelt, H.-J., Oppenheimer, S., Torroni, A., and Richards, M., 2005, *Single, rapid coastal settlement of Asia revealed by analysis of complete mitochondrial genomes: Science*, v. 308, no. 5724, p. 1034–1036.
- McClure, H.A., 1976, *Radiocarbon chronology of late Quaternary lakes in the Arabian Desert: Nature*, v. 263, p. 755–756.
- McClure, H.A., 1978, *Ar Rub' Al Khali*, in Al-Sayari, S.S. and Zoetl, J.G., ed., *Quaternary Period in Saudi Arabia: vol. 1: Wien, Springer*, p. 252–263.
- McCorrison, J., and Martin, L., 2009, *Southern Arabia's Early Pastoral Population History: Some Recent Evidence: The Evolution of Human Populations in Arabia: Paleoenvironments, Prehistory and Genetics*, Springer, p. 39–49.
- Mellars, P., 2006, *Going East: New genetic and archaeological perspectives on the modern human colonization of Eurasia: Science*, v. 313, no. 5788, p. 796–800.
- Parker, A.G., 2009, *Pleistocene Climate Change in Arabia: Developing a Framework for Hominin Dispersal over the Last 350 ka: The Evolution of Human Populations in Arabia: Paleoenvironments, Prehistory and Genetics*, Springer, p. 39–49.
- Petraglia, M. D., and Alsharekh, A., 2003, *The Middle Palaeolithic of Arabia: Implications for modern human origins, behaviour and dispersals: Antiquity* v. 77, p. 671-684.
- Petraglia, M., Korisettar, R., Boivin, N., Clarkson, C., Ditchfield, P., Jones, S., Koshy, J., Lahr, M.M., Oppenheimer, C., Pyle, D., Roberts, R., Schwenninger, J.-L., Arnold, L., and White, K., 2007, *Middle Paleolithic assemblages from the Indian subcontinent before and after the Toba super-eruption: Science*, v. 317, no. 5834, p. 114–116.
- Petraglia, M.D., Haslam, M., Fuller, D.Q., Boivin, N., and Clarkson, C., 2010, *Out of Africa: New hypotheses and evidence for the dispersal of Homo sapiens along the Indian Ocean rim: Annals of Human Biology*, v. 37, no. 3, p. 288–311.
- Petraglia, M. D., 2011, *Archaeology: Trailblazers across Arabia: Nature*, v. 470, no. 7332, p. 50-51.
- Petraglia, M. D., Alsharekh, A. M., Crassard, R., Drake, N. A., Groucutt, H., Parker, A. G., and Roberts, R. G., 2011, *Middle Paleolithic occupation on a Marine Isotope Stage 5*

-
- lakeshore in the Nefud Desert, Saudi Arabia: Quaternary Science Reviews*, v. 30, no. 13-14, p. 1555-1559.
- Radies, D., Preusser, F., Matter, A., and Mange, M., 2004, *Eustatic and climatic controls on the development of the Wahiba Sand Sea, Sultanate of Oman: Sedimentology*, v. 51, no. 6, p. 1359–1385.
- Shea, J.J., 2008, *Transitions or turnovers? Climatically-forced extinctions of Homo sapiens and Neanderthals in the east Mediterranean Levant: Quaternary Science Reviews*, v. 27, no. 23–24, p. 2253–2270.
- Siddall, M., Rohling, E.J., Almogi-Labin, A., Hemleben, C., Meischner, D., Schmelzer, I., and Smeed, D.A., 2003, *Sea-level fluctuations during the last glacial cycle: Nature*, v. 423, no. 6942, p. 853–858.
- Vaks, A., Bar-Matthews, M., Ayalon, A., Matthews, A., Halicz, L., and Frumkin, A., 2007, *Desert speleothems reveal climatic window for African exodus of early modern humans: Geology*, v. 35, no. 9, p. 831–834.
- Van Peer, P., 1998, *The Nile Corridor and the Out-of-Africa Model. An Examination of the Archaeological Record: Current Anthropology*, v. 39, no. S1, p. 115-140.
- Vermeersch, P. M., 2001, *Out of Africa' from an Egyptian point of view: Quaternary International*, v. 75, no. 1, p. 103-112.
- Walter, R.C., Buffler, R.T., Bruggemann, J.H., Guillaume, M.M.M., Berhe, S.M., Negassi, B., Libsekal, Y., Cheng, H., Edwards, R.L., von Cosel, R., Neraudeau, D., and Gagnon, M., 2000, *Early human occupation of the Red Sea coast of Eritrea during the last interglacial: Nature*, v. 405, no. 6782, p. 65–69.
- Whitney, J. W., 1983, *Erosional history and surficial geology of western Saudi Arabia: United States Geological Survey Technical Record 04–1*.

5 Late Pleistocene palaeolake in the interior of Oman: A potential key-area for the dispersal of anatomically modern humans out of Africa?

Thomas M. Rosenberg ^{a,b}, Frank Preusser ^{a,c}, Ingo Blechschmidt ^d,

Dominik Fleitmann ^{a,b}, Reto Jagher ^e, Albert Matter ^a

^a Institute of Geological Sciences, University of Bern, Switzerland

^b Oeschger Centre for Climate Change Research, University of Bern, Switzerland

^c Present address: Department of Physical Geography and Quaternary Geology, Stockholm University, Sweden

^d Nagra (National Co-operative for the Disposal of Radioactive Waste), Wettingen, Switzerland

^e Institut für prähistorische und naturwissenschaftliche Archäologie (IPNA), Basel, Switzerland

Accepted with minor revisions Journal of Quaternary Sciences

Abstract: Relicts of fluvial and lacustrine deposits in the interior of Oman near Saiwan consist of waterlain breccias with pebble imbrications and current ripples, covered by algal laminites containing calcified reeds and charcoal pieces. Geomorphological evidence suggests that the palaeolake covered a maximum surface of 1400 km² and had a maximum depth around 25 m. Optically stimulated luminescence (OSL) and thermally transferred OSL (TT-OSL) dating indicate that this palaeolake existed sometime between 132 and 104 ka. The rich archaeological evidence in the area suggests substantial human occupation, possibly at the same time when Palaeolake Saiwan existed. Interestingly, the lithic traditions of the archaeological material show no clear relation to coeval findings from neighbouring areas, putting a question mark on the origin of the culture found at Saiwan. This finding raises new questions in the context of the discussion on trans-Arabian migrations at times of modern human dispersal out of Africa.

5.1 Introduction

Until recently, it was assumed that the dispersal of anatomically modern humans (AMH, *Homo sapiens*) out of Africa followed the Nile into the Levant (Drake et al., 2011). However, the early appearance of AMH on the Indian sub-continent and in South East Asia is considered to be strong evidence that AMHs dispersed along a southern route across Southern Arabia (Macaulay et al., 2005; Petraglia et al., 2010; Armitage et al., 2011). However, AMHs were only capable to populate the area when the hostile environment of the Arabian deserts improved during periods of greatly enhanced precipitation. To date, speleothem records from Oman and Yemen (Fleitmann and Matter, 2009; Fleitmann et al., 2011) reveal the occurrence of more humid periods at ~6-11 ka, ~78-82 ka, ~100 ka and ~120-130 ka, caused by a northward shift of the Inter-Tropical Convergence Zone (ITCZ) and intensified monsoon circulation (Burns et al., 2001; Fleitmann et al., 2007). For the early to middle Holocene, radiocarbon-dated relict lake deposits in the interior of Arabia and abundant human artefacts along their shorelines indicate favourable environmental conditions (savannah-type) and a human occupation of the region (McClure, 1976; Whitney, 1983; Petraglia, 2010). Pre-Holocene relict lake deposits have been radiocarbon dated to 40-20 ka (McClure, 1976; Whitney, 1983), but these ages are in conflict with records indicating more arid conditions during the same period (Preusser, 2009). Re-dating of palaeolake deposits at Mundafan and Khujaymah revealed much older ages compared to the radiocarbon dates (Rosenberg et al., in press) with lake formation at ~80 ka, ~100 ka, and ~125 ka, in perfect agreement with speleothem records of Southern Arabia (Fleitmann et al., 2011). These results represent the first firmly dated evidence for pre-Holocene palaeolakes in southern Arabia (Rosenberg et al., in press). Other pre-Holocene palaeolakes - Mudawwara (Petit-Maire et al., 2010) and Jebel Qattar (Petraglia et al., 2011) - are located in northern Arabia and therefore not on the potential southern dispersal route of AMHs.

To enhance our knowledge of the hitherto poorly known environmental conditions for the time of AMH dispersal, we present new results obtained from relict lake deposits found at Saiwan in the interior of Oman. Dating of these deposits is crucial as Saiwan is located halfway between the Dhofar region and the Oman Mountains, both areas of presently rather favourable environmental conditions for human occupation. Numerous artefacts found in the vicinity of Palaeolake Saiwan indicate the presence of humans and underline the potential importance for AMH dispersal. The results of optically stimulated luminescence (OSL) and thermally-transferred OSL (TT-OSL) dating (see Appendix E for details) of relict lake deposits will be presented and discussed together with the archaeological context.

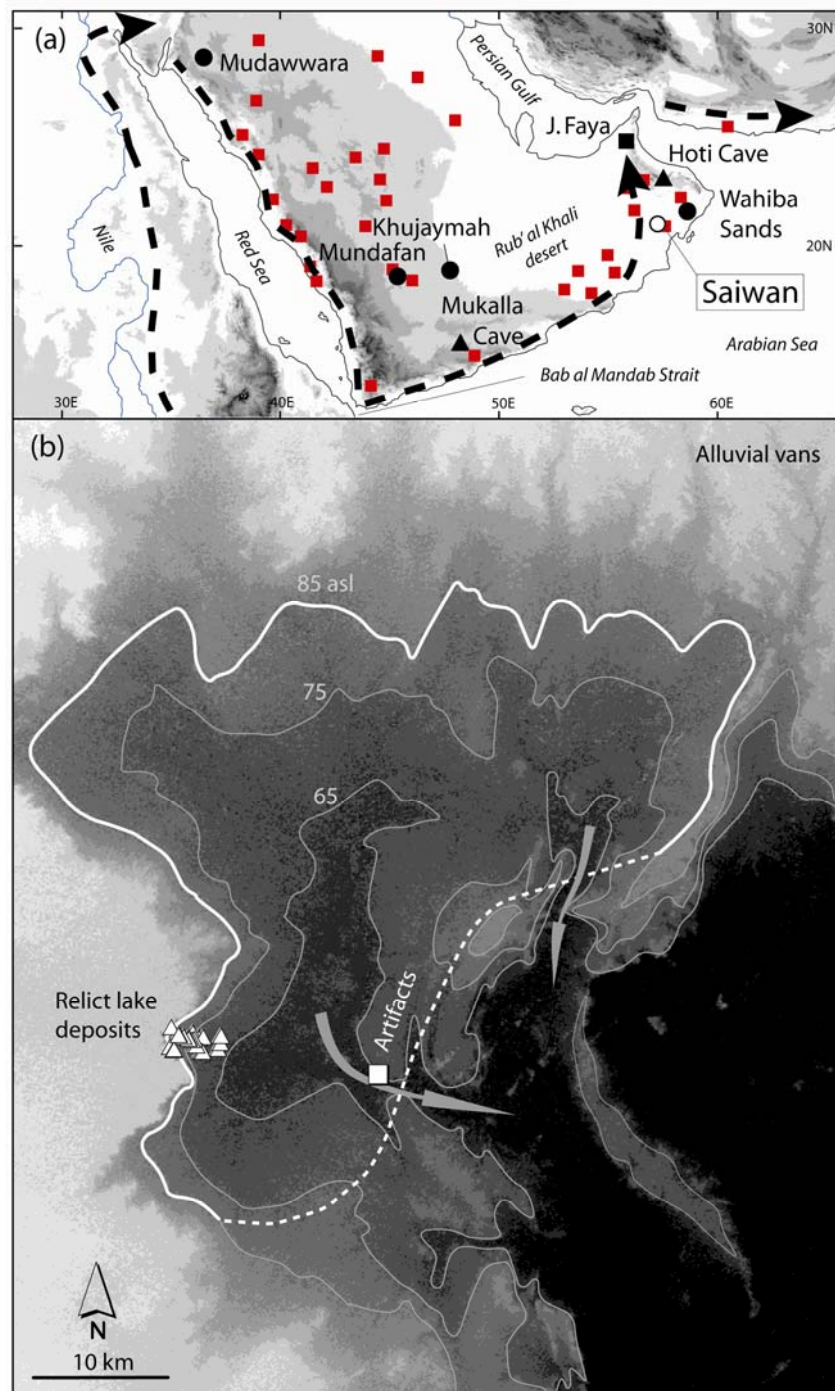


Fig. 5.1. (a) Location of sites and possible migration routes on the Arabian Peninsula. Circles indicate relict lake deposits of Pleistocene age and triangles cave sites. Red squares show a simplified distribution of Lower and Middle Palaeolithic archaeological sites (Petraglia and Alsharekh, 2003). (b) The Saiwan depression with the white line marking the extent of the inferred palaeolake. Arrows mark the channels of potential modern surface water flow.

5.2 Palaeolake Saiwan

The depression near Saiwan (20°58'N/57°22'E) is located just south of a system of large alluvial fans originating from the Oman Mountains (Fig. 5.1; cf. Blechschmidt et al., 2009). Relict lake deposits were found in the western part of the depression between a steep limestone cliff and the modern sabkha (Fig. 5.1). The deposits consist of inhomogeneous conglomerates and breccias with clasts of up to 25 cm in diameter made up of limestones (Fig. 5.2). The sandy matrix consists of carbonate and siliciclastic grains which are likely to originate from calcarenitic limestones cropping out towards the alluvial fans. The sedimentary structures include imbricated pebbles and current ripples in sand lenses indicating fluvial deposition. Towards the top, the breccias turn into sandy micro breccias and at a depth of 40-30 cm from the top charcoal pieces appear followed by the occurrence of well preserved calcified reeds and rarely the gastropod *Melanoides tuberculata*. Three sections show small inter layers of gypsum or calcified concretions. The top of the section consists of porous algal laminites, often homogenised by bioturbation. In some cases sand lenses occur within the lake carbonates. Based on the sedimentological features the Saiwan sequence reveals a change from fluvial deposition to a shallow lake with oscillating water-tables. Sand lenses of well rounded and well sorted quartz grains intercalated in the lake carbonates are clearly of aeolian origin, showing that the surroundings were at least occasionally relatively arid. Considering the geomorphology of the basin, the studied deposits represent a lake shore environment. Sediments in other parts of the basin have apparently been removed by erosion or are covered by sabkha deposits. Based on the present-day geomorphology, we estimate that Palaeolake Saiwan once covered an area of ca. 1400 km² and had a maximum depth of around 25 m. Given its modern geomorphology, the palaeolake depression would not retain a lake, as two incised fluvial channels drain the depression to the south-east (Fig. 5.1b). The channels must hence have formed after the deposition of the lake sediments.

Thirteen kilometres to the east of the relict lake deposits (Fig. 5.1b), a large number of chert artefacts were found on the surface, previously described by Biagi (1994). The artefact finds are located close to the margin of the former lake but within its estimated maximum extension. One of us investigated the findings of Biagi (1994) at the Ministry of Heritage and Culture in Muscat and artefacts of the same industry have been found in the wider surroundings of Palaeolake Saiwan (Fig. 5.3). The items were produced using chert nodules from the underlying limestone formation and detailed descriptions are given in Jagher and Pümpin (2010).

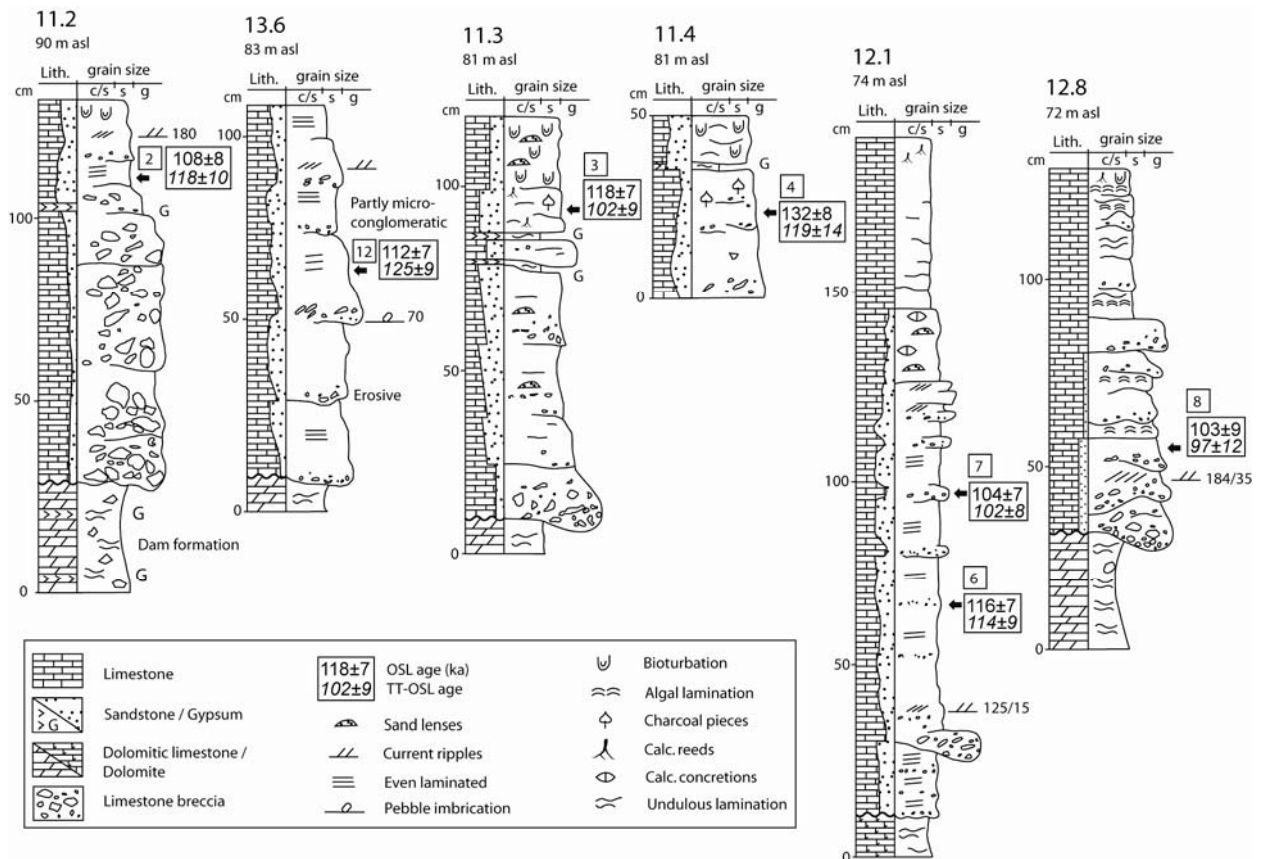


Fig. 5.2. Relict lake deposits from Saiwan, a selection of sedimentary sections.

5.3 Results and Discussion

Samples for luminescence dating were taken from sandy or micro conglomeratic layers often within the occurrence of charcoal pieces (Fig. 5.2). OSL and TT-OSL D_e s largely agree within errors and nine of the twelve OSL ages fall within the range 132 to 104 ka; three ages are between 18 to 26 ka. The three younger ages are from patchy breccia remnants which were not deposited in a lacustrine environment. We therefore interpret these younger deposits to represent occasional floods and not phases of pronounced humidity. The older OSL ages are from the sections described above and attributed to the onset of lake formation of the Paleolake Saiwan. It is important to note that the lacustrine phase between 132 to 104 ka coincides generally with enhanced speleothem growth in Oman (ca. 120-130 ka) and Yemen (ca. 100-105 ka and ca. 123-130 ka) (Fleitmann et al., 2011; Fleitmann and Matter, 2009). However, this phase was interrupted by a dry period with growth discontinuities in speleothems (between ca. 120-105) and deposition of aeolian sand (ca. 110-115 ka) (Preusser, 2009). In view of the dating uncertainties, the OSL and TT-OSL ages for Palaeolake Saiwan could eventually reflect two phases of increased humidity. Despite this uncertainty, there is clear evidence that Paleolake Saiwan was formed during the time of

the dispersal of AMHs and, is thus, a potentially important habitat. Indeed, substantial human occupation in the Palaeolake Saiwan area is evidenced by the presence of a very high number of artefacts (Biagi, 1994; Rose, 2006; Jagher and Pümpin, 2010). Interestingly, the artefacts from Saiwan lack any relation to industries known from the Levante (Jagher and Pümpin, 2010) and do not represent a Late Acheulian style, as originally proposed by Biagi (1994). Furthermore, the typology is also unrelated to any style known from eastern Africa. Moreover the south Arabian Palaeolithic legacy is alien to all its known neighbours and vice versa, except for a faint incursion from the Nubian realm during the early Late Pleistocene (Rose et al., submitted). The number of archaeological finds implies that human occupation must have temporarily been dense and lasting (Jagher and Pümpin, 2010). Due to the fresh appearance of the artefacts, we exclude substantial reworking and assume the artefacts were produced by humans who settled on the shore of the lake. As a consequence of the above, we interpret the artefacts from Saiwan to belong to an independent, so far not recognised Late Pleistocene culture in southern Arabia. Unsolved is, if these artefacts are related to AMHs who migrated out of Africa or belong to an older, possibly endemic population.

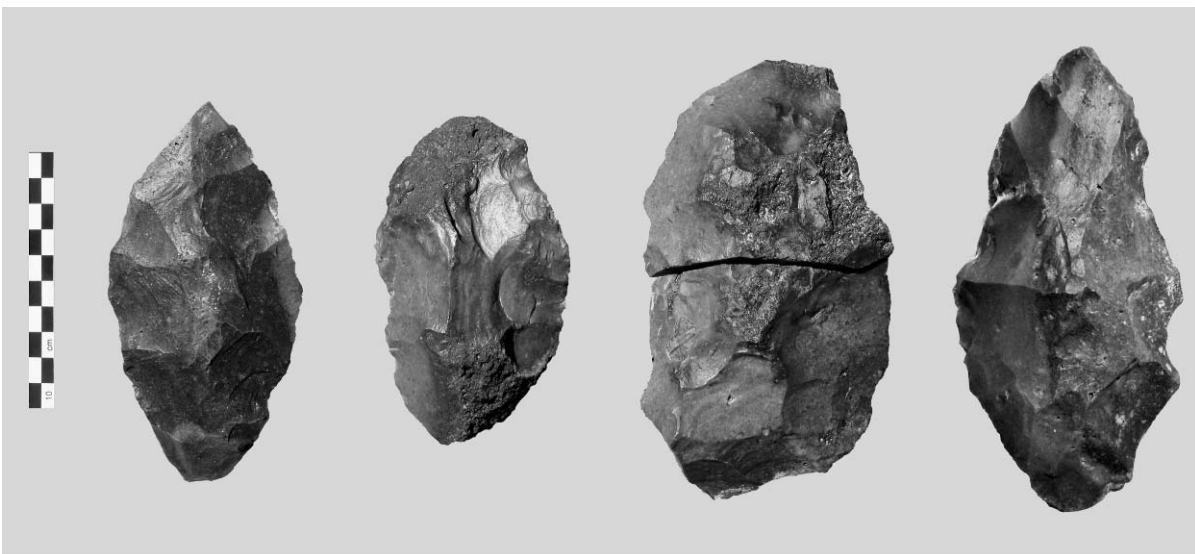


Fig. 5.3. Examples of hand axes from the Saiwan area.

5.4 References

- Biagi, P., 1994. *An Early Palaeolithic site near Saiwan (Sultanate of Oman)*. *Arabian Archaeology and Epigraphy* 5, 81-88.
- Blechs Schmidt, I., Matter, A., Preusser, F., Rieke-Zapp, D. 2009. *Monsoon triggered formation of Quaternary alluvial megafans in the interior of Oman*. *Geomorphology* 110, 128-137.
- Burns, S. J., Fleitmann, D., Matter, A., Neff, U., and Mangini, A., 2001. *Speleothem evidence from Oman for continental pluvial events during interglacial periods*. *Geology* 29, 623-626.
- Drake, N. A., Blench, R. M., Armitage, S. J., Bristow, C. S., and White, K. H., 2011. *Ancient watercourses and biogeography of the Sahara explain the peopling of the desert*. *Proceedings of the National Academy of Sciences* 108, 458-462.
- Fleitmann, D., Burns, S. J., Pekala, M., Mangini, A., Al-Subbary, A., Al-Aowah, M., Kramers, J., and Matter, A., 2011. *Holocene and Pleistocene pluvial periods in Yemen, southern Arabia*. *Quaternary Science Reviews* 30, 783-787.
- Fleitmann, D., and Matter, A., 2009. *The speleothem record of climate variability in Southern Arabia*. *Comptes Rendus Geosciences* 341, 633-642.
- Fleitmann, D., Burns, S. J., Mangini, A., Mudelsee, M., Kramers, J., Villa, I., Neff, U., Al-Subbary, A. A., Buettner, A., Hippler, D., and Matter, A., 2007. *Holocene ITCZ and Indian monsoon dynamics recorded in stalagmites from Oman and Yemen (Socotra)*. *Quaternary Science Reviews* 26, 170-188.
- Jagher, R., and Pümpin, C., 2010. *A New Approach to Central Omani Prehistory*. *Proceedings of the Arabian Seminar* 40, 145-160.
- Macaulay, V., Hill, C., Achilli, A., Rengo, C., Clarke, D., Meehan, W., Blackburn, J., Semino, O., Scozzari, R., Cruciani, F., Taha, A., Shaari, N. K., Raja, J. M., Ismail, P., Zainuddin, Z., Goodwin, W., Bulbeck, D., Bandelt, H.-J., Oppenheimer, S., Torroni, A., and Richards, M., 2005. *Single, Rapid Coastal Settlement of Asia Revealed by Analysis of Complete Mitochondrial Genomes*. *Science* 308, 1034-1036.
- McClure, H. A., 1976. *Radiocarbon chronology of late Quaternary lakes in the Arabian Desert*. *Nature* 263, 755-756.
- Petit-Maire, N., Carbonel, P., Reyss, J. L., Sanlaville, P., Abed, A., Bourrouilh, R., Fontugne, M., and Yasin, S., 2010. *A vast Eemian palaeolake in Southern Jordan (29°N)*. *Global and Planetary Change* 72, 368-373.
- Petraglia, M.D., Alsharekh, A.M., Crassard, R., Drake, N.A., Groucutt, H., Parker, A.G., Roberts, R.G., 2011. *Middle Paleolithic occupation on a Marine Isotope Stage 5 lakeshore in the Nefud Desert, Saudi Arabia*. *Quaternary Science Reviews* 30, 1555-1559.

-
- Petraglia, M. D., Haslam, M., Fuller, D. Q., Boivin, N., and Clarkson, C., 2010. Out of Africa: new hypotheses and evidence for the dispersal of Homo sapiens along the Indian Ocean rim. Annals of Human Biology 37, 288-311.*
- Petraglia, M. D., and Alsharekh, A. (2003). The Middle Palaeolithic of Arabia: Implications for modern human origins, behaviour and dispersals. Antiquity 77, 671-684.*
- Preusser, F., 2009. Chronology of the impact of Quaternary climate change on continental environments in the Arabian Peninsula. Comptes Rendus Geosciences 341, 621-632.*
- Rose, J. I., Usik, V. I., Marks, A. E., Hilbert, Y. H., Geiling, J. M., Galletti, C. S., Parton, A., Morley, M. W., Černý, V., and Roberts, R. G., submitted. The Nubian Complex of Dhofar, Oman and implications for early modern human occupation of southern Arabia. PLoS ONE.*
- Rose J. 2006. Among Arabian Sands: Defining the Palaeolithic of Southern Arabia. PhD thesis, Southern Methodist University, University Park, Texas. [Unpublished].*
- Rosenberg, T. M., Preusser, F., Fleitmann, D., Schwab, A., Penkman, K., Schmid, T. W., Kadi, K., Al-Shanti, M. A., and Matter, A., in press. Humid periods in southern Arabia - windows of opportunity for modern human dispersal. Geology, 39, 1115-1118.*
- Whitney, J. W., 1983. Erosional history and surficial geology of western Saudi Arabia. United States Geological Survey Technical Record 04-1.*

6 Nafud palaeolakes fill the gap between southern and northern Arabian climate archives

Thomas M. Rosenberg ^{a,b}, Frank Preusser ^{a,c}, Dominik Fleitmann ^{a,b},
Jan Risberg ^c, Anna Pliik ^c, Khalid Kadi ^d, Albert Matter ^a

^a Institute of Geological Sciences, University of Bern, Switzerland

^b Oeschger Centre for Climate Change Research, University of Bern, Switzerland

^c Department of Physical Geography and Quaternary Geology, Stockholm University, Sweden

^d Saudi Geological Survey, Jeddah, Saudi Arabia

In preparation for submission to Quaternary Science Reviews

Abstract: Relict palaeolake deposits in the Great Nafud desert of northern Saudi Arabia are evidence of a much wetter regional climate than today. At present, climate is hyper arid and moisture brought by northwesterly winds scarcely reaches the desert. The existing chronological framework of the palaeolake deposits is based on radiocarbon dating of questionable reliability. Recent studies indicate that the Pleistocene lake deposits are considerably older than the previously suggested 40-20 ka. This study provides new chronological data for the Nafud palaeolake deposits using luminescence dating techniques. The ages reveal humid periods centred at ca. 410, ca. 320, 125 ka and 100 ka, but no Holocene lake deposits were identified in interdune depressions. Geological characteristics of the deposits and diatom analysis suggest that a single, perennial lake covered the entire south-western Nafud ca. 320 ka ago. In contrast, lakes of the 125 and 100 ka phases were of much smaller scale and only occupied interdune depressions. A comparison with speleothem records of the southern Negev desert shows a very similar timing for humid periods. The agreement with the southern Negev and disagreement with the central and northern Negev makes a Mediterranean moisture source unlikely and suggests the origin of humidity is from enhanced African Monsoon circulation.

6.1 Introduction

Bare sand- and stone deserts dominate the landscape of modern Arabia. In contrast, the widespread occurrence of relict lake deposits is striking evidence of a more humid climate in the past. Today, the climate is governed by subtropical high pressure with very scarce moisture generally delivered by the northwesterlies, as well as a limited area in the far south which experiences tropical summer precipitation under the influence of the Inter Tropical Convergence Zone (ITCZ). The moisture brought by the northwesterlies comes as winter and spring precipitation in the form of Atlantic and Mediterranean frontal depression systems. From June to September strong south-westerly winds of the Indian Summer Monsoon (ISM) transport large quantities of moisture towards the ITCZ, released as heavy precipitation over south-western Arabia, namely the Yemeni highlands and the Dhofar region (Fig. 6.1).

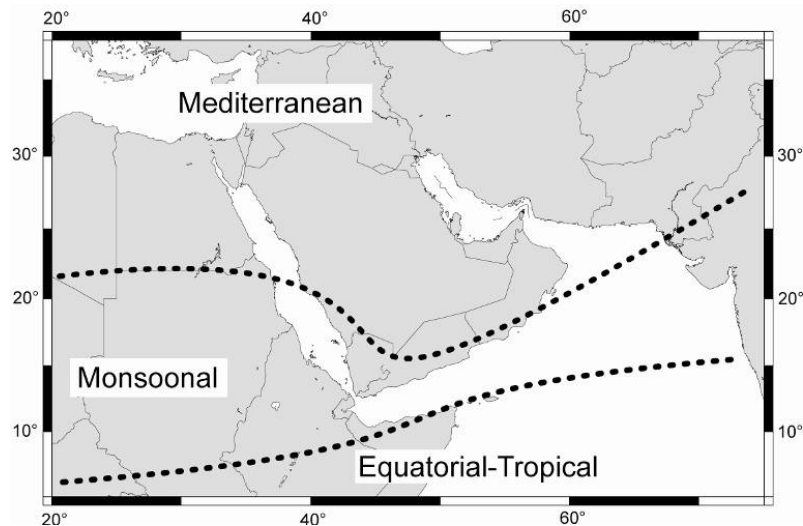


Fig. 6.1. Modern precipitation regimes (adapted by Gasse (2000)). “Mediterranean” = winter rainfall, “Monsoonal” = summer monsoon rainfall and “Equatorial-Tropical” = spring and autumn rainfall.

From speleothems and marine cores of the Arabian Sea (Clemens and Prell, 2003; Fleitmann et al., 2011) it is known that monsoon strength was highly variable over the last 350 ka. The growth and isotopic records of speleothems from Hoti cave in Oman (Burns et al., 2001) and Mukalla cave in Yemen (Fleitmann et al., 2011) indicate that during peak interglacial periods, the ITCZ was shifted far north of its present summer position. The environmental fate of the region largely depends on the oscillations of the ITCZ. Unfortunately, however, the major question of which latitudinal position the ITCZ has reached in the past remains unsolved. Despite being a key-area for understanding climate dynamics, the Pre-Holocene climate history of the Arabian Peninsula has large spatial and temporal gaps. Palaeoclimate archives (Fig. 6.2) do not cover the central part leaving a large gap

between clusters of archives in the south and north of the peninsula. Besides its key location for understanding past climate dynamics, Arabia is of crucial importance for reconstruction of when and where anatomically modern humans (AMH) moved out of Africa and spread over the planet. From genetic mutation rates it is assumed that the genetic diversion from the African gene-pool occurred some time between 85,000 and 65,000 years ago (Forster and Matsumura, 2005; Macaulay et al., 2005). This time slot, together with the nearly simultaneous first appearance of modern humans in Indonesia (Mellars, 2006; Oppenheimer, 2009), led a number of authors to suggest a single rapid southern dispersal across the Bab al Mandab strait and then on following the southern coast of Arabia. Regardless if AMH took the southern route over the Bab al Mandab Strait to Arabia or a northern route across the Sinai Peninsula, favourable environmental conditions with enough fresh water must have been a key factor. The palaeoclimate of the Arabian Peninsula therefore had a major influence on the timing of the migration out of Africa of AMH and therewith the global expansion of our species.

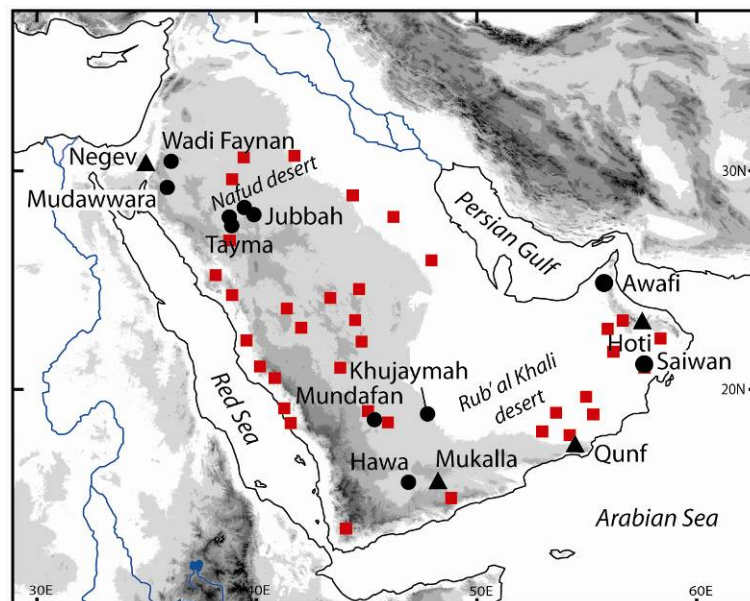


Fig. 6.2. Climate archives from the Arabian Peninsula. Circles indicate relict lake deposits, triangles speleothems. Red squares show a simplified distribution of Lower and Middle Palaeolithic archaeological sites (Petraglia and Alsharekh, 2003).

This study presents results from lake deposits in the Nafud Desert in northern Saudi Arabia (Fig. 6.2). As the peninsula's second largest desert after the Rub' al Khali, the Nafud Desert receives an average annual precipitation of ~50 mm (Edgell, 2006), mostly occurring between November and April. This is sufficient to allow for sparse vegetation including perennial shrubs and annual grasses. The Nafud desert is composed mainly of 60-120 m

high barchanoid dune ridges, transverse dunes and linear dunes. In the interdune depressions and on windward dune slopes relict lake deposits are occasionally exposed. The focus of this study is to establish a new chronology for the Nafud lake deposits previously dated by Whitney et al. (1983b) using optically stimulated luminescence (OSL) for dating and diatom assemblages as environmental proxy. Based on the location of the Nafud lake deposits and the new ages, it is hoped to contribute towards filling the spatial and temporal gaps of the Arabian climate archives.

6.2 Regional palaeoclimate history

Bringing together the climate archives of the Arabian Peninsula reveals a spatial gap between clusters of archives in the north and south but also a temporal gap due to chronologies often limited to the time range of radiocarbon dating. Recent studies using U/Th and optically stimulated luminescence (OSL) (Petit-Maire et al., 2010; Rosenberg et al., 2011a) indicate that most of the Pleistocene lake deposits in Arabia are considerably older than the previously suggested 40-20 ka (McClure, 1976; McClure, 1984; Sanlaville, 1992; Whitney, 1983a; Whitney et al., 1983b). All radiocarbon ages reported here are calibrated BP ages. While the moisture source for the southern cluster of archives was identified as the ISM, the origin of moisture for the northern cluster of archives remains speculative.

Only a handful of Arabian climate records reach further back than 150 ka. These comprise lake deposits from Jordan and the UAE (Abed et al., 2008; Fogg et al., 2002; Petit-Maire et al., 2010). The U/Th ages of these deposits show a lake phase at ~330 ka and a series of lake phases between 170 and 75 ka. In the Levant on the northern margin of the Arabian desert speleothem records of the Negev Desert (Vaks et al., 2010) reach as far back as 350 ka. Major humid periods in the southern Negev Desert are centred at ~330 ka and ~125 ka. Speleothem deposition in the northern Negev Desert differs, with additional phases at ~300 ka and ~205 ka and a less intensive phase at ~330 ka. No Holocene speleothem deposition is known from the southern Negev Desert. Fleitmann et al. (2011) found periods of enhanced speleothem growth in Oman (Hoti Cave) and Yemen (Mukalla Cave) centred at ~320 ka, ~235 ka, ~195 ka, ~125 ka, ~105 ka, ~80 ka and the early Holocene. Delta ^{18}O ratios suggest the ~125 ka phase to be the wettest, and the early Holocene phase, to be the driest. At Jebel Qattar within the Nafud Desert, Petraglia et al. (2011) dated palaeosols to 211 ± 16 ka and 95 ± 7 ka using OSL. They assume that the main calcrete formation occurred at ~125 ka. In southern Jordan lake deposits in the large depression at Mudawwara are U/Th dated to several periods between ~130 ka and ~80 ka with a concentration of ages around ~125 ka and an outlier at 170 ka (Petit-Maire et al., 2010). The environmental proxies

suggest rather brackish conditions and generally a perennial existence of the lake. No Holocene activity was found at Mudawwara. At Jebel Faya in the UAE shelter occupations by AMH are dated to 127 ± 16 ka, 123 ± 10 ka and 95 ± 13 ka (Armitage et al., 2011) suggesting humid conditions favourable for human dispersal being established by ~ 130 ka. In the south-western Rub' al Khali at Mundafan-Khujaymah (Rosenberg et al., 2011b) dated lake formation using OSL, to periods centred at ~ 125 ka, ~ 100 ka, ~ 80 ka and during the early Holocene. Environmental proxies indicate a savannah like environment surrounded the perennial lakes. In central Oman, at Saiwan, Rosenberg et al. (in review) recently presented a study on a palaeolake that existed for a few thousand years between 125 ka and 105 ka. Between 80 ka and the early Holocene there is no evidence to constrain humid periods, although episodic flooding events were reported from central Saudi Arabia dated to 54 ka and 39 ka using OSL on outwash fans (McLaren et al., 2008). Similarly, alluvial deposition in the interior of Oman was dated to ca. 45 ka using OSL on mega fans south of the Oman Mountains (Blechs Schmidt et al., 2009).

From the beginning of the Holocene to present, a humid period is indicated from a variety of climate archives, including palaeolake deposits, speleothems and fluvial sediments (Fleitmann et al., 2007; Fleitmann et al., 2003a; Hunt et al., 2004; Parker et al., 2006a; Parker et al., 2004; Parker et al., 2006b; Parker et al., 2006c; Radies et al., 2005). At Al-Hawa on the south-western limit of the Rub' al Khali in Yemen (300 km south of Mundafan) Lézine et al. (2010) dated lake deposits to 11.2- 7.7 ka using radiocarbon on gastropod shells and organic matter. Their sedimentological evidence suggests that humidity started to fade in southern Arabia after 7 ka. At Mundafan Rosenberg et al. (2011b) dated Holocene lake deposits using radiocarbon on organic matter and OSL, to a range between 9.6 ka and 7.6 ka. While the onset of lake formation is well constrained at Mundafan, its cessation is assumed to have taken place after 7.6 ka. At Awafi in the UAE Parker et al. (2004) thoroughly investigated a number of Holocene lake deposits and found a general onset of lake formation at 8.5 ka with a cessation at ~ 6 ka. Speleothems from Qunf cave and Hoti cave in Oman show the beginning of increased humidity at 10.6 and 10.0 ka (Fleitmann et al., 2007; Fleitmann et al., 2003a; Neff et al., 2001). Although numerous Holocene climate archives exist in Arabia, there is still a large gap between southern and northern archives. The most southern archives of the northern cluster are from the Nafud Desert where Whitney et al. (1983) and Schulz and Whitney (1986) found evidence for shallow lakes and swamps with radiocarbon ages between 9.5 ka and 5.8 ka. Engel et al. (2011) present results from a palaeo-environmental and hydrological study on the sabkha basin of the Tayma Oasis south-west to the Nafud desert. They found that a permanent lake existed at Tayma from 10.0 ka to 8.5 ka after which gradual aridification processes began. Hydrological modelling results led

them to suggest that a minimum annual precipitation of 150 mm was required to support a perennial lake.

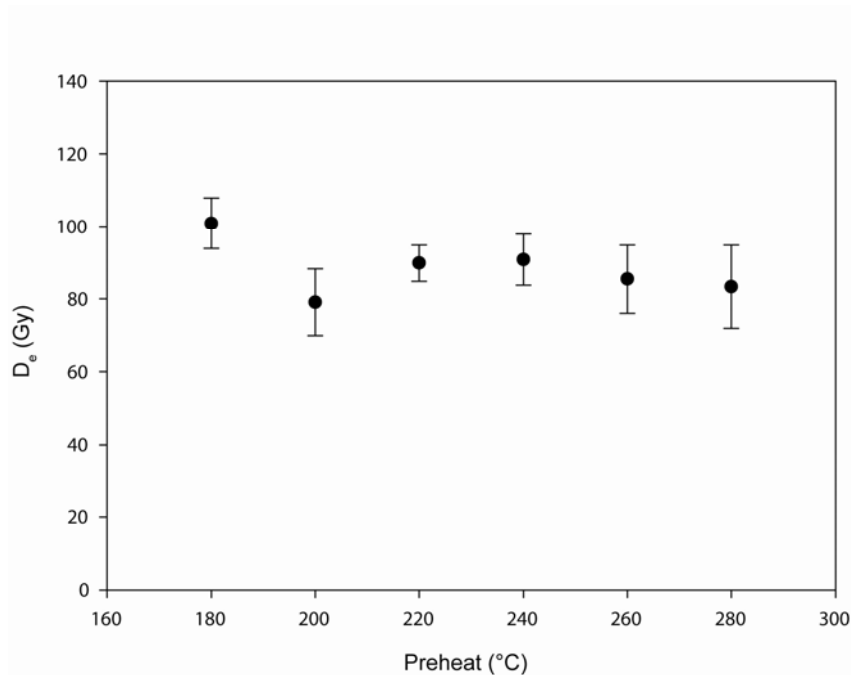


Fig. 6.3. D_e as a function of preheat temperature for sample 2 at site o16.4. Each point is the average of three 6 mm aliquots.

6.3 Materials and methods

6.3.1 Luminescence dating

Samples for luminescence dating were taken from aeolian sand beneath, above and, whenever possible, within lacustrine sequences, by forcing a steel tube into a freshly cleaned exposure, or by cutting out blocks of lithified deposits. The material from the tubes was carefully discharged into opaque plastic bags and block samples were double wrapped with opaque foil for transport. In the lab samples were opened under subdued light conditions and blocks were cut to obtain the inner part which had not been exposed to sunlight since deposition. The grain size 200-250 μm was isolated and treated with HCl and H₂O₂ to remove carbonates and organic matter. A two-step heavy-liquid separation using LST Fastfloat (2.70 and 2.58 g cm⁻³) was carried out and the quartz fraction was subsequently etched in HF (40%) for 60 min to remove feldspars, and the outer part of the quartz grains influenced by alpha irradiation during burial. Measurements were made in a Risø TL/OSL-DA-20 reader with blue diodes (470 \pm 30 nm; \sim 41 mW cm⁻²) and with a calibrated 40 mCi

$^{90}\text{Sr}/^{90}\text{Y}$ beta source delivering $\sim 0.13 \text{ Gy s}^{-1}$ to the grains. Luminescence signals were measured with an EMI 9635Q photomultiplier tube through a 7.5 mm Hoya U340 filter.

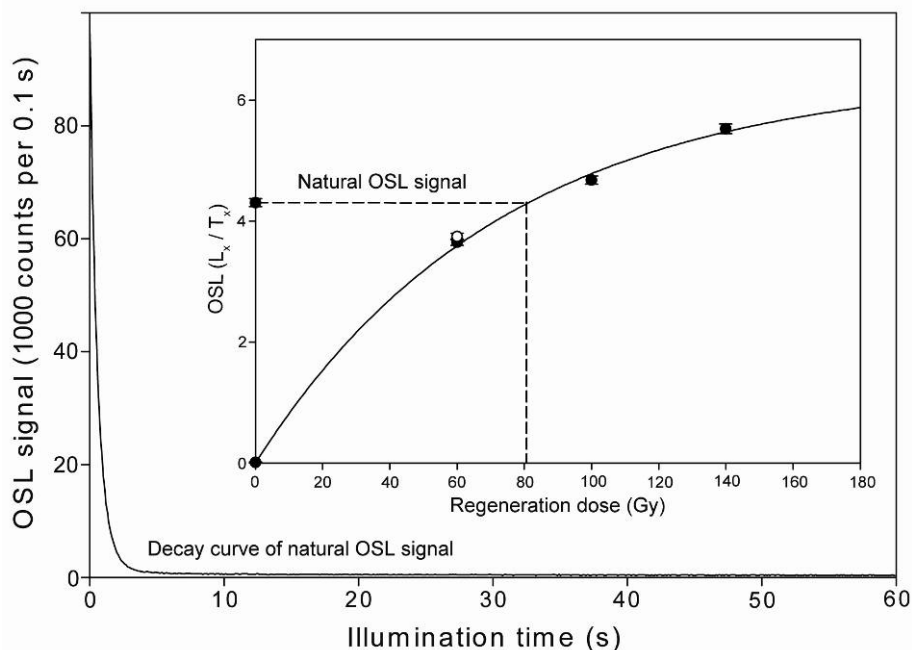


Fig. 6.4. Decay curve of natural OSL (L_N) as a function of illumination time. The inset shows the growth curve for an individual aliquot, showing L_x/T_x as a function of regeneration doses. This sample (o16.4/2) was dated to $117 \pm 8 \text{ ka}$. The open circle is a repeated measurement.

OSL was measured using the single aliquot regenerative dose (SAR) protocol of Murray and Wintle (2000). Samples were initially characterized using preheat tests (Fig. 6.3). A preheat of 240°C for 10 s, together with a cut-heat of 220°C were selected for D_e determination. The test dose (D_t) size was chosen to be 10 % of the expected dose. The initial 0.4 s OSL signal minus a background estimated from the 50-60 s integral was used for OSL dose determinations. Figure 6.4 shows a representative decay and growth curve. Aliquots were rejected if the recycling ratio was outside the range 1.0 ± 0.2 or the IR-OSL depletion ratio (Duller et al., 2003) was less than 0.8. All heating was ramped at 5°C s^{-1} . In order to obtain a central value that best reflects the average D_e for each sample, the central age model (Galbraith et al., 1999) was chosen. Figure 6.5 shows a typical dose distribution for a Nafud sample in a radial plot (Galbraith, 1990).

Twelve out of 30 samples were out of the dating range for the OSL SAR protocol of (Murray and Wintle, 2000) due saturation of the fast OSL signal (Fig. 6.4). In order to date these samples a previously published, single-aliquot regenerative-dose protocol (SAR) for thermally-transferred optically stimulated luminescence (TT-OSL) was applied (Porat et al., 2009; Rosenberg et al., 2011b). A test dose of 10 Gy was used and the aliquot size was 6 mm. The initial 0.4 s TT-OSL signal minus an early background estimated from the 0.4-10.4

s integral, as originally suggested by Ballarini et al. (2007), was used for TT-OSL dose determinations to better cope with sensitivity change and the build-up of background signal.

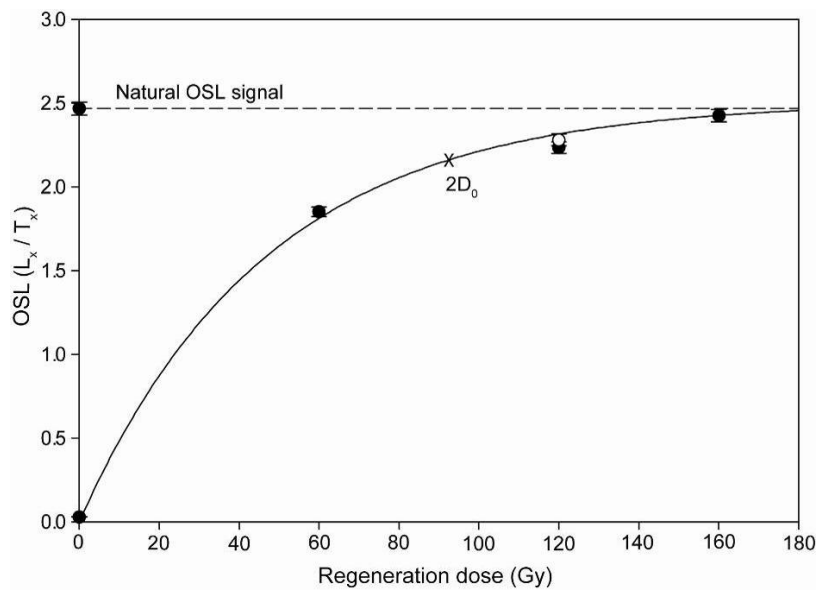


Fig. 6.5. OSL growth curve for sample d17.1/1B. The $2D_0$ value of the single saturating exponential are marked with a cross at 93 Gy. The dashed line shows the value of the natural L_n/T_n ratio. The open circle is a repeated measurement.

Radioactive elements (K, Th, U; Table 6.1) were measured for dose rate determination using high-resolution gamma spectrometry (Preusser and Kasper, 2001). These measurements imply some evidence for radioactive disequilibrium in the Uranium decay chain for some of the samples and these were also measured using Instrumental Neutron Activation Analysis (INAA). U-238 from INAA compared to Ra-226 from Gamma spectrometry (Table 6.1) shows an U-238 deficiency in sample i13.5/2 and j16.1/3. Modelling the dose rate history of the two samples with ADELE Software (Kulig, 2005) and allowing an U-238 input by carbonate precipitation during the lake period reduced the ages by 20 ka and 10 ka to 293 ± 19 ka and 307 ± 24 ka. Dose rates were calculated assuming average water content between 2% and 6% during burial. The contribution of cosmic rays to the total dose rate was calculated using present day depth considering full uncertainties due to actual position below surface (Prescott and Hutton, 1994). Total dose rates and resulting ages are summarized in Table 6.1.

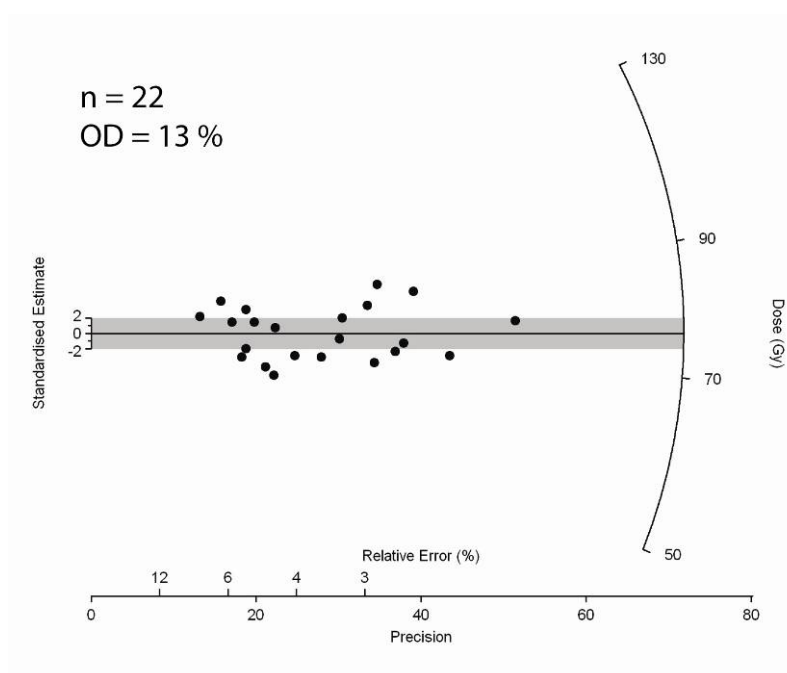


Fig. 6.6. Radial plot for sample p16.5/2 showing a typical dose distribution.

6.3.2 Diatoms

Diatoms and other siliceous microfossils were extracted from the diatomites using standard techniques (Battarbee 1986). 10 % HCl was added to remove possible carbonates and 17 % H₂O₂ to oxidize organic matter. Clay particles were decanted after sedimentation in 100 ml beakers in 2 hrs intervals. Sand grains were removed after 5 s of sedimentation. The residue was mounted in Naphrax and studied using X1000 magnification and immersion oil. Theriot and Stoermer (1984), Krammer and Lange-Bertalot (1986, 1988, 1991a, b), Håkansson and Kling (1989), Håkansson and Meyer (1994), Gasse (1987), Gasse et al. (1995), Morales (2001), Håkansson (2002) and Paull et al. (2008) were used as an aid for species identification and information on ecology. Diatoms have been grouped according to life habitat in different water depth (planktonic, facultatively planktonic, periphytic, aerophilic) and salinity preferences (eurysaline (marine), meso-polysaline (brackish), oligosaline (halophilous/indifferent), freshwater). Phytolith/diatom ratio was used as a rough indicator of the water depth at the sampling site.

Table 6.1. OSL Data

| Sample | Depth (m) | Cosmic-dose rate (mGy/ka) | Activities | | U-238 | Ra-226 | Dose-rate (Gy/ka) | n | OD | D _e (Gy) | Age (ka) | Protocol | |
|---------|-----------|---------------------------|------------|-------------|------------|-------------|-------------------|------------|----|---------------------|--------------|-----------|-----|
| | | | K | Th | | | | | | | | | |
| 10.2/1 | 0.7 | 208 | Y | 58.4 ± 1.7 | 8.6 ± 0.3 | 7.0 ± 1.6 | 7.1 ± 0.2 | 0.7 ± 0.04 | 15 | 16 | 266.3 ± 13.3 | 407 ± 32 | TT |
| | | | I | 30.4 ± 0.5 | 5.4 ± 0.1 | 6.2 ± 0.2 | | | | | | | |
| 10.2/2 | 0.2 | 223 | Y | 52.4 ± 0.9 | 7.4 ± 0.2 | 5.2 ± 1.3 | 6.6 ± 0.1 | 0.6 ± 0.04 | 15 | 22 | 210.7 ± 17.2 | 338 ± 34 | TT |
| | | | I | 70.8 ± 1.0 | 8.9 ± 0.1 | 4.8 ± 0.2 | | | | | | | |
| 11.2/1 | 0.6 | 210 | Y | 41.1 ± 0.9 | 6.8 ± 0.2 | 4.3 ± 1.6 | 5.7 ± 0.1 | 0.5 ± 0.06 | 19 | 25 | 194.7 ± 11.4 | 354 ± 30 | OSL |
| | | | I | 47.4 ± 0.8 | 7.2 ± 0.1 | 6.8 ± 0.2 | | | | | | | |
| 11.3/1 | 0.45 | 215 | Y | 48.4 ± 0.9 | 6.9 ± 0.4 | 7.3 ± 2.4 | 7.2 ± 0.4 | 0.6 ± 0.04 | 16 | 17 | 220.4 ± 12.9 | 406 ± 49 | TT |
| | | | I | 51.4 ± 0.9 | 6.6 ± 0.1 | 9.7 ± 0.3 | | | | | | | |
| 11.4-1 | 1.2 | 194 | Y | 43.6 ± 1.4 | 6.9 ± 0.1 | 10.6 ± 2.7 | 8.5 ± 0.1 | 0.6 ± 0.03 | 16 | 19 | 95.9 ± 4.8 | 161 ± 12 | OSL |
| 11.5/1 | 2.2 | 169 | Y | 33.3 ± 1.2 | 5.8 ± 0.2 | 9.1 ± 2.2 | 7.6 ± 0.1 | 0.5 ± 0.03 | 22 | 18 | 89.0 ± 3.5 | 177 ± 13 | OSL |
| | | | I | 26.2 ± 0.6 | 6.2 ± 0.1 | 8.9 ± 0.2 | | | | | | | |
| 12.3/1 | 1.6 | 183 | Y | 21.2 ± 0.9 | 5.9 ± 0.2 | 6.0 ± 1.6 | 5.5 ± 0.1 | 0.4 ± 0.03 | 16 | 27 | 158.9 ± 12.5 | 358 ± 37 | TT |
| | | | I | 16.9 ± 0.4 | 5.8 ± 0.1 | 5.2 ± 0.2 | | | | | | | |
| 13.2/1 | 0.75 | 202 | Y | 63.5 ± 3.0 | 8.8 ± 0.2 | 6.7 ± 1.5 | 6.6 ± 0.2 | 0.7 ± 0.04 | 15 | 30 | 174.7 ± 12.8 | 394 ± 39 | OSL |
| | | | I | 43.4 ± 0.8 | 6.2 ± 0.1 | 5.3 ± 0.2 | | | | | | | |
| 13.3/1 | 0.65 | 205 | Y | 75.6 ± 3.0 | 10.1 ± 0.2 | 12.2 ± 2.2 | 11.6 ± 0.5 | 0.8 ± 0.05 | 23 | 22 | 89.9 ± 4.2 | 109 ± 8 | OSL |
| | | | I | 37.9 ± 0.7 | 6.0 ± 0.1 | 9.4 ± 0.3 | | | | | | | |
| 13.4/1 | 0.4 | 212 | Y | 42.4 ± 0.9 | 6.7 ± 0.0 | 5.3 ± 2.5 | 11.8 ± 0.4 | 0.7 ± 0.04 | 15 | 23 | 255.2 ± 16.6 | 382 ± 33 | TT |
| | | | I | 25.3 ± 0.5 | 6.1 ± 0.1 | 9.0 ± 0.2 | | | | | | | |
| 13.5/1 | 1.9 | 173 | Y | 6.1 ± 0.9 | 4.4 ± 0.2 | 3.2 ± 1.1 | 4.4 ± 0.1 | 0.3 ± 0.03 | 16 | 32 | 204.8 ± 17.1 | 599 ± 70 | TT |
| | | | I | 2.7 ± 0.3 | 4.2 ± 0.1 | 4.0 ± 0.2 | | | | | | | |
| 13.5/2 | 0.3 | 215 | Y | 115.0 ± 3.0 | 7.7 ± 0.5 | 40.2 ± 15.9 | 19.0 ± 0.2 | 1.0 ± 0.06 | 10 | 14 | 228.6 ± 15.9 | 668 ± 71 | OSL |
| | | | I | 150.9 ± 2.2 | 12.0 ± 0.2 | 52.2 ± 0.7 | | | | | | | |
| 14.1/1 | 2.7 | 157 | Y | 54.5 ± 3.0 | 7.0 ± 0.3 | 9.2 ± 3.9 | 14.8 ± 0.4 | 0.7 ± 0.04 | 16 | 27 | 155.6 ± 11.5 | 219 ± 20 | TT |
| | | | I | 52.5 ± 0.9 | 6.8 ± 0.1 | 6.9 ± 0.2 | | | | | | | |
| 14.3-1 | 1.9 | 175 | Y | 52.3 ± 1.0 | 6.7 ± 0.1 | 7.2 ± 2.5 | 6.8 ± 0.3 | 0.6 ± 0.03 | 22 | 23 | 69.2 ± 3.5 | 122 ± 9 | OSL |
| 14.3/8 | 0.5 | 213 | Y | 39.3 ± 0.9 | 5.9 ± 0.2 | 5.0 ± 1.9 | 6.2 ± 0.1 | 0.5 ± 0.04 | 22 | 12 | 10.4 ± 0.3 | 19 ± 1 | OSL |
| | | | I | 50.2 ± 0.9 | 6.1 ± 0.1 | 9.4 ± 0.2 | | | | | | | |
| 14.4/1 | 1.45 | 188 | Y | 57.5 ± 3.0 | 5.2 ± 0.3 | 3.0 ± 3.6 | 5.3 ± 0.1 | 0.5 ± 0.04 | 14 | 12 | 213.2 ± 10.7 | 390 ± 34 | TT |
| | | | I | 50.9 ± 1.0 | 3.4 ± 0.1 | 4.9 ± 0.2 | | | | | | | |
| 15.1/1B | 2.9 | 189 | Y | 30.3 ± 1.5 | 8.3 ± 2.9 | 8.9 ± 1.0 | 8.7 ± 0.2 | 0.6 ± 0.08 | 16 | 21 | 212.2 ± 13.9 | 367 ± 57 | TT |
| | | | I | 22.7 ± 0.5 | 8.2 ± 0.1 | 7.4 ± 0.2 | | | | | | | |
| 15.2/1 | 0.5 | 217 | Y | 6.1 ± 0.6 | 5.1 ± 0.1 | 4.5 ± 0.6 | 4.5 ± 0.1 | 0.4 ± 0.03 | 14 | 25 | 188.5 ± 12.8 | 325 ± 51 | OSL |
| | | | I | 2.6 ± 0.2 | 5.4 ± 0.1 | 3.9 ± 0.2 | | | | | | | |
| 16.1/1 | 2 | 176 | Y | 236.0 ± 3.0 | 10.0 ± 0.5 | 5.5 ± 1.2 | 5.7 ± 0.2 | 1.1 ± 0.05 | 14 | 33 | 181.1 ± 17.3 | 158 ± 17 | TT |
| | | | I | 210.1 ± 2.7 | 9.8 ± 0.1 | 11.5 ± 0.3 | | | | | | | |
| 16.1/2 | 0.6 | 213 | Y | 71.1 ± 1.7 | 5.7 ± 0.2 | 9.5 ± 4.6 | 11.5 ± 0.4 | 0.7 ± 0.04 | 16 | 26 | 305.5 ± 21.5 | 419 ± 39 | TT |
| | | | I | 130.4 ± 1.8 | 10.6 ± 0.1 | 11.3 ± 0.3 | | | | | | | |
| 16.1/3 | 0.1 | 229 | Y | 39.5 ± 1.4 | 4.9 ± 0.5 | 32.9 ± 10.0 | 13.9 ± 0.2 | 0.7 ± 0.05 | 14 | 13 | 216.5 ± 11.1 | *307 ± 24 | TT |
| | | | I | 49.0 ± 0.9 | 7.5 ± 0.1 | 33.8 ± 0.5 | | | | | | | |
| 16.2/1 | 3.1 | 153 | Y | 6.8 ± 0.6 | 5.1 ± 0.4 | 3.1 ± 1.3 | 3.7 ± 0.1 | 0.3 ± 0.03 | 12 | 28 | 203.6 ± 17.8 | 286 ± 30 | OSL |
| | | | I | | | | | | | | | | |
| 16.3/1 | 2.35 | 168 | Y | 42.4 ± 1.5 | 7.4 ± 0.3 | 6.6 ± 1.0 | 7.6 ± 0.1 | 0.6 ± 0.03 | 22 | 13 | 191.7 ± 11.2 | 588 ± 61 | TT |
| | | | I | 29.9 ± 0.8 | 8.5 ± 0.1 | 5.6 ± 0.2 | | | | | | | |
| 16.4/1 | 2.55 | 164 | Y | 69.6 ± 1.2 | 7.7 ± 0.2 | 8.5 ± 1.6 | 6.3 ± 0.1 | 0.6 ± 0.03 | 21 | 20 | 60.6 ± 2.7 | 99 ± 7 | OSL |
| | | | I | 22.4 ± 0.6 | 7.0 ± 0.1 | 6.8 ± 0.2 | | | | | | | |
| 16.4/2 | 0.6 | 214 | Y | 63.5 ± 1.2 | 6.5 ± 0.2 | 12.9 ± 2.4 | 9.1 ± 0.1 | 0.7 ± 0.04 | 19 | 16 | 78.4 ± 2.9 | 117 ± 8 | OSL |
| | | | I | 54.7 ± 1.1 | 7.2 ± 0.1 | 17.4 ± 0.3 | | | | | | | |
| 16.5/1 | 1.35 | 193 | Y | 15.1 ± 0.6 | 6.4 ± 0.2 | 7.2 ± 1.2 | 6.7 ± 0.1 | 0.5 ± 0.03 | 23 | 19 | 59.0 ± 2.3 | 125 ± 10 | OSL |
| | | | I | 8.6 ± 0.4 | 7.5 ± 0.1 | 5.3 ± 0.2 | | | | | | | |
| 16.5/2 | 0.5 | 217 | Y | 39.3 ± 0.9 | 6.5 ± 0.3 | 9.7 ± 2.1 | 8.3 ± 0.2 | 0.6 ± 0.04 | 22 | 13 | 76.0 ± 2.1 | 128 ± 9 | OSL |
| | | | I | 23.3 ± 0.6 | 4.7 ± 0.1 | 10.5 ± 0.3 | | | | | | | |
| 17.1/1B | 1.05 | 201 | Y | 15.1 ± 0.6 | 7.3 ± 0.3 | 4.0 ± 1.6 | 6.2 ± 0.1 | 0.5 ± 0.03 | 16 | 22 | 153.3 ± 5.6 | 318 ± 25 | TT |
| | | | I | 5.1 ± 0.3 | 7.2 ± 0.1 | 6.7 ± 0.2 | | | | | | | |
| 17.2/1 | 1.9 | 179 | Y | 11.8 ± 1.1 | 6.5 ± 0.1 | 3.7 ± 1.2 | 5.5 ± 0.2 | 0.4 ± 0.03 | 18 | 13 | 157.8 ± 5.4 | 328 ± 26 | OSL |
| | | | I | | | | | | | | | | |
| 17.3/1 | 2.28 | 169 | Y | 33.3 ± 1.2 | 5.7 ± 1.8 | 8.8 ± 2.5 | 8.1 ± 0.1 | 0.5 ± 0.03 | 19 | 16 | 53.1 ± 2.1 | 99 ± 7 | OSL |

6.4 Results from the Nafud palaeolake deposits

All investigated lake deposits overlie white sands of a palaeodune system that differ significantly to the reddish sands of the modern dune system which partly covers the lake deposits. Every stage exists from covered to fully exhumed lake deposits. The lithologic succession of the palaeolake deposits shows great lateral variation with a thickness between 0.3 and 3 m. Figure 6.7 shows a location map of all sites on a digital elevation model, and Figure 6.8 and 6.9 display the sedimentary sections. All sites in the western Nafud are diatomite dominated except for site c16.1. Overall at ten out of 21 sites the lacustrine deposits are partly or completely calcareous. Drawings of the sedimentary sections are grouped according to known or assumed ages of the lake deposits to either Marine Isotope Stage (MIS) 11-9 (427-301 ka; Fig. 6.8) or MIS 5 (127-71 ka; Fig. 6.9).

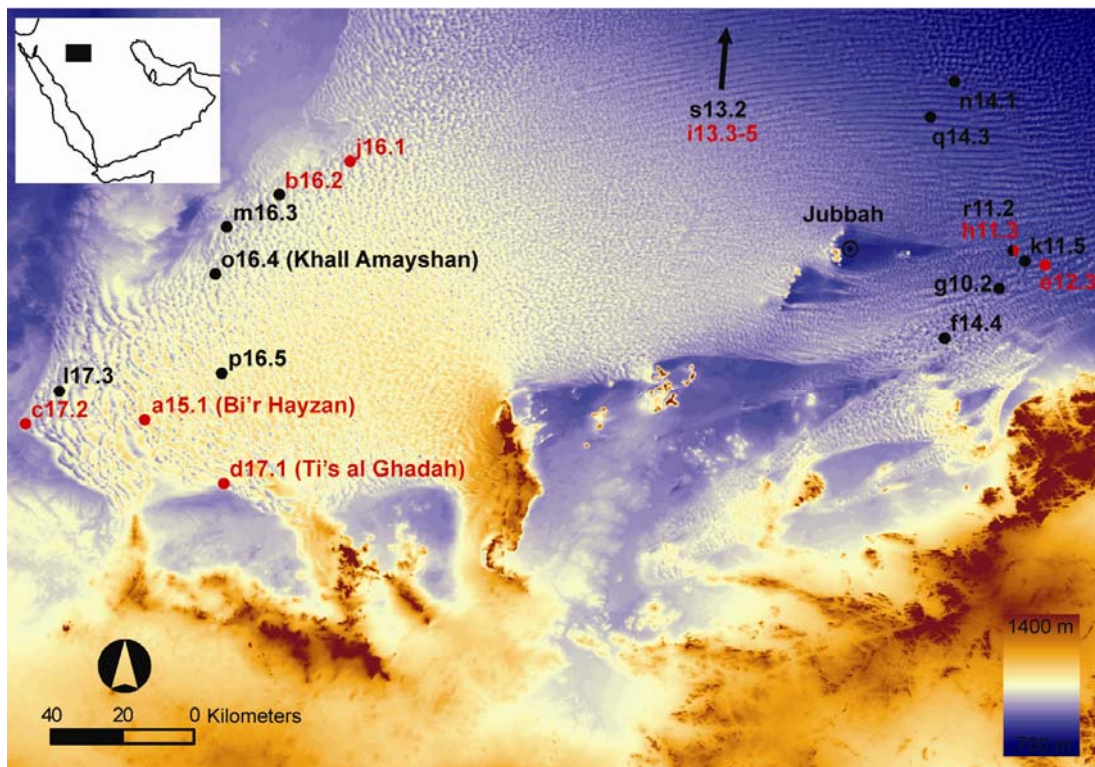


Fig. 6.7. Location of sites in the western Nafud desert. MIS 11-9 sites are in red and MIS 5 sites in black. The underlying digital elevation model (SRTM 90 m DEM from srtm.csi.cgiar.org) shows how the sand is piled onto the base rock.

6.4.1 MIS 11-9 deposits (Fig. 6.8)

All MIS 11-9 diatomites are horizontally bedded, have fine laminae, and show no bioturbation. Eight of the ten sites featuring limestone are from this time period. At site a15.1 (Bi'r Hayzan) a very pure and 2.2 m massive diatomite (Fig. 6.7, Fig. 6.8, Fig. 6.10b and Fig.

6.11) was previously studied by Whitney and Gettings (1982) and Le Nindre (1986) for mining. The deposit is attributed to MIS 9 with an OSL age in the aeolian sand beneath of 366 ± 57 ka and another OSL age of 104 ± 9 ka above. The latter age is separated from the diatomite by an unconformity. Except for the base and the erosional top of the sequence, the internal characteristics are extremely uniform. The entire bed is made up of laminated diatomite with slight variations in colour and in density of iron oxide stains (Fig. 6.10b). No interbeds of sand, silt, clay, or ash exist. While the average number of laminae per centimetre is about 10 in the lowest part, it decreases to about 4 in the upper part. The section is dominated by the diatoms *Stephanodiscus* cf. *rotula* and *Aulacoseira granulata* (Fig. 6.12). Both species indicate fresh and relatively deep water. The lowermost sample is dominated by meroplanktonic *A. granulata*, reflecting slightly shallower and more turbulent conditions. The shift towards the dominance of the euplanktonic *S. rotula* is interpreted as a change towards more stable conditions and deeper water. The lack of periphyton also indicates that the sediment was accumulated in deeper water. The diatomites at site b16.2 and c17.2 show similar laminae to the Bi'r Hayzan diatomite, although slightly less homogenous. The sequence at site c17.2 is continuous and has an OSL age of 369 ± 45 ka at the base. At site b16.2 an unconformity at the base of the lacustrine sequence means that the OSL age of 588 ± 61 ka beneath is a maximum age only.

Another site, d17.1 (Ti's al Ghadah) was previously known for its vertebrate fossil content with an assumed Late Pliocene to Early Pleistocene age. The fauna comprises savannah-like mammals similar to living zebra, wolf and hyena, plus a large fish of 155 cm length, and a tortoise (Thomas et al., 1998). Although these authors only show a rough map, it is possible to identify the place (Location 2) by using the explanatory notes of the geological map of the area (Janjou et al., 1998). The sequence starts with clayey silt containing the fossils, changing gradually into a fine laminated diatomite. On top of the diatomite lies a duricrust with roots and borings. The deposit is attributed to MIS 9 based on an OSL age of 318 ± 24 ka of the aeolian sand beneath. This is in apparent contrast to the higher age estimated from the fossil vertebrate fauna. The ^{13}C isotopic signature in mammal enamel implies an open savannah with arid grassland for the surroundings, however the remains of fish and tortoise suggest a large and permanent water body (Thomas et al., 1998).

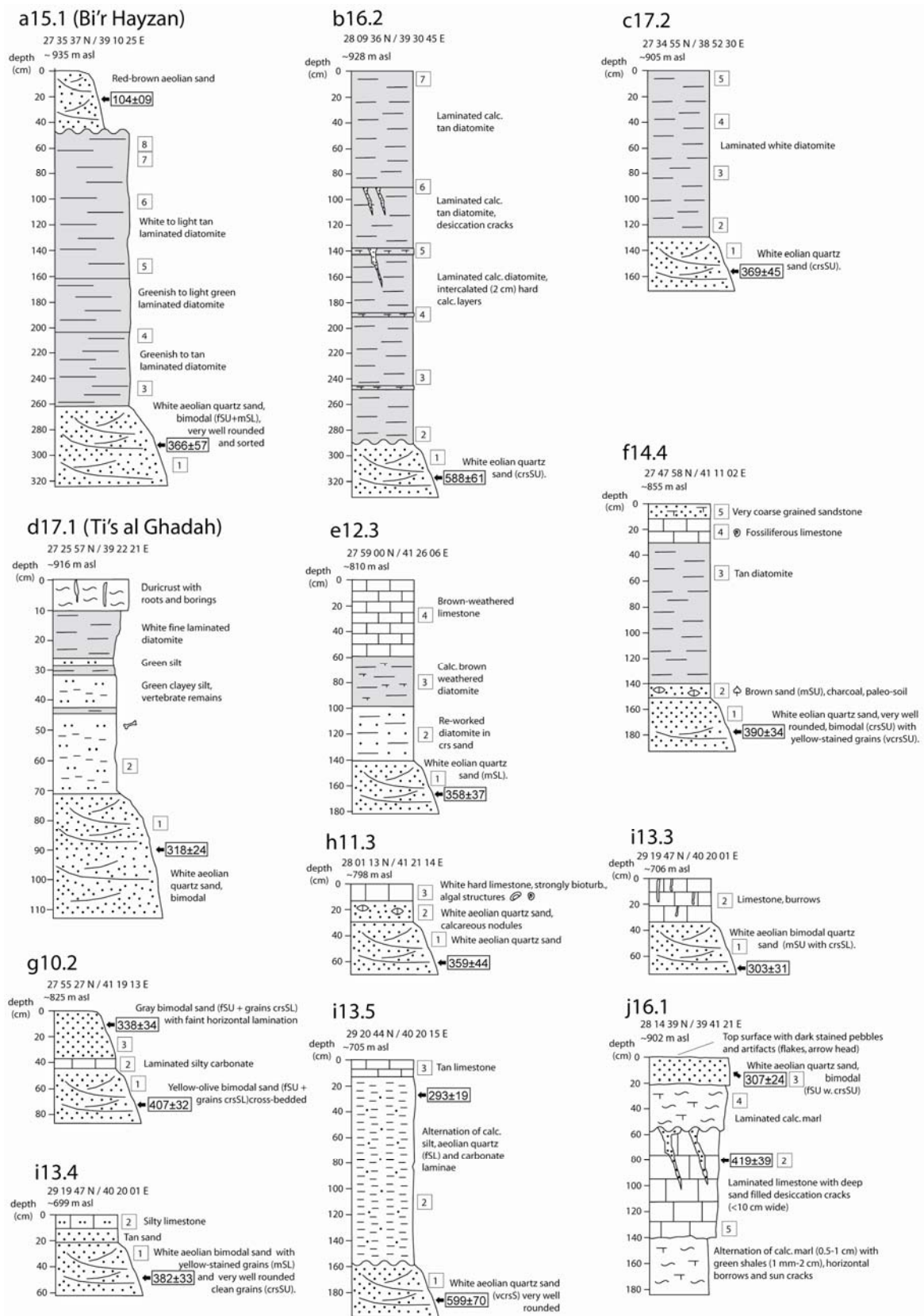


Fig. 6.8. MIS 11-9 sedimentary sections of the Nafud lake deposits. Legend in Fig. 6.9

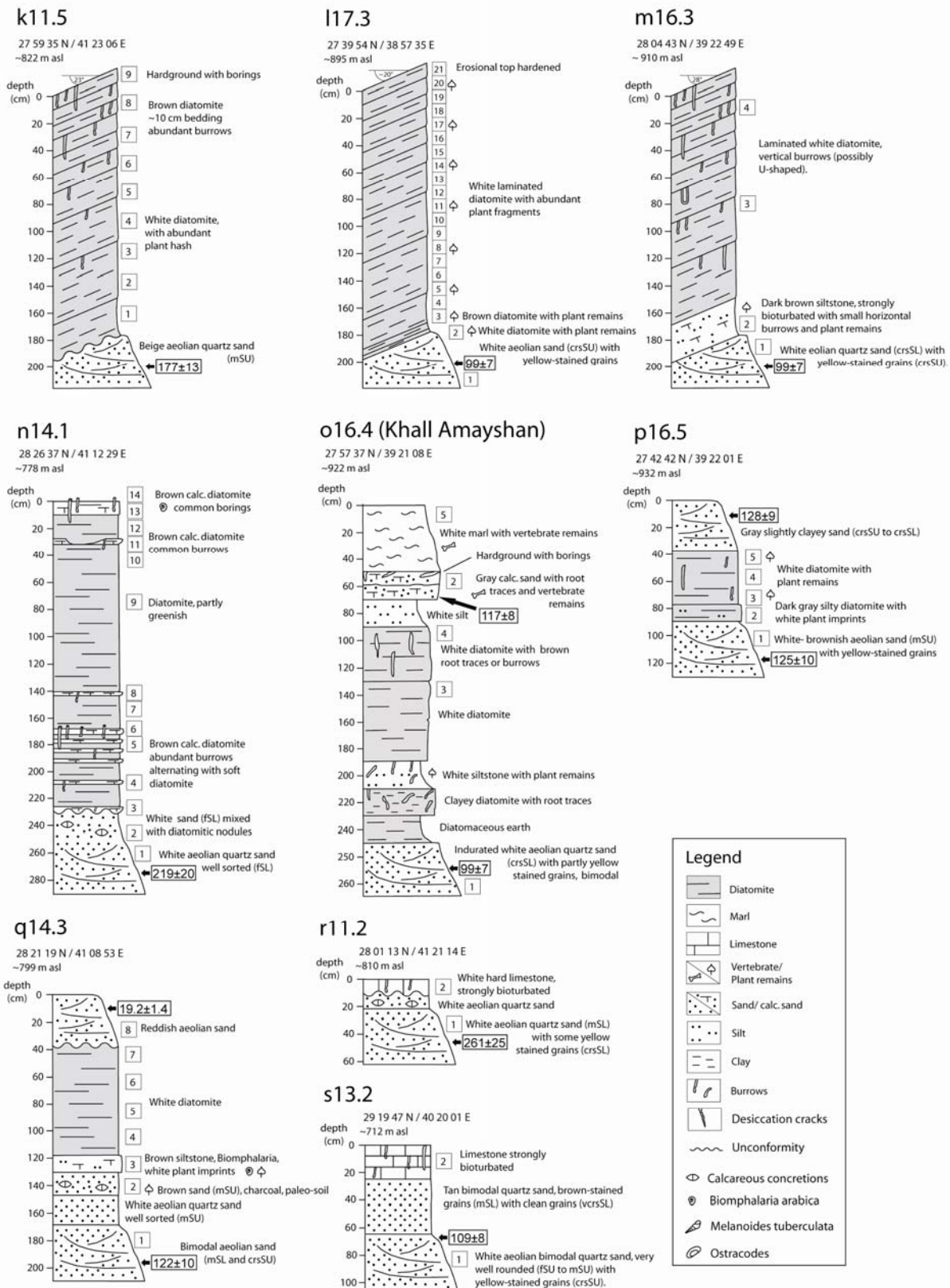


Fig. 6.9. MIS 5 sedimentary sections of the Nafud lake deposits.

At site e12.3 and f14.4 the initially diatomitic sequences turn into limestone indicating a shift from acidic to alkaline conditions. Further limestone containing sequences of MIS 9 age exist at site g10.2, h11.3, i13.3-5 and j16.1. Site j16.1 shows an alternation of calcareous marl (0.5- 1 cm) with green shale (1 mm- 2cm), horizontal burrows and sun cracks followed by a laminated limestone with deep, up to 10 cm wide, sand filled desiccation cracks, with an OSL age of 419 ± 39 ka. The top of the limestone is unconformably overlain by laminated calcareous marl, which is followed by calcified white aeolian bimodal quartz sand with another OSL age of 307 ± 24 ka.

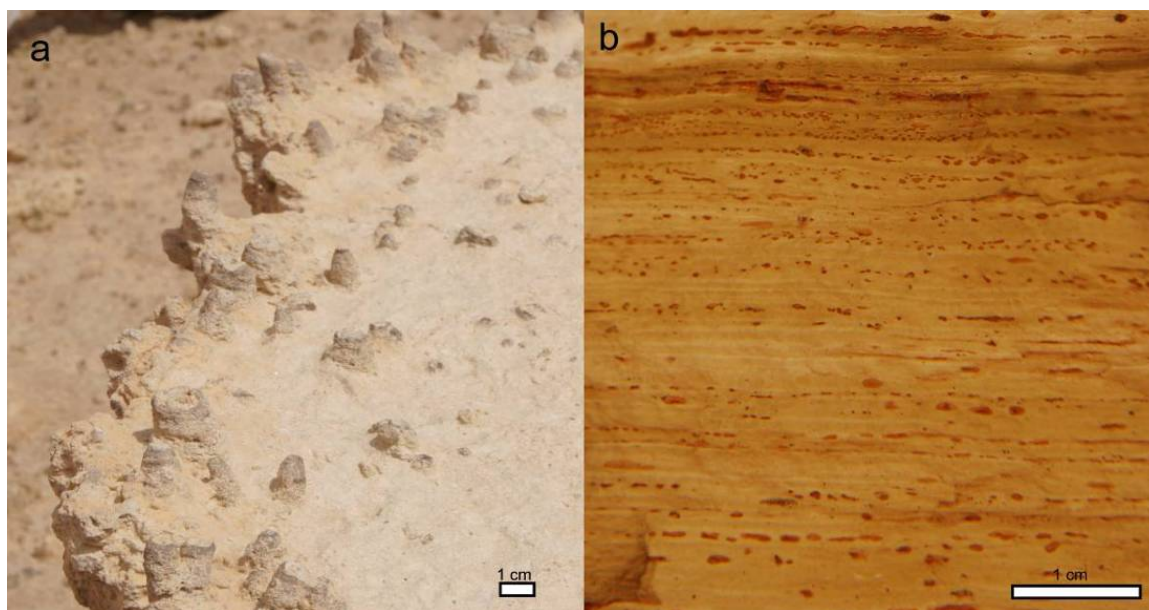


Fig. 6.10. (a) Burrows from section n14.1 possibly of crayfish. (b) Laminations and iron stains from the lower part of section a15.1 (Bi'r Hayzan).

6.4.2 MIS 5 deposits (Fig. 6.9)

Unlike MIS 11-9 deposits vertical burrows (Fig. 6.10a) and plant remains are common features of the MIS 5 diatomites. Three sequences are inclined at angles of 20° to 28° and a complete concave shape is preserved at site k11.5 indicating the shape an interdune lake (Fig. 6.15). Le Nindre (1986) first mentioned the diatomite at site l17.3 in the course of their prospection study. The 2 m massive laminated diatomite with abundant plant fragments and a hardened erosional top is dated using OSL on the aeolian sand beneath to an age of 99 ± 7 ka. The diatomite is dominated by the freshwater species *Fragilaria brevistriata*, *F. construens*, *F. construens v. venter*, *Aulacoseira granulata* and, in the upper part, *Cyclotella ocellata* (Fig. 6.12). The sequence is characterized by a gradual change from periphytic taxa in the lowermost part to planktonic and facultatively planktonic taxa in the upper part. This change reflects a shift towards deeper water, also indicated by the decreasing phytolith to diatom ratio. The two diatomites at sites k11.5 and m16.3 are very similar to l17.3 although

burrows are more abundant, and k11.5 has an unconformity at the base resulting in a higher OSL age of 177 ± 13 ka in the aeolian sand beneath. The burrows are tentatively identified as those of crayfish. At site n14.1 another massive diatomite was identified. With an erosive base and an OSL age of 219 ± 20 ka the deposit is suggested to originate from a humid period during MIS 5. Numerous intercalated calcified layers of diatomite show abundant burrows, which are again tentatively identified as being from crayfish.

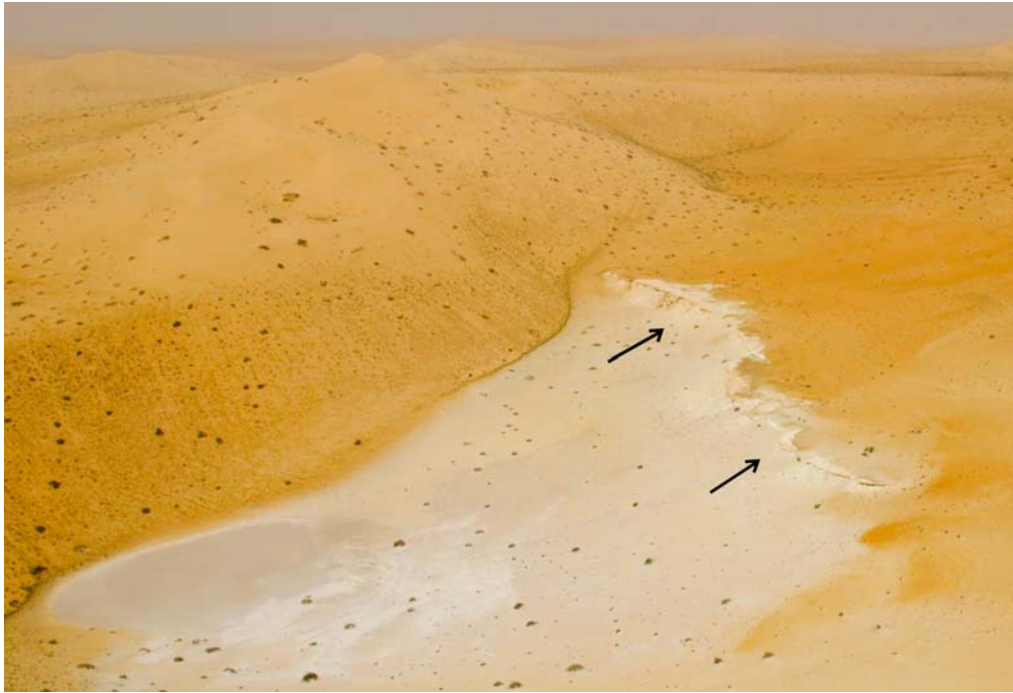


Fig. 6.11. Aerial view of the Bi'r Hayzan diatomite (a15.1) with a view towards NW. The diatomite outcrop (indicated by arrows) is about 30 m vertically above the bottom of the depression (white area) and extends for about 400 m.

Site o16.4 (Khall Amashan) coincides with Locality 1 of Thomas et al. (1998), also known previously for its vertebrate fossil content with an assumed Late Pliocene to Early Pleistocene age. The fauna comprises savannah-like mammals similar to living zebra and buffalo, as well remains of hippo (Thomas et al., 1998). Two OSL ages of 99 ± 7 ka and 117 ± 8 ka nicely constrain the age of the lake deposit at o16.4 (Khall Amayshan). The sequence shows a transition from diatomite in the lower part, to calcareous sand and lake marl in the upper part. In general, the diatom distribution is dominated by *Aulacoseira crenulata*, indicating a shallowing water body and an increase in pH. It is suggested that a decrease in precipitation allowed the formation of the lake marl. The associated diatom assemblage is dominated by periphytic species that may live in carbonate-rich environments (*Anomoeoneis sphaerophora*, *Campylodiscus clypeus*, *Mastogloia* spp, *A. crenulata* and *Meridion circulare*), and reflects an alkaline shallow water body (Fig. 6.12). The alkaline conditions also caused

corrosion of the diatom frustules. The ^{13}C isotopic signature in mammal enamel implies an open savannah with arid grassland for the surroundings, although the remains of hippo suggest a large and permanent water body (Thomas et al., 1998).

A diatomite of only 50 cm thickness at site p16.5 is dated with two OSL ages for the dune sands above (128 ± 9 ka) and below (125 ± 10 ka) the deposit, resulting in a well-defined MIS 5 age. Ten centimetres of dark gray silty diatomite are followed by 40 cm of white diatomite containing plant remains. The section shows a dominance of the freshwater diatoms *Fragilaria brevistriata*, *F. construens*, *F. construens v. venter* and *Aulacoseira granulata* (Fig. 6.13). Aerophilous taxa occur in the lowermost sample together with phytoliths, probably as a result of nearshore conditions, i.e. shallow water. The middle sample indicates deeper water reflected by a decrease in the phytolith percentages and an increase in planktonic and facultatively planktonic taxa. Similar conditions are recorded in the uppermost sample, although the increasing phytolith to diatom ratio indicates a return to more shallow water. This section shows a complete cycle from shallow to deep water, and back to shallow water, within 50 cm of diatomite.

At site q14.3 a small band of white diatomite is perched on a modern dune slope of reddish sand. The sequence is constrained by an OSL age of 122 ± 10 ka beneath the deposit. Another OSL of 19.2 ± 1.4 ka dates the burial of the diatomite by the modern dune system. The lacustrine sequence is dominated by the diatoms *Fragilaria construens* and *F. construens v. venter*. Meso-polysaline (e.g. *Anomeoneis sphaerophora*) and oligosaline taxa (e.g. *Navicula halophila*) occur in the lower and upper part of the sequence (Fig. 6.13). This stratigraphic occurrence is in accordance with aerophilous diatoms and phytoliths, both showing similar stratigraphic distributions. These trends are interpreted as a change from shallow to deep water followed by a return to shallow water. The occurrence of meso-polysaline and oligosaline taxa is thought to be the result of increased evaporation, in combination with decreased precipitation, resulting in an enhancement of ions in the lake water. The occurrence of limestone among the deposits attributed to MIS 5 is limited to site r11.2 and s13.2. At both sites the limestone beds extend less than 30 cm and are highly bioturbated.

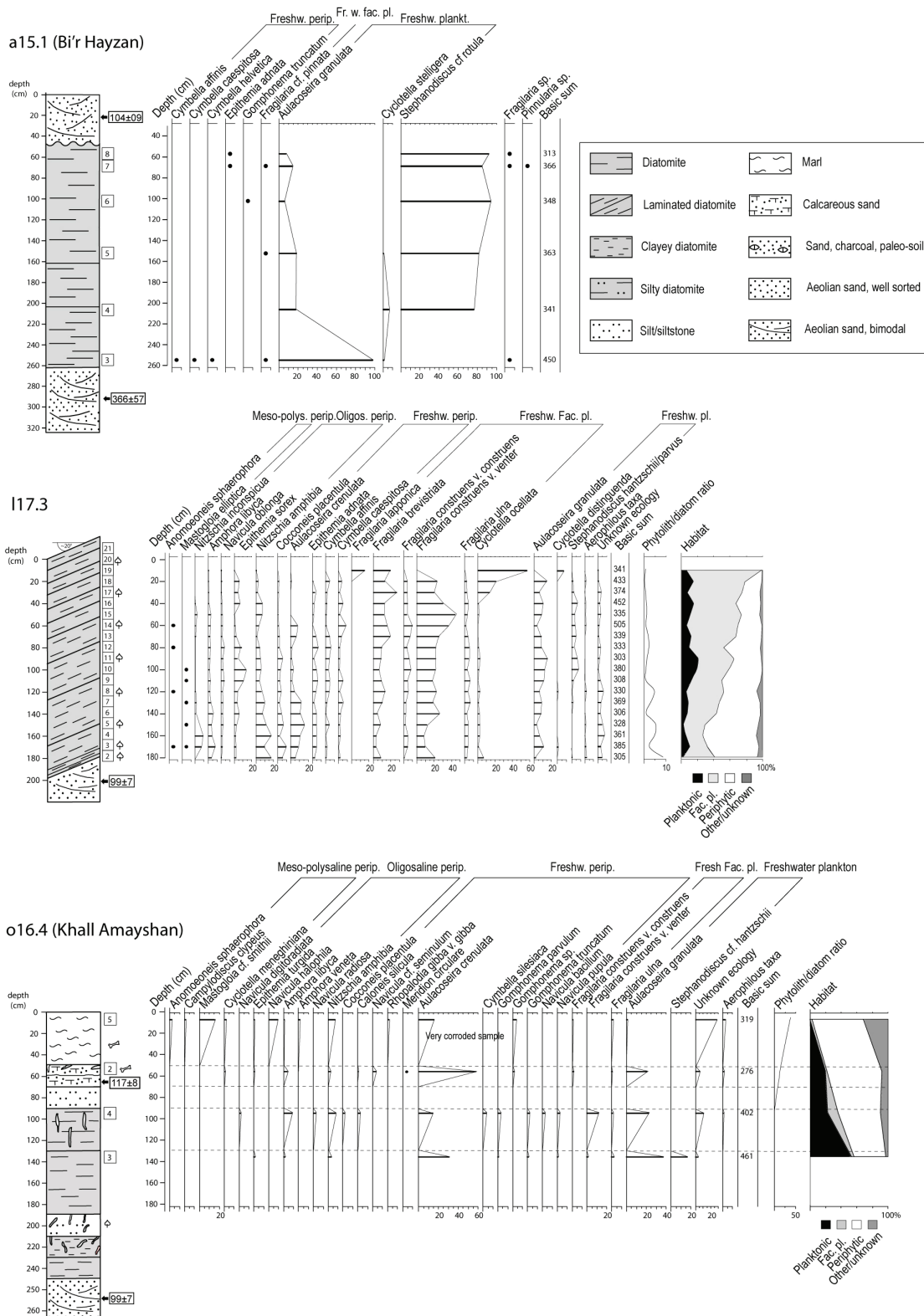


Fig. 6.12. Summary diagrams of diatom analysis. Relative abundances of taxa having percentages $\geq 1\%$ (a15.1 and o16.4) and $\geq 5\%$ (I17.3) in at least one level. At the very right of each diagram: calculation of phytolith/diatom ratio (x100) and habitat preferences of all counted species.

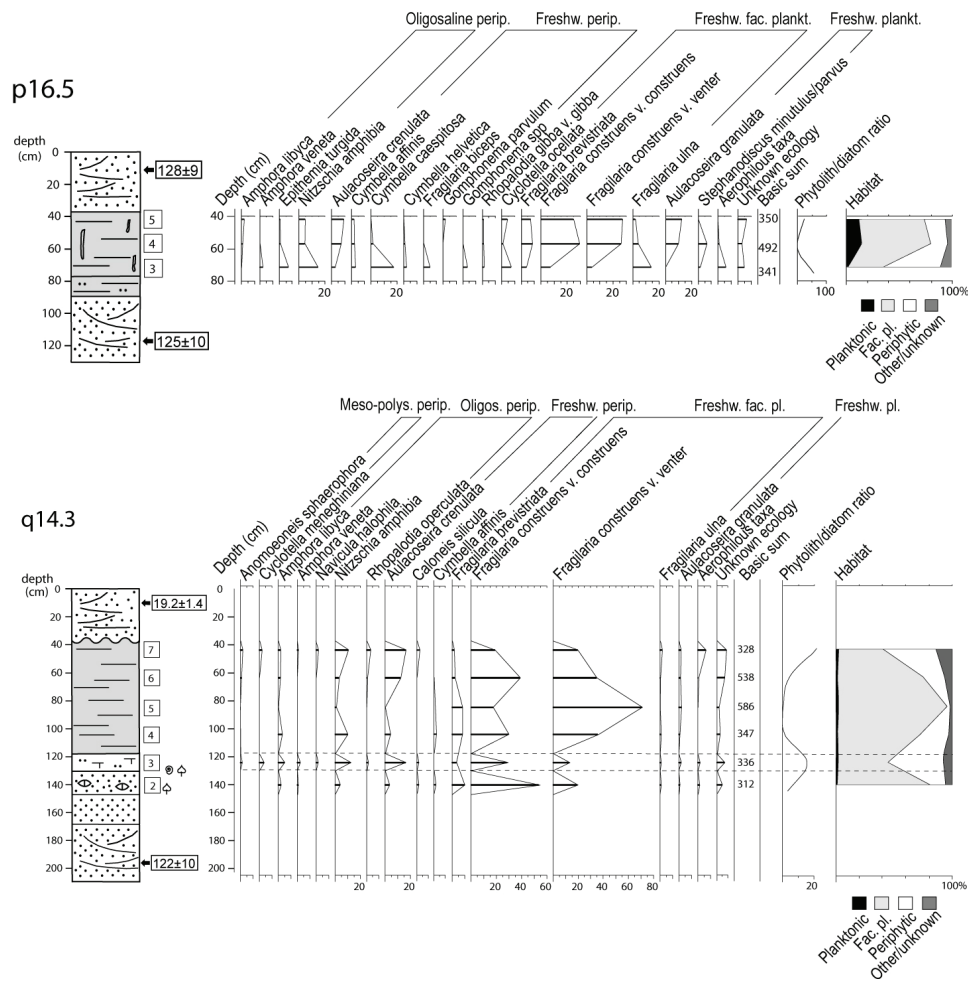


Fig. 6.13. Summary diagrams of diatom analysis. Relative abundances of taxa having percentages $\geq 1\%$ (q14.3 and p16.5) in at least one level. At the very right of each diagram: calculation of phytolith/diatom ratio (x100) and habitat preferences of all counted species.

6.5 Discussion

6.5.1 Pleistocene

All examined palaeolake deposits of the Nafud desert are of Middle to Late Pleistocene age. In Fig. 6.14, OSL ages of the Nafud deposits are plotted together with a compilation of proxy records from the Arabian Peninsula. Humid periods (blue shaded areas) are inferred from OSL ages from within lake deposits and from the population of OSL ages from beneath or above the deposits. The newly derived humid periods are centred in MIS 11, 9, 5e and 5c. The slight scatter of ages between MIS 8 and 6 seen in various archives, suggest that at least short phases of increased precipitation occurred. The OSL age in MIS 2 is the deposition of the reddish modern sand cover above the lake deposit at site q14.3. No lake deposits younger than MIS 5c (~100 ka) were found. Thomas et al. (1998) suggested an Early to Middle Pleistocene age for the Nafud vertebrate fossils now dated to 318 ± 24 and

117±8 ka. One of the reasons that such high ages were proposed is the African affinity of the vertebrate fauna and the missing European aspect. Vertebrate faunas of the Middle East typically have a European affinity from the Middle Pleistocene onwards. Although close to the Middle East climatically, an African affinity of the fauna would still make sense. Our OSL ages do not support a humid period between 40 and 20 ka (Whitney et al., 1983b). The obvious discrepancy between OSL and radiocarbon ages on carbonates and shells is most likely the result of contamination with younger ^{14}C from meteoric water during the Holocene, leading to consistently younger radiocarbon ages. This effect has been reported previously from similar environments (Fontes and Gasse, 1989; Petit-Maire et al., 2010; Rosenberg et al., 2011b).

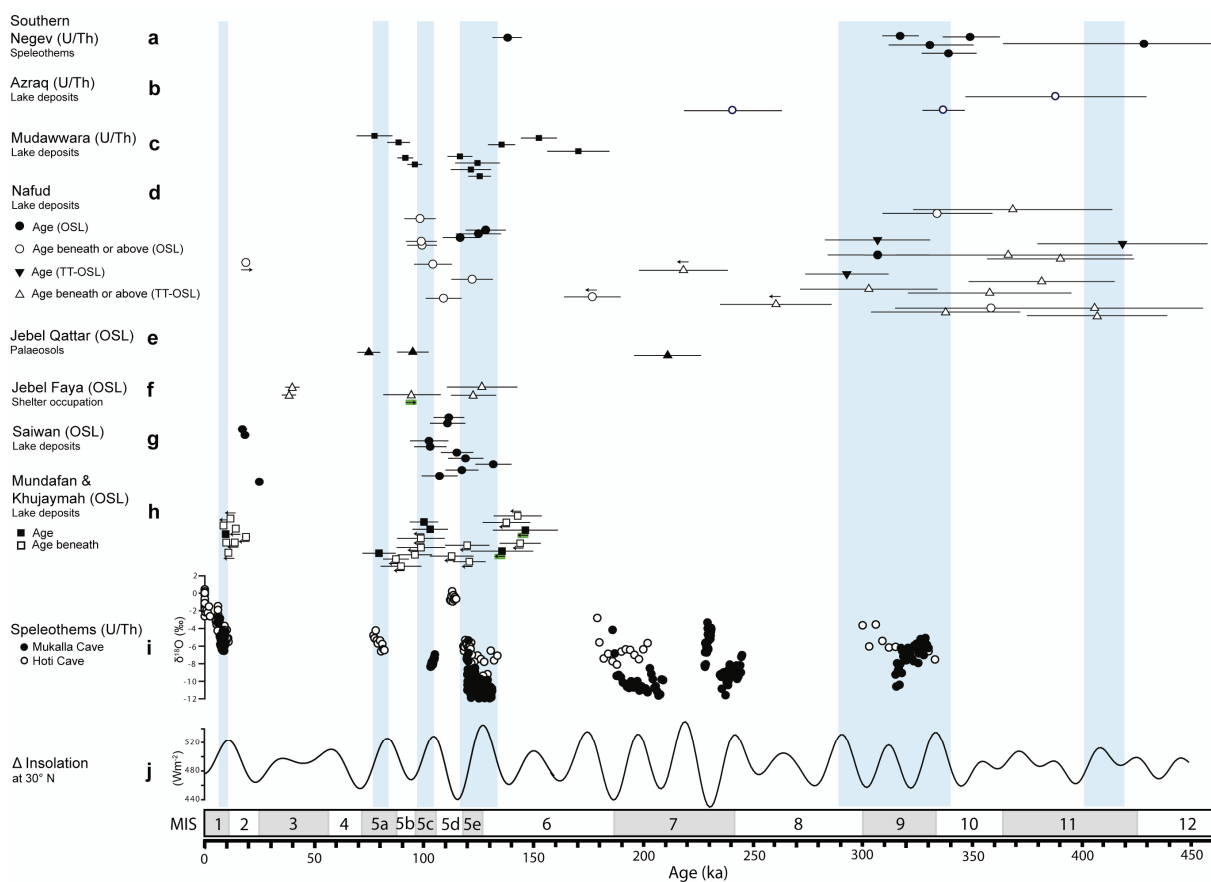


Fig. 6.14. Compilation of proxy records from the Arabian Peninsula. Blue bars represent humid periods. **(a)** U/Th ages from speleothems from the southern Negev desert (Vaks et al., 2010). **(b)** U/Th ages from southern Jordan (Abed et al., 2000). **(c)** U/Th ages from Mudawwara palaeolake, southern Jordan (Petit-Maire et al., 2010). **(d)** OSL ages of this study on the lake deposits of the Nafud desert. Ages from sand beneath or above the lake deposits are displayed as open symbols and ages from within lake deposits are shown as closed symbols. **(e)** OSL ages of Palaeosols near Jubbahh Oasis in the Nafud desert (Petraglia et al., 2011). **(f)** OSL ages from occupation phases at Jebel Faya (Armitage et al. 2011). **(g)** OSL ages from the lake deposits near Saiwan, Oman (Rosenberg et al., in review). **(h)** OSL ages lake deposits at Mundafan and Khujaymah (Rosenberg et al., in press). **(i)** Oxygen isotope ($\delta^{18}\text{O}$) data set from Mukalla and Hoti Cave (Fleitmann et al., 2011). **(j)** Summer insolation for 30°N (Berger and Loutre, 1991). Arrows indicate maximum and minimum ages.

6.5.1.1 MIS 11-9 deposits

The pure diatomite at a15.1 (Bi'r Hayzan), with its undisturbed fine laminae suggest a distal position in a larger lake. Diatoms also indicate deep fresh water in the lower part of the sequence. Assuming each lamination represents one year's deposition, the total time for sedimentation is approximately 1400 years. The large fossil fish (155 cm) found at d17.1 (Ti's al Ghadah) by Thomas et al. (1998) also supports the existence of a large lake. In the course of their reconnaissance study for diatom mining, Le Nindre (1986) postulated that the diatomite deposits extend beneath the entire south-western Nafud. This would imply a large lake covering the whole SW corner of the Nafud desert (Fig. 6.7). Only a dune morphology much less pronounced than today would allow for such a lake. The shape of the MIS 11-9 lake deposits would not contradict this assumption. From facies and digital elevation model (Fig. 6.7) a15.1 (Bi'r Hayzan) represents a central, and d17.1 (Ti's al Ghadah) a nearshore position in the assumed lake.



Fig. 6.15. The bedding of lake deposit k11.5 in the northern Nafud Desert dips towards the centre revealing the shape of a barchanoid interdune depression during the time of deposition. The maximum age for this deposit is 177 ± 13 ka dated on aeolian sand beneath the lake deposit.

6.5.1.2 MIS 5 deposits

From burrows, plant remains, inclined bedding and the diatom assemblages we infer generally small lakes governed by a variation in precipitation for the MIS 5 lake deposits. The concave shape of an interdune lake conserved at site k11.5 (Fig. 6.15) supports the interpretation of rather small lakes scattered in interdune depressions. Schultz and Whitney

(1986) analyzed the pollen spectra of some of the lake deposits and found that in general during the Pleistocene there were perennial fresh water lakes in contrast to the swampy Holocene lake reported from Jubbah. Pollen and plant remains led them to conclude that environmental changes never reached beyond a semi desert or savannah-like environment.

6.5.2 Early Holocene

As reported by Whitney et al. (1983b) and Engel et al. (2011) early Holocene lake deposits exist at Tayma- and Jubbah Oasis. At these places ground water was available a few meters below the surface up to historic times (Garrard et al., 1981). Apart from the oases, presumably no lakes existed in the Nafud desert during the early Holocene. Similarly, no Holocene deposits are reported from Mudawwara in southern Jordan (Petit-Maire et al., 2010), or speleothem deposition in the southern Negev desert (Vaks et al., 2010). Arz et al. (2003) concluded from sediment cores of the northernmost Red Sea, that monsoonal rains did not reach northern Arabia during the early to mid-Holocene. In the south of the peninsula at Hawa in the SW Rub' al Khali, Lézine et al. (2010) assume that the Holocene lake deposits were fed by wadi runoff and groundwater rather than by precipitation directly. This assumption matches with our observation from the Saudi side of the Rub' al Khali, where Holocene lake deposits occur preferentially in the peripheral region of the desert close to wadi systems, while the Pleistocene deposits are also found in the interior of the desert.

If one compares the radiocarbon dated onset of Holocene lake formation at Mundafan (9.6 ka; Rosenberg et al., in press) to that 300 km away to the south at Hawa (~11 ka; Lézine et al., 2010), there is a south-north time lag for the onset, supporting the evidence of Fleitmann et al. (2004) recorded in speleothems between Qunf cave (10.6 ka) and Hoti cave (10.0 ka). At Awafi in the UAE the onset of lake formation is even as late as at 8.5 ka (Parker et al., 2004).

6.5.3 Palaeoclimate implications

A comparison with speleothem records of the southern Negev desert (Vaks et al., 2010) shows a very similar timing for humid periods. The agreement with the southern Negev and disagreement with the central and northern Negev makes a Mediterranean moisture source unlikely and suggests the origin of humidity is from enhanced monsoon circulation. Considering the more traditional idea of an oscillating ISM monsoon it is difficult to explain how tropical humidity could reach as far north as the Nafud- and Negev desert. Models, however, proposed by Herold and Lohmann (2009) for Eemian (MIS 5e) moisture transport involve an increased participation of an Atlantic source of humidity. Their simulations show an increased precipitation over Africa between 10°N and 20°N and in the entire Red Sea

region (Fig. 6.16). Compared to the modern (pre-industrial) wind flow regime, with hardly any zonal component, the Eemian zonal wind component is present throughout the African continent bringing moisture from the Atlantic Ocean to Arabia. This model is further supported by the synchronous timing of MIS 9, 5e and 5c humid periods with speleothem growth in Oman (Fleitmann et al., 2003b). Since most of the Pleistocene African monsoon records do not match the Arabian climate records such a setting may have existed only during limited times of very particular conditions. According to the model of Herold and Lohmann (2009) the southern Levant would not receive additional precipitation (Fig. 6.16) and could possibly act as a natural barrier for human migrations, explaining why AMH dispersed first into Asia, and only later into Europe. Furthermore this scenario could also explain the absence of European faunal elements in the fossil vertebrate fauna of the Nafud desert.

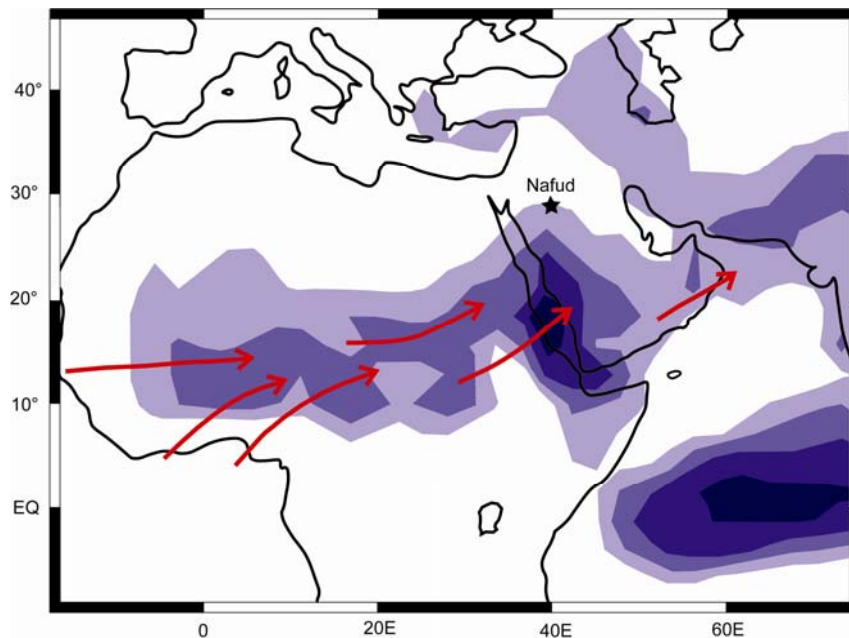


Fig. 6.16. Modelled anomalies (125 ka compared to pre-industrial) of annual mean precipitation in colour steps of 20 mm/month. Adapted from Herold and Lohmann (2009).

6.6 Conclusions

The first comprehensive chronology for Nafud palaeolake deposits shows humid periods centred on MIS 11, 9, 5e and 5c, with possibly some minor humid periods during MIS 8-6. No Pleistocene lake deposits younger than ~100 ka were found, and the new chronology does not therefore support a humid period between 40 and 20 ka as suggested by Whitney et al. (1983). The fossil faunas described by Thomas et al. (1998) were re-dated to 318 ± 24 (Locality 2) and 117 ± 8 ka (Locality 1). Geomorphology and environmental proxies suggest

larger and deeper lakes for MIS 11-9 than for MIS 5. It seems, however, that environmental changes never reached beyond a semi desert or savannah type environment. Based on a model proposed by Herold and Lohmann (2009) we speculate that the southern Levant remained dry and acted as a barrier for human migration during the MIS 5e humid period. Such a scenario could explain the African affinity but missing European aspect of the fossil vertebrate fauna and possibly the delayed migration of AMH into Europe. In the future it may be useful to investigate the Sinai Peninsula for the presence of lake deposits.

Acknowledgments

We thank A. Wetzel for the visual identification of burrows and Sally Lowick for constructive comments on earlier versions of the manuscript. This research is funded by the Swiss National Science Foundation (project 200021-117985/1) and fieldwork by the Saudi Geological Survey.

6.7 References

- Abed, A. M., Yasin, S., Sadaqa, R., and Al-Hawari, Z. (2008). The paleoclimate of the eastern desert of Jordan during marine isotope stage 9. *Quaternary Research* 69, 458-468.
- Armitage, S. J., Jasim, S. A., Marks, A. E., Parker, A. G., Usik, V. I., and Uerpmann, H.-P. (2011). The Southern Route "Out of Africa": Evidence for an Early Expansion of Modern Humans into Arabia. *Science* 331, 453-456.
- Arz, H. W., Lamy, F., Patzold, J., Muller, P. J., and Prins, M. (2003). Mediterranean Moisture Source for an Early-Holocene Humid Period in the Northern Red Sea. *Science* 300, 118-121.
- Ballarini, M., Wallinga, J., Wintle, A. G., and Bos, A. J. J. (2007). A modified SAR protocol for optical dating of individual grains from young quartz samples. *Radiation Measurements* 42, 360-369.
- Battarbee, R.W. (1986). Diatom analysis. In: B. E. Berglund (ed.): *Handbook of Holocene Palaeoecology and Palaeohydrology*, 527-570. John Wiley & Sons, Chichester.
- Berger, A., and Loutre, M. F. (1991). Insolation values for the climate of the last 10 million years. *Quaternary Science Reviews* 10, 297-317.
- Blechs Schmidt, I., Matter, A., Preusser, F., and Rieke-Zapp, D. (2009). Monsoon triggered formation of Quaternary alluvial megafans in the interior of Oman. *Geomorphology* 110, 128-139.
- Burns, S. J., Fleitmann, D., Matter, A., Neff, U., and Mangini, A. (2001). Speleothem evidence from Oman for continental pluvial events during interglacial periods. *Geology* 29, 623-626.
- Clemens, S. C., and Prell, W. L. (2003). A 350,000 year summer-monsoon multi-proxy stack from the Owen Ridge, Northern Arabian Sea. *Marine Geology* 201, 35-51.
- Duller, G. A. T., Botter-Jensen, L., and Murray, A. S. (2003). Combining infrared- and green-laser stimulation sources in single-grain luminescence measurements of feldspar and quartz. *Radiation Measurements* 37, 543-550.
- Edgell, H. S. (2006). *Arabian deserts: nature, origin and evolution*, Dordrecht, The Netherlands, Springer, 592 p.
- Engel, M., Brückner, H., Pint, A., Wellbrock, K., Ginau, A., Voss, P., Grottker, M., Klasen, N., and Frenzel, P. (in press). The early Holocene humid period in NW Saudi Arabia - Sediments, microfossils and palaeo-hydrological modelling. *Quaternary International*, doi:10.1016/j.quaint.2011.04.028.
- Fleitmann, D., Burns, S. J., Pekala, M., Mangini, A., Al-Subbary, A., Al-Aowah, M., Kramers, J., and Matter, A. (2011). Holocene and Pleistocene pluvial periods in Yemen, southern Arabia. *Quaternary Science Reviews* 30, 783-787.

-
- Fleitmann, D., Burns, S. J., Mangini, A., Mudelsee, M., Kramers, J., Villa, I., Neff, U., Al-Subbary, A. A., Buettner, A., Hippler, D., and Matter, A. (2007). Holocene ITCZ and Indian monsoon dynamics recorded in stalagmites from Oman and Yemen (Socotra). *Quaternary Science Reviews* 26, 170-188.
- Fleitmann, D., Burns, S. J., Neff, U., Mudelsee, M., Mangini, A., and Matter, A. (2004). Palaeoclimatic interpretation of high-resolution oxygen isotope profiles derived from annually laminated speleothems from Southern Oman. *Quaternary Science Reviews* 23, 935-945.
- Fleitmann, D., Burns, S. J., Mudelsee, M., Neff, U., Kramers, J., Mangini, A., and Matter, A. (2003a). Holocene Forcing of the Indian Monsoon Recorded in a Stalagmite from Southern Oman. *Science* 300, 1737-1739.
- Fleitmann, D., Burns, S. J., Neff, U., Mangini, A., and Matter, A. (2003b). Changing moisture sources over the last 330,000 years in Northern Oman from fluid-inclusion evidence in speleothems. *Quaternary Research* 60, 223-232.
- Fogg, T., Fogg, P., and Waltham, T. (2002). Magharat Qasir Hafit, a significant cave in the United Arab Emirates. *Tribulus* 12, 5-14.
- Fontes, J. C., and Gasse, F. (1989). On the ages of humid Holocene and Late Pleistocene phases in North Africa -- Remarks on "Late Quaternary climatic reconstruction for the Maghreb (North Africa)" by P. Rognon. *Palaeogeography, Palaeoclimatology, Palaeoecology* 70, 393-398.
- Forster, P., and Matsumura, S. (2005). *EVOLUTION: Enhanced: Did Early Humans Go North or South?* *Science* 308, 965-966.
- Galbraith, R. F. (1990). The radial plot: graphical assessment of spread in ages. *Nucl. Tracks Radiat. Meas.* 17, 207-214.
- Galbraith, R. F., Roberts, R. G., Laslett, G. M., Yoshida, H., and Olley, J. M. (1999). Optical dating of single and multiple grains of Quartz from Jinmium rock shelter, Northern Australia: Part I, Experimental design and statistical models. *Archaeometry* 41, 339-364.
- Garrard, A. N., Harvey, C. P. D., and Switsur, V. R. (1981). Environment and settlement during the Upper Pleistocene and Holocene at Jubba in the Great Nefud, northern Arabia. *Atlatl* 5, 137-148.
- Gasse, F. (1987). Diatoms for reconstructing palaeoenvironments and paleohydrology in tropical semi-arid zones. Example of some lakes from Niger since 12 000 BP. *Hydrobiologia* 154, 127-163.
- Gasse, F., Juggins, S. and Ben Khelifa, L. (1995). Diatom-based transfer functions for inferring past hydrochemical characteristics of African lakes. *Palaeogeography, Palaeoclimatology, Palaeoecology* 117, 31-54.
- Gasse, F. (2000). Hydrological changes in the African tropics since the Last Glacial Maximum. *Quaternary Science Reviews* 19, 189-211.

- Håkansson, H. (2002). A compilation and evaluation of species in the general *Stephanodiscus*, *Cyclostephanos* and *Cyclotella* with a new genus in the family *Stephanodisceae*. *Diatom Research* 17, 1-139.
- Håkansson, H. & Meyer, B. (1994). A comparative study of species in the *Stephanodiscus niagarae*-complex and a description of *S. heterostylus* sp. nov. *Diatom Research* 9, 65-85.
- Håkansson, H. & Kling, H. (1989). A light electron microscope study of previously described and new *Stephanodiscus* species (*Bacillariophyceae*) from central and Northern Canadian lakes, with ecological notes on species. *Diatom Research* 4, 269-288.
- Herold, M., and Lohmann, G. (2009). Eemian tropical and subtropical African moisture transport: an isotope modelling study. *Climate Dynamics* 33, 1075-1088.
- Hunt, C. O., Elrishi, H. A., Gilbertson, D. D., Grattan, J., McLaren, S., Pyatt, F. B., Rushworth, G., and Barker, G. W. (2004). Early-Holocene environments in the Wadi Faynan, Jordan. *The Holocene* 14, 921-930.
- Janjou, D., Halawani, M. A., Roobol, M. J., Memesh, A., Razin, P., Shorbaji, H., and Roger, J. (1998). "Explanatory Notes to the Geologic Map of the Jibal al Misma Quadrangle, Sheet 27d, Kingdom of Saudi Arabia." Ministry of Petroleum and Mineral Resources, Jiddah, Saudi Arabia.
- Krammer, K. & Lange-Bertalot, H. (1986). *Bacillariophyceae* 1. Teil *Naviculaceae*. In: Ettl, H., Gerloff, J., Heynig, H. & Mollenhauser, D. (eds.): *Süßwasserflora von Mitteleuropa* 2/1, 876 pp. Gustav Fischer Verlag. Stuttgart.
- Krammer, K. & Lange-Bertalot, H. (1988). *Bacillariophyceae* 2. Teil *Bacillariaceae*, *Epithemiaceae*, *Surirellaceae*. In: Ettl, H., Gerloff, J., Heynig, H. & Mollenhauser, D. (eds.): *Süßwasserflora von Mitteleuropa* 2/2, 596 pp. Gustav Fischer Verlag. Stuttgart.
- Krammer, K. & Lange-Bertalot, H. (1991a). *Bacillariophyceae* 3. Teil *Centrales*, *Fragilariaceae*, *Eunotiaceae*. In: Ettl, H., Gerloff, J., Heynig, H. & Mollenhauser, D. (eds.): *Süßwasserflora von Mitteleuropa* 2/3, 576 pp. Gustav Fischer Verlag. Stuttgart.
- Krammer, K. & Lange-Bertalot, H. (1991b). *Bacillariophyceae* 4. Teil *Achnanthaceae*. *Kritische Ergänzungen zu Navicula (Lineolate) und Gomphonema*. In: Ettl, H., Gerloff, J., Heynig, H. & Mollenhauser, D. (eds.): *Süßwasserflora von Mitteleuropa* 2/4, 437 pp. Gustav Fischer Verlag. Stuttgart.
- Kulig, G. (2005). *Preparation of a Software for Age Determination by Means of Luminescence Techniques (Faculty of Mathematics Informatics, Technische Universität Freiberg, Germany) (in German)*.
- Le Nindre, Y. M. (1986). *Exploration for diatomite in the Great Nafud: a sedimentologica guideline*. In "Open-File Report BRGM-OF-06-34." pp. 34. Saudi Arabian Deputy Ministry for Mineral Resources, Jiddah.
- Lézine, A.-M., Robert, C., Cleuziou, S., Inizan, M.-L., Braemer, F., Saliège, J.-F., Sylvestre, F., Tiercelin, J.-J., Crassard, R., Méry, S., Charpentier, V., and Steimer-Herbet, T.

(2010). *Climate change and human occupation in the Southern Arabian lowlands during the last deglaciation and the Holocene*. *Global and Planetary Change*.

Macaulay, V., Hill, C., Achilli, A., Rengo, C., Clarke, D., Meehan, W., Blackburn, J., Semino, O., Scozzari, R., Cruciani, F., Taha, A., Shaari, N. K., Raja, J. M., Ismail, P., Zainuddin, Z., Goodwin, W., Bulbeck, D., Bandelt, H.-J., Oppenheimer, S., Torroni, A., and Richards, M. (2005). *Single, Rapid Coastal Settlement of Asia Revealed by Analysis of Complete Mitochondrial Genomes*. *Science* 308, 1034-1036.

McClure, H. A. (1976). *Radiocarbon chronology of late Quaternary lakes in the Arabian Desert*. *Nature* 263, 755-756.

McClure, H. A. (1984). *"Late Quaternary palaeoenvironments of the Rub' Al-Khali*. Unpublished PhD Thesis, University College, London, 245p."

McLaren, S. J., Al-Juaidi, F., Bateman, M. D., and Millington, A. C. (2008). *First evidence for episodic flooding events in the arid interior of central Saudi Arabia over the last 60 ka*. *Journal of Quaternary Science* 24, 198-207.

Mellars, P. (2006). *Going East: New Genetic and Archaeological Perspectives on the Modern Human Colonization of Eurasia*. *Science* 313, 796-800.

Morales, E.A. (2001). *Morphological studies in selected fragilarioid diatoms (Bacillariophyceae) from Connecticut waters (U.S.A.)*. *Proceedings of the Academy of Natural Sciences of Philadelphia* 151, 105-120.

Murray, A. S., and Wintle, A. G. (2000). *Luminescence dating of quartz using an improved single-aliquot regenerative-dose protocol*. *Radiation Measurements* 32, 57-73.

Neff, U., Burns, S. J., Mangini, A., Mudelsee, M., Fleitmann, D., and Matter, A. (2001). *Strong coherence between solar variability and the monsoon in Oman between 9 and 6 kyr ago*. *Nature* 411, 290-293.

Oppenheimer, S. (2009). *The great arc of dispersal of modern humans: Africa to Australia*. *Quaternary International* 202, 2-13.

Parker, A. G., Davis, C., and Wilkinson, T. (2006a). *The early to mid-Holocene moist period in Arabia: some recent evidence from lacustrine sequences in eastern and south-western Arabia*. *Proceedings of the Seminar for Arabian Studies* 36, 243-255.

Parker, A. G., Goudie, A. S., Stokes, S., White, K., Hodson, M. J., Manning, M., and Kennet, D. (2006b). *A record of Holocene climate change from lake geochemical analyses in southeastern Arabia*. *Quaternary Research*, 465-476.

Parker, A. G., Preston, G., Walkington, H., and Hodson, M. J. (2006c). *Developing a framework of Holocene climatic change and landscape archaeology for the lower Gulf region, southeastern Arabia*. *Arabian Archaeology and Epigraphy* 17, 125-130.

Parker, A. G., Eckersley, L., Smith, M. M., Goudie, A. S., Stokes, S., Ward, S., White, K., and Hodson, M. J. (2004). *Holocene vegetation dynamics in the northeastern Rub' al-Khali desert, Arabian Peninsula: a phytolith, pollen and carbon isotope study*. *Journal of Quaternary Science*, 665-676.

- Paull, T.M., Hamilton, P.B., Gajewski, K. and LeBlanc, M. (2008). Numerical analysis of small Arctic diatoms (Bacillariophyceae) representing the *Stausosira* and *Stausosirella* species complexes. *Phycologia* 47, 213-224.
- Petit-Maire, N., Carbonel, P., Reyss, J. L., Sanlaville, P., Abed, A., Bourrouilh, R., Fontugne, M., and Yasin, S. (2010). A vast Eemian palaeolake in Southern Jordan (29°N). *Global and Planetary Change* 72, 368-373.
- Petraglia, M. D., and Alsharekh, A. (2003). The Middle Palaeolithic of Arabia: Implications for modern human origins, behaviour and dispersals. *Antiquity* 77, 671-684.
- Petraglia, M. D., Alsharekh, A. M., Crassard, R., Drake, N. A., Groucutt, H., Parker, A. G., and Roberts, R. G. (2011). Middle Paleolithic occupation on a Marine Isotope Stage 5 lakeshore in the Nefud Desert, Saudi Arabia. *Quaternary Science Reviews* 30, 1555-1559.
- Porat, N., Duller, G. A. T., Roberts, H. M., and Wintle, A. G. (2009). A simplified SAR protocol for TT-OSL. *Radiation Measurements* 44, 538-542.
- Prescott, J. R., and Hutton, J. T. (1994). Cosmic ray contributions to dose rates for luminescence and ESR dating: Large depths and long-term time variations. *Radiation Measurements* 23, 497-500.
- Preusser, F., and Kasper, H. U. (2001). Comparison of dose rate determination using high-resolution gamma spectrometry and inductively coupled plasma - mass spectrometry. *Ancient TL* 19, 19-23.
- Radies, D., Hasiots, S. T., Preusser, F., Neubert, E., and Matter, A. (2005). Paleoclimatic significance of Early Holocene faunal assemblages in wet interdune deposits of the Wahiba Sand Sea, sultanate of Oman. *Journal of Arid Environments* 62, 109-125.
- Rosenberg, T. M., Preusser, F., Fleitmann, D., Schwalb, A., Penkman, K., Schmid, T. W., Kadi, K., Al-Shanti, M. A., and Matter, A. (2011a). Humid periods in southern Arabia - windows of opportunity for modern human dispersal. *Geology* 39, 1115-1118.
- Rosenberg, T. M., Preusser, F., and Wintle, A. G. (2011b). A comparison of single and multiple aliquot TT-OSL data sets for sand-sized quartz from the Arabian Peninsula. *Radiation Measurements* 46, 573-579.
- Sanlaville, P. (1992). Changements climatiques dans la péninsule arabique durant le Pléistocène supérieure et l'Holocène. *Paléorient* 18, 5-26.
- Schulz, E., and Whitney, J. W. (1986). Upper Pleistocene and Holocene lakes in the An Nafud, Saudi Arabia. *Hydrobiologia* 143, 175-190.
- Theriot, E. & Stoermer, E.F. 1984. Principal component analysis of variation in *Stephanodiscus rotula* and *S. niagarae* (Bacillariophyceae). *Systematic Botany* 9, 53-59.
- Thomas, H., Geraads, D., Vaslet, D., Memesh, A., Billiou, D., Bocherens, H., Dobigny, G., Eisenmann, V., Gayet, M., France de Lapparent de, B., Petter, G., and Halawani, M. (1998). First Pleistocene faunas from the Arabian Peninsula: An Nafud desert, Saudi

Arabia. Comptes Rendus de l'Académie des Sciences - Series IIA - Earth and Planetary Science 326, 145-152.

Vaks, A., Bar-Matthews, M., Matthews, A., Ayalon, A., and Frumkin, A. (2010). Middle-Late Quaternary paleoclimate of northern margins of the Saharan-Arabian Desert: reconstruction from speleothems of Negev Desert, Israel. *Quaternary Science Reviews* 29, 2647-2662.

Whitney, J. W. (1983a). *Erosional history and surficial geology of western Saudi Arabia. United States Geological Survey Technical Record* 04-1.

Whitney, J. W., Faulkender, D. J., and Rubin, M. (1983b). *The environmental history and present condition of Saudi Arabia's northern sand seas. USGS Open-File Report* 83-749, 42.

Whitney, J. W., and Gettings, M. E. (1982). *Preliminary geological investigation of the Bir Hayzan diatomite deposit, Kingdom of Saudi Arabia. In "Saudi Arabian Deputy Ministry for Mineral Resources." Open-File Report USGS OF-02-7*

7 Conclusions and outlook

The main focus of this PhD study was on re-dating the Pleistocene relict lake deposits in the Arabian deserts using OSL. The few previous studies of the 80s relied on radiocarbon ages, which were contaminated and systematically underestimated the real ages. As about 25% of all collected samples were out of range of the standard OSL SAR protocol (Murray and Wintle, 2000) due to saturation of the fast signal, a recently published thermally-transferred OSL (TT-OSL) SAR protocol (Porat et al., 2009) has been extensively tested. The main conclusions for the samples under consideration are that the protocol can be used when the expected doses lie between ~100 and ~300 Gy. For doses above ~300 Gy the lack of proportionality observed between the TT-OSL and related OSL sensitivity measurement results in incorrect D_e determination. The divergent sensitivity change can be minimized by using dose response curves, which have only two regeneration doses; this is possible because doses of up to 500 Gy lie well within the linear part of the TT-OSL dose response curve. Application of the new TT-OSL protocol allowed dating of an additional 25 samples, out of a total of 85 samples, and supported 16 samples close to the dating limit of OSL.

Having developed a robust TT-OSL protocol, dating of all known Arabian relict lake deposits became possible. A first study in southern Arabia (Mundafan and Khujaymah) revealed humid phases with a savannah like environment at ~80 ka (MIS 5a), ~100 ka (MIS 5c) and ~125 ka (MIS 5e) in good agreement with periods of enhanced speleothem growth in Oman (Hoti Cave) and Yemen (Mukalla Cave) (Fleitmann et al., 2011). During these humid periods the region was suitable for occupation by anatomically modern humans (AMH).

A second study on fluvial and lacustrine deposits in the interior of Oman near Saiwan, indicates a humid period between 132 and 104 ka. The rich archaeological evidence in the vicinity of the deposits suggests substantial human occupation. Interestingly, the lithic traditions of the archaeological material show no clear relation to coeval findings from neighbouring areas, placing a question mark on the origin of the culture found at Saiwan. This raises new questions in the context of the discussion on trans-Arabian migrations at times of AMH dispersal out of Africa.

A third study on relict lake deposits in the Great Nafud desert of northern Saudi Arabia resulted in the first comprehensive chronology of the Nafud relict lake deposits. OSL and TT-OSL ages indicate humid periods centered at ~410 and ~320, 125 and 100 ka. Interestingly, no relict lake deposits younger than ~100 ka have been found, except in Jubbah and Tayma where ground water was present up to historic times (Engel et al., 2011;

Garrard et al., 1981). A comparison with speleothem records of the southern Negev desert (Vaks et al., 2010) shows a very similar timing for humid periods. The agreement with the southern Negev and disagreement with the central and northern Negev makes a Mediterranean moisture source unlikely and suggests the origin of humidity is from enhanced monsoon circulation. A new circulation model of Herold and Lohmann (2009) indicates strong zonal winds of the African monsoon at 125 ka, allowing Atlantic moisture to reach Arabia. The correlation of the Pleistocene humid periods in the Nafud desert with speleothem growth in Oman (Fleitmann et al., 2003b) also suggest a common moisture source. Based on the model of Herold and Lohmann (2009), we further speculate that the southern Levant remained dry and acted as a barrier for human migration during the MIS 5e humid period. Such a scenario could explain the African affinity but missing European aspect of the fossil vertebrate fauna and possibly the delayed migration of AMH into Europe. Situated between existing clusters of palaeoclimate archives, the results from the Nafud relict lake deposits contribute towards filling the spatial and temporal gaps in the Arabian climate archives.

In the future it may be useful to extend this spatial and temporal approach to fill the remaining gaps in the regional climate record. Spatially, it will be important to find archives in the central part of the Arabian Peninsula and on the Sinai Peninsula. Dating efforts should aim at better age control on the relict lake deposits. A small improvement when using existing OSL methodology could be to always sample the deposit itself, as well as the sand beneath. The experience of this thesis shows, that in this environment even the purest diatomite contains enough quartz grains to attempt OSL dating. Particularly interesting for further dating efforts are long lacustrine sequences such as Bi'r Hayzan. If continuous sampling of long sequences could be achieved, this would allow high resolution isotopic profiles and perhaps a comparison with speleothem records.

7.1 References

- Engel, M., Brückner, H., Pint, A., Wellbrock, K., Ginau, A., Voss, P., Grottker, M., Klasen, N., and Frenzel, P. (in press). The early Holocene humid period in NW Saudi Arabia - Sediments, microfossils and palaeo-hydrological modelling. *Quaternary International*, doi:10.1016/j.quaint.2011.04.028.
- Fleitmann, D., Burns, S. J., Pekala, M., Mangini, A., Al-Subbary, A., Al-Aowah, M., Kramers, J., and Matter, A. (2011). Holocene and Pleistocene pluvial periods in Yemen, southern Arabia. *Quaternary Science Reviews* 30, 783-787.
- Garrard, A. N., Harvey, C. P. D., and Switsur, V. R. (1981). Environment and settlement during the Upper Pleistocene and Holocene at Jubba in the Great Nefud, northern Arabia. *Atlatl* 5, 137-148.
- Herold, M., and Lohmann, G. (2009). Eemian tropical and subtropical African moisture transport: an isotope modelling study. *Climate Dynamics* 33, 1075-1088.
- Murray, A. S., and Wintle, A. G. (2000). Luminescence dating of quartz using an improved single-aliquot regenerative-dose protocol. *Radiation Measurements* 32, 57-73.
- Porat, N., Duller, G. A. T., Roberts, H. M., and Wintle, A. G. (2009). A simplified SAR protocol for TT-OSL. *Radiation Measurements* 44, 538-542.

Appendix A

Conference contributions

Oral presentations

- 26 Jul 2011 Evidence for pre-Holocene humid phases from lacustrine deposits on the Arabian Peninsula, *INQUA 2011, Bern, Switzerland*.
- 20 Jul 2011 Pre-Holocene palaeolakes in the Arabian deserts, *International Workshop: Climate change and prehistoric occupation of the Arabian Peninsula, University of Bern, Switzerland*.
- 07 Nov 2010 When was it wet on the Arabian Peninsula?, *German LED Meeting 2010, University of Innsbruck, Austria*.
- 27 Aug 2009 Aeolian quartz from Saudi Arabia with OSL-ages to beyond the Eemian. First results from a Palaeoclimate study on lakebeds, *UK Luminescence and ESR Meeting 2009, Royal Holloway University of London, UK*.
- 09 Jun 2009 „Neuere“ Klimageschichte der Rub' Al Khali, Saudi Arabien rekonstruiert aus fossilen Seeablagerungen, *Seminar am Institut für Umweltgeologie, TU Braunschweig, Germany*.
- 02 Nov 2008 Aeolian quartz from Saudi Arabia: Preliminary results from a Palaeoclimate study on lakebeds, *German LED Meeting 2008, Leipzig, Germany*.
- 01 Jul 2008 Aeolian quartz from Saudi Arabia: First tests and discussion of palaeodose distributions, *2nd International Symposium on Luminescence, Port Elizabeth, South Africa*.
- 21 Apr 2008 Paleoclimate History of the Rub' Al-Khali, Saudi Arabia: Humid phases recorded in Lake Deposits, *EuroCLIMATE Spring School, Piran, Slovenia*.

Posters

- 24 Jan 2011 Humid periods on Arabia - time windows for out of Africa migration of modern humans, *CH-QUAT bi-annual meeting on Geo&Archaeology, Bern, Switzerland*.
- 09 Sep 2010 Humid periods on Arabia - time windows for out of Africa migration of modern humans, *UK TL\OSL\ESR Meeting 2010, University of Oxford, UK*.
- 23 Apr 2008 Lake deposits in Saudi Arabian deserts, *EuroCLIMATE Spring School, Piran, Slovenia*.

Appendix B

A comparison of single and multiple aliquot TT-OSL data sets for sand-sized quartz from the Arabian Peninsula

Thomas M. Rosenberg, Frank Preusser, Ann G. Wintle

Preheat plateau and dose recovery test for OSL SAR protocol

Variation of D_e with preheat temperature

At different preheat temperatures the aliquots will undergo varying amounts of sensitivity change during the SAR procedure. Testing a series of preheat temperatures allows one to assess whether the D_e values remain constant over a certain range of temperatures, and, if not, to select the most suitable preheat temperature for a particular set of samples. The results of the preheat test for sample 8322.2/7 are displayed in Figure S1. The preheat of the regenerated dose was kept for 10 s while the preheat of the test dose was a hanging cut-heat (20°C lower and for 0 s). The data in Figure S1 shows a plateau from 240 to 280°C, suggesting to take preheat temperature in that range. The chosen preheat temperature was 260°C.

Dose recovery test at chosen preheat temperature

The successful recovery of a known radiation dose is a fundamental assumption of the OSL SAR protocol. A dose recovery test checks whether a known laboratory dose can be obtained through subsequent construction of a growth curve using the OSL measurements of the SAR protocol.

Thirty-six aliquots (6 mm) of sample 8322.2/7 were bleached at room temperature for 250 seconds, then stored for 10k seconds and bleached again for 250 seconds (Wintle and Murray, 2006). Subsequently the aliquots received a dose of 106 Gy. The dose response curve was constructed using doses of 80, 106 and 130 Gy, and a recycling dose of 106 Gy. A test dose of 12 Gy was used. The natural dose of sample 8322.2/7 is 92 ± 3 Gy, estimated from 26 aliquots. As in the preheat test, a hanging cut-heat was used for the chosen preheat temperature of 260°C. The results of the dose recovery test are shown in Figure S2. . An

average ratio of the measured to given dose of 0.99 demonstrates that the applied protocol is able to recover a laboratory dose of the given size.

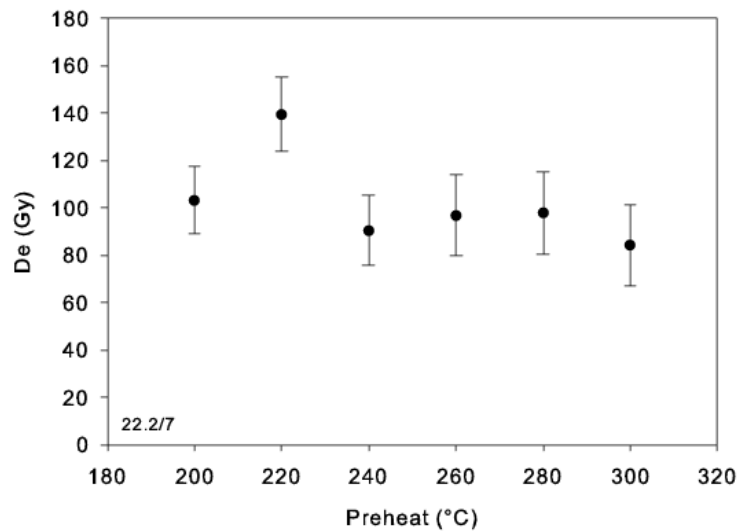


Fig. S1. Preheat test for sample 8322.2/7. A hanging cut-heat was used for the preheat of the test dose. The aliquot size was 6 mm. Averages of six aliquots with standard errors are shown.

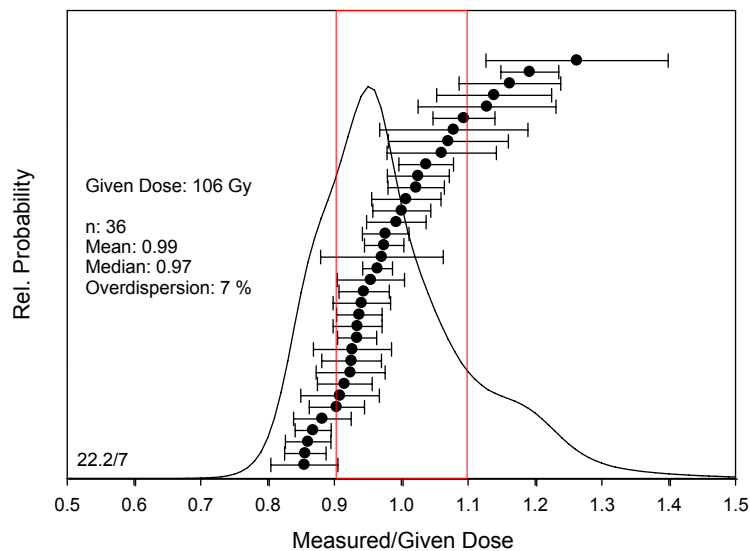


Fig. S2. Dose recovery test of sample 8322.2/7 with a natural D_e of 92 ± 3 Gy and a given dose to recover of 106 Gy. Shown are the ratios of the measured to given dose as well as the enveloping curve of the summed normal distributions. For each D_e a normal distribution was calculated with the D_e as the central value and the error as the standard deviation.

Appendix C

Faunal evidence of a Holocene pluvial phase in Southern Arabia with remarks on the morphological variability of *Helenina anderseni*

Giordana Gennari, Thomas M. Rosenberg, Silvia Spezzaferri, Jean-Pierre Berger, Dominik Fleitmann, Frank Preusser, Mahmoud Al-Shanti and Albert Matter

Taxonomic notes on *Helenina anderseni* (Warren).

***Helenina anderseni*, morphotype A.** The test of this type is calcareous, finely perforate, generally small to very small in size. The trochospire is low and consists of about two whorls. Six to eight chambers gradually increasing in size as added are present in the last whorl. On the umbilical side successive chambers extend toward the umbilicus producing umbilical flaps which conceal the umbilicus. The profile is subcircular and the peripheral margin is rounded. The sutures on the spiral side are tangential and deeply incised. On the umbilical side, sutures are curved to tangential. Elongated and slit-like supplementary apertures are present along the sutures on both sides. The primary aperture is a very umbilical-extraumbilical low arch at the base of the last chamber. The two small openings at the base of the apertural face as described in Warren (1957) are probably the opening along the insertion of the lobe like extension of the last chamber on the umbilical side.

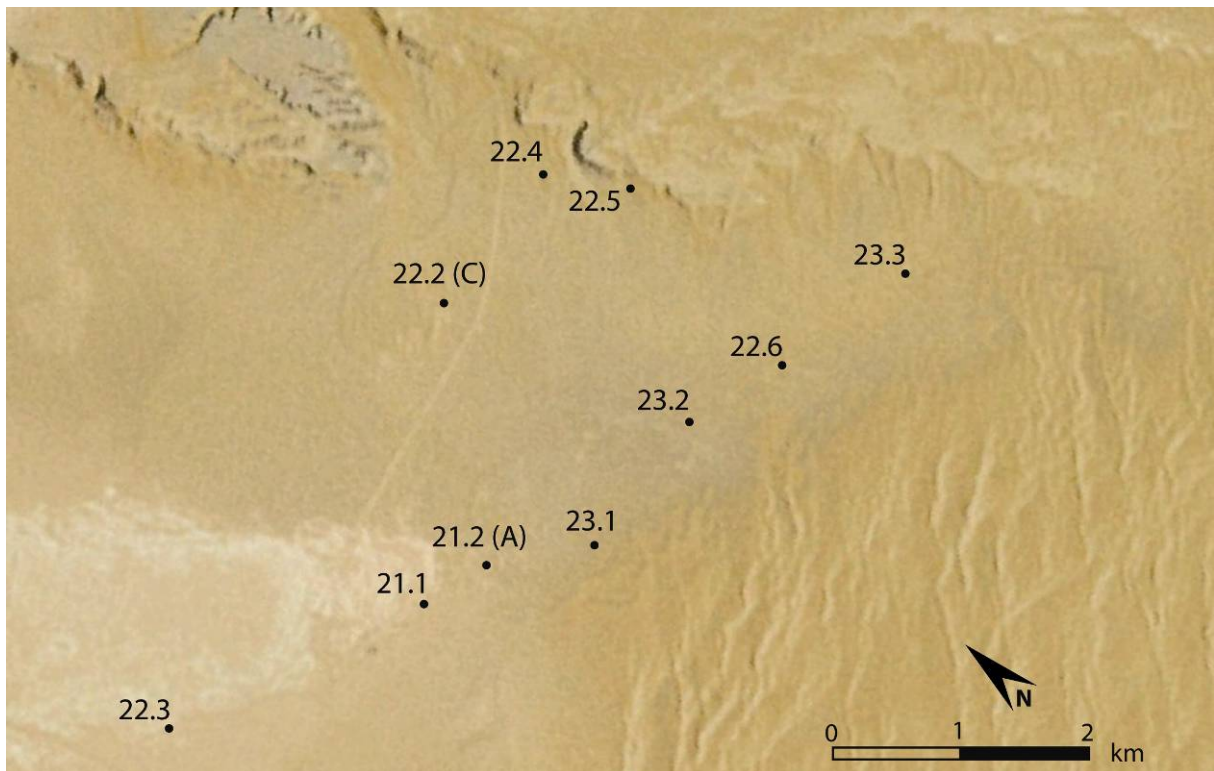
***Helenina anderseni*, morphotype B.** The test of this type is calcareous, finely to moderately coarsely perforate, small to very small in size. The trochospire is low and consists of two whorls. Six to eight chambers are present in the last whorl and increase rapidly in size as added. The profile is oval and the peripheral margin is rounded. The sutures on the spiral and umbilical sides are straight to slightly curved and deeply incised. Elongated and wide supplementary apertures are present along the sutures on both sides. The primary aperture is a very umbilical-extraumbilical low arch at the base of the last chamber. A flap-like prolongation of the chambers in the last whorl extends on the umbilical side and conceals the umbilicus.

Appendix D

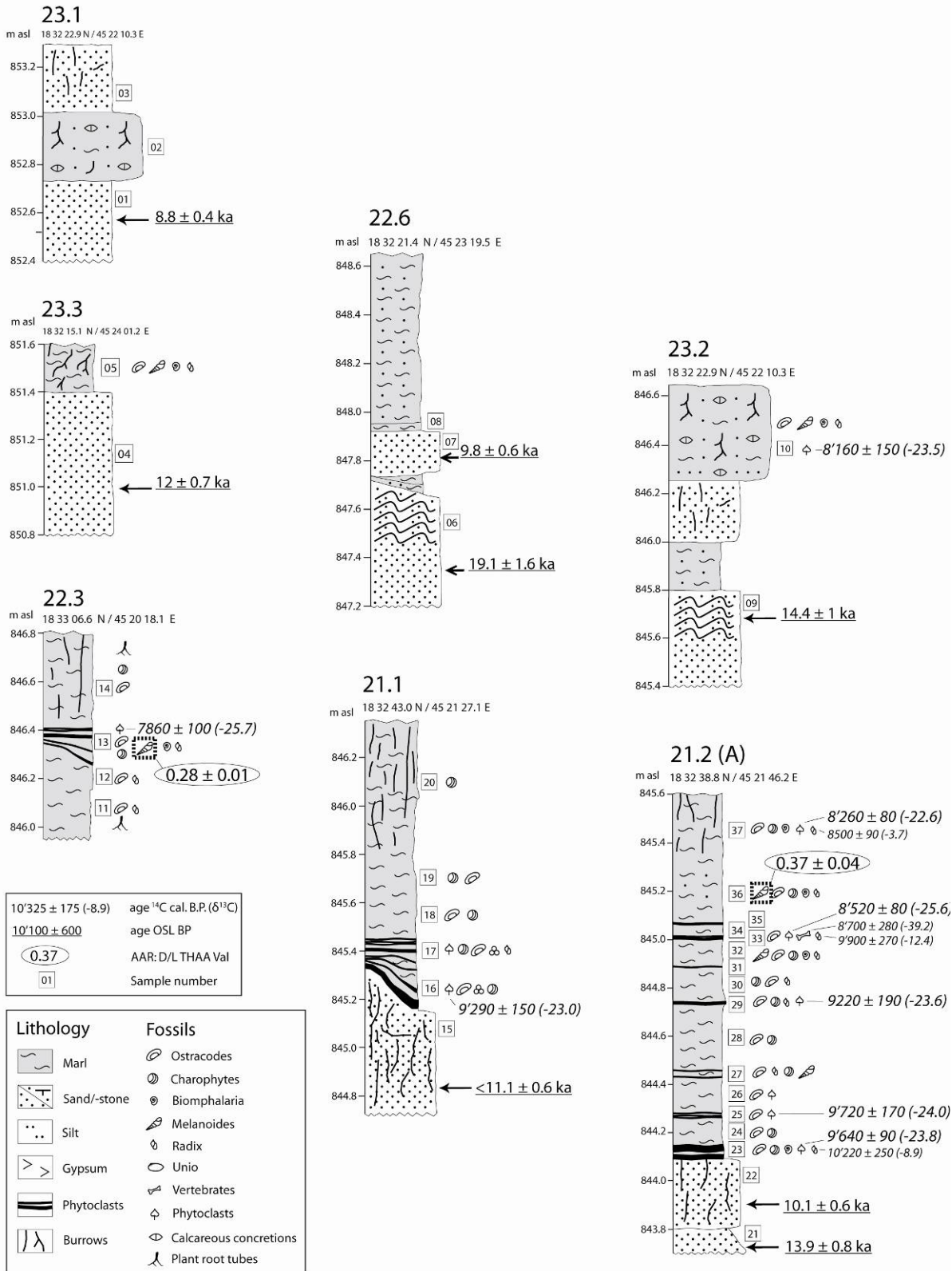
Humid periods in southern Arabia: windows of opportunity for modern human dispersal

*Thomas M. Rosenberg, Frank Preusser, Dominik Fleitmann, Antje Schwalb, Kirsty Penkman,
Thomas W. Schmid, Mahmoud Al-Shanti, Khalid Kadi, Albert Matter*

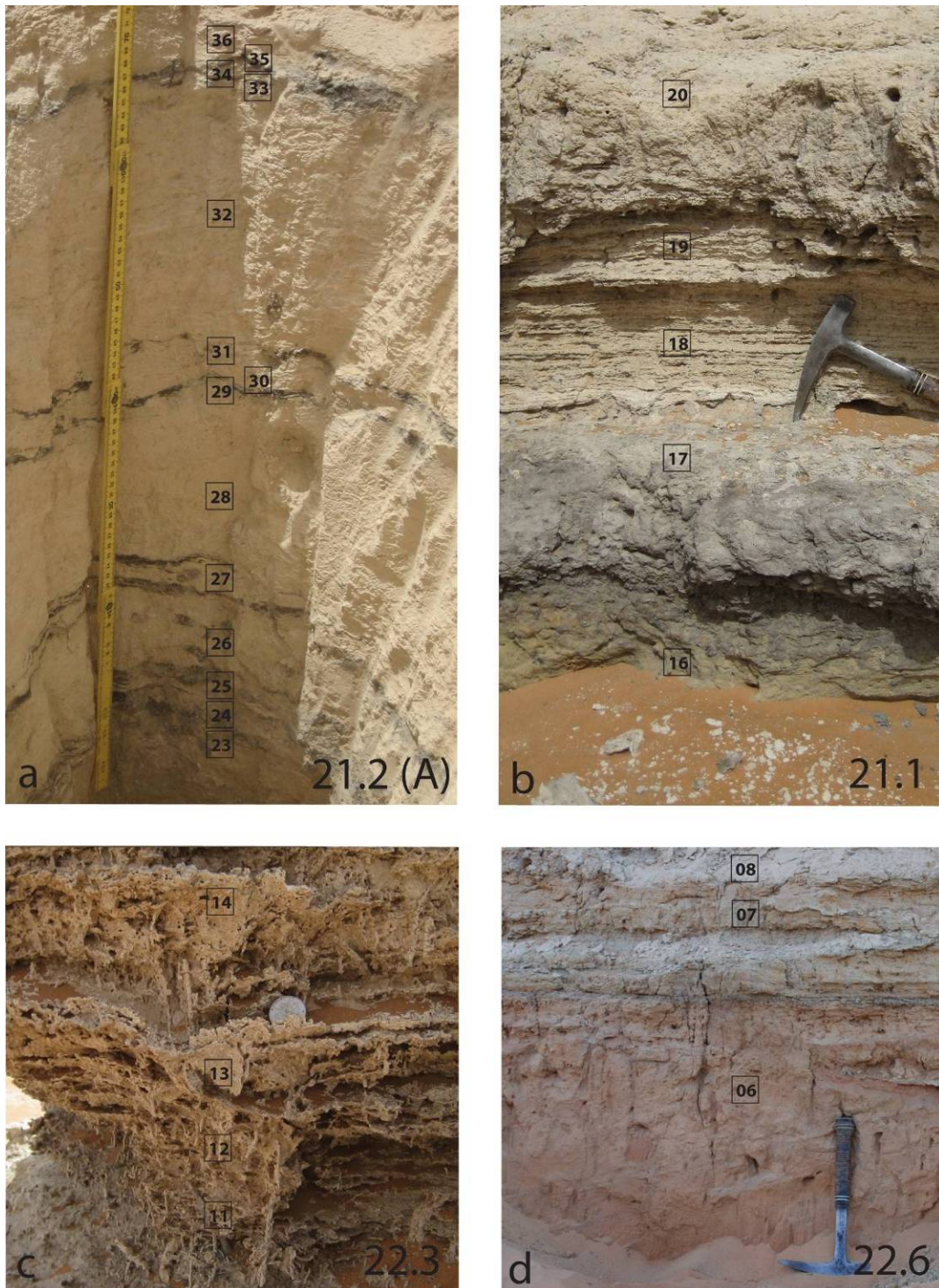
Supplementary Figures



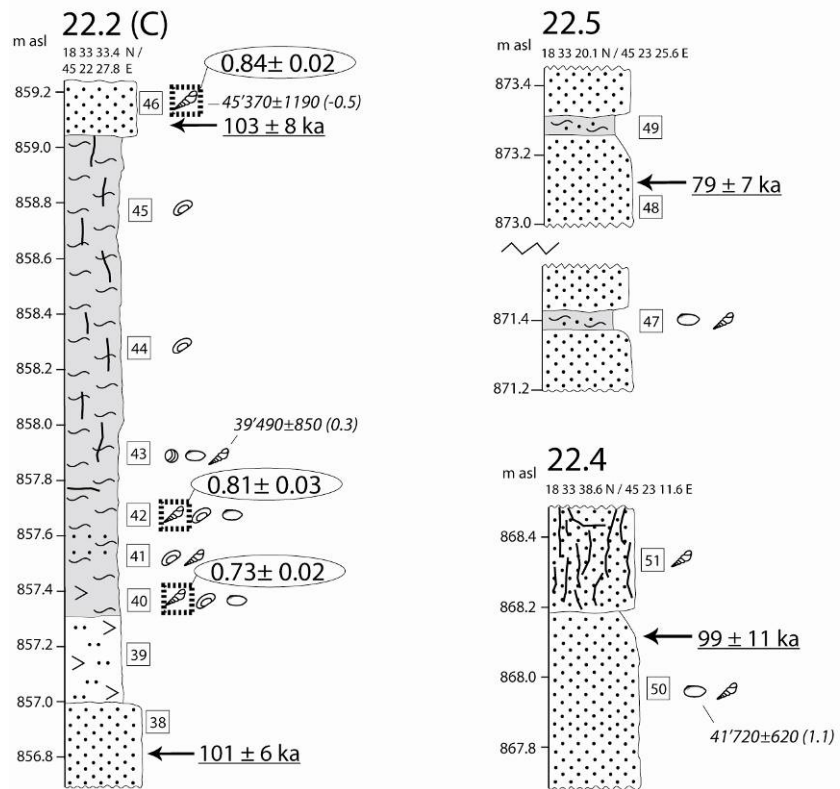
Supplementary Figure DR1. The Mundafan paleolake basin with the study sites (section numbers) and the Tuwayq escarpment in the north-east on a GoogleEarth image 2010.



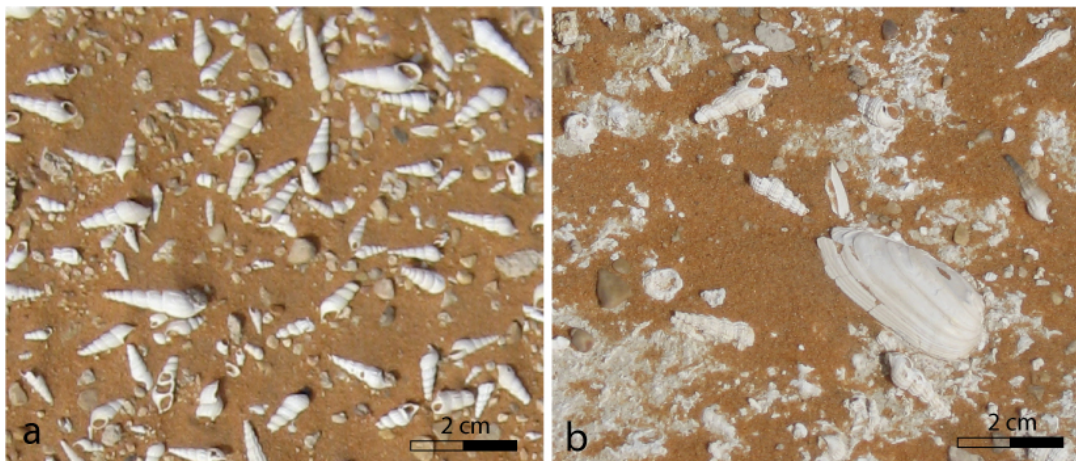
Supplementary Figure DR2. Holocene sections at Mundafan.



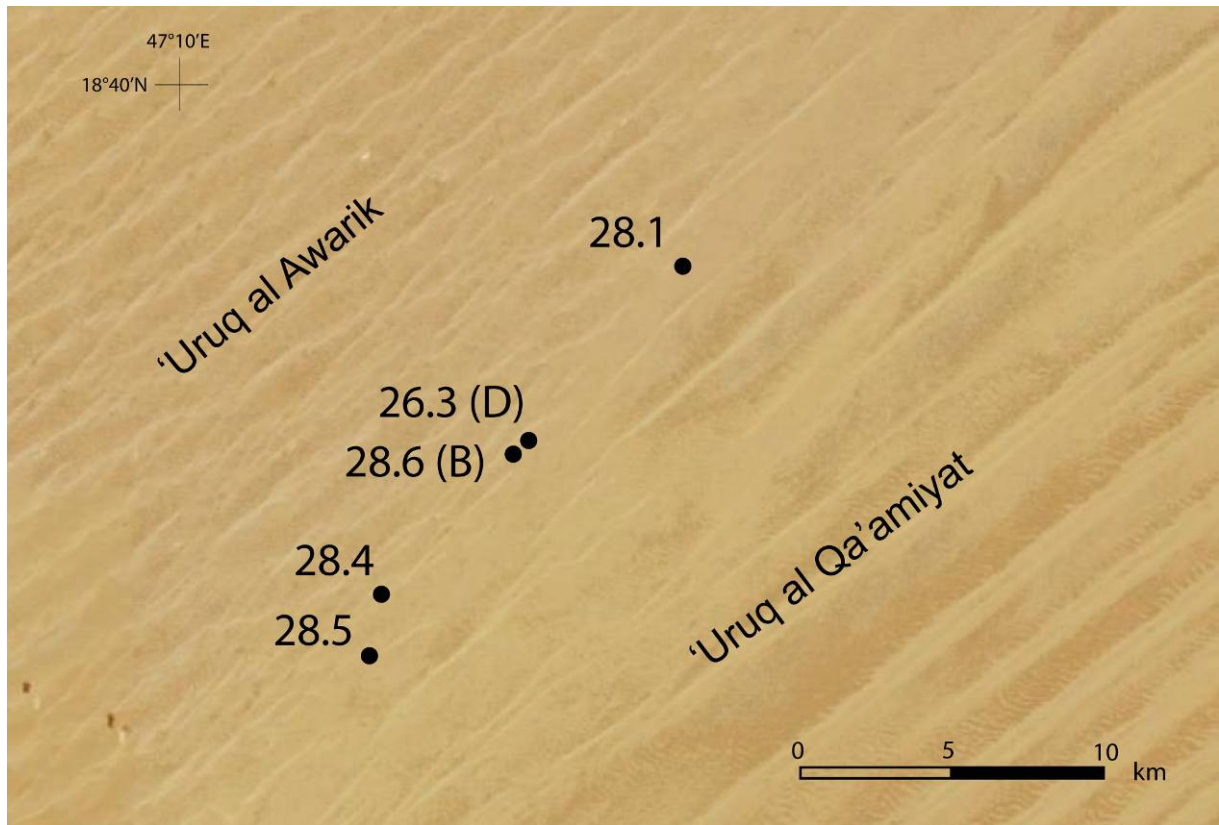
Supplementary Figure DR3. a, Section 21.2 (Sample 26-36), b, Section 21.1, c, Section 22.3, Plant root tubes and lamination. d, Section 22.6: Cross-bedded aeolian sand 06 below lacustrine sequence.



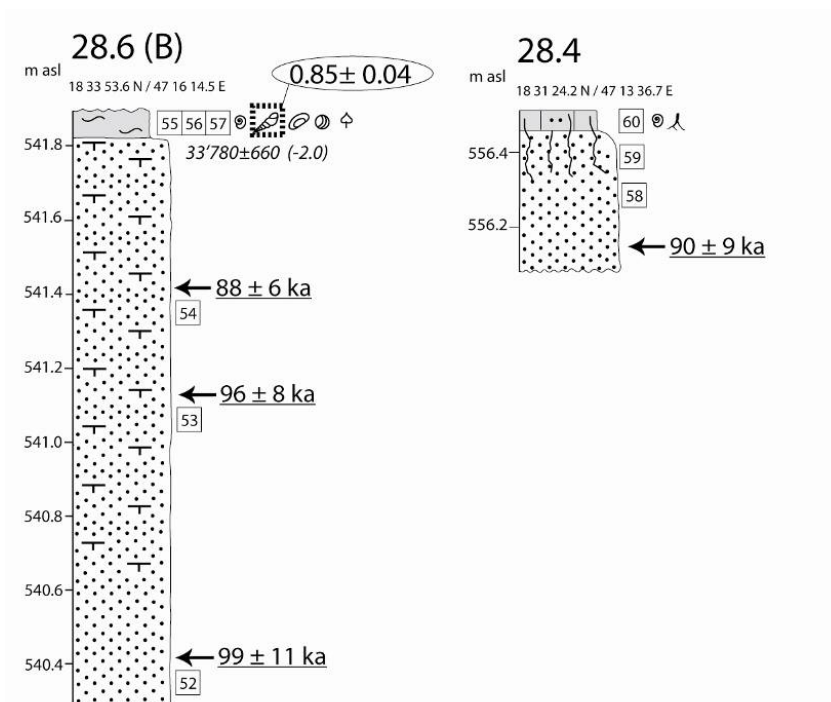
Supplementary Figure DR4. Sections at Mundafan (legend in Fig. DR2)



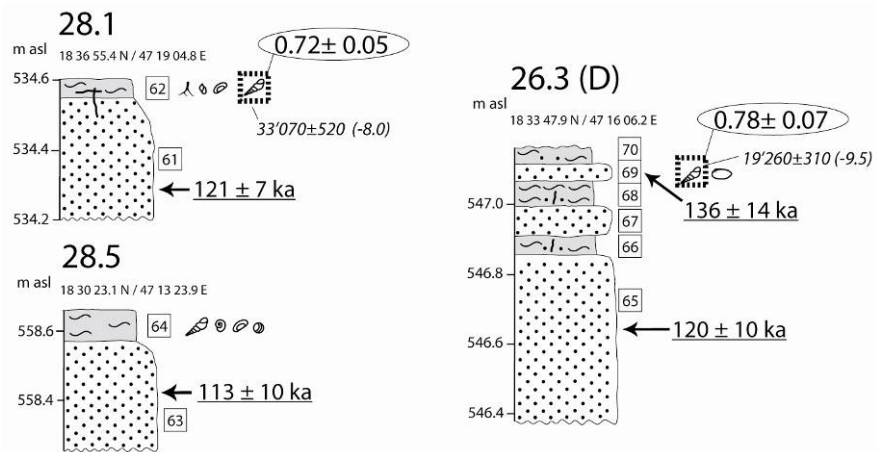
Supplementary Figure DR5. Section 22.2 (Sample 43). **a**, *Melanoides tuberculata*, **b**, *Unio* sp. and *Melanoides tuberculata*



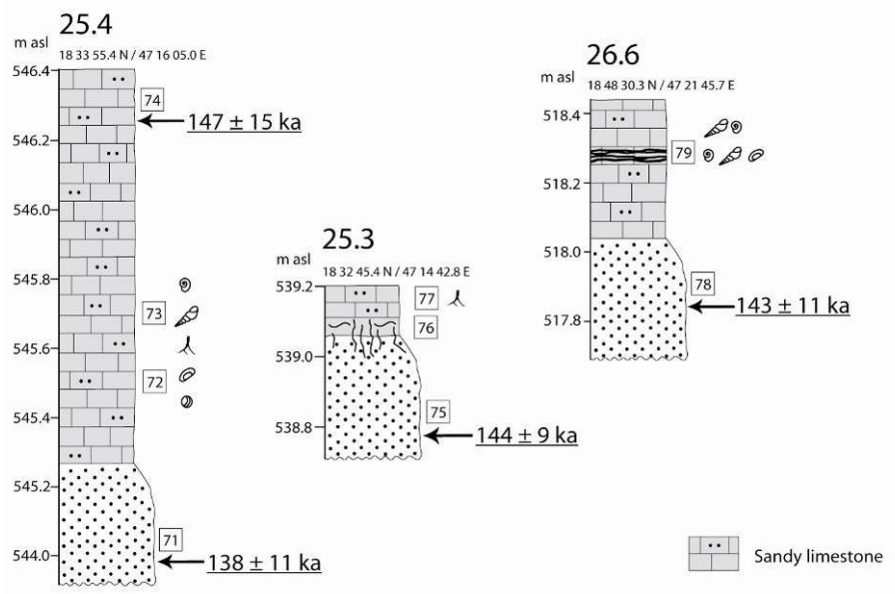
Supplementary Figure DR6. Sites (section numbers) in the Khujaymah study area, NASA World Wind image.



Supplementary Figure DR7. Sections at Khujaymah (legend in Fig. DR2)



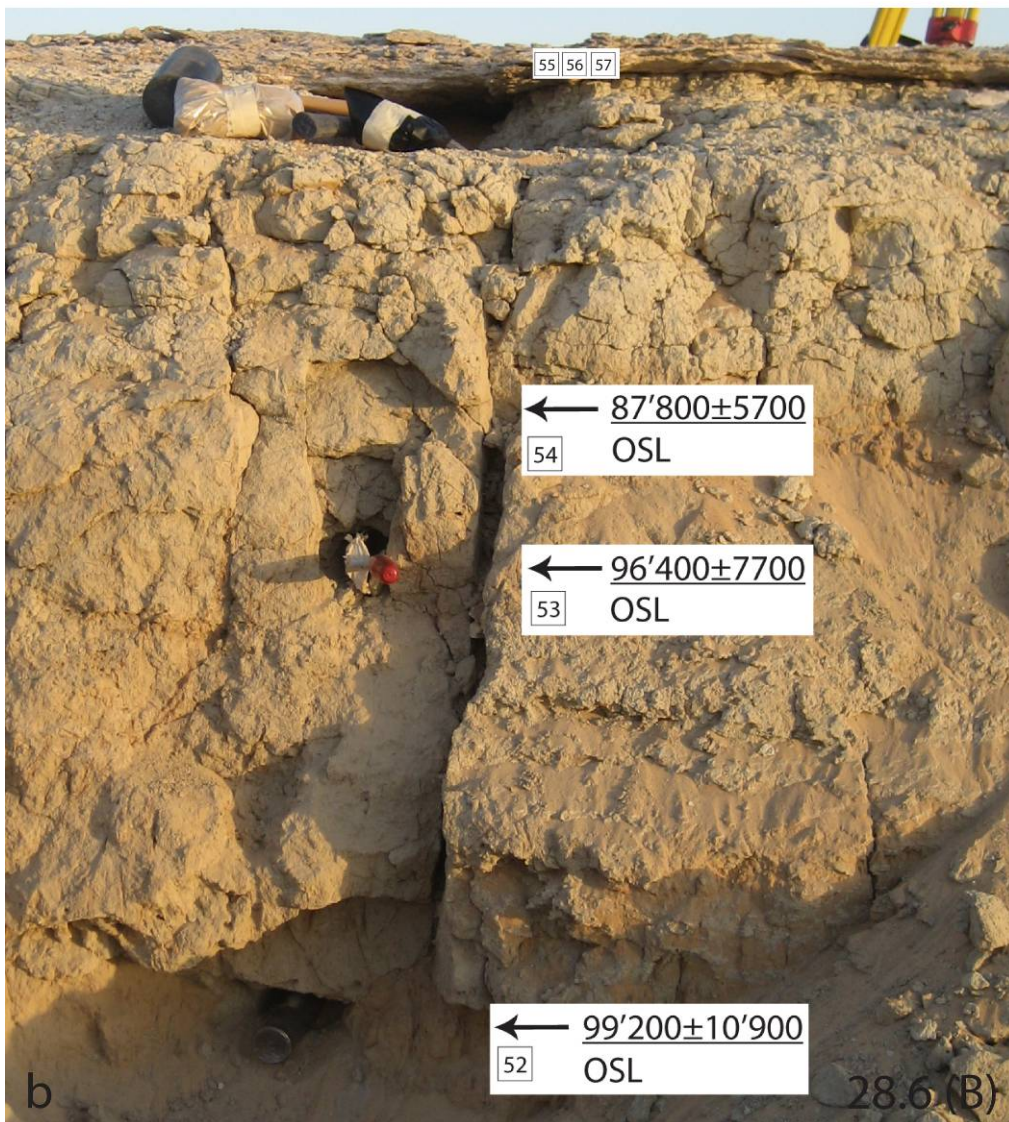
Supplementary Figure DR8. Sections at Khujaymah (legend in Fig. DR2)



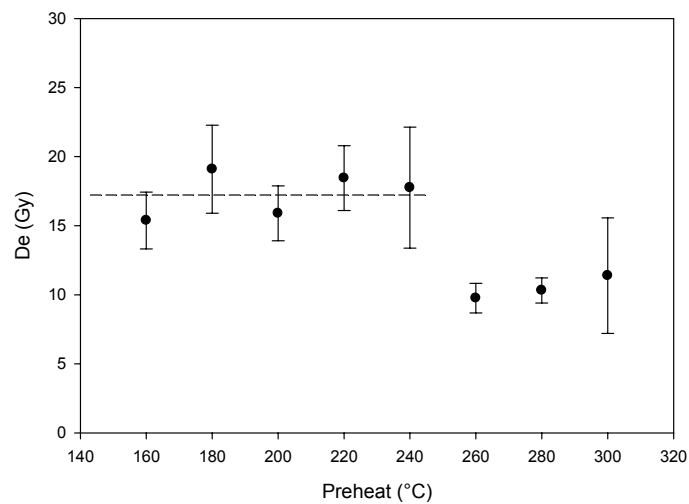
Supplementary Figure DR9. Sections at Khujaymah (legend in Fig. DR2)



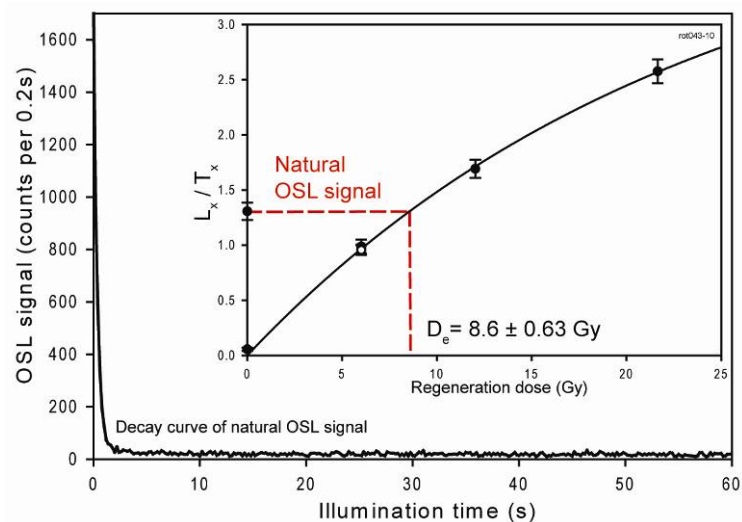
Supplementary Figure DR10. Section 26.6



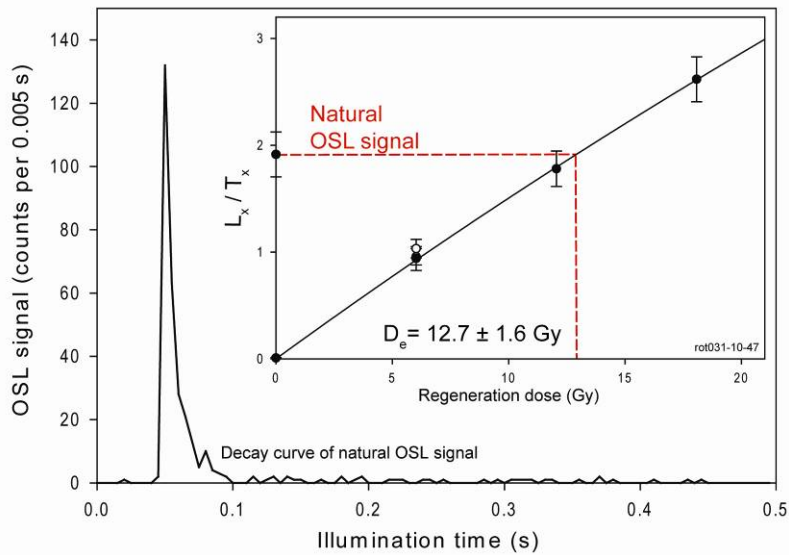
Supplementary Figure DR11. a, Section 26.3 (Fig. 4.2 D), b, Section 28.6 (Fig. 4.2 B)



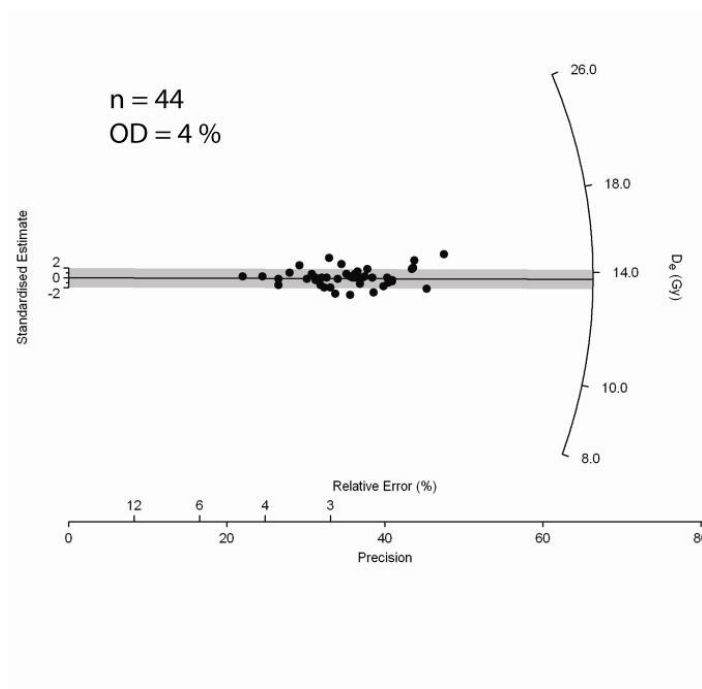
Supplementary Figure DR12. Preheat plateau test for sample 06 from section 22.6/1 (Supplementary Fig. DR2). Preheat and test dose preheat were at the same temperature and for 10 s each. Each data point is the average of 6 aliquots (2 mm).



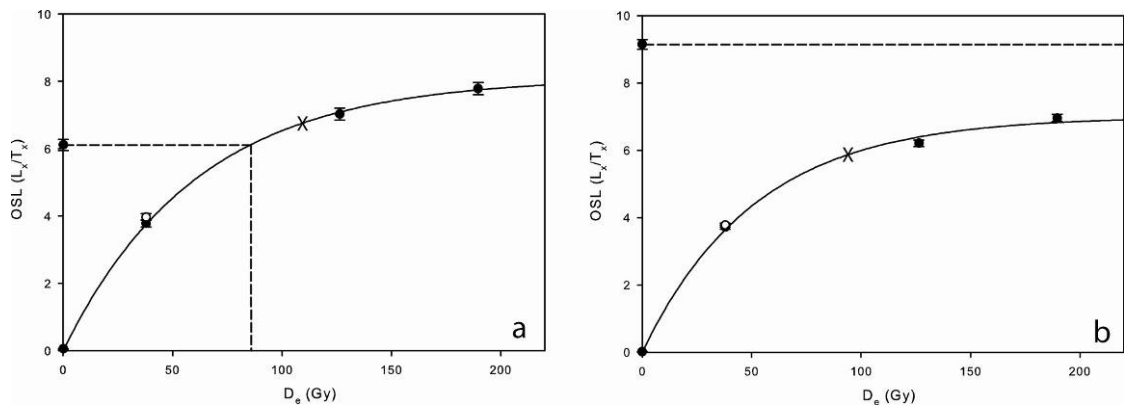
Supplementary Figure DR13. Decay curve of natural OSL (L_N) as a function of illumination time. The inset shows the growth curve of an individual aliquot, showing L_x/T_x as a function of regeneration doses. This sample (22 from section 21.2) was dated to 10.1 ± 0.6 ka.



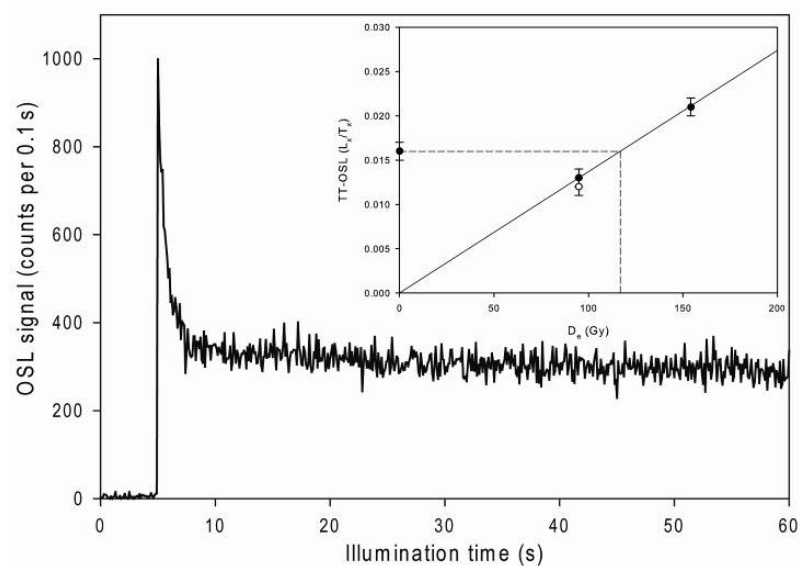
Supplementary Figure DR14. Decay curve of natural OSL (L_N) of a single grain as a function of illumination time. The inset shows the growth curve of an individual aliquot, showing L_x/T_x as a function of regeneration doses. This sample (7 from section 22.3; Supplementary Table DR4) was dated to 9.8 ± 0.5 ka.



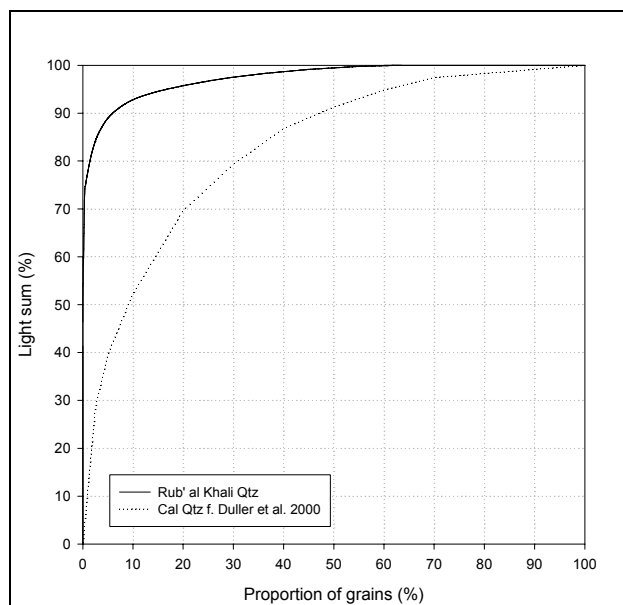
Supplementary Figure DR15. Radial plot of dose recovery test (sample 06 from section 22.6). The recovery ratio is 1.02 ± 0.02 . Preheat and test dose preheat were 210°C for 10s.



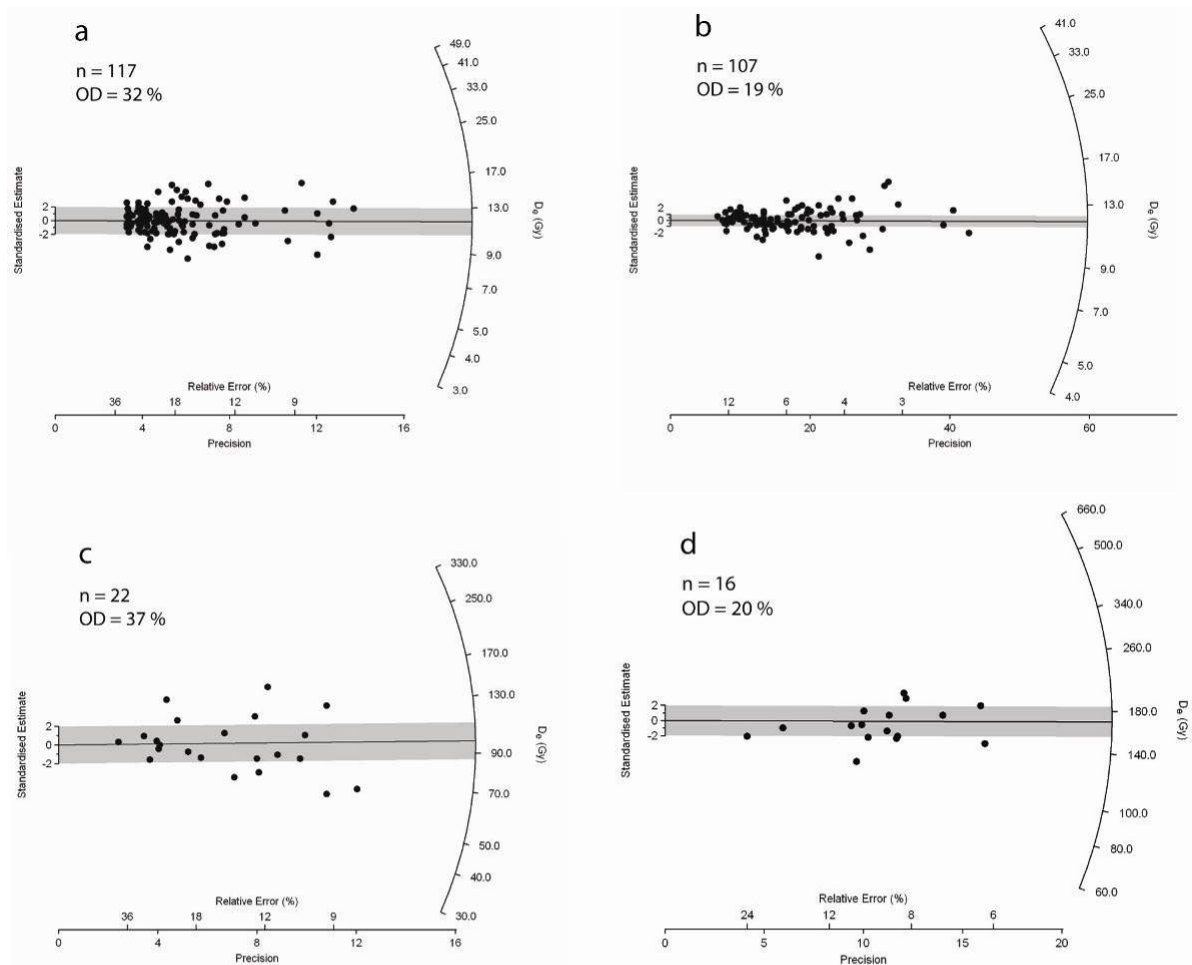
Supplementary Figure DR16. OSL dose response curves from sample 46 (section 22.2) obtained using 2 mm aliquots. The $2D_0$ values of the single saturating exponential are marked with a cross at 115 Gy (a) and 94 Gy (b). The dashed line shows the value of the natural L_n/T_n ratio. The open circle is a repeated measurement.



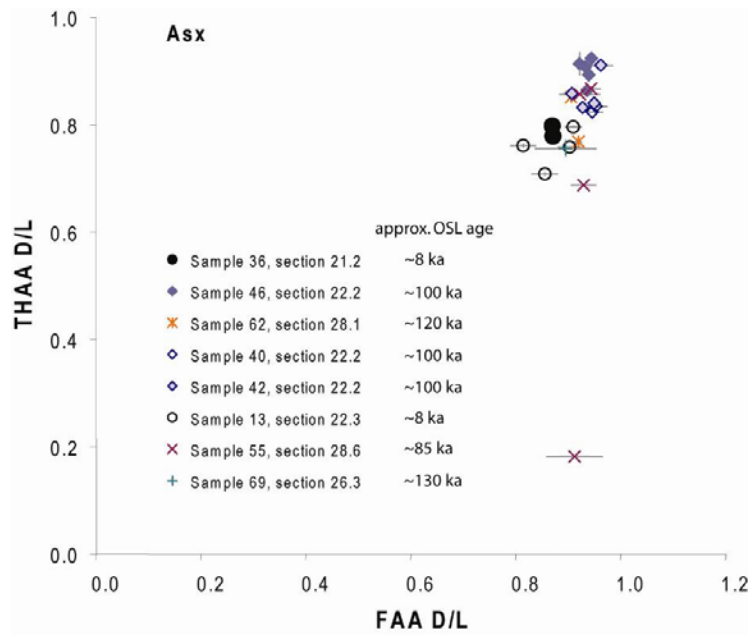
Supplementary Figure DR17. TT-OSL decay curve and TT-OSL dose response curve in the inset, both from sample 71 (section 25.4). Dose response points are linearly fitted and forced through the origin. The natural L_n/T_n ratio projected onto the curve results in a D_e of 118 ± 10 Gy. The recycling ratio is 0.92 ± 0.1 .



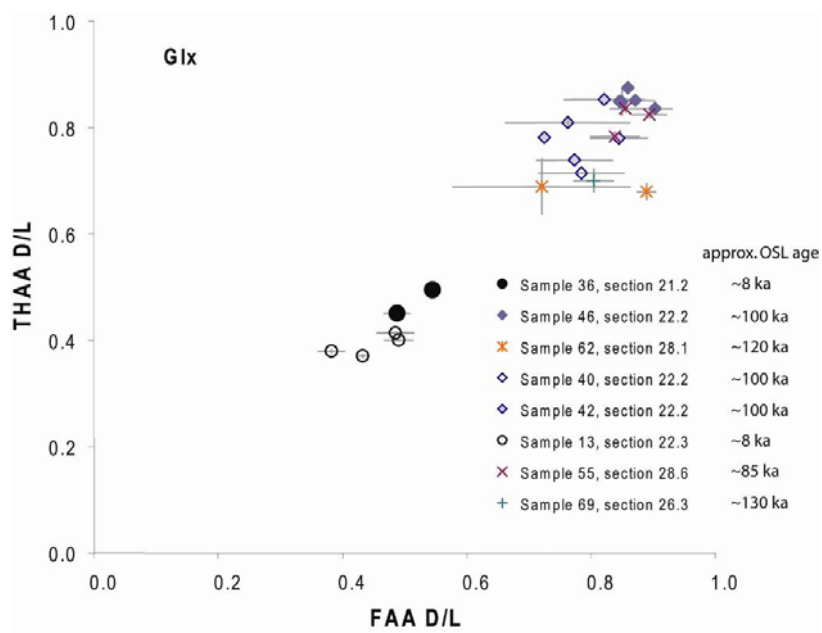
Supplementary Figure DR18. Cumulative light-sum curve from a total of 300 single grains from sample 46 compared to “calibration quartz” (Duller et al., 2000) showing that only 3 % of the grains contribute 85 % to the total light sum.



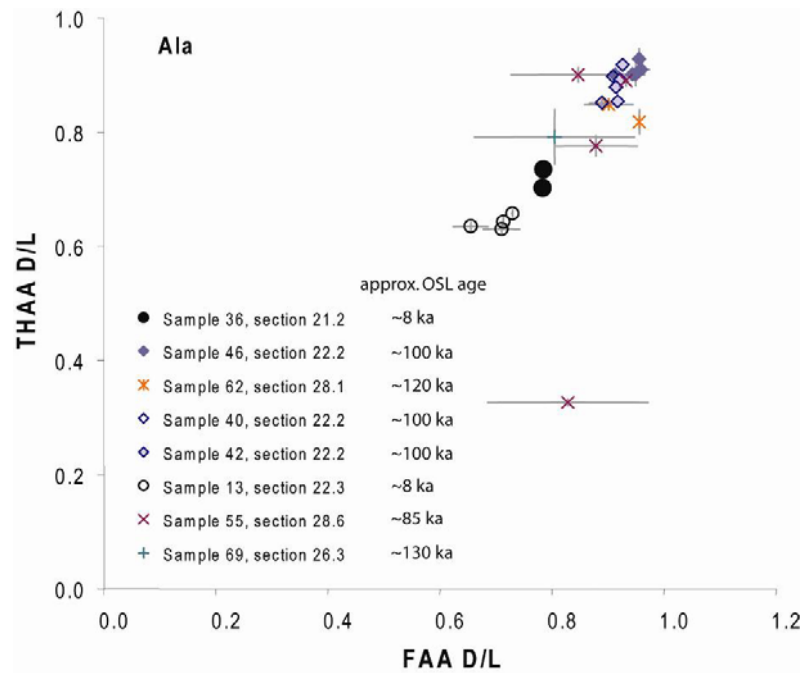
Supplementary Figure DR19. Radial plots for D_e distribution analysis. The equivalent dose for a grain is read by drawing a line from the origin of the y-axis ('Standardized Estimate') through the data point of interest, until the line intersects the radial axis (log scale) on the right-hand side. The measurement error on this equivalent dose is obtained by extending a line vertically to intersect the x-axis. The latter has two scales: the relative standard error and its reciprocal ('Precision'). **a**, Single grain D_e estimate obtained from 117 grains of quartz from a young sample (sample 6 section 22.6). **b**, 2 mm aliquot (ca. 80 grains per aliquot) D_e estimate obtained from 107 aliquots of the same young sample. **c**, Single grain D_e estimate obtained from 22 individual grains of quartz from a Pleistocene sample (sample 69 section 26.3). **d**, 6 mm aliquot (ca. 600 grains per aliquot) TT-OSL D_e estimate obtained from 16 aliquots of a Pleistocene sample (sample 54 section 28.6).



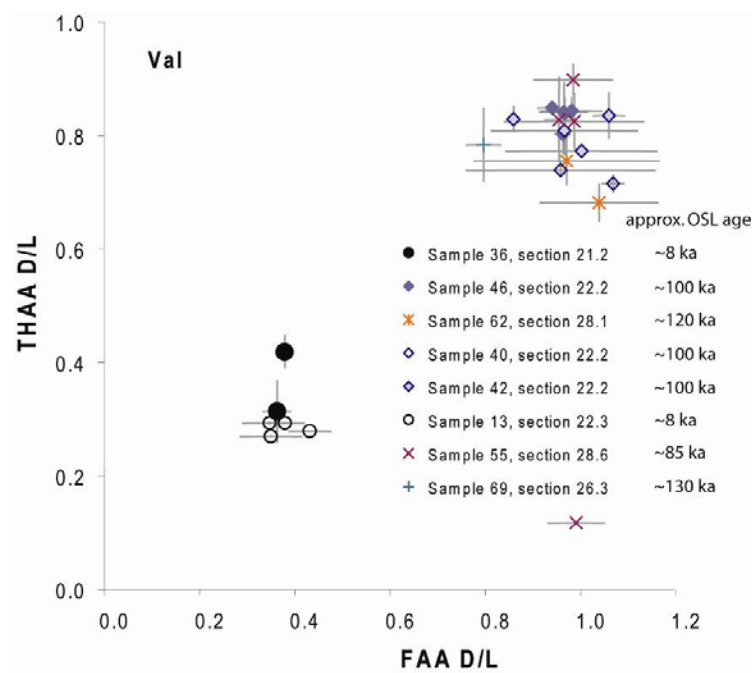
Supplementary Figure DR20. D/L THAA vs D/L FAA for Asx in *Melanoides tuberculata* shell from Mundafan.



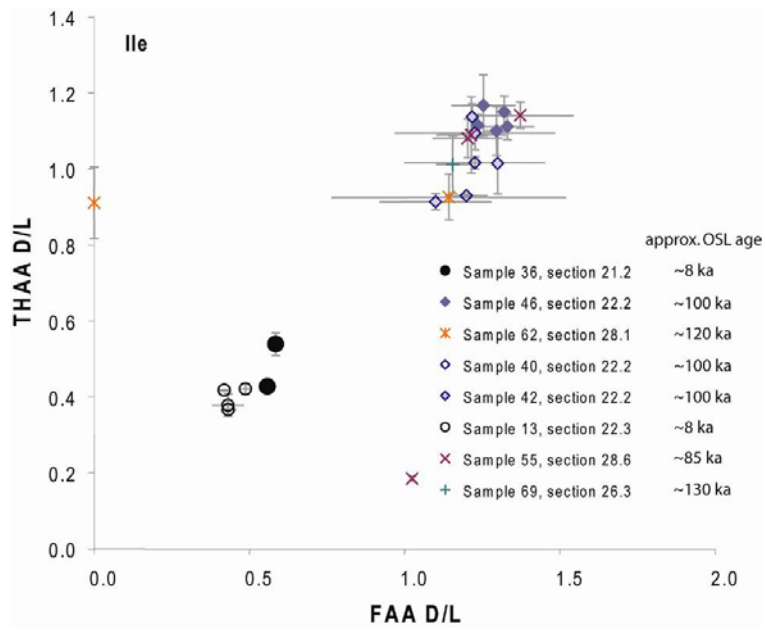
Supplementary Figure DR21. D/L THAA vs D/L FAA for Glx in *Melanoides tuberculata* shell from Mundafan and Khujaymah.



Supplementary Figure DR22. D/L THAA vs D/L FAA for Ala in *Melanoides tuberculata* shell from Mundafan and Khujaymah.



Supplementary Figure DR23. D/L THAA vs D/L FAA for Val in *Melanoides tuberculata* shell from Mundafan and Khujaymah.



Supplementary Figure DR24. D/L THAA vs D/L FAA for L-isoleucine / D-alloisoleucine (A/I) in *Melanoides tuberculata* shell from Mundafan and Khujaymah.

2. Supplementary Methods

OSL Dating Method

Optically stimulated luminescence (OSL) dating is a method to determine burial ages of sediments. Energy supplied by naturally occurring ionizing radiation in the sediment increases the number of trapped electrons in the crystal lattice of certain mineral grains (e.g. quartz). Sunlight exposure releases light-sensitive trapped electrons. As a consequence, the intensity of the OSL signal is a measure of the radiation dose absorbed by the sediment grains since they were last exposed to daylight. For purposes of dating, the OSL signal is measured and the dose producing an equivalent signal is determined. The equivalent dose divided by the dose rate of the surrounding sediment gives the OSL age of a sample (Huntley et al., 1985).

Common problems when sampling paleolake deposits are limited sediment thickness, low quartz content and sometimes vertical inhomogeneities. The spatial and temporal (water table changes, bioturbation) homogeneity is important as it affects the dose rate, and a homogenous dose rate is generally an assumption for age estimations. As a consequence, our sampling strategy mainly relied on sampling homogenous sand beneath the lake deposits for a maximum age, combined with further samples within and/or above the lake deposits to narrow the age range of deposition. We collected samples by forcing a steel tube into a freshly cleaned exposure. The material from the tubes was then carefully discharged into opaque plastic bags for transport to the lab. Dose rate samples were collected with a small shovel from the same holes. Block samples of lithified lake deposits were wrapped with two layers of black opaque foil. Documentation of outcrops included a detailed stratigraphic sketch (Supplementary Fig. DR2-9).

All samples were opened in the laboratory under the appropriate lighting conditions (dim red/orange illumination). In the case of block samples the outer surface was removed carefully using a diamond saw with water cooling. All dating was carried out on quartz grains. The samples were treated with HCl and H₂O₂ to remove carbonates and organic matter before the grain size 200-250 µm was isolated. A two-step heavy-liquid separation using LST Fastfloat (2.70 and 2.58 g cm⁻³) was applied and the quartz fraction was subsequently etched in HF (40%) for 60 min to reduce remaining feldspars and the outer part of the quartz grains influenced by alpha irradiation during burial. After washing with HCl to dissolve fluorides, the samples were re-sieved at 150 µm to remove remaining feldspar grains. The coarse-grained quartz was then mounted on steel discs using silicone spray or placed in special single grain discs.

The **dose rate** represents the rate of ionizing radiation to which the samples were exposed during burial and is mostly derived from the radioactive decay of ^{238}U , ^{235}U , ^{232}Th (plus their daughter products) and ^{40}K , with lesser contributions from cosmic rays. Radioactive elements (K, Th, U; Supplementary Table DR4) were measured by high-resolution gamma spectrometry by S. Szidat, Department of Chemistry and Biochemistry, University of Bern (Preusser and Kasper, 2001). These measurements imply some evidence for radioactive disequilibrium in the Uranium decay chain for some of the samples and these have been additionally measured using Instrumental Neutron Activation Analysis (INAA) by J. Kučera, Nuclear Physics Institute Řež, Czech Republic. U-238 from INAA compared to Ra-226 from Gamma spectrometry (Supplementary Table DR4) shows limited U-238 deficiency with a negligible effect on the Pleistocene ages. For example, the age of sample 38 with extreme scenario using the values determined U-238 or Ra-226 differs not more than 3 %. Dose rates were calculated assuming average water content between 1% and 3% during burial. The contribution of cosmic rays to the total dose rate was calculated using present day depth considering full uncertainties due to actual position below surface (Prescott and Hutton, 1994). Total dose rates and resulting OSL ages are summarized in Supplementary Table DR4.

Two of the samples are rather problematic with regard to dose rate determination, as these have been taken from near surface layers. Although problematic, these samples are important as they directly date the lake deposits. Sample 74 (section 25.4) is an almost pure carbonate with little aeolian sand content. This sample shows a deficit of the mother isotope U in the decay chain and extreme low K and Th concentrations. As the layer is highly porous it appears that rain water may have reduced the concentration of radioactive elements after deposition. As a consequence, the resulting age is regarded as maximum estimate. The second problematic sample 69 (section 26.3) is from a thin aeolian sand layer bracketed by lake marls. Unfortunately, we could not measure the gamma radiation field on site, which leaves some uncertainties with regard to homogeneity. Additionally, this sample also shows low K and Th values and therefore we also regard this age as a maximum estimate.

Luminescence measurements were made in a Risø TL/OSL-DA-20 reader with blue diodes ($470 \pm 30 \text{ nm}$; $\sim 41 \text{ mW cm}^{-2}$) and with a calibrated 40 mCi $^{90}\text{Sr}/^{90}\text{Y}$ beta source delivering $\sim 0.13 \text{ Gy s}^{-1}$ to the grains. Luminescence signals were measured with an EMI 9635Q photomultiplier tube through a 7.5 mm Hoya U340 filter. For optical stimulation of single sand-sized grains (SG) a laser attachment was used with a beam from a 10 mW Nd:YVO₄ diode-pumped green laser (532 nm) focused down to a 10 μm diameter spot with a power density of $\sim 50 \text{ W/cm}^2$ (Bøtter-Jensen et al., 2000).

Early saturation of the OSL signals with $2D_0$ values between 90 - 150 Gy made it necessary to use two different protocols. Equivalent doses (D_e) were either determined with a standard SAR protocol for OSL (Murray and Wintle, 2000) or a SAR protocol for thermally transferred OSL (TT-OSL, Porat et al., 2009).

For the **Holocene samples** the single aliquot regenerative dose (SAR) protocol (Supplementary Table DR1 and DR2) of Murray and Wintle (2000) was applied to the samples initially characterized using preheat plateau (Supplementary Fig. DR12) and dose recovery tests (Supplementary Fig. DR19).

For multi grain D_e determination a preheat of 220°C for 10 s was used and also applied to the test dose. For single grain D_e determination the conditions were the same except for the much shorter illumination of 0.5 s due to the high power density of the laser. The test dose (D_t) size was always 6 Gy. The dose response curve was constructed by plotting L_x/T_x versus dose, where L_x is the OSL signal from the regenerative dose and T_x is the response to the test dose. For multi grain the initial 0.4 s OSL signal minus a background estimated from the 50-60 s integral was used for OSL dose determinations while the much shorter intervals for single grains were 0.05-0.07 s for the signal minus a background from 0.4-0.5 s. Supplementary Figure DR13 and DR14 show representative decay and dose response curves. Aliquots were rejected if the recycling ratio was outside the range 1.0 ± 0.2 or the OSL IR depletion ratio (Duller et al., 2003) was less than 0.8. The recuperation threshold was 5 %. All heating was ramped at 5°C s^{-1} . Data analysis included a measurement error of 1 % for single aliquots and of 2.5 % for single grains. The total light sum figure (Supplementary Figure DR18) from a typical sample (48) shows that only 3 % of the grains contribute 85 % of the total light sum. We crossed-checked different aliquot sizes using single grains as well as 2 mm and 6 mm (spray mask size) multiple grain approaches (Supplementary Table DR4). The number of grains per aliquot is ~80 (2 mm) and ~600 (6 mm). The most intensively investigated samples (6 and 7) show almost identical results for the different approaches. For consistency, all ages related to the Holocene deposits shown in the figures are those determined for 2 mm aliquots (see: 4. Supplementary Discussion).

Most of the **Pleistocene samples** were out of range for the OSL SAR protocol of Murray and Wintle (2000) due to early signal saturation (Supplementary Fig. DR15). In order to date dune sands with greater expected doses, a previously published (Supplementary Table DR3, Porat et al. (2009)), single-aliquot regenerative-dose protocol (SAR) for TT-OSL was applied. A test dose of 10 Gy was used. The initial 0.4 s TT-OSL signal minus a background estimated from the 0.4-10.4 s integral, as suggested by Ballarini et al. (2007), was used for TT-OSL dose determinations (Supplementary figure DR17). For all measurements the aliquot size was 6 mm. Dose dependent dose recovery tests and

recycling ratios met the standard performance criteria (Porat et al., 2009) and dose response curves demonstrated the potential to extend the dose range to beyond 600 Gy. Multiple aliquot additive dose (MAAD) TT-OSL protocols were used to test for sensitivity changes in the SAR TT-OSL protocol up to doses of 1200 Gy. A strong dose dependent deviation of the SAR TT-OSL relative to the MAAD TT-OSL dose response is observed. Comparison of the TT-OSL and OSL sensitivity data obtained from the MAAD and SAR data sets show a lack of proportionality between TT-OSL and OSL for the SAR data which will result in a problem when SAR dose response curves are constructed using many regeneration points with doses above 300 Gy. As a consequence for the samples under consideration the SAR TT-OSL protocol of Porat et al. (2009) can only be used when the expected doses are below 300 Gy (Supplementary Fig. DR16). A detailed description of the TT-OSL testing results is given in Rosenberg et al. (2011).

AAR Dating Method

A technique of amino acid analysis has been developed for geochronological purposes (Penkman et al., 2008), combining a Reverse-Phase High Pressure Liquid Chromatography method of analysis (Kaufman and Manley, 1998) with the isolation of an “intra-crystalline” fraction of amino acids by bleach treatment (Sykes et al., 1995). This combination of techniques results in the analysis of D/L values of multiple amino acids from the chemically-protected protein within the biomineral; enabling both decreased sample sizes and increased reliability of the analysis. Amino acid analyses were undertaken on *Melanoïdes tuberculata* shells from Mundafan and Khujaymah. This involved isolating the intra-crystalline protein fraction of the gastropod *Melanoïdes tuberculata*, which is a novel species for amino acid studies. The rate of racemization is governed by a variety of factors, but the intra-crystalline amino acid fraction appears to operate as a closed system (Penkman et al., 2008; Penkman et al., 2007). Environmental factors in the intra-crystalline fraction of a particular species (e.g. water content, concentration of cations, pH) are constant and therefore the extent of racemization is a function of time and temperature. Over a small geographical area, such as that represented in this study, it can be assumed that the integrated temperature histories are effectively the same. Any differences in the extent of decomposition of protein within the sample are therefore age-dependent. The pattern of protein degradation with time is slightly different for each species and biomineral. Amino acid racemization is governed by the original protein sequence and conformation. Whilst developing the research into closed-system protein degradation it became clear that the reaction rates were species-specific, even in the intra-crystalline fraction. This necessitates the comparison of amino acid data only within a single species (Penkman et al., 2007). As

Melanooides tuberculata has not been characterized for amino acid geochronology before, this study provides the first data as to its usefulness.

Amino acid racemization (AAR) analyses were undertaken on *Melanooides tuberculata* shells from 8 samples:

- 2 subsamples from sample 36, section 21.2 (Supplementary Fig. DR2), NEaar 5774, 5807, **~8 ka**
- 2 subsamples from sample 40, section 22.2 (Supplementary Fig. DR4), NEaar 6003-6004, **~100 ka**
- 4 subsamples from sample 42, section 22.2 (Supplementary Fig. DR4), NEaar 6005-6008, **~100 ka**
- 5 subsamples from sample 46, section 22.2 (Supplementary Fig. DR4), NEaar 5775, 5808-5811, **~100 ka**
- 4 subsamples from sample 13, section 22.3 (Supplementary Fig. DR2), NEaar 6009-6012, **~8 ka**
- 2 subsamples from sample 69, section 26.3 (Supplementary Fig. DR8), NEaar 6017-6018, **~130 ka**
- 2 subsamples from sample 62, section 28.1 (Supplementary Fig. DR8), NEaar 5776, 5812, **~120 ka**
- 4 subsamples from sample 55, section 28.6 (Supplementary Fig. DR7), NEaar 6013-6016, **~85 ka**

All samples were prepared using the procedures of (Penkman et al., 2008) to isolate the intra-crystalline protein by bleaching. Two subsamples were then taken from each shell; one fraction was directly dematerialized and the free amino acids analyzed (referred to as the 'Free' amino acids, FAA, F), and the second was treated to release the peptide-bound amino acids, thus yielding the 'total' amino acid concentration, referred to as the 'Total Hydrolysable amino acid fraction' (THAA, H*). During preparative hydrolysis both asparagine and glutamine undergo rapid irreversible deamination to aspartic acid and glutamic acid respectively. It is therefore not possible to distinguish between the acidic amino acids and their derivatives and they are reported together as Asx and Glx.

Carbon Isotope $\delta^{13}\text{C}_{\text{org}}$

Carbon isotope composition (Supplementary Table DR7) were determined using a ThermoFisher Flash-EA 1112 coupled with a ConFlo IV interface to a ThermoFisher Delta V plus isotope ratio mass spectrometer (IRMS). Samples were combusted in the presence of O_2 in an oxidation column at 1030°C . Combustion gases were passed through a reduction column (650°C), and produced CO_2 gases transferred to the IRMS via an open split for on-line isotope measurements. Isotope ratios are reported in the conventional δ -notation with respect to V-PDB (Vienna Pee Dee Belemnite) standards. The methods were calibrated with NBS22 ($\delta^{13}\text{C} = -30.03\text{‰}$) and IAEA CH-6 ($\delta^{13}\text{C} = -10.46\text{‰}$) for carbon. Reproducibility of the measurements is better than 0.2‰ .

3. Supplementary Tables

Supplementary Table DR1 | OSL SAR protocol (Murray and Wintle, 2000) as used for 2 mm and 6 mm aliquots of Holocene age. For the natural sample, $x = 0$, $D_0 = 0$ Gy and the subscript n is used (L_n , T_n).

| Step | Procedure |
|------|---|
| 1 | Dose, D_x |
| 2 | Preheat 1 at 220°C for 10 s |
| 3 | Blue stimulation at 125°C for 60 s; L_x |
| 4 | Test dose, $D_t = 6$ Gy |
| 5 | Preheat 2 at 220°C for 10 s |
| 6 | Blue stimulation at 125°C for 60 s; T_x |
| | Return to 1 |

Supplementary Table DR2 | OSL SAR protocol (Murray and Wintle, 2000) as used for single grains of Holocene age. For the natural sample, $x = 0$, $D_0 = 0$ Gy and the subscript n is used (L_n , T_n).

| Step | Procedure |
|------|---|
| 1 | Dose, D_x |
| 2 | Preheat 1 at 220°C for 10 s |
| 3 | Green laser stimulation at 125°C for 0.5 s; L_x |
| 4 | Test dose, $D_t = 6$ Gy |
| 5 | Preheat 2 at 220°C for 10 s |
| 6 | Green laser stimulation at 125°C for 0.5 s; T_x |
| | Return to 1 |

Supplementary Table DR3 | Simplified TT-OSL SAR protocol as suggested by Porat et al. (2009). For the natural sample, $x = 0$, $D_0 = 0$ Gy and the subscript n is used (L_n , T_n).

| Step | Procedure |
|------|--|
| 1 | Dose, D_x |
| 2 | Preheat at 200°C for 10 s |
| 3 | Blue stimulation at 125°C for 300 s |
| 4 | Transfer preheat at 260°C for 10 s |
| 5 | Blue stimulation at 125°C for 100 s; L_x |
| 6 | Test dose, D_t |
| 7 | Preheat at 220°C for 10 s |
| 8 | Blue stimulation at 125°C for 100 s; T_x |
| 9 | Heat at 300°C for 100 s |
| | Return to 1 |

Supplementary Table DR4 | OSL and TT-OSL results. The grain size was always 200-250 µm and the water content 2±1 %. Doserates were calculated from high resolution Gamma spectrometry results. The highlighted data sets are the ones of the ages used.

| N | Section | Region | Depth (m) | Altitude (masl) | Cosmic-dose rate (mGy/ka) | Activities (Bq kg ⁻¹) | | | | | | De (Gy) | n | OD | Age (ka) | Aliquot size (mm) | Protocol |
|----|-------------|--------|-----------|-----------------|---------------------------|-----------------------------------|------------|-------------------------------|-----------------|------------|------------------|----------------|-----|----|-------------|-------------------|----------|
| | | | | | | K | Th | U-238 from 186 keV and Ra-226 | U-238 from INAA | Ra-226 | Doserate (Gy/ka) | | | | | | |
| 1 | 23.1 | Mund. | 0.9 | 860 | 196 | 271.0 ± 5.7 | 8.0 ± 0.4 | 5.0 ± 3.8 | | 7.2 ± 0.2 | 1.31 ± 0.06 | 11.51 ± 0.27 | 52 | 16 | 8.8 ± 0.4 | 2 | OSL |
| 1 | 23.1 | Mund. | 0.9 | 860 | 196 | 271.0 ± 5.7 | 8.0 ± 0.4 | 5.0 ± 3.8 | | 7.2 ± 0.2 | 1.31 ± 0.06 | 11.28 ± 0.97 | 7 | 18 | 8.6 ± 0.8 | SG | OSL |
| 4 | 23.3 | Mund. | 0.6 | 860 | 203 | 207.7 ± 4.5 | 4.3 ± 0.2 | 9.2 ± 1.7 | | 4.2 ± 0.1 | 1.00 ± 0.05 | 12.05 ± 0.41 | 28 | 17 | 12.0 ± 0.7 | 2 | OSL |
| 6 | 22.6 | Mund. | 1.3 | 860 | 184 | 98.0 ± 2.2 | 3.0 ± 1.1 | 3.2 ± 1.2 | | 3.7 ± 0.2 | 0.62 ± 0.05 | 11.88 ± 0.24 | 107 | 19 | 19.1 ± 1.6 | 2 | OSL |
| 6 | 22.6 | Mund. | 1.3 | 860 | 184 | 98.0 ± 2.2 | 3.0 ± 1.1 | 3.2 ± 1.2 | | 3.7 ± 0.2 | 0.62 ± 0.05 | 11.73 ± 0.40 | 117 | 32 | 18.9 ± 1.7 | SG | OSL |
| 6 | 22.6 | Mund. | 1.3 | 860 | 184 | 98.0 ± 2.2 | 3.0 ± 1.1 | 3.2 ± 1.2 | | 3.7 ± 0.2 | 0.62 ± 0.05 | 12.21 ± 0.45 | 23 | 17 | 19.6 ± 1.8 | 6 | OSL |
| 7 | 22.6 | Mund. | 0.9 | 860 | 195 | 248.5 ± 5.2 | 6.4 ± 0.2 | 9.6 ± 1.9 | | 6.6 ± 0.1 | 1.20 ± 0.05 | 11.72 ± 0.38 | 46 | 21 | 9.8 ± 0.5 | 2 | OSL |
| 7 | 22.6 | Mund. | 0.9 | 860 | 195 | 248.5 ± 5.2 | 6.4 ± 0.2 | 9.6 ± 1.9 | | 6.6 ± 0.1 | 1.20 ± 0.05 | 12.05 ± 0.52 | 86 | 30 | 10.0 ± 0.6 | SG | OSL |
| 7 | 22.6 | Mund. | 0.9 | 860 | 195 | 248.5 ± 5.2 | 6.4 ± 0.2 | 9.6 ± 1.9 | | 6.6 ± 0.1 | 1.20 ± 0.05 | 14.09 ± 0.31 | 38 | 13 | 11.7 ± 0.5 | 6 | OSL |
| 9 | 23.2 | Mund. | 1.0 | 860 | 192 | 207.9 ± 4.4 | 5.4 ± 0.1 | 7.6 ± 2.7 | | 5.2 ± 0.2 | 1.03 ± 0.04 | 14.81 ± 0.71 | 28 | 25 | 14.4 ± 0.9 | 2 | OSL |
| 9 | 23.2 | Mund. | 1.0 | 860 | 192 | 207.9 ± 4.4 | 5.4 ± 0.1 | 7.6 ± 2.7 | | 5.2 ± 0.2 | 1.03 ± 0.04 | 16.77 ± 1.02 | 10 | 9 | 16.3 ± 1.2 | SG | OSL |
| 15 | 21.1 | Mund. | 1.4 | 860 | 182 | 221.4 ± 4.6 | 6.0 ± 0.2 | 19.0 ± 2.6 | 27.1 ± 0.4 | 8.5 ± 0.1 | 1.13 ± 0.05 | 12.52 ± 0.40 | 47 | 15 | <11.1 ± 0.6 | 2 | OSL |
| 15 | 21.1 | Mund. | 1.4 | 860 | 182 | 221.4 ± 4.6 | 6.0 ± 0.2 | 19.0 ± 2.6 | 27.1 ± 0.4 | 8.5 ± 0.1 | 1.13 ± 0.05 | 12.03 ± 1.08 | 8 | 23 | <10.6 ± 1.0 | SG | OSL |
| 21 | 21.2 | Mund. | 1.8 | 860 | 172 | 172.2 ± 3.7 | 5.9 ± 0.3 | 39.9 ± 8.8 | | 6.8 ± 0.2 | 0.94 ± 0.04 | 13.10 ± 0.42 | 53 | 22 | <13.9 ± 0.8 | 2 | OSL |
| 21 | 21.2 | Mund. | 1.8 | 860 | 172 | 172.2 ± 3.7 | 5.9 ± 0.3 | 39.9 ± 8.8 | | 6.8 ± 0.2 | 0.94 ± 0.04 | 14.33 ± 0.52 | 22 | 16 | <15.3 ± 0.9 | 6 | OSL |
| 22 | 21.2 | Mund. | 1.6 | 860 | 177 | 172.4 ± 3.8 | 5.2 ± 0.3 | 21.4 ± 2.5 | 22.5 ± 0.4 | 6.1 ± 0.1 | 0.95 ± 0.04 | 9.51 ± 0.24 | 92 | 23 | <10.1 ± 0.5 | 2 | OSL |
| 22 | 21.2 | Mund. | 1.6 | 860 | 177 | 172.4 ± 3.8 | 5.2 ± 0.3 | 21.4 ± 2.5 | 22.5 ± 0.4 | 6.1 ± 0.1 | 0.95 ± 0.04 | 9.73 ± 0.19 | 52 | 14 | <10.3 ± 0.5 | 6 | OSL |
| 38 | 22.2 | Mund. | 2.5 | 860 | 157 | 433.8 ± 9.0 | 20.5 ± 0.1 | 10.6 ± 4.4 | 20.9 ± 0.4 | 16.2 ± 0.3 | 1.98 ± 0.05 | 201.05 ± 10.66 | 15 | 19 | 101 ± 6 | 6 | TT-OSL |
| 38 | 22.2 | Mund. | 2.5 | 860 | 157 | 433.8 ± 9.0 | 20.5 ± 0.1 | 10.6 ± 4.4 | 20.9 ± 0.4 | 16.2 ± 0.3 | 1.98 ± 0.05 | 165.65 ± 11.87 | 17 | 18 | >83 ± 7 | SG | OSL |
| 38 | 22.2 | Mund. | 2.5 | 860 | 157 | 433.8 ± 9.0 | 20.5 ± 0.1 | 10.6 ± 4.4 | 20.9 ± 0.4 | 16.2 ± 0.3 | 1.98 ± 0.05 | 130.70 ± 9.52 | 21 | 30 | >65 ± 5 | 2 | OSL |
| 38 | 22.2 | Mund. | 2.5 | 860 | 157 | 433.8 ± 9.0 | 20.5 ± 0.1 | 10.6 ± 4.4 | 20.9 ± 0.4 | 16.2 ± 0.3 | 1.98 ± 0.05 | 141.30 ± 6.77 | 24 | 23 | >71 ± 4 | 6 | OSL |
| 46 | 22.2 | Mund. | 0.3 | 860 | 212 | 182.3 ± 4.0 | 5.9 ± 0.4 | 6.4 ± 3.2 | 11.9 ± 0.3 | 10.3 ± 0.1 | 0.97 ± 0.05 | 109.30 ± 6.76 | 12 | 18 | 103 ± 8 | 6 | TT-OSL |
| 46 | 22.2 | Mund. | 0.3 | 860 | 212 | 182.3 ± 4.0 | 5.9 ± 0.4 | 6.4 ± 3.2 | 11.9 ± 0.3 | 10.3 ± 0.1 | 0.97 ± 0.05 | 87.60 ± 6.55 | 30 | 33 | >83 ± 7 | SG | OSL |
| 46 | 22.2 | Mund. | 0.3 | 860 | 212 | 182.3 ± 4.0 | 5.9 ± 0.4 | 6.4 ± 3.2 | 11.9 ± 0.3 | 10.3 ± 0.1 | 0.97 ± 0.05 | 108.53 ± 7.21 | 23 | 30 | >103 ± 8 | 2 | OSL |
| 46 | 22.2 | Mund. | 0.3 | 860 | 212 | 182.3 ± 4.0 | 5.9 ± 0.4 | 6.4 ± 3.2 | 11.9 ± 0.3 | 10.3 ± 0.1 | 0.97 ± 0.05 | 92.02 ± 3.28 | 26 | 18 | >87 ± 5 | 6 | OSL |
| 48 | 22.5 | Mund. | 0.8 | 860 | 198 | 429.8 ± 8.9 | 11.5 ± 0.6 | 12.4 ± 1.9 | | 8.8 ± 0.3 | 1.79 ± 0.06 | 150.18 ± 11.40 | 11 | 24 | 79 ± 7 | 6 | TT-OSL |
| 48 | 22.5 | Mund. | 0.8 | 860 | 198 | 429.8 ± 8.9 | 11.5 ± 0.6 | 12.4 ± 1.9 | | 8.8 ± 0.3 | 1.79 ± 0.06 | 154.61 ± 15.00 | 15 | 29 | >82 ± 9 | SG | OSL |
| 48 | 22.5 | Mund. | 0.8 | 860 | 198 | 429.8 ± 8.9 | 11.5 ± 0.6 | 12.4 ± 1.9 | | 8.8 ± 0.3 | 1.79 ± 0.06 | 137.11 ± 12.54 | 24 | 43 | >72 ± 7 | 2 | OSL |
| 48 | 22.5 | Mund. | 0.8 | 860 | 198 | 429.8 ± 8.9 | 11.5 ± 0.6 | 12.4 ± 1.9 | | 8.8 ± 0.3 | 1.79 ± 0.06 | 164.08 ± 6.82 | 24 | 16 | >87 ± 5 | 6 | OSL |
| 50 | 22.4 | Mund. | 0.8 | 860 | 198 | 363.1 ± 7.5 | 9.1 ± 0.1 | 8.4 ± 2.0 | | 9.0 ± 0.2 | 1.81 ± 0.12 | 161.63 ± 16.45 | 14 | 36 | 99 ± 11 | 6 | TT-OSL |
| 50 | 22.4 | Mund. | 0.8 | 860 | 198 | 363.1 ± 7.5 | 9.1 ± 0.1 | 8.4 ± 2.0 | | 9.0 ± 0.2 | 1.81 ± 0.12 | 145.52 ± 23.45 | 16 | 59 | >89 ± 15 | SG | OSL |
| 50 | 22.4 | Mund. | 0.8 | 860 | 198 | 363.1 ± 7.5 | 9.1 ± 0.1 | 8.4 ± 2.0 | | 9.0 ± 0.2 | 1.81 ± 0.12 | 149.43 ± 13.67 | 19 | 37 | >92 ± 9 | 2 | OSL |
| 50 | 22.4 | Mund. | 0.8 | 860 | 198 | 363.1 ± 7.5 | 9.1 ± 0.1 | 8.4 ± 2.0 | | 9.0 ± 0.2 | 1.81 ± 0.12 | 154.26 ± 5.72 | 18 | 15 | >95 ± 5 | 6 | OSL |

| Activities (Bq kg ⁻¹) | | | | | | | | | | | | | | | | | |
|-----------------------------------|---------|--------|-----------|-----------------|---------------------------|-------------|------------|-------------------------------|-----------------|------------|------------------|----------------|----|-----------|-----------|-------------------|----------|
| Nr | Section | Region | Depth (m) | Altitude (masl) | Cosmic-dose rate (mGy/ka) | K | Th | U-238 from 186 keV and Ra-226 | U-238 from INAA | Ra-226 | Doserate (Gy/ka) | De (Gy) | n | OD | Age (ka) | Aliquot size (mm) | Protocol |
| 52 | 28.6 | Khuj. | 1.5 | 560 | 172 | 303.7 ± 6.3 | 5.4 ± 0.1 | 5.0 ± 1.7 | | 6.3 ± 0.2 | 1.23 ± 0.03 | 128.86 ± 13.32 | 8 | 18 | 99 ± 11 | 6 | TT-OSL |
| 52 | 28.6 | Khuj. | 1.5 | 560 | 172 | 303.7 ± 6.3 | 5.4 ± 0.1 | 5.0 ± 1.7 | | 6.3 ± 0.2 | 1.23 ± 0.03 | 63.49 ± 11.74 | 11 | 57 | >49 ± 9 | SG | OSL |
| 52 | 28.6 | Khuj. | 1.5 | 560 | 172 | 303.7 ± 6.3 | 5.4 ± 0.1 | 5.0 ± 1.7 | | 6.3 ± 0.2 | 1.23 ± 0.03 | 75.90 ± 7.50 | 25 | 47 | >58 ± 6 | 2 | OSL |
| 53 | 28.6 | Khuj. | 1.2 | 560 | 179 | 337.7 ± 7.1 | 11.3 ± 0.3 | 11.7 ± 3.2 | | 15.0 ± 0.4 | 1.68 ± 0.06 | 161.51 ± 11.34 | 8 | 19 | 96 ± 8 | 6 | TT-OSL |
| 53 | 28.6 | Khuj. | 1.2 | 560 | 179 | 337.7 ± 7.1 | 11.3 ± 0.3 | 11.7 ± 3.2 | | 15.0 ± 0.4 | 1.68 ± 0.06 | 144.00 ± 18.00 | 23 | 39 | >86 ± 11 | SG | OSL |
| 53 | 28.6 | Khuj. | 1.2 | 560 | 179 | 337.7 ± 7.1 | 11.3 ± 0.3 | 11.7 ± 3.2 | | 15.0 ± 0.4 | 1.68 ± 0.06 | 137.69 ± 12.59 | 14 | 32 | >82 ± 8 | 2 | OSL |
| 53 | 28.6 | Khuj. | 1.2 | 560 | 179 | 337.7 ± 7.1 | 11.3 ± 0.3 | 11.7 ± 3.2 | | 15.0 ± 0.4 | 1.68 ± 0.06 | 131.03 ± 4.67 | 23 | 16 | >78 ± 4 | 6 | OSL |
| 54 | 28.6 | Khuj. | 0.5 | 560 | 197 | 406.4 ± 8.4 | 12.8 ± 0.4 | 15.7 ± 4.3 | | 16.2 ± 0.2 | 1.94 ± 0.06 | 170.10 ± 9.36 | 16 | 20 | 88 ± 6 | 6 | TT-OSL |
| 54 | 28.6 | Khuj. | 0.5 | 560 | 197 | 406.4 ± 8.4 | 12.8 ± 0.4 | 15.7 ± 4.3 | | 16.2 ± 0.2 | 1.94 ± 0.06 | 99.92 ± 11.83 | 18 | 46 | >51 ± 6 | SG | OSL |
| 54 | 28.6 | Khuj. | 0.5 | 560 | 197 | 406.4 ± 8.4 | 12.8 ± 0.4 | 15.7 ± 4.3 | | 16.2 ± 0.2 | 1.94 ± 0.06 | 120.62 ± 11.22 | 9 | 10 | >62 ± 6 | 2 | OSL |
| 58 | 28.4 | Khuj. | 0.4 | 577 | 200 | 311.3 ± 6.5 | 5.4 ± 0.2 | 5.8 ± 2.7 | | 5.2 ± 0.2 | 1.30 ± 0.01 | 119.76 ± 11.18 | 16 | 34 | 90 ± 9 | 6 | TT-OSL |
| 58 | 28.4 | Khuj. | 0.4 | 577 | 200 | 311.3 ± 6.5 | 5.4 ± 0.2 | 5.8 ± 2.7 | | 5.2 ± 0.2 | 1.30 ± 0.01 | 46.60 ± 7.00 | 13 | 54 | >35 ± 5 | 2 | OSL |
| 61 | 28.1 | Khuj. | 0.3 | 555 | 203 | 315.8 ± 6.6 | 6.5 ± 0.4 | 22.5 ± 5.6 | | 15.4 ± 0.2 | 1.48 ± 0.07 | 188.88 ± 8.81 | 8 | 9 | 121 ± 7 | 6 | TT-OSL |
| 61 | 28.1 | Khuj. | 0.3 | 555 | 203 | 315.8 ± 6.6 | 6.5 ± 0.4 | 22.5 ± 5.6 | | 15.4 ± 0.2 | 1.48 ± 0.07 | 120.70 ± 15.50 | 14 | 46 | >77 ± 10 | 2 | OSL |
| 63 | 28.5 | Khuj. | 0.3 | 580 | 203 | 285.8 ± 6.0 | 6.1 ± 0.2 | 7.1 ± 1.9 | | 7.7 ± 0.1 | 1.03 ± 0.04 | 147.69 ± 11.44 | 8 | 17 | 113 ± 10 | 6 | TT-OSL |
| 63 | 28.5 | Khuj. | 0.3 | 580 | 203 | 285.8 ± 6.0 | 6.1 ± 0.2 | 7.1 ± 1.9 | | 7.7 ± 0.1 | 1.03 ± 0.04 | 143.60 ± 4.65 | 13 | 8 | >110 ± 6 | 2 | OSL |
| 65 | 26.3 | Khuj. | 0.8 | 570 | 189 | 253.2 ± 5.4 | 5.5 ± 0.3 | 8.1 ± 3.0 | 7.7 ± 0.3 | 6.7 ± 0.2 | 1.12 ± 0.01 | 141.14 ± 10.01 | 8 | 15 | 120 ± 10 | 6 | TT-OSL |
| 65 | 26.3 | Khuj. | 0.8 | 570 | 189 | 253.2 ± 5.4 | 5.5 ± 0.3 | 8.1 ± 3.0 | 7.7 ± 0.3 | 6.7 ± 0.2 | 1.12 ± 0.01 | 107.74 ± 6.33 | 17 | 23 | >92 ± 7 | 2 | OSL |
| 65 | 26.3 | Khuj. | 0.8 | 570 | 189 | 253.2 ± 5.4 | 5.5 ± 0.3 | 8.1 ± 3.0 | 7.7 ± 0.3 | 6.7 ± 0.2 | 1.12 ± 0.01 | 113.50 ± 4.82 | 18 | 17 | >97 ± 6 | 6 | OSL |
| 68 | 26.3 | Khuj. | 0.1 | 570 | 210 | 143.7 ± 3.1 | 2.5 ± 0.2 | 3.9 ± 2.4 | 5.5 ± 0.2 | 5.9 ± 0.1 | 0.73 ± 0.01 | 108.07 ± 9.83 | 8 | 20 | 136 ± 14 | 6 | TT-OSL |
| 68 | 26.3 | Khuj. | 0.1 | 570 | 210 | 143.7 ± 3.1 | 2.5 ± 0.2 | 3.9 ± 2.4 | 5.5 ± 0.2 | 5.9 ± 0.1 | 0.73 ± 0.01 | 97.65 ± 8.55 | 22 | 34 | >123 ± 12 | SG | OSL |
| 71 | 25.4 | Khuj. | 1.3 | 570 | 177 | 275.1 ± 5.8 | 5.3 ± 0.2 | 6.1 ± 2.6 | 10.2 ± 0.3 | 9.2 ± 0.3 | 1.3 ± 0.05 | 175.64 ± 11.68 | 16 | 24 | 138 ± 11 | 6 | TT-OSL |
| 71 | 25.4 | Khuj. | 1.3 | 570 | 177 | 275.1 ± 5.8 | 5.3 ± 0.2 | 6.1 ± 2.6 | 10.2 ± 0.3 | 9.2 ± 0.3 | 1.3 ± 0.05 | 136.83 ± 21.03 | 12 | 44 | >108 ± 17 | SG | OSL |
| 74 | 25.4 | Khuj. | 0.2 | 570 | 206 | 22.7 ± 0.8 | 0.7 ± 0.2 | 11.0 ± 4.9 | 18.0 ± 0.3 | 25.0 ± 0.3 | 0.8 ± 0.04 | 111.15 ± 9.46 | 12 | 32 | 147 ± 15 | 6 | TT-OSL |
| 74 | 25.4 | Khuj. | 0.2 | 570 | 206 | 22.7 ± 0.8 | 0.7 ± 0.2 | 11.0 ± 4.9 | 18.0 ± 0.3 | 25.0 ± 0.3 | 0.8 ± 0.04 | 93.90 ± 3.17 | 10 | 9 | >124 ± 8 | 2 | OSL |
| 74 | 25.4 | Khuj. | 0.2 | 570 | 206 | 22.7 ± 0.8 | 0.7 ± 0.2 | 11.0 ± 4.9 | 18.0 ± 0.3 | 25.0 ± 0.3 | 0.8 ± 0.04 | 103.27 ± 3.56 | 20 | 15 | >140 ± 8 | 6 | OSL |
| 75 | 25.3 | Khuj. | 0.5 | 560 | 197 | 263.9 ± 5.5 | 4.5 ± 0.2 | 4.9 ± 2.0 | 6.0 ± 0.2 | 1.2 ± 0.05 | 170.91 ± 8.32 | 7 | 26 | 144 ± 9 | 6 | TT-OSL | |
| 75 | 25.3 | Khuj. | 0.5 | 560 | 197 | 263.9 ± 5.5 | 4.5 ± 0.2 | 4.9 ± 2.0 | 6.0 ± 0.2 | 1.2 ± 0.05 | 155.50 ± 27.30 | 15 | 66 | >131 ± 24 | SG | OSL | |
| 75 | 25.3 | Khuj. | 0.5 | 560 | 197 | 263.9 ± 5.5 | 4.5 ± 0.2 | 4.9 ± 2.0 | 6.0 ± 0.2 | 1.2 ± 0.05 | 157.40 ± 16.20 | 10 | 30 | >133 ± 15 | 2 | OSL | |
| 78 | 26.6 | Khuj. | 0.7 | 540 | 191 | 275.7 ± 5.7 | 4.3 ± 1.2 | 6.5 ± 1.7 | 7.7 ± 0.1 | 1.2 ± 0.06 | 177.96 ± 9.79 | 8 | 7 | 143 ± 11 | 6 | TT-OSL | |
| 78 | 26.6 | Khuj. | 0.7 | 540 | 191 | 275.7 ± 5.7 | 4.3 ± 1.2 | 6.5 ± 1.7 | 7.7 ± 0.1 | 1.2 ± 0.06 | 157.84 ± 12.40 | 10 | 22 | >127 ± 12 | 2 | OSL | |

Supplementary Table DR5 | Amino acid data for *Melanoides tuberculata* from Mundafan and Khujaymah. Error terms represent one standard deviation about the mean. Each sample was bleached, with the free amino acid fraction signified by 'FAA' and the total hydrolysable fraction by 'THAA'.

| Sample | Near r | FAA | | | | | | | | THAA | | | | | | | |
|------------------|--------|--------------|--------------|--------------|--------------|--------------|--------------|--------------|--------------|--------------|--------------|--------------|--------------|--------------|--------------|--------------|--------------|
| | | Asx D/L | | Glx D/L | | Ala D/L | | Val D/L | | Asx D/L | | Glx D/L | | Ala D/L | | Val D/L | |
| | | x | σ | x | σ | x | σ | x | σ | x | σ | x | σ | x | σ | x | σ |
| Sample 13 | 6009 | 0.910 | 0.016 | 0.485 | 0.030 | 0.729 | 0.002 | 0.347 | 0.058 | 0.796 | 0.002 | 0.414 | 0.003 | 0.658 | 0.007 | 0.293 | 0.003 |
| Sample 13 | 6010 | 0.903 | 0.023 | 0.490 | 0.024 | 0.713 | 0.001 | 0.350 | 0.066 | 0.758 | 0.001 | 0.400 | 0.003 | 0.643 | 0.012 | 0.270 | 0.002 |
| Sample 13 | 6011 | 0.814 | 0.025 | 0.382 | 0.022 | 0.655 | 0.032 | 0.380 | 0.042 | 0.761 | 0.003 | 0.380 | 0.004 | 0.635 | 0.008 | 0.293 | 0.002 |
| Sample 13 | 6012 | 0.856 | 0.026 | 0.433 | 0.011 | 0.710 | 0.034 | 0.432 | 0.045 | 0.708 | 0.003 | 0.371 | 0.004 | 0.630 | 0.012 | 0.279 | 0.001 |
| Sample 13 | | 0.871 | 0.044 | 0.448 | 0.051 | 0.702 | 0.032 | 0.377 | 0.039 | 0.756 | 0.036 | 0.391 | 0.020 | 0.642 | 0.012 | 0.284 | 0.011 |
| Sample 36 | 5774 | 0.870 | 0.008 | 0.545 | 0.012 | 0.785 | 0.010 | 0.379 | 0.006 | 0.798 | 0.000 | 0.495 | 0.009 | 0.735 | 0.004 | 0.419 | 0.029 |
| Sample 36 | 5807 | 0.871 | 0.007 | 0.488 | 0.022 | 0.783 | 0.004 | 0.363 | 0.031 | 0.778 | 0.001 | 0.451 | 0.007 | 0.702 | 0.007 | 0.314 | 0.055 |
| Sample 36 | | 0.870 | 0.001 | 0.516 | 0.040 | 0.784 | 0.001 | 0.371 | 0.011 | 0.788 | 0.014 | 0.473 | 0.031 | 0.718 | 0.023 | 0.366 | 0.074 |
| Sample 40 | 6003 | 0.953 | 0.022 | 0.763 | 0.101 | 0.909 | 0.013 | 1.068 | 0.024 | 0.835 | 0.001 | 0.809 | 0.009 | 0.898 | 0.003 | 0.715 | 0.016 |
| Sample 40 | 6004 | 0.946 | 0.021 | 0.785 | 0.069 | 0.889 | 0.024 | 0.958 | 0.200 | 0.824 | 0.001 | 0.714 | 0.002 | 0.852 | 0.013 | 0.739 | 0.014 |
| Sample 40 | | 0.949 | 0.022 | 0.774 | 0.085 | 0.899 | 0.018 | 1.013 | 0.112 | 0.829 | 0.008 | 0.762 | 0.067 | 0.875 | 0.033 | 0.727 | 0.017 |
| Sample 42 | 6005 | 0.962 | 0.024 | 0.822 | 0.066 | 0.926 | 0.005 | 1.060 | 0.034 | 0.911 | 0.002 | 0.853 | 0.002 | 0.918 | 0.004 | 0.835 | 0.041 |
| Sample 42 | 6006 | 0.949 | | 0.725 | | 0.922 | | 0.859 | | 0.840 | 0.003 | 0.782 | 0.001 | 0.892 | 0.004 | 0.829 | 0.023 |
| Sample 42 | 6007 | 0.907 | 0.017 | 0.774 | 0.062 | 0.917 | 0.007 | 0.966 | 0.155 | 0.858 | 0.005 | 0.739 | 0.006 | 0.854 | 0.006 | 0.809 | 0.044 |
| Sample 42 | 6008 | 0.927 | 0.013 | 0.845 | 0.047 | 0.914 | 0.014 | 1.002 | 0.160 | 0.832 | 0.002 | 0.780 | 0.006 | 0.879 | 0.001 | 0.773 | 0.013 |
| Sample 42 | | 0.937 | 0.024 | 0.791 | 0.053 | 0.920 | 0.005 | 0.972 | 0.084 | 0.860 | 0.035 | 0.788 | 0.047 | 0.886 | 0.027 | 0.811 | 0.028 |
| Sample 46 | 5775 | 0.936 | 0.005 | 0.903 | 0.029 | 0.943 | 0.024 | 0.965 | 0.052 | 0.864 | 0.009 | 0.836 | 0.010 | 0.901 | 0.001 | 0.841 | 0.053 |
| Sample 46 | 5808 | 0.933 | 0.008 | 0.872 | 0.032 | 0.913 | 0.000 | 0.967 | 0.014 | 0.908 | 0.010 | 0.851 | 0.012 | 0.900 | 0.014 | 0.839 | 0.028 |
| Sample 46 | 5809 | 0.922 | 0.003 | 0.846 | 0.002 | 0.959 | 0.017 | 0.940 | 0.032 | 0.914 | 0.022 | 0.849 | 0.009 | 0.910 | 0.006 | 0.849 | 0.012 |
| Sample 46 | 5810 | 0.944 | 0.011 | 0.859 | 0.010 | 0.955 | 0.001 | 0.982 | 0.064 | 0.924 | 0.012 | 0.875 | 0.009 | 0.928 | 0.019 | 0.844 | 0.024 |
| Sample 46 | 5811 | 0.939 | 0.004 | 0.850 | 0.000 | 0.949 | 0.000 | 0.963 | 0.018 | 0.893 | 0.006 | 0.848 | 0.027 | 0.902 | 0.021 | 0.802 | 0.035 |
| Sample 46 | | 0.935 | 0.008 | 0.866 | 0.023 | 0.944 | 0.018 | 0.963 | 0.015 | 0.900 | 0.023 | 0.852 | 0.014 | 0.908 | 0.012 | 0.835 | 0.019 |
| Sample 55 | 6013 | 0.943 | 0.019 | 0.894 | 0.029 | 0.932 | 0.007 | 0.987 | 0.148 | 0.868 | 0.004 | 0.825 | 0.008 | 0.891 | 0.011 | 0.825 | 0.050 |
| Sample 55 | 6014 | 0.912 | 0.054 | 0.836 | 0.005 | 0.828 | 0.144 | 0.991 | 0.061 | *0.1817 | *0.000 | *0.138 | *0.001 | *0.326 | *0.007 | *0.117 | *0.001 |
| Sample 55 | 6015 | 0.922 | 0.039 | 0.855 | 0.025 | 0.846 | 0.121 | 0.984 | 0.083 | 0.857 | 0.000 | 0.836 | 0.008 | 0.901 | 0.014 | 0.898 | 0.027 |
| Sample 55 | 6016 | 0.929 | 0.025 | 0.839 | 0.040 | 0.879 | 0.075 | 0.955 | 0.031 | 0.688 | 0.002 | 0.783 | 0.009 | 0.776 | 0.019 | 0.828 | 0.076 |
| Sample 55 | | 0.927 | 0.013 | 0.856 | 0.027 | 0.871 | 0.045 | 0.979 | 0.016 | 0.804 | 0.101 | 0.815 | 0.028 | 0.856 | 0.069 | 0.850 | 0.041 |
| Sample 62 | 5776 | 0.920 | 0.007 | 0.890 | 0.016 | 0.901 | 0.044 | 1.039 | 0.125 | 0.768 | 0.001 | 0.680 | 0.016 | 0.848 | 0.004 | 0.682 | 0.034 |
| Sample 62 | 5812 | 0.906 | 0.006 | 0.721 | 0.144 | 0.956 | 0.000 | 0.971 | 0.196 | 0.851 | 0.009 | 0.689 | 0.053 | 0.818 | 0.022 | 0.755 | 0.043 |
| Sample 62 | | 0.913 | 0.010 | 0.805 | 0.119 | 0.929 | 0.038 | 1.005 | 0.048 | 0.810 | 0.059 | 0.684 | 0.007 | 0.833 | 0.021 | 0.718 | 0.052 |
| Sample 69 | 6017 | 0.895 | 0.059 | 0.804 | 0.033 | 0.804 | 0.144 | 0.797 | 0.038 | 0.756 | 0.016 | 0.701 | 0.022 | 0.792 | 0.049 | 0.784 | 0.065 |
| Sample 69 | 6018 | 0.902 | 0.052 | 0.798 | 0.002 | 0.801 | 0.167 | 0.855 | 0.007 | | | | | | | | |
| Sample 69 | | 0.898 | 0.005 | 0.801 | 0.004 | 0.803 | 0.002 | 0.826 | 0.041 | 0.756 | 0.016 | 0.701 | 0.022 | 0.792 | 0.049 | 0.784 | 0.065 |

*not included in average due to contamination

Supplementary Table DR6 | Radiocarbon dating results. Calibration was done with OxCal 4.10 using the IntCal09 curve (Bronk Ramsey, 2009). Preparation and measurement procedure are described in Hajdas et al. (2004). Samples with the comment “leach+” were subject to additional HCl leaching.

| Sec | Nr | Lab Nr. | Material | DeltaC13 (‰) | C14 age BP | Cal (2σ) age (OxCal 4.10) BP | |
|------|----|-------------|-------------------|-----------------|---------------|---------------------------------|--------|
| 21.2 | 37 | ETH-38514 | Phytoclasts | -22.6 ± 1.1 | 7420 ± 35 | 8260 ± 80 | |
| 21.2 | 37 | ETH-36454 | Shell, Lymnea | -3.7 ± 1.2 | 7720 ± 55 | 8500 ± 90 | |
| 21.2 | 33 | ETH-36452 | Bone, Vertebrate | -39.2 ± 1.1 | 7810 ± 70 | 8700 ± 280 | |
| 21.2 | 33 | ETH-36453 | Shell, Lymnea | -12.4 ± 1.2 | 8820 ± 65 | 9900 ± 270 | |
| 21.2 | 33 | ETH-37794 | Phytoclasts | -25.6 ± 1.1 | 7755 ± 40 | 8520 ± 80 | |
| 21.2 | 29 | ETH-37793 | Phytoclasts | -23.6 ± 1.1 | 8255 ± 45 | 9220 ± 190 | |
| 21.2 | 25 | ETH-38512 | Phytoclasts | -24.0 ± 1.1 | 8710 ± 35 | 9720 ± 170 | |
| 21.2 | 23 | ETH-38511 | Phytoclasts | -23.8 ± 1.1 | 8685 ± 35 | 9640 ± 90 | |
| 21.2 | 23 | ETH-36567 | Phytoclasts (raw) | -2.2 ± 1.2 | 9300 ± 40 | 10480 ± 175 | |
| 21.2 | 23 | ETH-36451 | Shell, Lymnea | -8.9 ± 1.2 | 9075 ± 60 | 10220 ± 250 | |
| 21.1 | 16 | ETH-37792 | Phytoclasts | -23.0 ± 1.1 | 8300 ± 45 | 9290 ± 150 | |
| 22.3 | 13 | ETH-37906 | Phytoclasts | -25.7 ± 1.1 | 7030 ± 40 | 7860 ± 100 | |
| 23.2 | 10 | ETH-37907 | Phytoclasts | -23.5 ± 1.4 | 7325 ± 50 | 8160 ± 150 | |
| 22.2 | 43 | ETH-36455 | Shell, Melanoides | 0.3 ± 1.2 | 31570 ± 420 | 35930 ± 870 | |
| 22.2 | 43 | ETH-36455-2 | Shell, Melanoides | -4.1 ± 1.2 | 34350 ± 320 | 39490 ± 850 | leach+ |
| 22.2 | 46 | ETH-36456 | Shell, Melanoides | -0.5 ± 1.2 | 38065 ± 895 | 42830 ± 1350 | |
| 22.2 | 46 | ETH-36456-2 | Shell, Melanoides | -1.9 ± 1.2 | 41785 ± 770 | 45370 ± 1190 | leach+ |
| 22.4 | 50 | ETH-36457 | Shell, Unio | 1.1 ± 1.2 | 34065 ± 580 | 39040 ± 1630 | |
| 22.4 | 50 | ETH-36457-2 | Shell, Unio | -2.5 ± 1.2 | 36755 ± 415 | 41720 ± 620 | leach+ |
| 28.6 | 55 | ETH-38709 | Marl, bulk | -2.0 ± 1.1 | 28970 ± 135 | 33780 ± 660 | |
| 26.3 | 55 | ETH-38710 | Shell, Unio | -9.5 ± 1.1 | 16230 ± 50 | 19260 ± 310 | |
| 28.1 | 62 | ETH-38711 | Shell, Melanoides | -8.0 ± 1.1 | 28685 ± 125 | 33070 ± 520 | |

Supplementary Table DR7 | Carbon isotope $\delta^{13}\text{C}_{\text{org}}$ ratios

| Sample (Fig. DR2) | Weight (mg) | Run | $\delta^{13}\text{C}_{\text{org}}$ VPDB (‰) |
|----------------------|----------------|--------|--|
| 16 | 4.856 | NC0183 | -24.830 |
| 23 | 6.077 | NC0183 | -24.844 |
| 29 | 4.791 | NC0183 | -25.976 |
| 37 | 9.142 | NC0183 | -26.141 |
| 13 | 6.489 | NC0183 | -25.918 |
| 10 | 6.206 | NC0183 | -23.233 |

4. Supplementary Discussion

Discussion of OSL dating

Sources of scatter in D_e distributions include the variability in luminescence sensitivity and dose saturation characteristics (Roberts et al., 1999; Duller et al., 2000), incomplete bleaching (Olley et al., 1998), variations in microdosimetry (Murray and Roberts, 1997; Kalchgruber et al., 2003; Vandenberghe et al., 2003), and post-depositional mixing (Roberts et al., 1999). While incomplete bleaching and post-depositional mixing increases the spread of the distribution by skewed distributions or a mixture of different populations, variations in microdosimetry and the variability in sensitivity and saturation characteristics only generally increases the spread of the distribution. The samples from Mundafan and Khujaymah were tested for mixed populations by single grain methodology. Single grain D_e distributions (Supplementary Fig. DR19a,c) show little skewness and only a single population ruling out problems of incomplete bleaching and post-depositional mixing.

In order to describe D_e distributions quantitatively, a parameter defining the spread of the distribution was calculated. The over-dispersion parameter (OD) is defined as the spread in a population that is additional to the spread expected from the error on each individual D_e value (Galbraith et al., 1999), which is strongly influenced by differences in signal intensity. The OD of the samples under consideration (Supplementary Table DR4) is on average 20 %, ranging from 15 to 25 % for the Holocene samples (2 mm aliquots). Such broad distributions have previously been observed for dune sands from Southern Australia and have been attributed to variations in microdosimetry (Kalchgruber et al. 2003). Applying the decision process of Bailey and Arnold (2006) shows that none of the distributions from Holocene samples has a skew that indicates a mixture of populations. In order to obtain a central value that best reflects the average D_e of each sample, the central age model (Galbraith et al., 1999) was chosen for calculations.

For the Holocene deposits (Supplementary Fig. DR2), it is shown that all OSL ages for the dune sands below the lake deposits are predating the onset of lake formation, as given by radiocarbon, by not more than a few thousand years. We hence assume that the deposition of aeolian sand below the lake deposits in general usually just predates the onset of lake formation. This assumption has been applied for the Pleistocene deposits and is supported by evidence from sections 22.2 (Supplementary Fig. DR4), 26.2 (Supplementary Fig. DR8) and 25.4 (Supplementary Fig. DR9).

Discussion AAR geochronology

The DL ratios of Asx, Glx, serine (Ser), alanine (Ala) and valine (Val) provide an overall estimate of protein decomposition. These indicators of protein decomposition have been selected as their peaks are cleanly eluted with baseline separation and they cover a wide range of rates of reaction. It is expected that with increasing age, the extent of racemization (D/L) will increase.

If the amino acids were contained within a closed system, the relationship between the FAA and the THAA fractions should be highly correlated, with non-concordance enabling the recognition of compromised samples (Preece and Penkman, 2005). The plot of FAA to THAA data from each sample can also be used as a relative timescale, with younger samples falling towards the bottom left corner of the graph and older samples falling towards the upper right corner, along the line of expected decomposition. The data from the Mundafan samples have been plotted in this way for each of the amino acids. As the site of Mundafan has experienced a different temperature history to that of previous studies of intra-crystalline protein degradation, correlation to absolute dates requires the development of an aminostratigraphic framework for this area.

Asparagine (Asx) is one of the fastest racemizing of the amino acids discussed here (due to the fact that it can racemize whilst still peptide bound). This enables good levels of resolution at younger age sites, but decreased resolution with older material. The D/L Asx data from the Holocene samples have the lowest values of the samples analyzed, as expected. However, most of the other horizons are nearing equilibrium, meaning that Asx is not particularly useful for age resolution for sites of this age. The subsamples of sample 55 are divergent – 6014bH* shows very low D/L values in the THAA fraction, falling away from the line of expected decomposition, along with high concentrations and a differing amino acid composition. This sample shows clear signs of contamination, so although the data is presented in the figures, it should not be used for age determination.

Glutamine (Glx) is one of the slower racemizing amino acids discussed here and so the low levels of racemization do help discriminate between material of the ages of this study. It is noteworthy that Glx has a slightly unusual pattern of racemization in the free form, due to the formation of a lactam. This results in difficulties in measuring Glx in the Free form, as the lactam cannot be derivitized and is therefore unavailable for analysis. The Glx D/L values from sample 13 show the lowest values (Supplementary Fig. DR23), with sample 36 yielding slightly higher D/L values, consistent with their relative radiocarbon dates within the Holocene. Again, the 6014bH* subsamples from sample 55 show that their closed system has been compromised and should be rejected. The other sites show high levels of

racemization, nearing equilibrium, although sample 62 and sample 69 exhibit the lower values of the group. Sample 46, sample 51 and sample 40 show similar levels of protein breakdown, consistent with relatively rapid deposition of this sequence.

Alanine (Ala) is a hydrophobic amino acid, whose concentration is partly contributed from the decomposition of other amino acids (notably serine). Ala racemizes at an intermediate rate, so is one of the amino acids that may help distinguishing samples of the timescales under consideration. The results for Ala are broadly similar to that seen in the other amino acids (Supplementary Fig. DR24). The alanine data supports the interpretation that sample 13 is the youngest in age, with sample 36 slightly older. The 6014bH* subsamples from sample 55 again show divergence from closed system behavior. The replication of sample 55 and sample 69 samples is not particularly good, so further samples are being run to confirm this. Sample 62 tend to show a slightly younger age, with sample 46, sample 42 and sample 40 showing tight clustering at almost equilibrium levels.

Valine (Val) has extremely low rates of racemization, and as the concentration of Val is quite low, the difficulty of measuring the D/L accurately results in higher variability. It does however still prove useful for age discrimination within material of Pleistocene age. The Val D/L in the FAA and THAA fractions again support the other amino acid data (Supplementary Fig. DR23). The Holocene samples are demonstrably younger, while the one subsample from sample 55 is compromised. Data from sample 62 is more variable, but still consistent with a younger age than sample 46, sample 42 and sample 40 (but significantly older than the Holocene samples). Again, the older samples show values nearing equilibrium; it is therefore likely that AAR dating has reached its temporal limit for this area.

Isoleucine (Ile) also has extremely low rates of racemization, and baseline separation is not very accurate using the RP-HPLC technique, so is usually separated by ion exchange chromatography. However, results are presented here as they support the data obtained from the other amino acids. Isoleucine has two chiral centers, but the important geochronological reaction is the breakdown of L-isoleucine to its diastereomer D-alloisoleucine, which is reported to equilibrate at D/L values of 1.3 (often reported as an A/I value). Again, the Holocene samples are clearly distinguishable, and the other sites are tending towards equilibrium.

The *Melanoides tuberculata* samples seem to show relatively good closed system behavior, although a higher degree of variability is seen within sample 62, and there is clear contamination in sample 55. While optical thin section analysis showed that the structure of the shells is well preserved, there were indications of epitaxial calcite growth. Our preparation isolates the intra-crystalline material within a shell, therefore we are theoretically

analyzing a closed system of protein. However, if any re-crystallization has occurred, then this compromises the intra-crystalline fraction, meaning it has not been closed system for the history of the sample, and therefore cannot be used for dating. It may be that the variability is due to re-crystallization, but the relative consistency between the amino acids would argue against any significant effect. The two samples of well-constrained Holocene age: Sample 13 (~ 8000 years BP) and sample 36 (~9000 years BP) show levels of protein degradation consistent with these ages. The rest of the samples show levels of racemization nearing equilibrium, limiting their relative resolution. At what point equilibrium is achieved with these species in this tropical environment is unknown. Further study will inform on this. Using AAR, it is not possible to discriminate between the three samples analyzed which have been excavated within a sequence (sample 46, sample 42 and sample 40).

In this study the amino acid data has been used as a relative dating technique to present a pilot aminostratigraphy for the area in question. The conversion of relative sequences into absolute dates and accurate correlation between different areas requires further studies on the patterns of breakdown in *Melanoides tuberculata*. However, it is concluded that sample 13 and sample 36 are the youngest within the sequence, consistent with their radiocarbon ages. Very high levels of protein degradation are observed in the other samples, inconsistent with a Holocene age. Amino acid geochronology has the potential to yield useful information on the relative age of these deposits in this area, but it is vital to establish the time point where equilibration occurs to constrain these ages.

Discussion Radiocarbon dating

For understanding the discrepancy between Pleistocene OSL and radiocarbon ages, it is important to realize that samples (mainly porous mollusk shells; e.g. *Melanoides tuberculata*) used for radiocarbon dating of pre-Holocene deposits will have strongly been affected by epitaxial calcite growth due to the interaction with water during the Holocene humid period, leading to an incorporation of younger ^{14}C . In section 22.2 (Supplementary Fig. DR4) radiocarbon ages of *Melanoides tuberculata* shells ($39,490 \pm 850$ cal BP (sample 43) and $45,370 \pm 1190$ cal BP (sample 46)) are stratigraphically inverted. OSL ages of ~100 ka for aeolian deposits from above and below the same lacustrine sequence are considered to reflect the real depositional age. Additional leaching on the same samples (43, 46 and also 50) had only increased the age by 3.5 ka, 2.5 ka and 2.7 ka but was not able to remove all of the epitaxial calcite due to the porous structure of the shells. This problem has been reported on other occasions from similar environments (Fontes and Gasse, 1989). The Holocene

radiocarbon ages (Supplementary Fig. DR2) on shells on the other hand show some hard water effect with the ages on shells being up to 1.4 ka older than the ages on phytoclasts.

Discussion Ostracodes

Ostracode species from Mundafan and Khujaymah are typical of fresh- to brackish, shallow water environments. Most prominent species include *Cyprideis torosa* that mainly occurs in marine brackish waters with fluctuating salinities but is also characteristic of a wide range of continental water bodies down to a water depth of 30 m (McClure, 1980; Meisch, 2000). Other species that tolerate an increase in salinity are *Cypris* sp., *Cypris bispinosa*, and *Heterocypris salina* (Meisch, 2000). Freshwater species include *Cypretta* sp., a genus usually found in warm (often subtropical), shallow, vegetated waters (Bronstein, 1947; Smith and Delorme, 2010) and *Paracandona* sp. that prefers small water bodies with a swampy or boggy bottom and the littoral zone of lakes (Meisch, 2000). A species that needs stable conditions and cannot survive in desiccating environments is *Darwinula stevensoni*. This species lives in aquifers and seeps (Bronstein, 1947; Griffiths et al., 2001; Martens et al., 1997; Schwalb, 2003; Smith and Delorme, 2010) and also occurs in the littoral of lakes, rivers, bogs and springs (Dumont et al., 1986; Martens et al., 1997). Less characteristic and less abundant are *Candona* sp. and *Limnocythere* sp., both benthonic species as well as *Candonocypris* sp., a nektobenthonic species that is an indicator for running shallow waters (Pérez et al., 2010).

Each humid phase is characterized by a typical species assemblage (number of samples):

Holocene (16), *Paracandona* sp. is accompanied by *Cypris* sp., *Darwinula stevensoni*, and *Heterocypris salina*. This suggests small and shallow, permanent and possibly slightly saline environments.

~80 ka (3), *Darwinula stevensoni* is the dominant ostracode. This species is accompanied by *Paracandona* sp., *Cypris* sp., and a few specimen of *Cyprideis torosa*. This suggests significantly fresher conditions than during the Holocene and at ~100 ka with permanent water bodies.

~100 ka (5), The dominance of *Cyprideis torosa* hints at brackish waters. The presence of *Candonocypris* sp., *Darwinula stevensoni*, and *Limnocythere* sp. suggests the existence of permanent, shallow water bodies with possibly running water.

~125 ka (1), *Darwinula stevensoni* is the dominant species accompanied by *Cypris* sp. and *Paracandona* sp. This suggests significantly fresher conditions than during the Holocene and at ~100 ka with permanent water bodies.

References Supplementary Materials

- Bailey, R. M., and Arnold, L. J., 2006, *Statistical modelling of single grain quartz De distributions and an assessment of procedures for estimating burial dose: Quaternary Science Reviews*, v. 25, no. 19-20, p. 2475-2502.
- Ballarini, M., Wallinga, J., Wintle, A. G., and Bos, A. J. J., 2007, *A modified SAR protocol for optical dating of individual grains from young quartz samples: Radiation Measurements*, v. 42, no. 3, p. 360-369.
- Bøtter-Jensen, L., Bulur, E., Duller, G. A. T., and Murray, A. S., 2000, *Advances in luminescence instrument systems: Radiation Measurements*, v. 32, no. 5-6, p. 523-528.
- Bronk Ramsey, C., 2009, *Bayesian analysis of radiocarbon dates. Radiocarbon*, v. 51, p. 337-360.
- Bronshtein, Z. S., 1947, *Fresh-water Ostracoda Fauna of the USSR Crustaceans (Amerind Publishing for the U.S. Dept. of the Interior / N.S.F., New Delhi). [English transl., 1988.]*, v. 2 (1), no. i-xv, p. 1-470.
- Duller, G. A. T., 2003, *Distinguishing quartz and feldspar in single grain luminescence measurements: Radiation Measurements*, v. 37, no. 2, p. 161-165.
- Duller, G. A. T., Bøtter-Jensen, L., and Murray, A. S., 2000, *Optical dating of single sand-sized grains of quartz: sources of variability: Radiation Measurements*, v. 32, no. 5-6, p. 453-457.
- Dumont, H. J., Maas, S., and Martens, K., 1986, *Cladocera, Copepoda and Ostracoda (Crustacea) from Fresh Waters in South Yemen: Fauna of Saudi Arabia*, v. 8, no. 12-19.
- Fontes, J. C., and Gasse, F., 1989, *On the ages of humid Holocene and Late Pleistocene phases in North Africa -- Remarks on "Late Quaternary climatic reconstruction for the Maghreb (North Africa)" by P. Rognon: Palaeogeography, Palaeoclimatology, Palaeoecology*, v. 70, no. 4, p. 393-398.
- Galbraith, R. F., Roberts, R. G., Laslett, G. M., Yoshida, H., and Olley, J. M., 1999, *Optical dating of single and multiple grains of Quartz from Jinmium rock shelter, Northern Australia: Part I, Experimental design and statistical models: Archaeometry*, v. 41, no. 2, p. 339-364.
- Griffiths, H. I., Schwalb, A., and Stevens, L. R., 2001, *Environmental change in southwestern Iran: the Holocene ostracod fauna of Lake Mirabad: The Holocene*, v. 11, no. 6, p. 757-764.
- Hajdas, I., Bonani, G., Thut, J., Leone, G., Pfenninger, R., and Maden, C., 2004, *A report on sample preparation at the ETH/PSI AMS facility in Zurich: Nuclear Instruments and Methods in Physics Research Section B: Beam Interactions with Materials and Atoms*, v. 223-224, p. 267-271.
- Huntley, D.J., Godfrey-Smith, D.I. and Thewalt, M.L.W., 1985, *Optical dating of sediments: Nature*, v. 313, p. 105-107
-

-
- Kalchgruber, R., Fuchs, M., Murray, A. S., and Wagner, G. A., 2003, *Evaluating dose-rate distributions in natural sediments using δ -Al₂O₃:C grains: Radiation Measurements*, v. 37, no. 4-5, p. 293-297.
- Kaufman, D. S., and Manley, W. F., 1998, *A new procedure for determining dl amino acid ratios in fossils using reverse phase liquid chromatography: Quaternary Science Reviews*, v. 17, no. 11, p. 987-1000.
- Martens, K., Rossetti, G., and Fuhrmann, R., 1997, *Pleistocene and Recent species of the family Darwinulidae: Hydrobiologia*, v. 357, p. 99-116.
- McClure, H. A., Swain, F.M., 1980, *Fresh-water and Brackish-water fossils Quaternary Ostracoda from the Rub' al Khali ("Empty Quater"), Saudi Arabia: Actes du VI Colloque Africain de Micropaléontologie - Tunis 1974, Annales des Mines et de la Géologie*, v. 28, p. 427-441.
- Meisch, C., 2000, *Freshwater Ostracoda of Western and Central Europe, Süßwasserfauna von Mitteleuropa 8/3: Heidelberg, Spektrum Akademischer Verlag*, 1-522 p.
- Murray, A. S., and Roberts, R. G., 1997, *Determining the burial time of single grains of quartz using optically stimulated luminescence: Earth and Planetary Science Letters*, v. 152, no. 1-4, p. 163-180.
- Murray, A. S., and Wintle, A. G., 2000, *Luminescence dating of quartz using an improved single-aliquot regenerative-dose protocol: Radiation Measurements*, v. 32, no. 1, p. 57-73.
- Olley, J., Caitcheon, G., and Murray, A., 1998, *The distribution of apparent dose as determined by optically stimulated luminescence in small aliquots of fluvial quartz: implications for dating young sediments: Quaternary Science Reviews*, v. 17, no. 11, p. 1033-1040.
- Penkman, K. E. H., Kaufman, D. S., Maddy, D., and Collins, M. J., 2008, *Closed-system behaviour of the intra-crystalline fraction of amino acids in mollusc shells: Quaternary Geochronology*, v. 3, no. 1-2, p. 2-25.
- Penkman, K. E. H., Preece, R. C., Keen, D. H., Maddy, D., Schreve, D. C., and Collins, M. J., 2007, *Testing the aminostratigraphy of fluvial archives: the evidence from intra-crystalline proteins within freshwater shells: Quaternary Science Reviews*, v. 26, no. 22-24, p. 2958-2969.
- Pérez, L., Lorenschat, J., Bugja, R., Brenner, M., Scharf, B., and Schwalb, A., 2010, *Distribution, diversity and ecology of modern freshwater ostracodes (Crustacea), and hydrochemical characteristics of Lago Petén Itzá, Guatemala: Journal of Limnology*, v. 69, no. 1, p. 146-159.
- Porat, N., Duller, G. A. T., Roberts, H. M., and Wintle, A. G., 2009, *A simplified SAR protocol for TT-OSL: Radiation Measurements*, v. 44, no. 5-6, p. 538-542.
- Preece, R. C., and Penkman, K. E. H., 2005, *New faunal analyses and amino acid dating of the Lower Palaeolithic site at East Farm, Barnham, Suffolk: Proceedings of the Geologists Association*, v. 116, p. 363-377.

-
- Prescott, J. R., and Hutton, J. T., 1994, *Cosmic ray contributions to dose rates for luminescence and ESR dating: Large depths and long-term time variations: Radiation Measurements*, v. 23, no. 2-3, p. 497-500.
- Preusser, F., and Kasper, H. U., 2001, *Comparison of dose rate determination using high-resolution gamma spectrometry and inductively coupled plasma - mass spectrometry: Ancient TL*, v. 19, no. 1, p. 19-23.
- Roberts, R. G., Galbraith, R. F., Olley, J. M., Yoshida, H., and Laslett, G. M., 1999, *Optical dating of single and multiple grains of quartz from Jinmium rock shelter, Northern Australia: Part II, Results and implications: Archaeometry*, v. 41, no. 2, p. 365-395.
- Rosenberg, T. M., Preusser, F., and Wintle, A. G., 2011, *A comparison of single and multiple aliquot TT-OSL data sets for sand-sized quartz from the Arabian Peninsula: Radiation Measurements*, 46, 573-579.
- Schwalb, A., 2003, *Lacustrine ostracodes as stable isotope recorders of late-glacial and Holocene environmental dynamics and climate: Journal of Paleolimnology*, v. 29, no. 3, p. 265-351.
- Smith, A. J., and Delorme, L. D., 2010, *Ostracoda, Ecology and Classification of North American Freshwater Invertebrates* p. 725-771.
- Sykes, B., Leiboff, A., Low-Beer, J., Tetzner, S., and Richards, M., 1995, *The origins of the Polynesians: An interpretation from mitochondrial lineage analysis: Am. J. Hum. Genet.*, v. 57, p. 1463 - 1475.
- Vandenbergh, D., Hossain, S. M., De Corte, F., and Van den haute, P., 2003, *Investigations on the origin of the equivalent dose distribution in a Dutch coversand: Radiation Measurements*, v. 37, no. 4-5, p. 433-439.
- Wintle, A. G., and Murray, A. S., 2006, *A review of quartz optically stimulated luminescence characteristics and their relevance in single-aliquot regeneration dating protocols: Radiation Measurements*, v. 41, no. 4, p. 369-391.

Appendix E

Late Pleistocene palaeolake in the interior of Oman: A potential key-area for the dispersal of anatomically modern humans out of Africa?

Thomas M. Rosenberg, Frank Preusser, Ingo Blechschmidt, Dominik Fleitmann, Reto Jagher, Albert Matter

Luminescence dating

Samples for luminescence dating were taken as large blocks of breccias or lithified sand, wrapped with opaque foil for transport, and to later be cut under subdued light conditions to uncover the inner part which has not been exposed to sunlight since deposition. Twelve samples from which quartz grains of 200-250 µm in diameter were extracted and prepared for luminescence dating were investigated. For OSL measurements the aliquot size was 2 mm and for TT-OSL measurements 6 mm. Measurements were made in a Risø TL/OSL-DA-20 reader with blue diodes using a 7.5 mm Hoya U340 filter.

Two protocols were applied to determine the equivalent dose (D_e) for each of the samples: a standard single aliquot regenerative (SAR) protocol for OSL (Murray and Wintle, 2000) and a SAR protocol for TT-OSL (Porat et al. 2009; Rosenberg et al. 2011). Samples were initially characterized using preheat plateau and dose recovery tests. A preheat of 240°C for 10 s together with a cut-heat of 220°C were selected for D_e determination. The initial 0.4 s OSL signal minus a background estimated from the 50-60 s integral was used for OSL dose determinations. For TT-OSL the test dose was 10 Gy. The initial 0.4 s TT-OSL signal minus an early background estimated from the 0.4-10.4 s integral was used for TT-OSL dose determinations.

The dose rates were measured by high-resolution gamma spectrometry (Preusser and Kasper, 2001). Comparing the activities calculated for ^{238}U and ^{226}Ra indicates some evidence for radioactive disequilibrium in the Uranium decay chain (cf. Zander et al., 2007), mainly as deficit in ^{238}U . The likely process behind this observation is the removal of carbonate from the system as ^{238}U is highly soluble in contrast to its daughter isotopes. Such a process is only possible during periods of pronounced humidity. The most likely

period during which the disequilibrium occurred is the Holocene. Following this assumption we calculate different scenarios using ADELE software (Kulig, 2005), all of which indicate a negligible effect of disequilibrium on age determination. Dose rates were calculated assuming average water content between 1% and 3% during burial. The contribution of cosmic rays to the total dose rate was calculated using present day depth considering full uncertainties due to actual position below surface. Total dose rates and resulting OSL ages are summarized in Table 1.

Table 1. OSL and TT-OSL ages.

| Sample | Section | Depth (m) | Cosmic-dose rate (mGy/ka) | Activities (Bq/kg) | | | | U-238 from 186 keV and Ra-226 | Ra-226 | Dose rate (Gy/ka) | TT-OSL De (Gy) | n | OD (%) | OSL De (Gy) | n | OD (%) | TT-OSL Age (ka) | OSL Age (ka) |
|--------|---------|-----------|---------------------------|--------------------|-----------|-----------|------------|-------------------------------|------------|-------------------|----------------|-------------|------------|-------------|----------|---------|-----------------|--------------|
| | | | | K | Th | U-238 | Th | | | | | | | | | | | |
| 1 | 11.1 | 1.3 | 165 | 125.2 ± 1.6 | 4.0 ± 0.1 | 5.4 ± 1.0 | 7.8 ± 0.2 | 0.73 ± 0.03 | | | | | 19.1 ± 1.0 | 21 | 21 | | 26 ± 2 | |
| 2 | 11.2 | 0.6 | 182 | 195.7 ± 2.1 | 4.0 ± 0.1 | 7.0 ± 1.6 | 11.2 ± 0.3 | 1.05 ± 0.04 | 123.9 ± 9 | 12 | 21 | 113.7 ± 7.3 | 24 | 30 | 118 ± 10 | 108 ± 8 | | |
| 3 | 11.3 | 0.5 | 185 | 163.3 ± 2.3 | 2.8 ± 0.2 | 7.1 ± 1.4 | 11.9 ± 0.3 | 0.95 ± 0.04 | 97.1 ± 8 | 12 | 20 | 112.3 ± 5.1 | 27 | 22 | 102 ± 9 | 118 ± 7 | | |
| 4 | 11.4 | 0.4 | 187 | 120.5 ± 1.9 | 2.4 ± 0.1 | 6.9 ± 1.9 | 10.5 ± 0.2 | 0.79 ± 0.03 | 93.8 ± 10 | 12 | 32 | 104.7 ± 4.4 | 26 | 21 | 119 ± 14 | 132 ± 8 | | |
| 5 | 11.5 | 0.8 | 177 | 169.9 ± 2.0 | 4.9 ± 0.4 | 7.3 ± 0.8 | 7.6 ± 0.2 | 0.92 ± 0.04 | 119.7 ± 11 | 10 | 25 | 109.9 ± 5.4 | 23 | 23 | 131 ± 13 | 120 ± 8 | | |
| 6 | 12.1/1 | 1.3 | 165 | 106.7 ± 1.6 | 1.9 ± 0.1 | 7.8 ± 2.5 | 4.3 ± 0.1 | 0.60 ± 0.03 | 68.3 ± 4 | 20 | 11 | 69.6 ± 2.9 | 30 | 22 | 114 ± 9 | 116 ± 7 | | |
| 7 | 12.1/2 | 1.0 | 172 | 170.8 ± 1.7 | 3.0 ± 0.1 | 5.4 ± 0.9 | 5.3 ± 0.1 | 0.84 ± 0.03 | 85.3 ± 6 | 12 | 16 | 87.0 ± 5.1 | 27 | 30 | 102 ± 8 | 104 ± 7 | | |
| 8 | 12.8 | 0.7 | 180 | 40.4 ± 3.0 | 1.8 ± 0.1 | 4.1 ± 0.6 | 8.3 ± 0.2 | 0.49 ± 0.04 | 47.6 ± 5 | 10 | 12 | 50.5 ± 2.1 | 24 | 19 | 97 ± 12 | 103 ± 9 | | |
| 9 | 13.1A | 0.3 | 190 | 35.1 ± 1.1 | 2.1 ± 0.2 | 5.2 ± 0.7 | 8.3 ± 0.1 | 0.49 ± 0.03 | | | | 9.5 ± 0.7 | 23 | 30 | | 19 ± 2 | | |
| 10 | 13.1B | 0.3 | 190 | 29.3 ± 0.9 | 1.9 ± 0.1 | 6.5 ± 1.6 | 7.2 ± 0.1 | 0.45 ± 0.03 | | | | 8.2 ± 0.7 | 28 | 45 | | 18 ± 2 | | |
| 11 | 13.4 | 0.1 | 195 | 46.8 ± 1.1 | 2.6 ± 0.1 | 3.0 ± 1.6 | 7.7 ± 0.1 | 0.53 ± 0.03 | 64.8 ± 7 | 12 | - | 58.7 ± 2.5 | 20 | 18 | 123 ± 15 | 112 ± 8 | | |
| 12 | 13.6 | 0.8 | 177 | 103.4 ± 1.9 | 3.3 ± 0.1 | 5.2 ± 0.6 | 6.7 ± 0.1 | 0.67 ± 0.03 | 83.9 ± 5 | 12 | - | 75.4 ± 3.0 | 20 | 16 | 125 ± 9 | 112 ± 7 | | |

References

- Kulig, G. (2005). *Preparation of a Software for Age Determination by Means of Luminescence Techniques (Faculty of Mathematics Informatics, Technische Universität Freiberg, Germany) (in German)*.
- Murray, A. S., and Wintle, A. G., 2000. *Luminescence dating of quartz using an improved single-aliquot regenerative-dose protocol. Radiation Measurements 32, 57-73.*
- Porat, N., Duller, G. A. T., Roberts, H. M., and Wintle, A. G., 2009. *A simplified SAR protocol for TT-OSL. Radiation Measurements 44, 538-542.*
- Preusser, F., and Kasper, H. U., 2001. *Comparison of dose rate determination using high-resolution gamma spectrometry and inductively coupled plasma - mass spectrometry. Ancient TL 19, 19-23.*
- Rosenberg, T. M., Preusser, F., and Wintle, A. G., 2011. *A comparison of single and multiple aliquot TT-OSL data sets for sand-sized quartz from the Arabian Peninsula. Radiation Measurements 46, 573-579.*
- Zander, A., Degering, D., Preusser, F., Kasper, H.U., Brückner, H., 2007. *Optically stimulated luminescence dating of sublittoral and intertidal sediments from Dubai, UAE.: Radioactive disequilibria in the uranium decay series. Quaternary Geochronology 2, 123-128.*

Erklärung

gemäss Art. 28 Abs. 2 RSL 05

Name/Vorname: Rosenberg Thomas

Matrikelnummer: 01-908-276

Studiengang: PhD Sc in Climate Sciences

Bachelor Master Dissertation

Titel der Arbeit: Palaeoclimate history of the Arabian Peninsula:
humid phases recorded in lake deposits

LeiterIn der Arbeit: Prof. Dr. F. Preusser und Prof. Dr. D. Fleitmann

Ich erkläre hiermit, dass ich diese Arbeit selbständig verfasst und keine anderen als die angegebenen Quellen benutzt habe. Alle Stellen, die wörtlich oder sinngemäss aus Quellen entnommen wurden, habe ich als solche gekennzeichnet. Mir ist bekannt, dass andernfalls der Senat gemäss Artikel 36 Absatz 1 Buchstabe o des Gesetzes vom 5. September 1996 über die Universität zum Entzug des auf Grund dieser Arbeit verliehenen Titels berechtigt ist.

Bern, 1. November 2011

Ort/Datum

.....
Unterschrift

Curriculum vitae

Thomas M. Rosenberg

Date of birth: 22.07.1979

Place of origin: Beinwil AG, Switzerland

Education

12. 2007 – 11. 2011 **PhD student** at the Geological Institute and the Oeschger Centre of Climate Change Research, **University of Bern**.

Thesis: Palaeoclimate history of the Arabian Peninsula:
humid phases recorded in lake deposits

Supervisors Prof Dr F Preusser and Prof Dr D Fleitmann

10. 2001 – 10. 2006 **Studies** for a Diploma equivalent to a **MSc in Geology** at the Department of Earth Sciences, **ETH Zurich**

Thesis: Sedimentological- and geochemical analysis of the Karakoram-Kohistan suture zone in Yasin, northern Pakistan

Supervisor Prof Dr Jean-Pierre Burg

20. 03. 2000 Swiss Federal Matura C (Natural Sciences)